Highly siderophile elements in planetary materials as tracers for late accretion

Mario Fischer-Gödde

Dissertation submitted to obtain
the academic degree

Doktor der Naturwissenschaften
(Dr. rer. nat.)

Fachbereich Geowissenschaften
Freie Universität Berlin

Freie Universität Berlin

Berlin, April 2010

Referees:

1. Prof. Dr. Harry Becker
   Institut für Geologische Wissenschaften, FR Geochemie
   Freie Universität Berlin
   Malteserstr. 74-100, Haus B
   12249 Berlin
   Germany

2. Prof. Dr. Gerhard Franz
   Institut für Angewandte Geowissenschaften, FG Mineralogie
   Technische Universität Berlin
   Ackerstr. 76
   13355 Berlin
   Germany

Date of Disputation: 26.05.2010

Contents

List of figures and tables

Figures

Tables

1. Preface

1.1 Structure of the Thesis

The structure of this thesis is arranged in three major parts. The first part provides a general outline of the scientific framework of the thesis and a brief introduction into the geo- and cosmochemistry of highly siderophile elements (Chapter 2). The second part comprises three manuscripts, in which the scientific work and the results carried out in this study are documented and discussed (Chapters 3 – 5). The third part represents a synthesis of the results and conclusions of the manuscripts and provides a short outlook (Chapter 6).

1.2 Scientific manuscripts

The main part of the thesis comprises three scientific manuscripts. The first manuscript (Chapter 3) is already published in Geochimica et Cosmochimica Acta (Fischer-Gödde et al., 2010a). The second manuscript (Chapter 4) is currently under review for publication in Chemical Geology (Fischer-Gödde et al., 2010b). The third manuscript (Chapter 5) will be submitted to Earth and Planetary Science Letters in a revised version.

The scientific work schedule and the manuscripts are based on research proposals by Harry Becker, which were funded through the Deutsche Forschungsgemeinschaft (Be 1820 / 3-1, 6-1).

The authors of the three manuscripts are: Mario Fischer-Gödde, Harry Becker and Frank Wombacher. Mario Fischer-Gödde and Harry Becker are affiliated with the Freie Universität Berlin. Frank Wombacher was formerly affiliated with the Freie Universität Berlin and is now affiliated with the Universität zu Köln.

Data tables for each respective manuscript are provided after the main text and before the appendix.

1.2.1 CHAPTER 3

"Rhodium, gold and other highly siderophile element abundances in chondritic meteorites".

Mario Fischer-Gödde, Harry Becker and Frank Wombacher were responsible for sample preparation and data collection at the Freie Universität Berlin. Harry Becker provided assistance in the clean laboratory and in the TIMS laboratory. Frank Wombacher provided assistance in the ICP-MS laboratory. Mario Fischer-Gödde wrote preliminary and final versions of the manuscripts. Harry Becker and Frank Wombacher contributed to discussions and improved focus and clarity of the manuscript. Meteorite samples were applied by Harry Becker and Frank Wombacher.

In the thesis this chapter will be referenced as Fischer-Gödde et al. (2010a). The appendix of this chapter contains a comparison between data obtained in this study and literature data in order to assess accuracy of the analytical method.

1.2.2 CHAPTER 4

"Rhodium, gold and other highly siderophile elements in orogenic peridotites and peridotite xenoliths".

Mario Fischer-Gödde, Harry Becker and Frank Wombacher were responsible for sample preparation and data collection at the Freie Universität Berlin. Mario Fischer-Gödde wrote preliminary and final versions of the manuscripts. Harry Becker and Frank Wombacher contributed to discussions and improved focus and clarity of the manuscript. Peridotite samples were provided by Harry Becker. Samples from Beni Bousera, internal and external Ligurides, and West Eifel xenoliths were prepared by Mario Fischer-Gödde.

In the thesis this chapter will be referenced as Fischer-Gödde et al. (2010b). The appendix of this chapter provides major element data for peridotites determined by XRF, some detailed information on analytical techniques, and a comparison to literature data.

1.2.3 CHAPTER 5

"Highly siderophile element abundances and $^{187}Os/^{188}Os$ in lunar impact melt rocks: implications for late accretion processes in the Earth-Moon system".

Mario Fischer-Gödde and Harry Becker were responsible for scientific content and sample preparation. Apollo samples were selected by Mario Fischer-Gödde. A proposal to apply for the Apollo samples was written by Harry Becker and Mario Fischer-Gödde. Mario Fischer-Gödde contributed to the proposal on the scientific background, analytical techniques and information on the requested samples. The proposal was submitted to the NASA lunar sample curator and peer-reviewed by the Curation and Analysis Planning Team for Extraterrestrial Materials (CAPTEM). The lunar meteorite DaG400 was applied by Mario Fischer-Gödde.

Mario Fischer-Gödde, Harry Becker and Frank Wombacher were responsible for data collection at the Freie Universität Berlin. Mario Fischer-Gödde wrote preliminary and final versions of the manuscripts. Harry Becker contributed to discussions and improved focus and clarity of the manuscript. The manuscript will be submitted in a revised form to Earth and Planetary Science Letters.

2. Introduction

2. 1 Abstract

In the course of this study different planetary materials have been analyzed in order to evaluate the origin of the excess abundances of highly siderophile elements (HSE: Re, Os, Ir, Ru, Pt, Rh, Pd, Au) in the Earth's mantle and lunar crustal rocks. Concentrations of HSE and $^{187}Os/^{188}Os$ have been determined for chondritic meteorites, terrestrial peridotites and lunar impact melt rocks.

In the case of chondrites the obtained data further substantiated differences in the HSE abundance patterns and ratios such as Re/Os, $^{187}Os/^{188}Os$, Pd/Ir, Rh/Ir and Au/Ir among chondrite classes. Well-defined linear correlations of HSE, in particular for bulk samples of ordinary and EL chondrites, are explained by binary mixing and, possibly, dilution by silicates. The HSE carrier phases responsible for these correlations have a uniform chemical composition, indicating efficient homogenization of local nebular heterogeneities during or prior the formation of the host minerals in chondrite components. These correlations also suggest that metamorphism, alteration or igneous processes on the chondrite parent bodies had negligible influence on relative HSE abundances on scales larger than bulk rocks.

Depletion patterns for Rh, Pd and Au in carbonaceous chondrites other than CI are smoothly related to condensation temperatures and therefore are consistent with the general depletion of moderately volatile elements in carbonaceous chondrites. Subtle fractionations among refractory siderophile elements within ordinary and enstatite chondrites relative to carbonaceous chondrites may be explained by fractional condensation combined with the removal of early condensates and mixing of early and late formed alloys. Planetary fractionation processes that may have affected precursor material of chondrite components cannot explain the HSE abundance patterns of chondrite groups.

New HSE data on peridotites were used to further constrain HSE abundances in the Earth's mantle and to place constraints on the distribution processes accounting for observed HSE variations between fertile and depleted mantle lithologies.

Non-systematic variation of Rh abundances and constant Rh/Ir displayed by fertile lherzolites indicate a compatible behaviour of Rh during low to moderate degrees of partial melting. In contrast, Au and Au/Ir correlate with peridotite fertility, indicating incompatible behaviour of Au during magmatic processes in the mantle. Correlations displayed by Pd/Ir, Re/Ir and Au/Ir with Al_2O_3 suggest HSE fractionation during partial melting, or may reflect refertilization of previously melt depleted peridotites due to reactive infiltration of silicate melts.

Relative abundances of Rh and Au for the primitive mantle HSE model composition are similar to values of ordinary and enstatite chondrites. In combination with the results of previous studies, the inferred HSE composition of the primitive mantle does not match with the HSE abundance patterns of chondritic meteorites.

HSE abundances and $^{187}Os/^{188}Os$ in lunar impact melt rocks serve as important tracers to place constraints on the late accreted meteoritic materials during the late accretion period in the Earth-Moon system. Excellent linear correlations displayed among HSE abundances of subsamples from a given impact melt rock are explained by dilution processes or binary mixing between a high HSE end-member composition of the meteoritic impactor and a low-HSE end-member composition corresponding to the lunar target rocks. The high-HSE meteoritic end-member compositions are characterized by the slopes of the correlation lines.

Some of the high HSE impactor end-member compositions identified in granulitic lunar impact melts are similar to chondrites. Suprachondritic impactor components inferred for Apollo 14 and 16 impact melt rocks may reflect ancient meteoritic material with distinct chemical compositions not recognized in the present meteorite record or differentiated meteoritic material. The strongly fractionated HSE abundance pattern of some Apollo 16 samples is similar to magmatic iron meteorites and suggests a IVA iron meteorite projectile for the Nectaris impact. The first sufficiently precise Re-Os model age reported for Apollo 16 impact melt rock 67935 in this study indicates that the Nectaris basin may be as old as 4.1 Ga.

Excess HSE abundances of the Earth's mantle and suprachondritic Pd/Ir and Ru/Ir inferred for the primitive mantle may be explained by binary mixing of chondritic material with some fractionated HSE component similar to that recorded in Apollo 16 impact melt rocks.

2.2 Introduction and scientific framework

The highly siderophile elements (HSE) include the platinum-group elements Os, Ir, Ru, Pt, Rh and Pd, along with Re and Au. Owing to their unique chemical and physical properties, including high melting points and high resistance to oxidation, they are widely used for industrial and technical processes, catalytic converters, and jewellery. In Earth sciences the HSE have emerged as well suited tracer elements and are widely used to study geo- and cosmochemical differentiation processes. Because of their high siderophile and chalcophile behaviour, HSE are sensitive tracers for metal-silicate, sulphide-silicate, solid sulphide-sulphide liquid and solid metal-liquid metal partitioning processes. During these processes HSE show a range of different properties concerning their distribution behaviour between metal, silicate, sulphide and oxide phases.

The HSE include three radioisotope decay systems. The ^{187}Re-^{188}Os (half-life = 4.16×10^{10} y) and ^{190}Pt-^{186}Os (half-life = 4.5×10^{11} y) are long-lived systems, while the now-extinct ^{107}Pd-^{107}Ag is a short-lived chronometer, with a half-life of 6.5 million years. The Re-Os system has been most widely used for geochemical and cosmochemical studies, in order to study the chemical evolution of the Earth's mantle and asteroidal cores (e.g. Meisel et al., 1996; Smoliar et al., 1996; Shirey and Walker, 1998). In comparison to traditionally lithophile isotope systems like Rb-Sr and Sm-Nd, where both elements behave incompatible during mantle melting, the Re-Os system consists of a moderately incompatible parent (Re) and a compatible daughter (Os). Partial melt generation in the mantle results in a Re-depleted residual mantle and Re-enriched silicate melt. Thus, Os isotopic compositions of melt depleted peridotites retain the Os isotopic composition corresponding to the age of melt depletion. Consequently the Re-Os isotope system has been used to date ancient mantle derived rocks and to obtain melt depletion model ages

for residual mantle samples (Allègre and Luck, 1980; Luck and Allègre, 1984; Walker et al., 1989). On the other hand, Re and/or Os could be affected by redistribution processes in the mantle and the system could yield misleading age information (e.g. Becker et al., 2001; Pearson et al., 2004; van Acken et al., 2008; Lorand et al., 2009). Both, the Re-Os and Pt-Os decay systems have been used to study possible effects of core-mantle interaction at the core-mantle boundary (Walker et al., 1997; Brandon et al., 1999; Brandon and Walker, 2005), or possible mixing effects of silicate and sulphide melts derived from subducted oceanic crust with mantle derived melts or depleted mantle (e.g. Lorand et al., 1993; Rehkämper et al., 1999a; Luguet et al., 2008; van Acken et al., 2010). The short-lived ^{107}Pd-^{107}Ag decay system was used to study the timing of processes in the early solar system like volatile element depletion and the chronology of iron meteorite formation (Chen and Wasserburg, 1996; Schönbächler et al., 2008).

Over the past decades analytical progress resulted in improved precision and significantly reduced scatter of HSE abundance data for planetary materials. An increasing number of precise Re, Os, Ir, Ru, Pt and Pd concentration and ^{187}Os/^{188}Os data obtained by isotope dilution on chondrites, terrestrial peridotites and lunar impact melt rocks provide a resolution of differences in HSE composition not attained by previous neutron activation analysis (e.g. Becker et al., 2001a,b; Norman et al., 2001; Walker et al., 2002; Horan et al., 2003; Pearson et al., 2004; Brandon et al., 2005a,b; Becker et al., 2006; Luguet et al., 2007; Puchtel et al., 2008; van Acken et al., 2008; Horan et al., 2009). Despite an increasing data base, precise abundance data for Rh and Au in planetary materials are largely lacking, because both are monoisotopic and can not be analyzed by isotope dilution. Both, Rh and Au may be critical elements for (1) a comprehensive understanding of the different HSE patterns of the chondrite groups and their origin, (2) constraining the compositions and the origin of likely impactor populations accreted to the early Earth-Moon system, and (3) for a complete characterization of the HSE pattern of the Earth's primitive mantle (PM) and assessment of the influence of late accretion processes on the origin of the excess HSE abundances in the mantle.

In the course of this study, new and improved low-blank analytical methods for precise analysis of Rh, Au and other HSE concentrations in various types of planetary materials were developed. Rhodium and Au are difficult to analyse precisely because they are monoisotopic. Gold is also known to be a labile element in the laboratory, which may

easily get lost by adsorption and precipitation from solution. The analytical methods thus must ensure quantitative recovery of these elements along with other HSE. The development and improvement of a chemical separation technique for all HSE from the same digestion aliquot of different sample matrixes was a major goal of this study. The applied analytical techniques comprise high-pressure acid digestion, chemical separation, isotope dilution, standardization, inductively coupled plasma mass spectrometry (ICP-MS) and negative thermal ionisation mass spectrometry (N-TIMS) analyses. Concentrations of Re, Os, Ir, Ru, Pt and Pd were determined by isotope dilution. Rhodium and gold were quantified by a standardization technique relative to the abundances of other HSE determined by isotope dilution (Meisel et al., 2003; Fischer-Gödde et al., 2010a,b). Osmium concentrations and isotope compositions were determined by N-TIMS, all other HSE concentrations were determined by ICP-MS analysis.

2.2.1 Highly siderophile elements as tracers for late accretion

The main objective of this study focuses on the late accretion period in the Earth-Moon system. Precise abundance data for Rh, Au and other highly siderophile elements (HSE) obtained on planetary materials such as chondrites, peridotites and lunar impact melt rocks will be used as tracers to evaluate the origin of the HSE signature of the Earth's mantle and lunar crust.

Because HSE strongly partition into metal relative to silicates, during core formation the HSE will be almost quantitatively removed from the silicate portion of a planet or planetesimal. Excess abundances and broadly chondritic proportions of HSE in the Earth's mantle are commonly explained by late accretion of meteoritic materials after core formation. Late accretion is suggested to have taken place 4 billion years ago during a period of intense bombardment in the inner solar system. The timing of the late influx is inferred from radiometric ages obtained on lunar impact melt rocks, which mostly fall within a restricted range from 4.0 to 3.8 Ga. Lunar impact melt rocks were formed during large basin forming impact events on the lunar surface. Because of the narrow time interval defined by ages obtained on these rocks, this period is also referred to as "late heavy bombardment" or "final cataclysm". The HSE compositions contained in ancient

lunar impact melt rocks provide a unique record of the late accreted meteoritic materials accreted to the early Earth-Moon system.

In the case of the Earth the late accreted materials have been mixed back into the mantle. If the HSE in the Earth's mantle were added by late accretion of meteoritic materials, relative HSE abundances in the mantle should broadly reflect the HSE characteristics of the late influx, provided that HSE were not significantly fractionated since their incorporation into the mantle. Because HSE will get fractionated during magmatic and metasomatic processes in the mantle, constraining the origin of HSE in the Earth's mantle requires a detailed characterization of the HSE composition of the Earth's primitive mantle (PM). PM refers to the composition of a hypothetical mantle reservoir that has never undergone melt depletion or enrichment. For the purpose of this study, PM is used equivalent to primitive upper mantle (PUM, Meisel et al., 2001; Becker et al., 2006) or bulk silicate Earth (BSE). Because most of the peridotite samples derived from the upper mantle experienced prior melt extraction, relative abundances of moderately incompatible HSE in the PM have to be estimated via extrapolation (e.g. Morgan, 1986; Meisel et al., 2001; Becker et al., 2006). HSE abundances for a hypothetical primitive mantle (PM) model composition shown in Fig. 2.1 are calculated based on abundance data for fertile lherzolites and covariations observed for incompatible HSE with lithophile melt extraction indicators (e.g. Al_2O_3), assuming that the primitive mantle has a composition similar to fertile lherzolites (McDonough and Sun, 1995).

2.2.2 Highly siderophile elements in chondritic meteorites

Analysis of HSE abundances in meteorites provide information on the prevailing conditions and processes when the earliest solids were formed from the solar nebular, and the subsequent evolution of the first protoplanetary and planetary bodies within our solar system. The cosmochemical behaviour of highly siderophile elements is constrained from the study of primitive meteorites and their constituting components (chondrules, refractory calcium aluminium rich inclusions (CAIs) and metal grains). Highly siderophile element abundances in chondritic meteorites are commonly assumed to record fractionation processes in the solar nebula, such as volatile element depletion and phase

separation prior to the formation of chondrite parent bodies (e.g. Palme, 2000). These processes are largely controlled by volatility. The volatility of an element is given by its 50% condensation temperature from a gas of solar composition and corresponds to the temperature where 50% of the element has condensed into the solid phase and 50% is left in the gas phase (Wasson, 1985; Lodders, 2003). Because of their low vapour pressures under reducing solar nebular conditions, most HSE condense at high temperatures, well above the condensation temperature of iron (Table 2.1). Calculated equilibrium condensation curves for siderophile elements from a gas of solar composition show that refractory HSE (Re, Os, Ir, Ru, Pt, Rh) are nearly completely condensed before the condensation of Pd and Au, which both condense at lower temperatures and into solid solution with Fe (e.g. Palme and Wlotzka, 1976; Sylvester et al., 1990; Campbell et al., 2001). Most of the condensation calculations assume equilibrium between gas and solid phases, and ideal solid solution in the condensate. The HSE composition of a condensed alloy depends on the temperature, when it was removed out of equilibrium with the gas phase (e.g. Palme and Wlotzka, 1976; Campbell et al., 2003). Partial condensation or evaporation under solar nebular conditions is consistent with HSE abundance patterns observed for carbonaceous chondrites other than CI, which show increasing depletion of the more volatile HSE from Pt to Au (Palme et al., 1988; Wasson and Kallemeyn, 1988; Humayun and Caesson, 2000).

Table 2.1. Cosmochemical classification of HSE, 50% condensation temperatures (50% T_C in °K) in a gas of solar composition and major host phase.

	Refractory						Moderately volatile		
	Re	**Os**	**Ir**	**Ru**	**Pt**	**Rh**	**Fe**	**Pd**	**Au**
50% T_C[a]	1821	1812	1603	1551	1408	1392	1334	1324	1060
	Refractory metal alloy						Fe alloy		

[a] 50% condensation temperatures from Lodders et al. (2003).

Recent studies applying analytical techniques with improved precision, revealed abundances variations in ordinary and enstatite chondrites compared to carbonaceous chondrites, even among the refractory HSE. These variations are inconsistent with single phase condensation processes (e.g. Walker et al., 2002; Horan et al., 2003) and may be explained by fractional condensation combined with the removal of early formed refractory condensates and mixing of early and late formed alloys (Horan et al., 2009; Fischer-Gödde et al., 2010).

On the other hand, the results of radiometric studies on differentiated meteorites and chondrite components suggest that some differentiated planetesimals formed earlier than chondrites (Bizzarro et al., 2004; Baker et al., 2005; Kleine et al., 2005). Early formed differentiated planetary bodies could have been disrupted during collisions, and differentiated material from such bodies could have contributed material to chondrites and their components. From petrologic studies on chondrite components it was claimed that granoblastic olivine-rich aggregates within chondrules represent inherited components from an earlier generation of differentiated objects (Libourel et al., 2006; Libourel and Krot, 2007). Fractionated HSE abundance patterns displayed by ordinary, enstatite and R chondrites may reflect the influence of phases formed by very early metal-silicate, liquid metal-solid metal or liquid sulphide-solid sulphide segregation. Possible effects of HSE fractionation processes affecting chondrite precursor materials and their relevance for fractionated HSE abundances observed for bulk samples of chondrites are discussed in Chapter 3.

2.2.3 Highly siderophile elements in the Earth's mantle

Abundances and ratios of HSE in the silicate part of the terrestrial planets and the Moon may provide constraints on the conditions of planetary core formation and late accretion processes in the inner solar system (e.g. Chou, 1978; Kimura et al., 1974; Jones and Drake, 1986; O'Neill et al., 1991). Some partitioning studies performed at low pressure and relatively reducing f_{O2} conditions indicate that metal-silicate partition coefficients of HSE are in the range of 10^5-10^8, or even higher (Borisov and Palme, 1995; Ertel et al., 1999; Ertel et al., 2001). Consequently, during metal-silicate segregation the

HSE will be quantitatively stripped off the silicate portion of a planet or planetesimal and concentrate in the metallic core. Contrary to their expected complete removal, HSE abundances in the Earth's PM are several orders of magnitude elevated compared to metal-silicate equilibrium (Fig. 2.1). Excess siderophile abundances in the Earth's mantle are commonly explained by the addition of late accreted meteoritic materials after core formation (Chou, 1978; Jagoutz et al., 1979; Morgan, 1986; O'Neill, 1991; Schmidt et al., 2000; Meisel et al., 2001; Morgan et al., 2001; Schmidt, 2004; Becker et al., 2006).

A strong argument favouring the late veneer hypothesis stems from broadly chondritic relative HSE abundances in conjunction with $^{187}Os/^{188}Os$ and $^{186}Os/^{188}Os$ similar to ordinary and enstatite chondrites deduced for fertile peridotites and mantle materials (Morgan et al., 1981; Meisel et al., 1996; Brandon et al., 2000; Meisel et al., 2001; Walker et al., 2005a; Brandon et al., 2006).

Alternative explanations invoke inefficient core formation scenarios (Arculus and Delano, 1981; Jones and Drake, 1986), contributions from outer core material (Snow and Schmidt, 1998) or decreasing partition coefficients at high pressure-temperature core formation conditions (Murthy, 1991; Righter and Drake, 1997; Righter et al., 1997; Li and Agee, 2001; Righter et al., 2008). While the effect of pressure has little influence on the HSE partitioning behaviour (Holzheid et al., 2000; Ertel et al., 2006), high temperatures can cause a decrease in metal-silicate partition coefficients of Re, Pt, Pd and Au (Ohtani and Yurimoto, 1996; Righter and Drake, 1997; Danielson et al., 2005; Cottrell and Walker, 2006; Righter et al., 2008; Brenan and McDonough, 2009). However, abundances of other HSE like Os, Ir, Ru and Rh would still require the addition of a late meteoritic veneer (Cottrell and Walker, 2006; Righter et al., 2008; Brenan and McDonough, 2009).

The chondritic $^{187}Os/^{188}Os$ and $^{186}Os/^{188}Os$ isotope compositions inferred for the Earth's fertile mantle places strong constraints on the Re, Os and Pt relative abundances in the mantle. In order to preserve chondritic relative abundances, metal-silicate partition coefficients of Re, Os and Pt should be almost identical during core segregation. Combined literature data on the partitioning of Re and Os (Ohtani and Yurimoto, 1996; Righter and Drake, 1997; Brenan and McDonough, 2009) indicate that the Re/Os ratio would by far exceed the ratio required to account for the chondritic $^{187}Os/^{188}Os$ of the mantle. Partition coefficients obtained for Pt at the same conditions display significant variation (Fig. 2.1, Cottrell and Walker, 2006; Ertel et al., 2006). In summary, metal-

silicate partitioning at high temperature conditions for some HSE may decline towards values appropriate to account for their mantle abundances, but this hypothesis at present reveals some major problems.

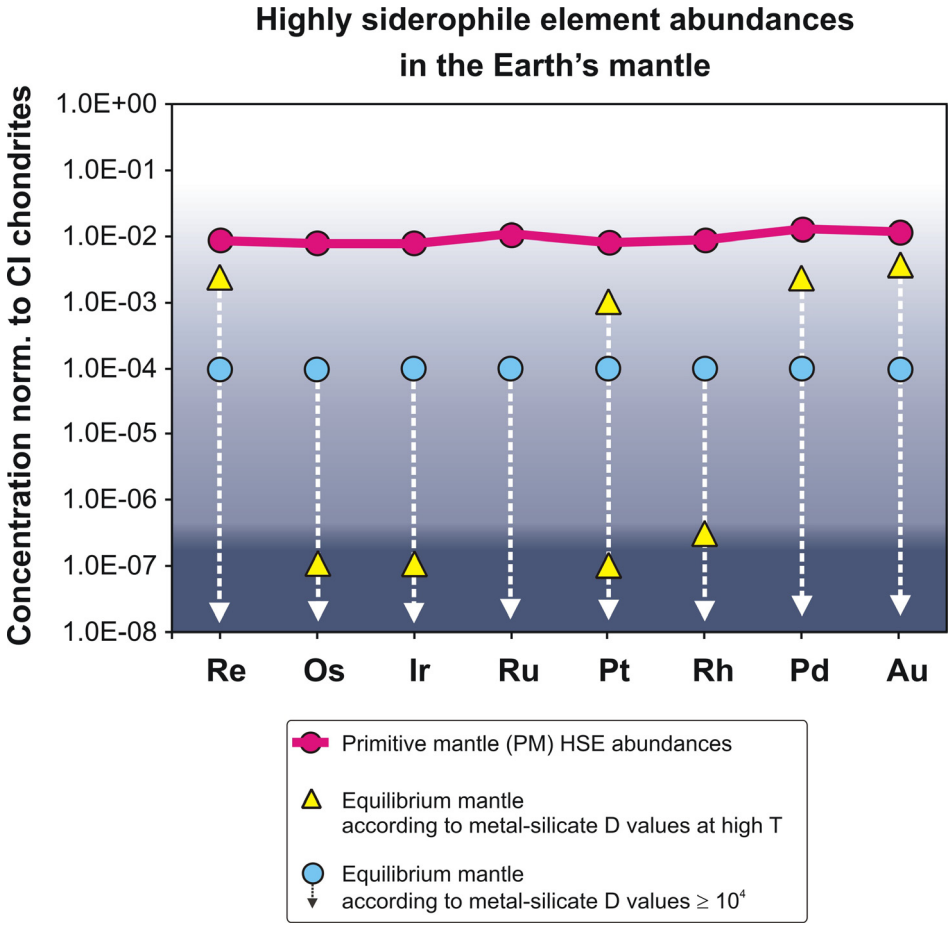

Fig. 2.1. CI chondrite normalized HSE abundances inferred for the primitive mantle (PM) according to Becker et al. (2006) and this study (Rh, Au), in comparison to calculated HSE abundances assuming equilibrium metal-silicate fractionation using D values obtained at different temperature and pressure conditions. CI abundances used from Fischer-Gödde et al. (2010). Elements are listed in the order of decreasing 50% condensation temperature in a gas of solar composition from left to right (Lodders, 2003). Blue points represent maximum D values inferred for metal-silicate equilibration at low pressure and moderate temperature conditions (e.g. Borisov and Palme, 1995; O'Neill et al., 1995; Ertel et al., 1999; Holzheid et al., 2000; Walter et al., 2000; Ertel et al., 2001). Yellow triangles correspond to maximum D values obtained at high temperatures (1900°C-2500°C) according to Ohtani and Yurimoto (1996) (Re), Righter and Drake (1997) (Re), Fortefant et al. (2003) (Rh), Danielson et al. (2005) (Au), Cottrell and Walker (2006) (Pt), Ertel et al. (2006) (Pt), Righter et al. (2008) (Pd), Brenan and McDonough (2009) (Os, Ir, Au). Dashed lines below the points illustrate that D values for each element extent to values lower than the scale of the diagram, depending on the experimental conditions (P, T, f_{O2}).

An increasing number of precise HSE abundance data sets on mantle peridotites and komatiites (Pattou et al., 1996; Lorand et al., 1999; Rehkämper et al., 1999a,b; Schmidt et al., 2000; Puchtel et al., 2004a; Puchtel et al., 2004b; Puchtel and Humayun, 2005; Puchtel et al., 2007; Liu et al., 2009; Maier et al., 2009) and Os isotopic data (Meisel et al., 1996; Brandon et al., 2000; Meisel et al., 2001; Walker et al., 2005a; Brandon et al., 2006) indicate that the HSE composition of the PM is characterized by $^{187}Os/^{188}Os$, $^{186}Os/^{188}Os$, Re/Os, Os/Ir, Pt/Ir and Pt/Os ratios within the range of chondritic meteorites, whereas suprachondritic ratios have been inferred for Ru/Ir, Pd/Ir, Pd/Pt.

While abundances and ratios of Re, Os, Ir, Ru, Pt and Pd for the Earth's mantle are precisely constrained, most of the HSE data sets on mantle peridotites obtained by acid digestion and isotope dilution did not include abundance data for monoisotopic Rh and Au (e.g. Pearson et al., 2004; Becker et al., 2006), with the notable exception of the data by Handler and Bennett, 1999, which include Rh data. Other studies reported Rh and Au data obtained using NiS fire assay pre-concentration followed by INAA (Lorand et al., 1993; Lorand et al., 1999; Lorand et al., 2000; Snow et al., 2000; Schmidt et al., 2003) or ICP-MS analysis (Pattou et al., 1996; Lorand et al., 1999; Luguet et al., 2003; Luguet et al., 2004). These studies reported both chondritic and suprachondritic Rh/Ir, and revealed that Rh may behave as a compatible element during magmatic processes in the mantle similar to Os, Ir and Ru. An incompatible behaviour of Au is indicated by correlations with other moderately incompatible elements like Re and Al_2O_3 (Morgan, 1986; Lorand et al., 1999). Abundances of Au in fertile peridotites in some of these studies showed considerably strong scatter. Thus, one of the main objectives of this study is to report precise abundance data for Rh and Au together with other HSE, in order to constrain Rh and Au abundances and their ratios with other HSE in the Earth's mantle.

2.2.4 Late accretion in the Earth-Moon system

Based on HSE concentrations and $^{187}Os/^{188}Os$ inferred for the primitive mantle (PM), mass balance calculations require the addition of a meteoritic late veneer of up to 0.4 - 0.5% of the total mass of the Earth, assuming that the late accreted meteoritic materials had an average chondrite composition. However, a detailed comparison between the HSE

composition inferred for the Earth's primitive mantle (PM) (Meisel et al., 2001; Becker et al., 2006; Fischer-Gödde et al., 2010b) and the HSE abundance patterns of chondritic meteorites (Walker et al., 2002; Horan et al., 2003; Fischer-Gödde et al., 2010a) reveals that none of the chondrite groups provides a good match for the PM composition (Fig. 2.2). In particular, the inferred suprachondritic ratios of Ru/Ir and Pd/Ir for the PM HSE composition are irreconcilable with the addition of one specific chondrite group. It was supposed that the HSE composition of the Earth's primitive mantle may reflect mixing of different types of meteoritic materials (Morgan et al., 2001; Norman et al., 2002; Becker et al., 2006; Puchtel et al., 2008; Walker, 2009; Fischer-Gödde et al., 2010c), but indigenous contributions inherited from high-temperature metal-silicate segregation may remain a viable option (e.g. Righter et al., 2008; Brenan and McDonough, 2009; Walker, 2009).

In the case of the Earth the late accreted materials have been mixed back into the mantle due to convection. In contrast, the lunar crust preserves a record of events after its formation 4.5 billion years ago, and the composition of the late meteoritic influx is recorded in ancient lunar impact melt rocks. Thus, lunar impact rocks are key samples to place constraints on the nature and origin of the late accreted meteoritic materials. Ancient lunar impact melt rocks have revealed details about the composition of impacting bodies during the Hadean history of the Earth-Moon system (Morgan et al., 1974; Hertogen et al., 1977). Recent studies on lunar impact melts indicate that some of the meteoritic components accreted to the lunar surface prior to 3.8 Ga may have had a HSE composition different from the known chondrite groups (Norman et al., 2002; Puchtel et al., 2008; Fischer-Gödde et al., 2010c). The meteoritic components contained in ancient lunar impact melt rocks bear evidence for the late accretion of meteoritic material with elevated Pd/Ir and Ru/Ir similar to the suprachondritic ratios inferred for the PM model HSE composition (Fig. 2.2, Norman et al., 2002; Puchtel et al., 2008; Fischer-Gödde et al., 2010c). Thus, one intriguing option to explain the suprachondritic Ru/Ir and Pd/Ir of the Earth's primitive mantle seems to be the addition of meteoritic material with a HSE composition different from the known chondrite groups.

In this study new HSE abundance and $^{187}Os/^{188}Os$ data on lunar impact melt rocks from the Apollo 14, 16 and 17 landing sites will be acquired. While previous studies basically focused on impact melt rock samples from Apollo 17 (Norman et al., 2002;

Puchtel et al., 2008), no comprehensive HSE data sets on Apollo 16 impact melt rocks obtained using modern analytical techniques are available. In addition to one Apollo 14 sample analyzed by Puchtel et al. (2008), we report new data on another Apollo 14 impact melt rock. The new HSE data will allow further constraints to be placed on the chemical composition and the origin of the late accreted meteoritic materials in the Earth-Moon system.

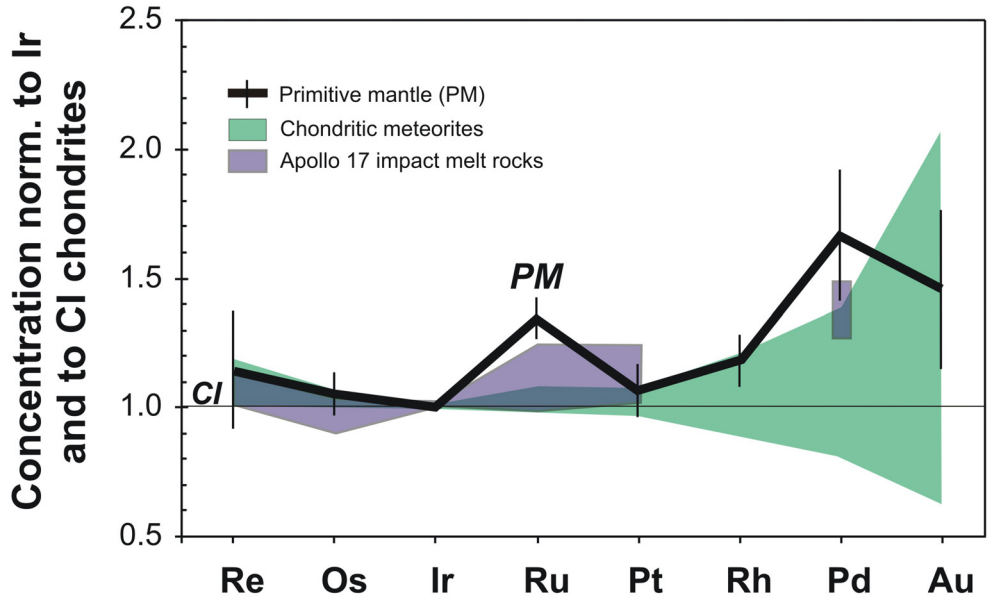

Fig. 2.2. Double normalized HSE abundance diagram (normalized to Ir and CI chondrite values, CI values from Fischer-Gödde et al., 2010a) showing the Earth's primitive mantle (PM) model HSE composition (Becker et al., 2006, Rh and Au from Fischer-Gödde et al., 2010b) in comparison to the range of HSE abundance patterns observed for chondritic meteorites (Walker et al., 2002; Horan et al., 2003; Fischer-Gödde et al., 2010a), and HSE abundance patterns of lunar impact melt rocks from the Apollo 17 landing site (Norman et al., 2002; Puchtel et al., 2008). Relative abundances of Ru and Pd inferred for the PM composition are clearly out of the range defined by chondritic meteorites. A reasonably good match can be observed between the PM and HSE patterns of Apollo 17 poikilitic lunar impact melt rocks, which also display Ru and Pd enhancements.

3. Rhodium, gold and other highly siderophile element abundances in chondritic meteorites

3.1 Abstract

The abundances of the highly siderophile elements (HSE) Re, Os, Ir, Ru, Pt, Rh, Pd and Au, and $^{187}Os/^{188}Os$ isotope ratios have been determined for a set of carbonaceous, ordinary, enstatite and Rumuruti chondrites, using an analytical technique that permits the precise and accurate measurement of *all* HSE from the same digestion aliquot. Concentrations of Re, Os, Ir, Ru, Pt and Pd were determined by isotope dilution ICP-MS and N-TIMS analysis. The monoisotopic elements Rh and Au were quantified relative to the abundance of Ir.

Differences in HSE abundances and ratios such as Re/Os, $^{187}Os/^{188}Os$, Pd/Ir and Au/Ir between different chondrite classes are further substantiated with new data, and additional Rh and Au data, including new data for CI chondrites. Systematically different relative abundances of Rh between different chondrite classes are reminiscent of the behaviour of Re. Carbonaceous chondrites are characterized by low average Rh/Ir of 0.27 ± 0.03 (1s) which is about 20 % lower than the ratio for ordinary (0.34 ± 0.02) and enstatite chondrites (EH: 0.33 ± 0.01; EL: 0.32 ± 0.01). R chondrites show higher and somewhat variable Rh/Ir of 0.37 ± 0.07.

Well-defined linear correlations of HSE, in particular for bulk samples of ordinary and EL chondrites, are explained by binary mixing and/or dilution by silicates. The HSE carriers responsible for these correlations have a uniform chemical composition, indicating efficient homogenization of local nebular heterogeneities during or prior to the formation of the host minerals in chondrite components. Excepting Rumuruti chondrites

and Au in carbonaceous chondrites, these correlations also suggest that metamorphism, alteration and igneous processes had negligible influence on the HSE distribution on the bulk sample scale.

Depletion patterns for Rh, Pd and Au in carbonaceous chondrites other than CI are smoothly related to condensation temperatures and therefore consistent with the general depletion of moderately volatile elements in carbonaceous chondrites. Fractionated HSE abundance patterns of ordinary, enstatite and Rumuruti chondrites, however, are more difficult to explain. Fractional condensation combined with the removal of metal phases at various times, and later mixing of early and late formed metal phases may provide a viable explanation. Planetary fractionation processes that may have affected precursor material of chondrite components cannot explain the HSE abundance patterns of chondrite groups. HSE abundances of some, but not all Rumuruti chondrites may be consistent with solid sulphide-liquid sulphide fractionation processes during impact induced melting.

3.2 Introduction

Osmium isotopic compositions and precise concentration data for some highly siderophile elements (HSE, which include the platinum group elements, Re and Au) display resolvable differences between the different chondrite groups (e.g. Wasson and Kallemeyn, 1988; Walker et al., 2002; Horan et al., 2003; Brandon et al., 2005a,b). Even though these data may be applied to study the processes that fractionated these elements in chondrites and their precursor materials, the detailed origin of these fractionations has remained obscure. HSE data on some chondrites also serve as important proxies for the composition of the solar system and are commonly used as a baseline for comparison with the HSE patterns of differentiated planetary and asteroidal samples.

Elemental abundances in chondritic meteorites are commonly assumed to record fractionation processes in the solar nebula such as volatile element depletion and phase separation prior to the formation of chondrite parent bodies (e.g. Palme, 2000). Walker et al. (2002) discuss differences in Re/Os and $^{187}Os/^{188}Os$ between carbonaceous chondrites relative to ordinary and enstatite chondrites that could have been achieved by high-temperature nebular condensation processes or subsequent lower temperature processes

such as oxidation and volatilization. However, the detailed process that fractionated Re/Os is unknown. Ratios of Al/Mg and Al/Si for chondrites show that carbonaceous chondrite groups other than CI are enriched in refractory siderophile and lithophile elements, while ordinary and enstatite chondrites are depleted in refractory elements (e.g. Wasson and Kallemeyn, 1988; Jochum, 1996; Palme 2000; Horan et al., 2003; Brandon et al., 2005b; Tagle and Berlin, 2008). Enstatite chondrites, particularly EH chondrites, are enriched in the more volatile elements Fe, Si, Ni, Pd and Au with condensation temperatures < 1400 K relative to refractory elements. Hence, they might have lost a refractory component (Ehman et al., 1970; Baedecker and Wasson, 1975; Wasson and Kallemeyn, 1988; Horan et al., 2003). Complementary siderophile element patterns have been observed between EH chondrites and CK and CV carbonaceous chondrite groups, suggesting that CK and CV chondrites might have gained a component similar to that lost from the EH chondrite formation region (Tagle and Berlin, 2008). A direct relationship between those groups is incompatible with their different oxygen isotopic composition.

Recent radiometric studies suggested that some differentiated planetesimals formed earlier than chondrites (Bizzarro et al., 2004; Baker et al., 2005; Kleine et al., 2005). Petrologic studies on chondrules suppose that granoblastic olivine-rich aggregates within chondrules have been derived from an earlier generation of differentiated objects (Libourel et al., 2006; Libourel and Krot, 2007). According to these rather controversial interpretations, material from early formed differentiated bodies could have been incorporated in some chondrite components, notably certain chondrules. The question arises whether some of the resolvable HSE fractionations (e.g. Re/Os) observed for ordinary and enstatite chondrites could reflect the influence of differentiated precursor materials, or if volatility control or redox processes may be more plausible explanations (Palme et al., 1998; Becker et al., 2001a; Walker et al., 2002; Horan et al., 2003).

While abundances and ratios of Re, Os, Ir, Ru, Pt, Pd and Au are now precisely constrained in important falls of chondritic meteorites, only limited concentration data for Rh in chondrites are available (e.g. Jochum, 1996; McDonald et al., 2001; McDonald and Russell, 2001; Tagle and Berlin, 2008). Rhodium and Au were not analyzed in the study by Horan et al. (2003), and thus no comprehensive data sets on the same digestion aliquot of chondrites are available in the literature. For CI chondrites only two analysis for Rh in Orgueil and Ivuna are currently available (Jochum, 1996). Here, we present new precise

and accurate concentration data for all HSE and $^{187}Os/^{188}Os$ obtained on the same aliquot from 30 bulk samples of carbonaceous, ordinary, enstatite and Rumuruti type chondrites. The analytical technique applies isotope dilution for Os, Ir, Ru, Pt, Pd and Re, and internal standardization for Rh and Au, using a modification of a technique by Meisel et al. (2003a). Along with previous data, the present study allows better constraints to be placed on HSE systematics in chondrites and their possible origin. We also provide updates of CI reference values for the comparison with HSE data in other planetary materials.

3.3 Analytical techniques

3.3.1 Sample preparation

Most of the chondrites analyzed in this study are falls. The Rumuruti chondrites NWA 978 (R3.8), NWA 753 (R3.9), EET 96026 (R3) and the EH3 chondrite Sahara 97072 are desert finds. Two EL3 chondrites (MAC 02839 and MAC 88136) are Antarctic finds. Altered and cut surfaces of the chondrite samples were abraded with corundum paper. Unweathered fresh looking chondrite pieces were crushed into coarse grained chips using an agate mortar. The chips were milled to a fine powder with a Retsch^{TM} MM200 agate swing mill.

Aliquots of sample powder between 50 and 100 mg were weighted into quartz glass digestion vessels and mixed ^{185}Re-^{190}Os and ^{191}Ir-^{99}Ru-^{194}Pt-^{105}Pd spike solutions were added, followed by 2.5 ml conc. HCl and 5 ml conc. HNO_3. The vessels were sealed with teflon-tape and heated in a high-pressure asher (HPA-S, Anton Paar^{TM}) for 6 h at 320°C (Meisel et al., 2003a). For comparison sample aliquots of the Smithsonian Allende standard powder were digested using both the HPA-S and a high-temperature Carius tube technique (Table 3.1) as described by Becker et al. (2006).

3.3.2 Chemical separation

Osmium was extracted immediately after digestion by solvent extraction from the reverse *aqua regia* into CCl_4, back extraction into HBr (Cohen and Waters, 1996), and further purification by microdistillation from a H_2SO_4-dichromate solution into a drop of HBr (Roy-Barman, 1993).

About 2-3 ml of the *aqua regia* solution were transferred into a PFA beaker and evaporated to near dryness. To ensure that Rh and Au are completely present as their chloro complex species, the solution was taken to near dryness twice with 2 ml 8.3 M HCl and once with 1 ml 1.25 M HCl. Rhenium, Ir, Ru, Pt, Rh, Pd and Au were separated from the matrix by cation exchange chromatography using Biorad™ Econo-columns filled with 10 ml of pre-cleaned Eichrom™ AG50W-X8 (100-200 mesh) resin. The resin was equilibrated with 20 ml 0.5 M HCl-60 % acetone (4 ml 1.25 M HCl + 6 ml ultrapure acetone). The sample solution was adjusted to the same HCl-acetone concentration before loading onto the column to avoid the formation of neutral and positive species of Rh and Au during the separation chemistry (Strelow et al., 1971). All HSE were eluted together in 14 ml 0.5 M HCl-60 % acetone. We used sample solutions of Allende to conduct column calibrations and recovery tests. We observed that Ir, Ru, Pt, Pd, Rh and Au showed parallel elution curves, while Re was slightly shifted to larger acid volumes. After the elution of the HSE fraction the remaining matrix elements were eluted from the resin within 30 ml of 6 M HCl and analyzed in order to test the HSE recovery. Matrix elution was also conducted for some samples during the course of this study. Recoveries were > 95 % for all HSE.

The eluted HSE fraction was split in half: one split for the analysis of Au, Re, Ir, Pt, and Pd, and the other for analysing Rh along with Ru, Ir, and Pt. Iridium and Pt were analysed in both splits. Before the analysis of the Au-Re-Ir-Pt-Pd split the acetone was evaporated by placing the beakers onto a hot plate for one hour at 60°C and for another hour at 80°C. The Rh-Ru-Ir-Pt cut was evaporated to near dryness and the residue was taken up in 0.28 M HNO_3 for ICP-MS analysis.

Because of the use of 0.5 M HCl during the chemical separation step Cd passed simultaneously with the HSE through the column. To avoid interferences from Cd isotopes on Pd a clean-up procedure using smaller columns filled with 2 ml Eichrom

AG50W-X8 (100-200 mesh) cation resin was performed in 0.2 M HCl. The clean-up procedure was conducted using the remaining solution from the Au-Re-Ir-Pt-Pd split after analysis of Au, Re, Ir and Pt. The eluted HSE fraction was evaporated to near dryness and the residue taken up into 0.28 M HNO_3 for ICP-MS analysis of Pd.

3.3.3 Mass spectrometry

Osmium isotopic compositions were measured by negative thermal ionisation mass spectrometry using a Thermo-Finnigan^{TM} Triton at the FU Berlin. Measured ratios were corrected for isobaric OsO_3^- interferences. Mass fractionation was corrected using $^{192}Os/^{188}Os = 3.0827$. Values and long-term reproducibility for $^{187}Os/^{188}Os$ of the UMD Os standard solution were 0.11379 ± 0.00006 (2s, n = 18) on Faraday cups and 0.1138 ± 0.0004 (2s, n = 4) for measurements on the secondary electron multiplier in pulse counting mode.

All other HSE were measured by sector-field inductively coupled plasma mass spectrometry using the ThermoElectron^{TM} Element XR equipped with an ESI^{TM} SC-autosampler at FU Berlin. Concentrations of Re, Ir, Ru, Pt and Pd were determined by isotope dilution (ID) analysis. Rhodium and Au concentrations were calculated using an internal-external standardization technique (Meisel et al., 2003a).

Signals were detected in low resolution by a secondary electron multiplier operating in pulse counting mode. One analysis contained 100 measurements, each made up of 3 scans (i.e. 300 scans in total) of the following analyte and interfering isotope masses: 99, 101, 102, 104 (Ru), 103 (Rh), 105, 106, 108, 110 (Pd), 111 (Cd), 185, 187 (Re), 189 (Os), 191, 193 (Ir), 194, 195, 196, 198 (Pt), 197 (Au), 199 (Hg). Each mass was integrated for 45 ms during each scan. The HSE spike isotopes ^{185}Re, ^{191}Ir, ^{99}Ru, ^{194}Pt and ^{105}Pd were not affected by isobaric interferences. Of the other isotopes used for concentration calculations, only ^{108}Pd was in some cases affected by the isobaric interference of ^{108}Cd. Corrections for the interference on ^{108}Pd were always conducted but insignificant in most cases, with few exceptions where corrections were < 4 %. Internal precision of measured isotopic ratios ranged from 0.1 to 1 % ($2s_m$, with n = 100).

The two splits derived from column chemistry were run with different sample introduction setups. For the Au-Re-Ir-Pt-Pd split a glass spray chamber (either cyclonic or Peltier-cooled Scott-type) was used, while the Rh-Ru-Ir-Pt split and the Pd clean-up fraction of the Au-Re-Ir-Pt-Pd split were run with an Aridus membrane desolvator, which reduced oxide interferences and increased signal intensities. While the glass spray chamber setup yielded better reproducibilities for Au and Re, the setup with the Aridus was required for precise and accurate Ru-Rh-Pd data, obviously due to suppressed interferences in this mass range. Sample solutions were aspirated with a Glass Expansion™ MicroMist nebulizer or an ESI™ PFA microconcentric nebulizer. Uptake rates of the analysed solutions were 80-140 µl/min depending on the nebulizer and tubing used. Acid blank solutions were measured at the start of each measurement session and after every 3-4 sample solutions to monitor background intensities and memory effects. Background corrections were occasionally carried out, if the background intensities were > 1 % of the sample intensities. At the start, in the middle and at the end of each measurement session a Re, Ir, Ru, Pt, Rh, Pd, Au standard solution with roughly chondritic HSE ratios and ~1 ppb Ir was measured. Mass fractionation was determined and corrected by the comparison of the ratios measured in the standard solution with IUPAC reference values. The long-term external reproducibility of isotopic compositions in the standard solution is < 1 % (1s).

Because both Rh and Au are monoisotopic, a combined internal-external standardization technique was used for concentration determination similar to that employed by Meisel et al. (2003a). The ^{193}Ir abundance of the sample measured by isotope dilution was used as internal standard as it provided the best reproducibility. This approach is reasonable since elution curves for Rh, Au and Ir are parallel during column chemistry, and their recoveries are > 95 %. The relative intensities of Rh, Au and Ir were calibrated using the external HSE standard solution.

In the course of this study we have continuously reduced our total chemistry blank levels. Initially, blanks were high and to some extent erratic (17-58 pg Re, 5-65 pg Ru, 19-372 pg Pt, 15-321 pg Pd, Fischer-Gödde et al., 2007). Some of these high blanks were produced by the sample introducion system of the ICP-MS instrument (e.g. by the Aridus membrane desolvator). Increasing wash times between samples and a periodically applied rinse protocol for the Aridus desolvator system reduced the blank levels substantially to

22±10 pg Re, 9±3 pg Os, 0.5±0.3 pg Ir, 3±2 pg Ru, 13±7 pg Pt, 0.6±0.1 pg Rh, 12±6 pg Pd, 7±3 pg Au (n = 4). Blank corrections were always applied, but usually less than 1 %. For Re blank corrections were less than 2 %, except for St.Severin (4 %) and Hvittis (7 %) which both have low HSE concentrations compared to all other samples. Osmium blank corrections were less than 0.1 % except in the case of Hvittis (0.16 %).

3.3.4 Data quality and comparison to literature data

Accuracy and reproducibility of the method were tested by repeated analysis of the Smithsonian Allende reference powder and by comparison with data obtained by other techniques such as spark source mass spectrometry (SSMS: Jochum, 1996) and neutron activation analysis (NAA: Jarosewich et al., 1987) (Table 3.1, Fig. 3.1). HSE abundances for the Smithsonian Allende standard powder determined in this study by isotope dilution (ID) are reproducible within 2.7 to 6.4 % (1s). Rhodium and Au abundances in Allende determined by standardization to Ir are reproducible to 4.1 % and 7.8 % (1s), respectively (Table 3.1, Fig. 3.1). HSE ratios reproduce within a few per cent (Re/Os < 4.3 %, HSE/Ir ratios < 7.3 %). Averaged absolute abundances and HSE ratios for the Smithsonian Allende standard powder (USNM 3529) from this study compare well with previous ID data from Horan et al. (2003), Brandon et al. (2005a) and Becker et al. (2006) (Table 3.1). HSE abundances and ratios for repeated analysis of Allende aliquots from this study, Walker et al. (2002) and Horan et al. (2003) agree within < 5 % and are consistent within analytical uncertainties. The 3 to 8 % reproducibility level for concentrations and the 0.2 % variation in Os isotope compositions in Table 3.1 may reflect heterogeneity of the Smithsonian Allende standard powder at the 50 mg sample aliquot scale used.

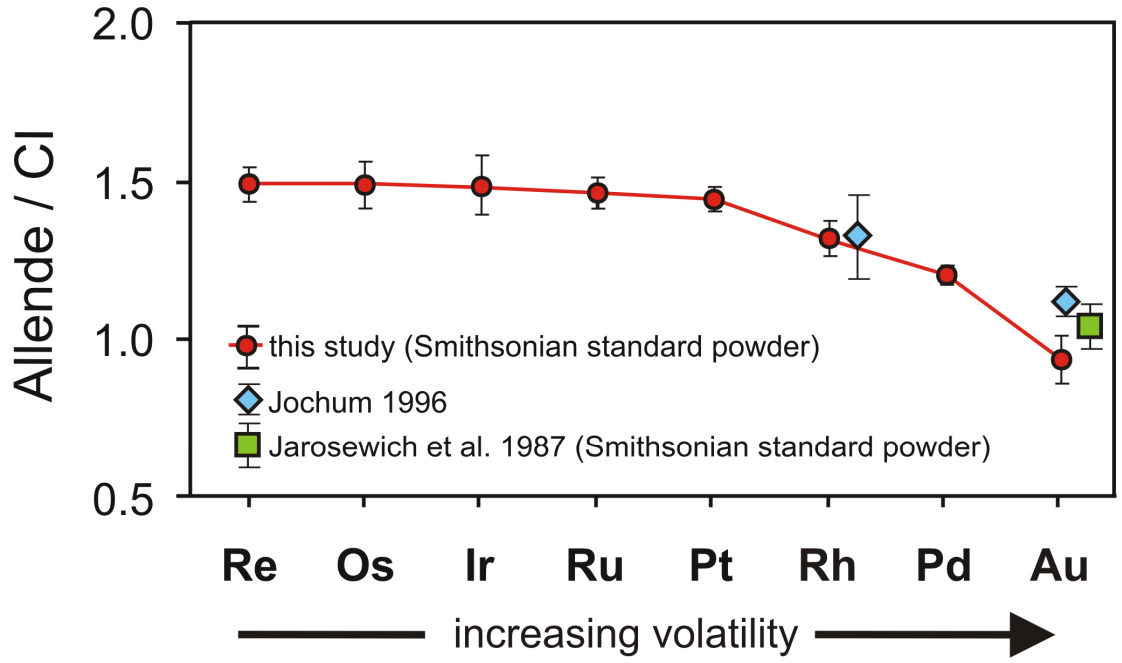

Fig. 3.1. Results for the Allende CV3 chondrite and comparison of Au and Rh data with spark source mass spectrometry (SSMS: Jochum, 1996) and neutron activation analysis (NAA: Jarosewich et al., 1987). Uncertainties (1s) derived from repeated analysis of the Smithsonian standard powder (Table 3.1).

Replicate analyses of the same sample powders were also conducted in the case of Orgueil (CI), Ivuna (CI), Ninqiang (CK3), Pillistfer (EL6), St.Marks (EH5) and NWA753 (R3.9) (Table 3.2). Relative standard deviations (1s) for HSE concentration data from replicate analysis of these samples are: Re <6.0%, Os <7.3%, Ir <10%, Ru <5.3%, Pt <7.1%, Rh <10%, Pd <6.5% and Au <12%. In the case of NWA 753, however, duplicate analyses reveals a difference of a factor of two in Au concentration, which suggests that its strong Au depletion resulted in a very heterogeneous Au distribution, while other HSE are reproducible within the range stated above. HSE ratios of replicates reproduce within < 8.3 %, again with the exception of NWA 753 (3.0 to 40 %), most probably reflecting sample heterogeneity. The reproducibilities for powders from chondrite bulk samples are essentially in accordance with the ones obtained for Allende (Table 3.1). Replicate analysis of chondrite powders reported by Horan et al. (2003) show similar or larger variation, which is best explained by the small sample weights and inhomogeneous

sampling of HSE carrier phases such as metal and sulphides (Walker et al., 2002; Horan et al., 2003). Taking into account the small amount of less than 500 mg for the preparation of bulk chondrite sample powders, this reproducibility is sufficient to assess the HSE variations between chondrite classes and groups.

Rhenium, Os, Ir, Ru, Pt and Pd abundances (Tables 3.1 and 3.2) and ratios of Re/Ir, Os/Ir, Ru/Ir and Pd/Ir compare well with data from previous isotope dilution analysis (Fig. 3.4, Walker et al., 2002; Horan et al., 2003, Brandon et al. 2005a,b). Our Pt/Ir ratios tend to be slightly higher than those reported by Horan et al. (2003), but both agree within a few %. A more detailed comparison of HSE concentrations and ratios obtained on the same samples from our study Walker et al. (2002) and Horan et al. (2003) is given in the appendix (3.8.1, Figs. 3.11 and 3.12).

Our technique produced Rh data that agrees within 1-10 % with data obtained previously by spark source mass spectrometry (SSMS: Jochum, 1996) for key samples such as Orgueil (CI), Ivuna (CI), Allende (CV3), Murchison (CM2) and Karoonda (CK4). Rhodium concentration data for Allende obtained by ICP-MS after Ni-sulphide fire assay pre-concentration by Tagle and Berlin (2008) are about 20 % higher than our average data and the values determined by Jochum (1996). Our Rh concentration data and average Rh/Ir ratios for ordinary and enstatite chondrites agree within < 5 % with previous studies using ICP-MS analysis after NiS fire assay pre-concentration from McDonald and Russell (2001) and McDonald et al. (2001), and within < 10 % with data from Tagle and Berlin (2008) (Fig. 3.4).

Our data for Au from carbonaceous chondrites agree within < 10 % with results from previous studies using instrumental and radiochemical neutron activation analysis (INAA and RNAA) and SSMS (e.g. Kallemeyn and Wasson, 1981; Kallemeyn et al., 1991; Jochum, 1996). The concentration data for Au and Au/Ir ratios obtained for ordinary and enstatite chondrites compare well with data from McDonald and Russell (2001) and McDonald et al. (2001) using NiS fire assay ICP-MS techniques (Fig. 3.4). Some of our Au data for ordinary and enstatite chondrites, however, show deviations up to 20 % from previously published RNAA and INAA data (Baedecker and Wasson, 1975; Morgan et al., 1985; Kallemeyn et al., 1989).

3.4 Results

3.4.1 Re/Os and Osmium isotope compositions

New Re, Os, $^{187}Re/^{188}Os$ and $^{187}Os/^{188}Os$ data of chondrites are listed in Tables 3.1 and 3.2. Concentrations of Re and Os span a range from 9.6 – 88 ng/g for Re and 107 - 965 ng/g for Os, where Hvittis (EL6) has the lowest and Dhajala (H3) the highest concentrations. As noted before significant differences in Re/Os and $^{187}Re/^{188}Os$ exist between chondrite classes (Morgan et al., 1985; Meisel et al., 1996; Walker et al, 2002; Brandon et al., 2005a,b). Ratios of $^{187}Re/^{188}Os$ for carbonaceous chondrites span a range from 0.293 for Karoonda (CK4) to 0.425 for one Allende (CV3) aliquot. This range becomes more narrow (0.370 to 0.425) if unusually low values from Karoonda (CK4) and Kainsaz (CO3) are excluded, in accordance with the average of 0.389 ± 0.021 (1s) reported for carbonaceous chondrites by Walker et al. (2002). Ordinary chondrites display ranges in $^{187}Re/^{188}Os$ from 0.342 (St.Severin, LL6) to 0.484 (Mt.Tazerzait, L5). Excluding the unusually low $^{187}Re/^{188}Os$ of St.Severin the ordinary chondrite range (0.413 to 0.484) is in good agreement with the average of 0.422 ± 0.025 (1s) reported by Walker et al. (2002) and data reported by Brandon et al. (2005b). Enstatite chondrites display a similar range as ordinary chondrites from 0.413 for MAC 88136 (EL3) to 0.480 for St.Marks (EH5), in agreement with the reported average (0.421 ± 0.013) of Walker et al. (2002). Two R chondrite samples display $^{187}Re/^{188}Os$ from 0.356 and 0.377 at the lower end of the carbonaceous chondrites range, while the Antarctic find EET 96026 (R3) has by far the lowest $^{187}Re/^{188}Os$ (0.136) of all analysed chondrite samples.

Because of the ß-decay of ^{187}Re to ^{187}Os, elemental Re/Os ratios should be correlated with $^{187}Os/^{188}Os$ in an isochron diagram (Fig. 3.2), provided that the Re/Os ratio was not disturbed since the formation of the chondrites. Similar to previous observations by Chen et al. (1998), Walker et al. (2002) and Brandon et al. (2005a), most chondrites in this study fall close to a 4.558 Ga reference isochron for IIIA iron meteorites from Smoliar (1996) (Fig. 3.2). Thus carbonaceous and R chondrites do not only display lower $^{187}Re/^{188}Os$, but also lower average $^{187}Os/^{188}Os$ than ordinary and enstatite chondrites (Figs. 3.2, 3.3).

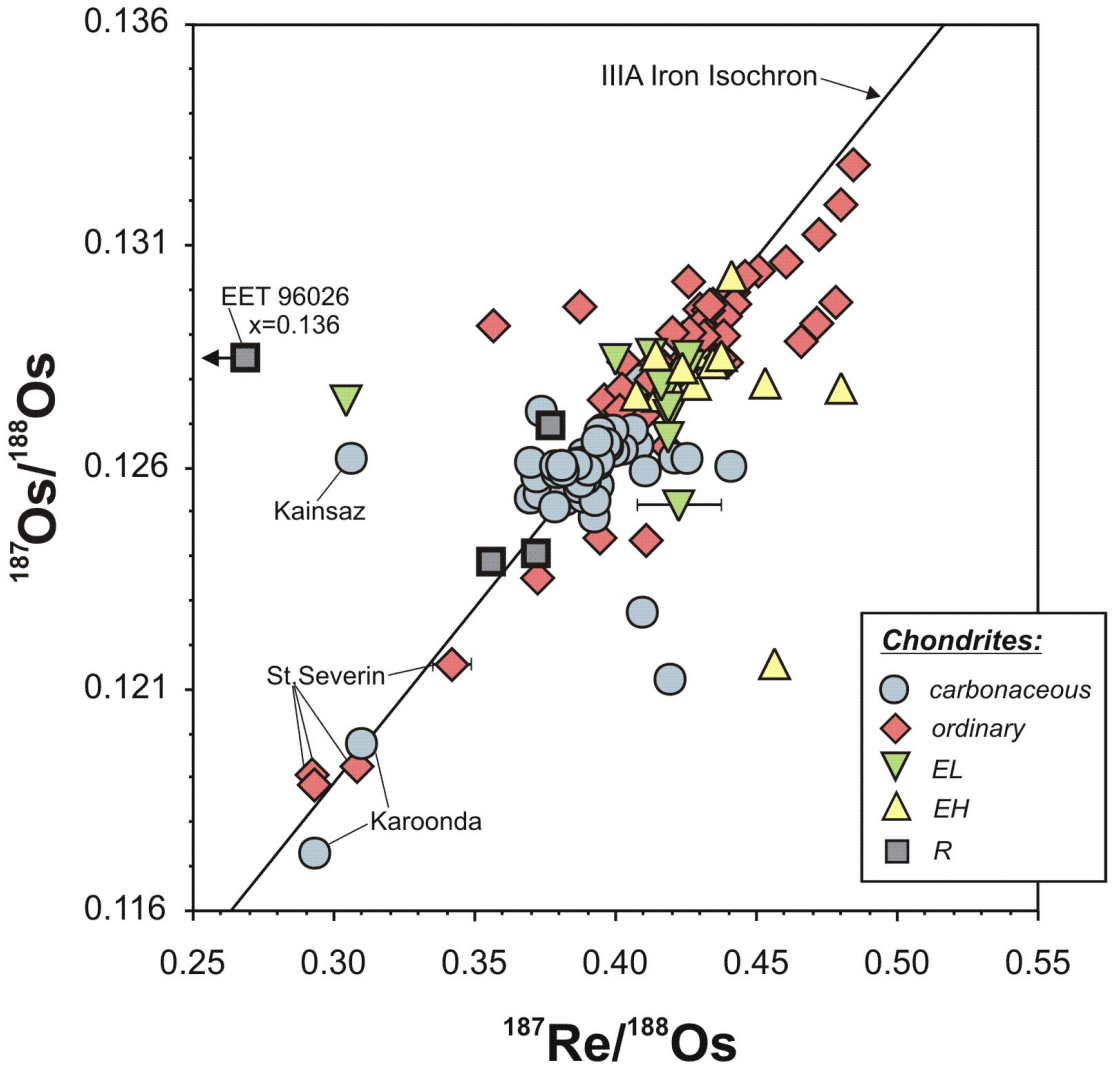

Fig. 3.2. $^{187}Os/^{188}Os$ vs. $^{187}Re/^{188}Os$ for chondrite bulk samples analysed in this study, Chen et al. (1998), Walker et al. (2002) and Brandon et al. (2005a,b). The 4.558 Ga isochron for IIIA iron meteorites from Smoliar (1996) is shown for reference. More than half of the chondrite samples analyzed in this study plot of the isochron beyond analytical uncertainties. Uncertainties (2s) are ~1 % for $^{187}Re/^{188}Os$ and 0.05 % for $^{187}Os/^{188}Os$ and reflect the uncertainty of the Re blank correction and the long term external reproducibility of $^{187}Os/^{188}Os$ of the Os standard. Uncertainties in $^{187}Re/^{188}Os$ for St.Severin and Hvittis are 2 % and 3.5 %, respectively, due to high blank corrections. Uncertainties are not shown if they do not exceed sample symbols. A distinction between the data from this study and the literature is provided in the appendix (3.8.3, Fig.3.15).

Ranges in $^{187}Os/^{188}Os$ for carbonaceous (0.12490 to 0.12624, excluding Karoonda), ordinary (0.12799 to 0.13282, excluding St.Severin) and enstatite chondrites (0.12518 to 0.13029) are essentially in accordance with previously reported averages of 0.12596 ± 0.00131 (1s), 0.12833 ± 0.00166, and 0.12815 ± 0.00044, respectively (Walker et al., 2002), and also compare well with $^{187}Os/^{188}Os$ data on chondrite bulk samples from Brandon et al. (2005a, b). Carbonaceous chondrites show only limited variation in $^{187}Os/^{188}Os$. Karoonda (CK4) and St.Severin (LL6) both have unusually low $^{187}Os/^{188}Os$ and $^{187}Re/^{188}Os$ (Fig. 3.2; Table 3.2). Mt.Tazerzait (L5) has the highest $^{187}Os/^{188}Os$ (0.13282) of all chondrites analyzed so far (Chen et al., 1998; Walker et al., 2002; Brandon et al., 2005b). A more detailed comparison with Re and Os concentration data and osmium isotopic data obtained on the same samples from this study and Walker et al. (2002) is given in the appendix (3.8.1, Figs. 3.11 and 3.12).

The unusually low Re/Os for Karoonda (CK4) was set in the early history of the meteorite, because it is supported by its low $^{187}Os/^{188}Os$ (Fig. 3.2), as already observed by Walker et al. (2002). The same reasoning applies to St.Severin (LL6), which also displays low $^{187}Os/^{188}Os$, in accordance with the results from Chen et al. (1998). In the case of Kainsaz (CO3) and EET 96026 (R3), however, low Re/Os is not accompanied by correspondingly low $^{187}Os/^{188}Os$ and therefore most likely reflects recent loss of Re, also documented by Rankenburg et al. (2007), who reported disturbed Re/Os for ureilites most likely produced by mobilization of Re during weathering.

Only about half of the chondrites analyzed in this study plot within analytical uncertainty of the IIIA isochron. Non-isochronous behaviour is not uncommon for chondrite bulk samples and components (Meisel et al., 1996; Chen et al., 1998; Becker et al., 2001a; Walker et al., 2002; Brandon et al., 2005a). Non-isochronous behaviour of chondrites is most probably caused by late stage open system disturbances of the Re/Os system as suggested above for Kainsaz and EET 96026 (Meisel et al., 1996; Chen et al., 1998; Becker et al., 2001a; Walker et al., 2002). However, while the Kainsaz and EET 96026 samples apparently lost significant amounts of Re, smaller scale non-isochronous behaviour is observed for many other chondrite samples. Because the measured Re abundances in some meteorites are obviously disturbed time-integrated Re concentrations were calculated (Re* in Tables 3.1, 3.2) based on the measured Os concentrations and Os isotopic compositions assuming the samples evolved from an initial solar system

$^{187}Os/^{188}Os$ of 0.09531 at 4.558 Ga and $\lambda = 1.666 \times 10^{-11}$ yr^{-1} (Shirey and Walker, 1998). Most of the calculated Re abundances agree within < 5 % with the measured abundances, except for particular samples with high Δ_{Os} (see Table 3.1 footer for explanation).

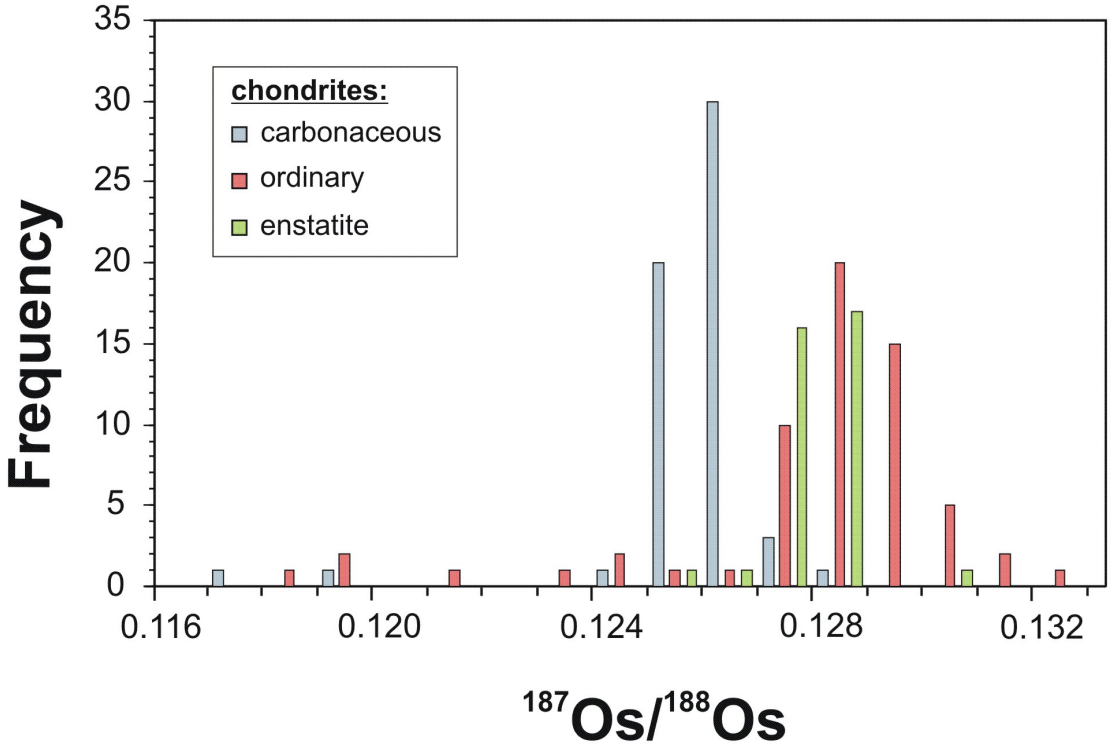

Fig. 3.3. Histogram of $^{187}Os/^{188}Os$ for carbonaceous, ordinary and enstatite chondrites. Data from this study, Chen et al. (1998), Walker et al. (2002) and Brandon et al. (2005a,b) are shown. Carbonaceous chondrites are distinct from ordinary and enstatite chondrites.

Recently, Brandon et al. (2005b) and Yokoyama et al. (2007) observed deficits of up to 0.5 ‰ in the s-process dominated isotope ^{186}Os in bulk carbonaceous chondrites and deficits of only 0.1 ‰ or less for one enstatite and one ordinary chondrite. These deficits are due to the incomplete digestion of an s-process isotope-bearing Os carrier phase (Brandon et al., 2005b; Yokoyama et al., 2007). If incomplete digestion affected our chondrite samples, deficits of similar magnitude than observed for ^{186}Os are to be expected for ^{187}Os, because ^{187}Os is an s-process only isotope. The denominator isotope ^{188}Os (which is also the denominator in the ratio ($^{192}Os/^{188}Os$) used for the correction of the instrumental mass discrimination) has a smaller s-process component (18 %). The combined effect of a 0.5 ‰ deficit for ^{187}Os and the corresponding smaller deficit for

^{188}Os translates in Δ_{Os} of about -0.5. Even if extreme nucleosynthetic anomalies from Murchison acid leachates (-1.4 to +1.3 ‰ for ^{186}Os, Reisberg et al., 2009) are assumed, corresponding Δ_{Os} values range from -1.4 to +1.2. Because Δ_{Os} reported in Table 3.2 is commonly much larger, incomplete digestion of an s-process Os carrier phase can only result in negligible non-isochronous behaviour.

One analysis of the Smithsonian Allende standard is ~8% higher in Re/Os but only slightly (0.2 %) more radiogenic in ^{187}Os/^{188}Os compared to the average Allende data. This particular sample was digested in a Carius Tube (320°C). If high Re/Os phases were preferentially digested for this Allende aliquot, one would expect ^{187}Os/^{188}Os to be more radiogenic by about 30 per mil rather than 2 per mil. The non-isochronous behaviour of the Allende aliquots either requires Re/Os fractionation in the digestion process or late Re and/or Os redistribution at the sample aliquot scale. While decoupling of Re from Os via incomplete spike-sample equilibration in the digestion process appears unlikely (Becker et al., 2001a), the latter suggestion is consistent with the mobilization of Re from Kainsaz and EET 96026 observed above and with earlier in-depth discussions provided by Becker et al. (2001a) and Walker et al. (2002) for CAI and chondrite samples.

3.4.2 Highly siderophile element abundances in CI chondrites

Element abundances in CI chondrites are widely used for normalization and comparison purposes. A crucial point is: what are the “right” CI data and which CI data should be used for normalization. Although there are a lot of data for CI abundances available in the literature, reported abundances for specific elements can easily differ up to 10 % between different data sets and compilations. In the following section we discuss our new CI values and compare them with literature data.

Averaged abundances of Rh and Au for the CI chondrites Orgueil and Ivuna calculated from replicate analysis of the present work are 130 ± 5 ppb Rh and 149 ± 37 ppb Au (Table 3.3, 1s, n=5) and agree well with literature data (Rh: 140 ± 4 ppb, Au: 148 ± 6, Jochum 1996) and compiled values (Rh: 134 ± 11 ppb, Au: 140 ± 21 ppb, Anders and Grevesse, 1989; Rh: 139 ± 14, Au: 146 ± 15, Lodders, 2009). The Au abundance in our sample split of Ivuna is almost 40 % lower compared to Orgueil. However, Au

abundances from replicate analysis of Orgueil (n=3) and Ivuna (n=2) are reproducible within < 10 %, in accordance with the reproducibility deduced from Allende replicates (7.8 %, 1s). The greater heterogeneity of Au abundances in CI chondrites (also seen in the data compilation by Tagle and Berlin, 2008) may reflect redistribution by aqueous alteration processes (e.g. Ebihara et al., 1982) and introduces additional uncertainty in normalization values.

Refractory HSE (Re, Os, Ir, Ru, Pt) and Pd concentration data for both CI chondrites Orgueil and Ivuna from this study compare well with previous isotope dilution (ID) ICP-MS data (Table 3.3, Walker et al., 2002; Horan et al., 2003). Mean abundances and ratios of HSE analyzed using ID techniques agree within a few %. The averaged ID data (Mean ID in Table 3.3) for aliquots of Orgueil and Ivuna are systematically about 10 % lower in the refractory HSE (Re, Os, Ir, Ru, Pt), while refractory HSE/Ir ratios compare well with literature data (Table 3.3, Anders and Grevesse, 1989; Jochum, 1996; Tagle and Berlin, 2008; Lodders et al., 2009). The ~10 % difference in absolute abundances displayed by the ID dilution data exceeds the precision for the concentration determinations, which is usually < 5 %. In contrast absolute abundances of the moderately volatile elements Pd and Au compare well with the above literature data, but Pd/Ir and Au/Ir ratios are about 10 % higher due to the lower refractory HSE abundances in the ID data.

We note that the samples were not dried before weighting, thus the generally lower abundances of refractory HSE observed in this study, Walker et al. (2002) and Horan et al. (2003) may in part result from the high volatile (H_2O, C, S) contents of CI chondrites (Horan et al., 2003; Palme, 2008). Because drying of CI samples may not be reproducible and drying procedures are not usually specified in the literature (Anders and Grevesse, 1989), and previous ID studies did not attempt drying, we preferred to analyze the samples without drying. However, if the lower refractory HSE abundances originate from different contents of volatiles, we would expect the same offset for Pd and Au.

Obviously Pd and Au data from this study and Pd data from Horan et al. (2003) are enriched relative to the refractory HSE. Such fractionated abundances of refractory relative to moderately volatile elements have not been observed before in NAA data. A possible explanation might be redistribution of these elements during aqueous alteration as already discussed for Au (Ebihara et al., 1982). Another reason may be inhomogeneous

sampling of HSE bearing components that differ in their proportions of refractory to moderately volatile siderophiles.

In order to obtain representative CI abundances for normalization purposes, we have adjusted abundances of the refractory HSE (Re, Os, Ir, Ru and Pt) to a mean Ir CI abundance of 462 ± 38 ng/g (1s, n=39) using the refractory HSE/Ir ratios of the combined ID data (Mean ID in Table 3.3). The value for Ir was calculated based on a large number of concentration data reported for the CI chondrites Alais, Ivuna and Orgueil (data from this study; Horan et al., 2003; Tagle and Berlin, 2008, and references therein; plus additional data from Hermann and Wichtl, 1974; Chou et al., 1976 and Friedrich et al., 2002). The value obtained is very similar to the averaged Orgueil based CI Ir abundance of 469 ± 25 ng/g (n=44) compiled by Lodders et al. (2009). A population density histogram of the Ir data used to calculate the mean CI Ir abundance is shown in the appendix (3.8.2, Fig. 3.13). In the case of Rh, so far only two measured values have been reported for Orgueil and Ivuna (Jochum, 1996). The average Rh abundance of 133 ± 7 ng/g (1s) in CI chondrites was calculated from our new data and values from Jochum (1996). The adjusted CI values are indicated as Mean CI in Table 3.3 and were used for normalization in the following. Fig. 3.14 in the appendix shows CI data from recent ID studies and the literature normalized to the adjusted Mean CI values obtained in this study. Our Mean CI abundances and the HSE/Ir ratios agree within < 5 % with another recent data compilation of Lodders et al. (2009). The new Mean CI abundances and ratios also agree within < 10 % with the data compilations of Anders and Grevesse (1989) and Tagle and Berlin (2008), except that the Re abundance given by Anders and Grevesse (1989) is too low.

3.4.3 Highly siderophile element (HSE) variation in chondrites

Osmium, Ru and Pt data for all chondrite classes are well correlated with Ir, except for R chondrites for which only few data are available. Plots of Re, Rh, Pd and Au against Ir are best correlated for ordinary and EL chondrites, while trends for carbonaceous, EH and R chondrites are less tightly defined (Fig. 3.4).

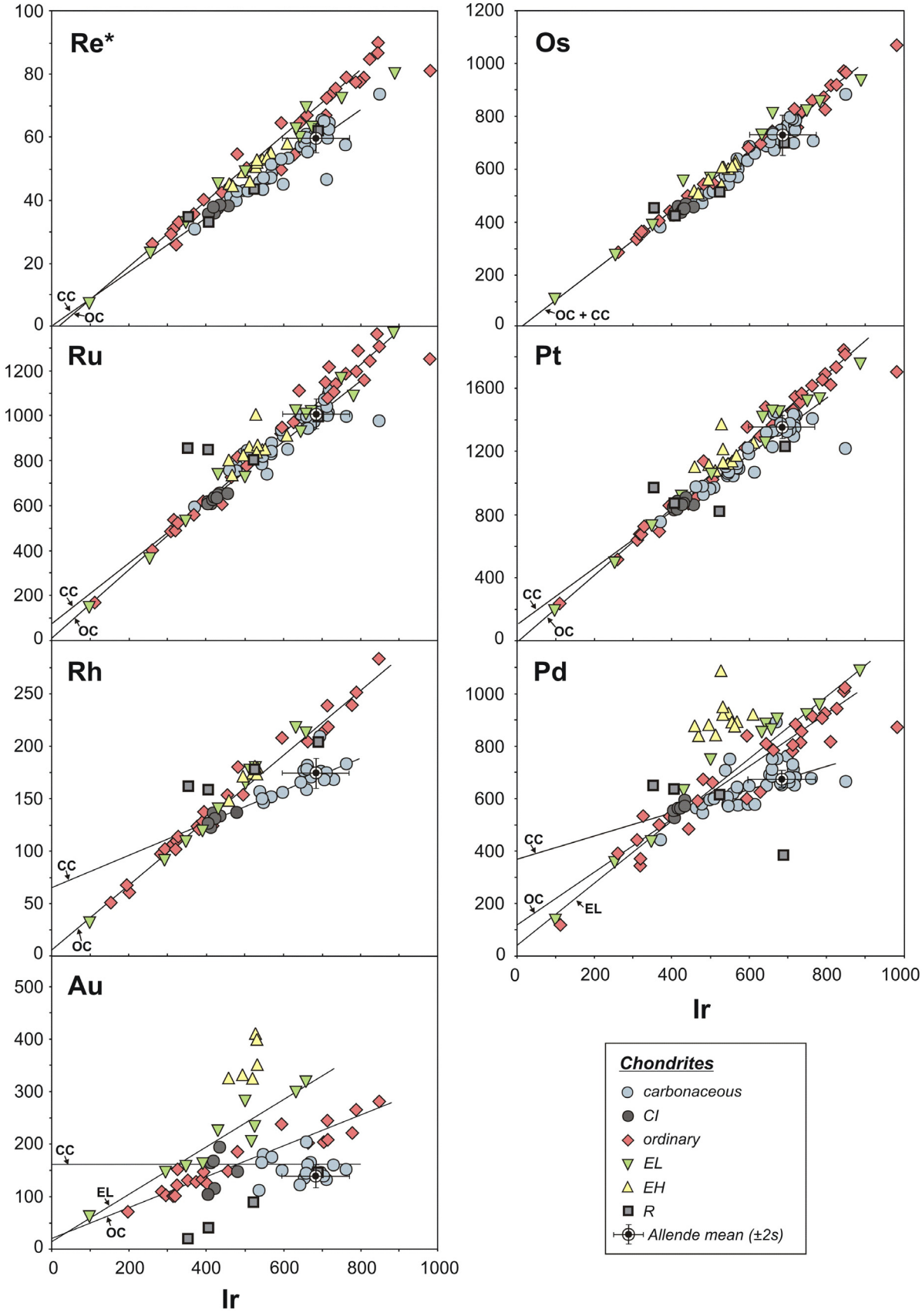
Re*
CC
OC
Os
OC + CC
Ru
CC
OC
Pt
CC
OC
Rh
CC
OC
Pd
CC
OC
EL
Au
CC
EL
OC
Ir
Ir
Chondrites
carbonaceous
CI
ordinary
EL
EH
R
Allende mean (±2s)

Fig. 3.4 (previous page). Chondrite HSE abundances plotted versus Ir (all data in ng/g). Precise ID ICP-MS data for Re*, Os, Ir, Ru, Pt, and Pd are from this study, Walker et al. (2002), Horan et al. (2003) and Brandon et al. (2005a,b). For Rh and Au data from this study, Jochum (1996), McDonald and Russell (2001), McDonald et al. (2001) and Tagle and Berlin (2008) are plotted. Regression lines are indicated for individual chondrite classes and groups: carbonaceous (CC), ordinary (OC) and enstatite chondrites (EL). For comparison we show the mean value and standard deviation for Allende (2s) obtained by repeated analysis of the Smithsonian standard powder (Table 3.1). Excellent correlations obtained for some element pairs and some chondrite classes indicate that the relatively large standard deviation for Ir abundances in Allende may reflect intrinsic small-scale heterogeneity of this element in the Allende meteorite and in the Smithsonian Allende standard powder. A distinction between the data from this study and the literature is provided in the appendix (3.8.3, Fig. 3.16). Re* = calculated time-integrated Re abundances as described in the text.

The HSE concentration data in Fig. 3.4 includes precise ID data from previous studies of Walker et al. (2002), Horan et al. (2003) and Brandon et al. (2005a,b), and additional data for Ir, Rh and Au from Jochum (1996), McDonald and Russell (2001), McDonald et al. (2001) and Tagle and Berlin (2008). Rhenium and Rh are strongly correlated in ordinary and enstatite (particularly EL) chondrites, but not in others (Fig. 3.5). Consequently ratios like Re/Ir, Re/Os and Rh/Ir also correlate well. Similar correlations for ordinary and enstatite chondrites are observed in diagrams of Os vs. Rh and Pt vs. Rh (not shown). Concentration data of Pd and Au from this study, McDonald and Russell (2001), McDonald et al. (2001) and Hertogen et al. (1983) shown in Fig. 3.6 are well correlated for ordinary and enstatite chondrite classes, while R chondrites define a different trend. In contrast Pd and Au abundances of carbonaceous chondrites show no covariation.

Linear regressions shown in Figs. 3.4 to 3.6 were calculated using the robust regression option in ISOPLOT (Ludwig, 2003). This option does not account for analytical errors of the concentration determination which are difficult to quantify precisely for these elements because of the heterogeneity of sample powders as observed from replicate analysis of Allende aliquots (Table 3.1). The slopes and intercepts of the linear regression calculations are provided in Table 3.4. The slopes of Re-Ir, Os-Ir, Ru-Ir and Pt-Ir regressions are essentially the same for ordinary and EL chondrites and regression lines pass through the origin. Ordinary chondrites have slightly lower Rh/Ir and lower Pd/Ir and Au/Ir than EL chondrites. In the case of carbonaceous chondrites the slopes of Re-Ir, Rh-Ir, Pd-Ir and Au-Ir regressions are shallower compared to ordinary and

EL chondrites and correlation lines yield positive intercepts for Rh, Pd and Au (Au in carbonaceous chondrites does not correlate with Ir). Carbonaceous chondrites also show resolvable positive intercepts for Ru-Ir and Pt-Ir regressions with somewhat shallower slopes compared to ordinary and EL chondrites.

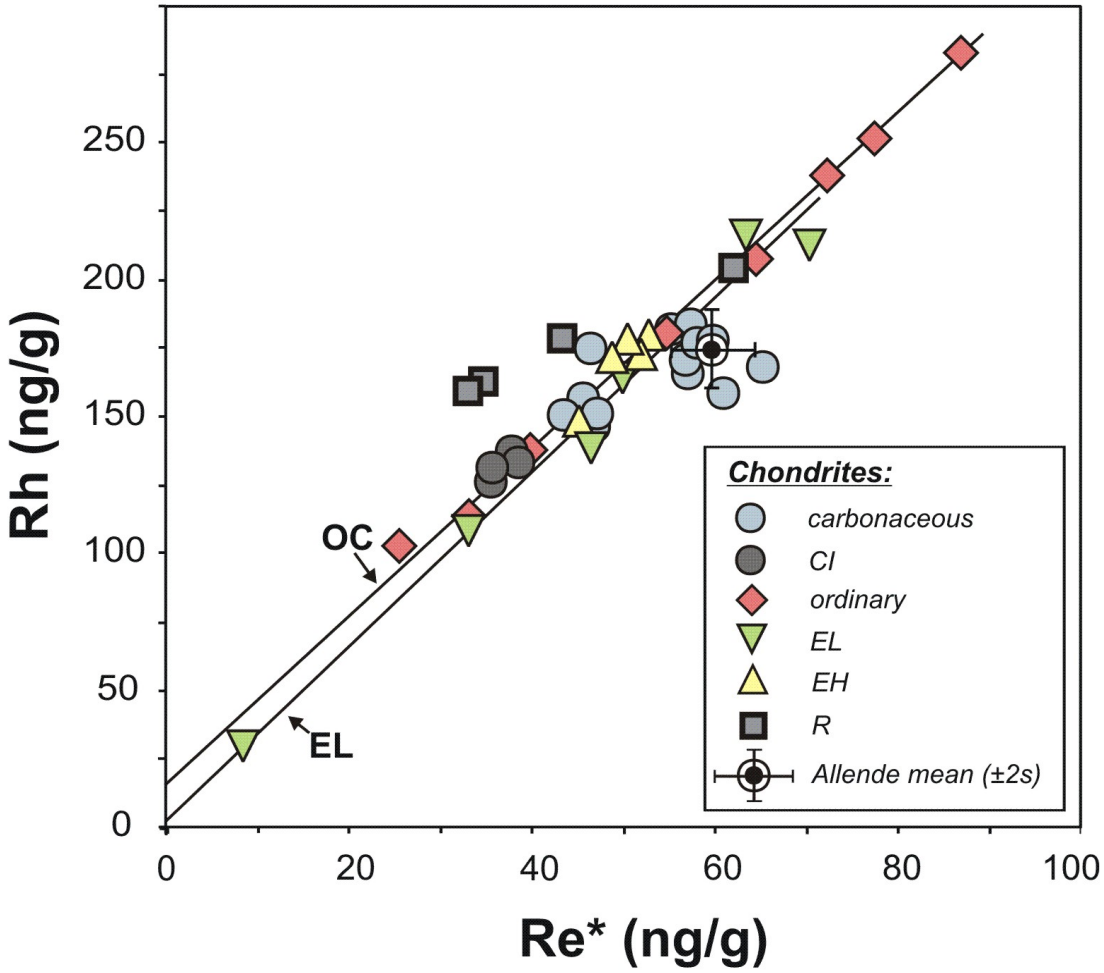

Fig. 3.5. Concentration data for Re* and Rh correlate well for different chondrite classes, in spite of the large difference in condensation temperatures. Subtle differences exist for different chondrite classes. The regression line for ordinary chondrite data (OC) may reflect binary mixing of a CI like component (matrix?) with variable amounts of a high Rh/Re-component with high HSE abundances (large metal grains or chondrules?) and some dilution with silicate material. EL chondrites define a parallel trend at lower Rh/Re, while Rumuruti chondrites plot towards higher Rh/Re ratios. The EL correlation line (EL) passes through the origin and thus can be interpreted as reflecting variable dilution of a single HSE bearing component. Carbonaceous and EH chondrites display more scatter. Re* = calculated time-integrated Re abundances as described in the text.

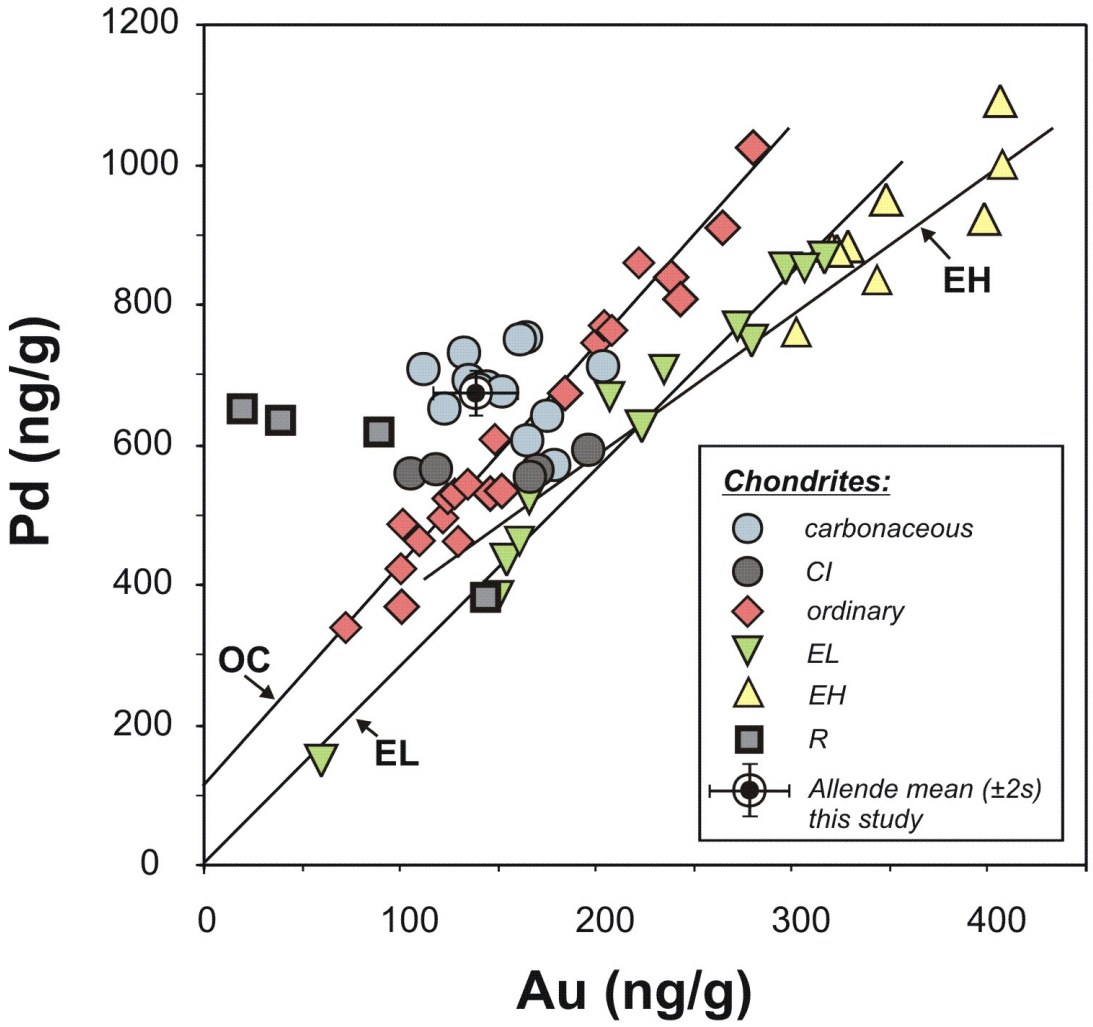

Fig. 3.6. Concentration data for Pd and Au with regression lines for ordinary (OC) and enstatite (EL, EH) chondrites. Data from this study, Hertogen et al. (1983), McDonald and Russell (2001) and McDonald et al. (2001) are in good agreement and are shown using the same symbols. A distinction between the data is provided in the appendix (3.8.3, Fig. 3.17). Ordinary and EL chondrite data are well correlated. Most carbonaceous and R chondrites plot to the left of the ordinary chondrite correlation. Enstatite chondrites are enriched in Au and plot to the right of the ordinary chondrite trend. The EL data appears to reflect dilution of a single HSE component. The regression line for EH chondrites passes near CI chondrite values, but not through the origin, and may indicate binary mixing of a Pd-Au enriched component with a CI like (matrix?) component. The ordinary chondrite data hint at the presence of two components, because the regression line does not pass through the origin.

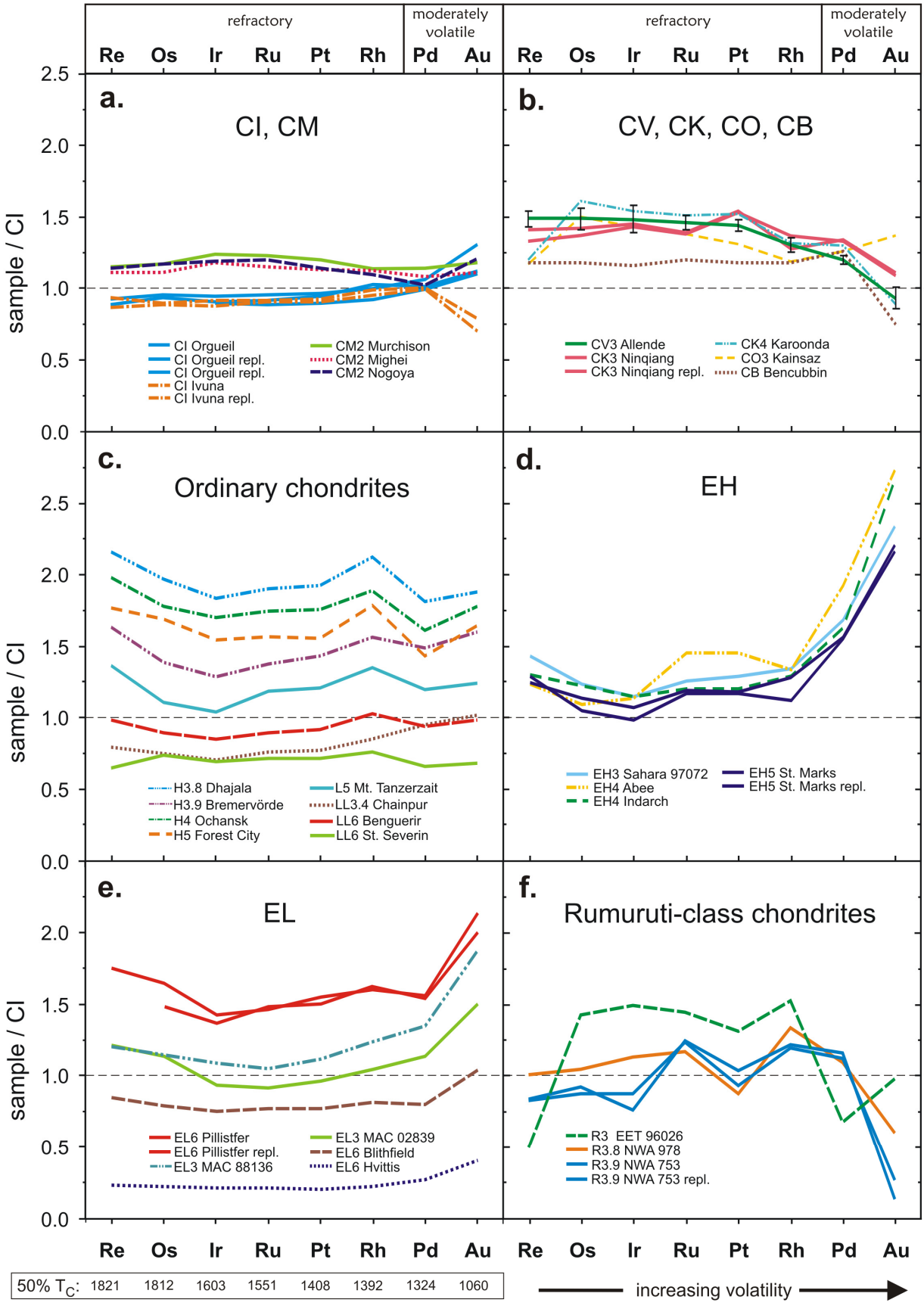
refractory
moderately volatile
Re Os Ir Ru Pt Rh Pd Au
a.
CI, CM
CI Orgueil
CI Orgueil repl.
CI Orgueil repl.
CI Ivuna
CI Ivuna repl.
CM2 Murchison
CM2 Mighei
CM2 Nogoya
b.
CV, CK, CO, CB
CV3 Allende
CK3 Ninqiang
CK3 Ninqiang repl.
CK4 Karoonda
CO3 Kainsaz
CB Bencubbin
c.
Ordinary chondrites
H3.8 Dhajala
H3.9 Bremervörde
H4 Ochansk
H5 Forest City
L5 Mt. Tanzerzait
LL3.4 Chainpur
LL6 Benguerir
LL6 St. Severin
d.
EH
EH3 Sahara 97072
EH4 Abee
EH4 Indarch
EH5 St. Marks
EH5 St. Marks repl.
e.
EL
EL6 Pillistfer
EL6 Pillistfer repl.
EL3 MAC 88136
EL3 MAC 02839
EL6 Blithfield
EL6 Hvittis
f.
Rumuruti-class chondrites
R3 EET 96026
R3.8 NWA 978
R3.9 NWA 753
R3.9 NWA 753 repl.
sample / CI
0.0
0.5
1.0
1.5
2.0
2.5
50% T_C: 1821 1812 1603 1551 1408 1392 1324 1060
increasing volatility

Fig. 3.7 (previous page). Highly siderophile element abundances for bulk chondrites analyzed in this study normalized to mean CI chondrite values (Table 3.3), (a, b) carbonaceous chondrites, (c) ordinary chondrites, (d, e) enstatite chondrites, and (f) Rumuruti chondrites. Elements listed in the order of decreasing 50% condensation temperature (50% T_C) in a gas of solar composition (Lodders, 2003). Uncertainties (1s) shown for Allende derived from repeated analysis of the Smithsonian standard powder (Table 3.1). repl. = replicate analysis from the same sample powder.

In Figures 3.7a-f the chondrite HSE data from this study were normalized to mean concentrations in CI chondrites calculated from the present study in combination with data from Walker et al. (2002), Horan et al. (2003) and other literature data (Mean CI in Table 3.3). The CM2 chondrite group has 20-25 % higher refractory HSE concentrations than CI chondrites, but the more volatile elements Rh, Pd and Au tend to be depleted in CM chondrites compared to the refractory HSE. CV3, CO3 and CK3 & 4 chondrites are even more enriched in refractory HSE than the CM2 group, about 50% higher than CI abundances (Fig. 3.7b). Carbonaceous chondrites other than CI show CI-like or lower Re/Ir and nearly flat or weakly decreasing normalized HSE abundances from Ir to Pt. Compared to the refractory HSE like Ir, the more volatile HSE Rh, Pd and Au are depleted in carbonaceous chondrite groups other than CI and consequently ratios of Rh/Ir, Pd/Ir and Au/Ir are significantly lower than in enstatite and ordinary chondrites.

Gold, the most volatile HSE, is commonly more depleted in CV and CK carbonaceous chondrites than Pd but slightly enriched relative to Pd in Nogoya (CM2) and Kainsaz (CO3). The metal-rich CB chondrite Bencubbin shows an unfractionated CI-like abundance pattern from Re to Rh, while Pd and Au are slightly enriched relative to the refractory HSE (Fig. 3.7b). The low HSE abundance obtained for Bencubbin indicates that we have sampled a silicate-rich portion of the meteorite, because the data are comparable to data obtained for silicate portions by Kallemeyn et al. (1978). Campbell et al. (2002) observed similar CI-normalized abundance patterns for metal grains from Bencubbin, where the refractory HSE are unfractionated relative to CI while Pd and Au are fractionated. Karoonda is slightly enriched in Os relative to Ir consistent with data from Walker et al. (2002) and Horan et al. (2003).

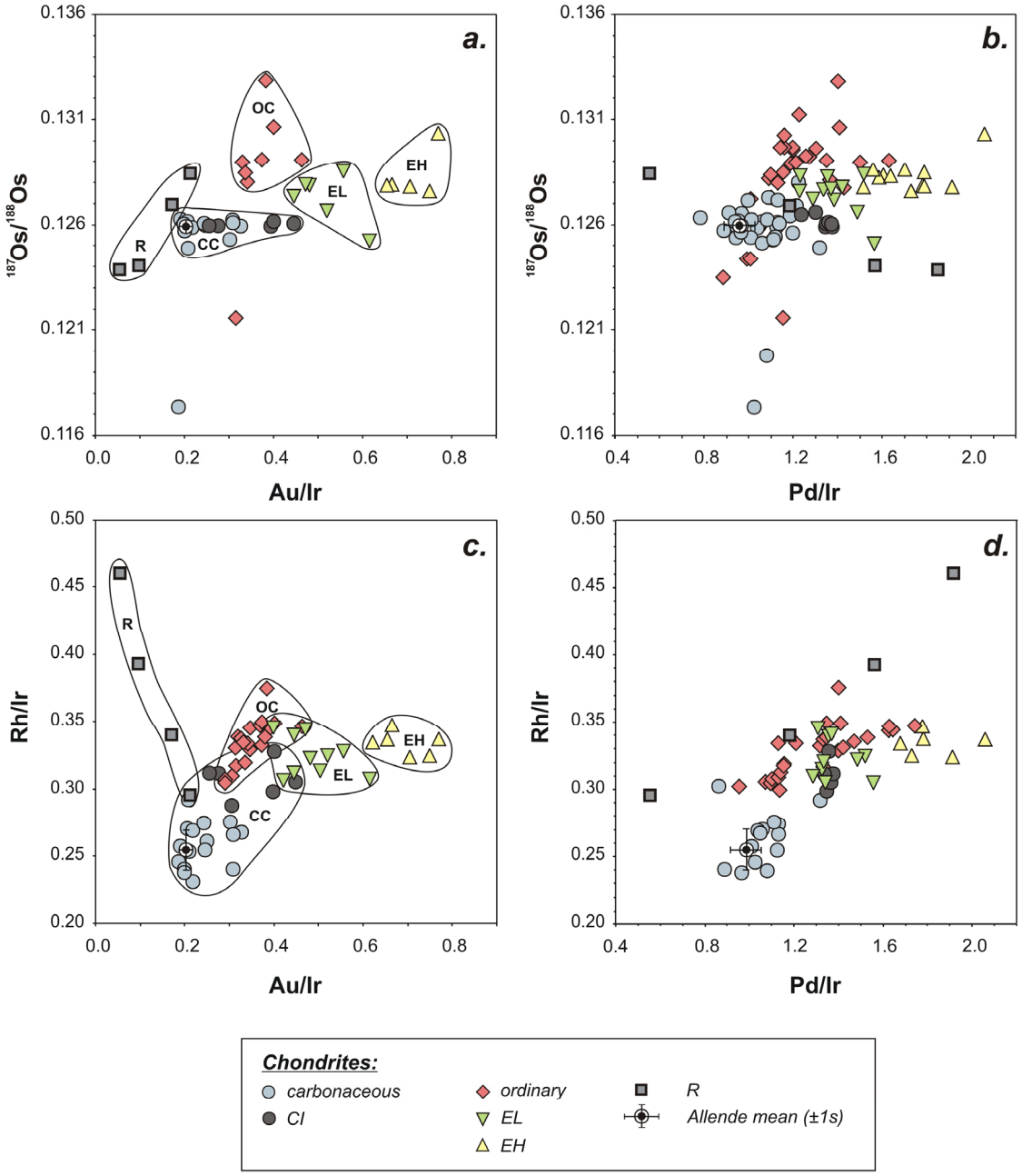

Fig. 3.8. $^{187}Os/^{188}Os$ (as a proxy for Re/Os), Rh/Ir, Pd/Ir and Au/Ir for carbonaceous (CC), ordinary (OC), enstatite (EL, EH) and Rumuruti-class (R) chondrites from this study in combination with additional $^{187}Os/^{188}Os$ and Pd/Ir data from Walker et al. (2002), Horan et al. (2003) and Brandon et al. (2005a,b), and Rh/Ir, Pd/Ir and Au/Ir data from Jochum (1996), McDonald and Russell (2001), McDonald et al. (2001) and Tagle and Berlin (2008). In a. and c. different chondrite classes are best resolved from each other based on diagnostic HSE ratios. Carbonaceous chondrites have a small range in $^{187}Os/^{188}Os$ and differ significantly from ordinary, enstatite and R chondrites which are more variable in $^{187}Os/^{188}Os$ (a, b). Carbonaceous chondrites are characterized by lower Rh/Ir, Pd/Ir and Au/Ir compared to ordinary and enstatite chondrites (c, d). Rh/Ir is similar for ordinary and enstatite chondrites. EH group chondrites show the highest Pd/Ir and Au/Ir observed, R chondrites have the lowest Au/Ir.

Ordinary chondrites show complex, but uniform CI-normalized HSE abundance patterns with more variation in absolute HSE abundances compared to the carbonaceous chondrites (Fig. 3.7c). As in previous studies, Re is slightly enriched compared to Os and Ir, and slightly increasing normalized abundances from Ir to Rh are noted. The more volatile HSE Pd and Au are somewhat variable and Au/Pd ratios are slightly higher compared to CI. Absolute HSE abundances decrease with metal abundances from H > L > LL in accordance with previous studies. We find no correlation of HSE abundances with petrological type, thus absolute concentrations of HSE are not controlled by thermal metamorphism in the parent bodies. The ordinary chondrites analyzed here include only weakly shocked specimens from shock stage S1 to S3 according to Stöffler et al. (1991). We did not note any peculiarities regarding HSE abundances and shock stage of ordinary chondrites. A more detailed discussion of shock effects is given in Horan et al. (2003).

The CI-normalized HSE patterns of enstatite chondrites bear striking similarities to ordinary chondrites, except for Pd and Au, which are strongly enriched in EH chondrites, but less enriched in EL chondrites compared to ordinary chondrites (Figs. 3.7d, e and Horan et al., 2003, and references therein). Aliquots of Blithfield (EL6) and especially Hvittis (EL6) were strongly depleted in all HSEs (~0.25 x CI). Refractory HSE are similarly well correlated in enstatite and ordinary chondrites, while Pd and Au behave different from refractory HSE (Figs. 3.4, 3.6). No systematic differences in abundance variations between different petrologic types of enstatite chondrites were found.

The Rumuruti chondrites NWA 978 (R3.8) and NWA 753 (R3.9) show unique fractionated HSE abundances patterns, where Au is strongly depleted, while Pd and Pt are depleted to a lesser extent (Fig. 3.7f). Both have CI-like Re/Os. NWA 753 differs in its lower abundances of Re, Os, and Ir compared to NWA 978. EET 96026 (R3) shows a similar pattern, except for its low measured Re abundance, which is inconsistent with the time-integrated Re abundance, indicating recent Re loss. This aliquot is also markedly depleted in Pd. Rumuruti chondrites have the lowest Au/Ir ratios of all analysed chondrite classes. Highly fractionated HSE patterns and strong depletions in Au have been reported before, but some R chondrite samples (e.g. Rumuruti) do not show Au depletion relative to CI (Kallemeyn et al., 1996).

The new Os isotope, HSE and especially Rh and Au data underscores the diversity of chondrite HSE systematics. The Au/Ir ratio can be used as a diagnostic tool because of the

large differences in enstatite and R chondrites compared to other classes (Figs. 3.8a,c). Rhodium also helps to distinguish chondrite classes (Figs. 3.8c,d). Carbonaceous chondrite groups other than CI display lower Rh/Ir ratios compared to ordinary and enstatite chondrites, which show similar Rh/Ir ratios. One Rumuruti chondrite (NWA 753) displays the highest Rh/Ir in this study (Fig. 3.8c). Resolvable differences also exist in Pd/Ir, Re/Os and $^{187}Os/^{188}Os$ as reported before (Figs. 3.8b,d, Walker et al., 2002; Horan et al., 2003; Brandon et al., 2005a,b).

3.5 Discussion

3.5.1 Carbonaceous chondrites

Most carbonaceous chondrite groups contain high temperature components (chondrules, calcium aluminium rich inclusions (CAIs) and metal grains), with increasing contents from CI chondrites (essentially free of such components) to CK, CM, CV and CO chondrites (Brearley and Jones, 1998). Coupled enrichments of both siderophile and lithophile refractory elements in CM, CV, CO and CK groups suggest that these elements are contained within the high temperature components (e.g. Wasson and Kallemeyn, 1988; Palme et al. 1988). The fractionated CI chondrite normalized HSE abundance patterns of carbonaceous chondrites (Figs. 7a, b, Horan et al., 2003) must relate to these high temperature components, but exactly how has been obscure. Gradually decreasing abundances from Rh to Au in carbonaceous chondrites other than CI are most likely related to their volatility, and mirror HSE abundance patterns of bulk CAIs and refractory metal nuggets (fremdlinge) included in CAIs from carbonaceous chondrites, however, chondrules must also contribute to the HSE budget of carbonaceous chondrites (Palme and Wlotzka, 1976; Mason and Taylor, 1982; Bischoff and Palme, 1987; Sylvester et al., 1990; Eisenhour and Buseck, 1992; Palme et al., 1994; Becker et al., 2001a; Walker et al., 2002; Campbell et al., 2003, Palme, 2008). A popular model has been that the increasing

depletion of moderately volatile elements might be related to incomplete condensation of the refractory component in carbonaceous chondrites (Palme et al., 1988).

Here, we discuss a variation of the incomplete condensation model that involves binary mixing of two components with different nebular histories. This interpretation is based on the observation that trends of carbonaceous chondrite data for Rh and Pd vs. Ir pass through CI values and yield positive intercepts (Fig. 3.4). These data are consistent with binary mixing of a CI-like component with a component depleted in Rh and Pd relative to the refractory HSE and CI.

In the Au vs. Ir diagram (Fig. 3.4) carbonaceous chondrites plot horizontally, with an intercept at about 160 ng/g Au, which is approximately the CI abundance. Compiled abundance data for carbonaceous chondrites from Tagle and Berlin (2008) also indicate that Au is essentially invariant in carbonaceous chondrites. The broadly CI-like abundance of Au in carbonaceous chondrites also suggests that the component which caused the enrichment of refractory HSE relative to CI was strongly depleted in Au and did not significantly contribute to the Au budget of carbonaceous chondrites. Analysis of bulk CAIs from carbonaceous chondrites show that Au is strongly depleted relative to the refractory HSE (e.g. Grossman and Ganapathy, 1976; Sylvester et al., 1993). Kong and Palme (1999) analyzed Au in Renazzo (CR2) components. In that study Au abundances in matrix (141 ppb), chondrules (124 ppb), chondrule rims (172 ppb) and the bulk meteorite (174 ppb) are in the range of the CI abundances measured in this study (103-194 ppb, Table 3.3) and compiled data by Tagle and Berlin (2008). Thus, CI-normalized HSE abundance patterns of carbonaceous chondrite groups are consistent with mixing of matrix with CI-like composition with a CAI-like refractory component rich in refractory siderophiles and depleted in the more volatile siderophiles Rh, Pd and Au. Mixing of two or more components that have been processed under different nebular conditions has been invoked by several other studies (e.g. Wolf et al., 1980; Humayun and Cassen, 2000; Horan et al., 2003, Brandon et al., 2005b). Further analyses of HSE in carbonaceous chondrite components such as CAIs and chondrules are required to elucidate the relative contribution of these components to the budget of bulk chondrites.

The lack of any covariation between Pd and Au in carbonaceous chondrites is in stark contrast to the well correlated behaviour of these elements in other chondrite classes (Fig. 3.6). We interpret this decoupling of Pd and Au, and the heterogeneity of Au abundances

in aliquots of some meteorites (e.g. Ivuna) as a likely result of small-scale partial redistribution of Au in carbonaceous chondrites due to aqueous alteration (Ebihara et al., 1982). Secondary processes at lower temperatures and under more oxidizing conditions might have caused low Re/Os observed for Karoonda (CK4) (Figs. 3.2 and 3.7b, Walker et al., 2002). The CK chondrites are highly oxidized and contain only rare FeNi-metal. Most of the metal has been oxidized and resulted in the formation of secondary phases like magnetite, FeO-rich silicates and HSE-rich sulfides, tellurides and arsenides (Geiger and Bischoff, 1989, 1995; Kallemeyn et al., 1991; Rubin, 1993; Choi and Wasson, 2003). Low Re/Os ratios may have been acquired during aqueous alteration or metamorphism on the parent body where Re might be more mobile than other refractory HSE (Palme et al., 1998).

3.5.2 Ordinary chondrites

The new HSE data confirms previous observations (e.g. Kallemeyn et al., 1989) that no systematic compositional differences among different petrologic types exist for refractory and moderately volatile elements in bulk rocks, consistent with isochemical thermal metamorphism. This is evident in Fig. 3.7c, where the H4 and H5 chondrites plot between two unequilibrated samples, and the unequilibrated LL chondrite plots between two LL6 chondrites. Even the moderately volatile siderophiles Pd and Au are well correlated with each other (Fig. 3.6), effectively ruling out large-scale redistribution of these elements during metamorphism. Kong and Ebihara (1997) described similar HSE abundance patterns for metal phases from unequilibrated and equilibrated ordinary chondrites, in accordance with our data (Fig. 3.7c). These data and the good correlations displayed by all HSE (Figs. 3.4 to 3.6) clearly indicate that HSE fractionation took place before accretion of the ordinary chondrite parent bodies, and not during or after accretion as suggested by some workers (Kong and Ebihara, 1996, 1997; Chen et al., 1998).

Uniform relative HSE abundances of ordinary chondrites reflect the close genetic relationship of the H, L and LL groups. Obviously the processes which led to more or less abundant metal in ordinary chondrites did not significantly fractionate the HSE from each other, i.e. relative HSE abundances in bulk rocks are not related to the degree of

oxidation, but absolute abundances are. If, as often argued, oxidation state and abundance of Fe and other siderophile elements in ordinary chondrites reflect nebular processes, the uniform HSE pattern of ordinary chondrites must have been established even before the components of ordinary chondrites were formed.

The linear correlation lines for ordinary chondrites shown in Figs. 3.4 to 3.6 indicate that HSE abundances are mainly controlled by mixing and/or dilution of components. Only correlations for Os, Ru, Pt and Rh vs. Ir pass through CI chondrite values and through the origin, indicating that these elements are contained in a component with CI like composition. Correlations of Au, Pd and Re with Ir, pass through or near CI chondrite values, but not through the origin. This may reflect binary mixing of a CI-like or Pd-Au enriched component with a Pd-Au depleted component rich in refractory siderophiles. The Pd-Au enriched component may be contained in coarse metal (Widom et al., 1986; Horan et al., 2009). Previous studies on metal phases of ordinary chondrites indicate that the major fraction of HSE is contained in chondrite metals (Rambaldi, 1977a,b; Kong and Ebihara, 1996, 1997; Campbell and Humayun, 2003). Recent HSE data on metal and non-magnetic fractions for Dhajala and Ochansk (Horan et al., 2009) also indicate mixing of distinct HSE carrier phases within ordinary chondrites. The metal phase contains about 80 % of the HSE and is characterized by unfractionated abundances relative to the bulk chondrite. Non-magnetic fractions have lower absolute abundances and are markedly depleted in Pd and slightly depleted in Re, Ru, Pt (Ochansk) and Re, Pt (Dhajala) relative to the bulk chondrite.

3.5.3 Enstatite chondrites

EH chondrites are strongly enriched in Pd and Au, while EL chondrites are only enriched in Au relative to the refractory HSE (Figs. 3.7d,e, Baedecker and Wasson, 1975; Hertogen et al., 1983, Kallemeyn and Wasson, 1986; Horan et al., 2003). This feature and the somewhat different overall HSE patterns of EH and EL chondrites contrasts with the observation for ordinary chondrites, where H, L and LL groups display very similar HSE patterns. The good correlations of Pd, Au and other elements with Ir for EL chondrites pass through the origin, indicating that the HSE occur in a single component diluted by

HSE free material. Extensions of trends defined by EH chondrites seem to pass near CI chondrite values, but not through the origin (Figs. 3.4, 3.6). These trends can be interpreted as reflecting binary mixing of a component with high Pd/Ir and Au/Ir located in coarse metal (Sears et al., 1983) and chondrules, with minor fractions of a CI-like component (matrix?). The restricted spread in HSE abundances of EH chondrites, however, limits the significance of the observed trends. If condensation or evaporation and phase separation played a role in the history of enstatite chondrites, a later homogenization event must have set the rather constant Pd/Au ratio of the Pd-Au rich component in EL chondrites, and maybe EH chondrites (Fig. 3.6). As with ordinary chondrites, it is difficult to envision that metamorphism or metasomatism on the parent body could have produced well-correlated data arrays such as the one for EL chondrites in Fig. 3.6. Therefore, the homogeneous Pd/Au in EL chondrites must have been established before accretion of the components of enstatite chondrites.

Low abundances of refractory elements relative to Fe, Ni and Si and the moderately volatiles Pd and Au have been interpreted that enstatite chondrites might have lost a refractory (CAI-like?) component (Larimer and Anders, 1970; Baedecker and Wasson, 1975). It should be noted, however, that abundances of refractory HSE in EH and most EL chondrites are not depleted relative to CI. Indeed it is most likely that the depletion of refractory elements occurred prior to the formation of enstatite chondrite components. Tagle and Berlin (2008) discuss a complementary compositional relationship between CV-CK carbonaceous and EH enstatite chondrite groups, deduced from their CI-normalized siderophile element abundance patterns. The new data does not add any further insight on whether this complementarity might be accidental or not.

Very similar correlations and slopes of refractory HSE in enstatite and ordinary chondrites and comparable, subtle fractionations in Re/Os, Os/Ir and Rh/Ir (Figs. 3.4 and 3.7) and lithophile refractories (e.g. Y and Ho, Pack et al., 2007) suggest a similar history of the components that host the main fraction of the refractory elements in these chondrite classes. Possible explanations for the subtle fractionations of the refractory siderophiles will be discussed below.

3.5.4 Rumuruti-class chondrites

R chondrites are highly oxidized as indicated by their high Fe content in olivine, abundant troilite and very low abundance of Fe-Ni metal (Bischoff et al., 1994; Schulze et al., 1994; Kallemeyn et al., 1996). Even though their major and trace element composition is similar to ordinary chondrites, R chondrites are distinct by having higher $\delta^{17}O$ compared to ordinary chondrites (Bischoff et al., 1994; Schulze et al., 1994; Kallemeyn et al., 1996). Weisberg et al. (1991) suggested the formation of R chondrites by oxidation of ordinary chondrite-like precursor material. Other studies suggest an independent nebular origin of R chondrites in an environment similar to ordinary chondrites (e.g. Schulze et al., 1994).

Abundances and ratios of HSE from R chondrites are distinct from other major chondrite classes (Figs. 3.7f, 3.8) and support their distinction as a separate class. The R chondrite samples analyzed in the present study are strongly depleted in Au (0.1-0.6 × CI). Kallemeyn et al. (1996) analysed a more comprehensive set of R chondrites including Rumuruti (R3.8) which is a fall. They also found a large range in Au concentration (0.2-1.0 × CI), while the Rumuruti sample shows no Au depletion relative to CI. Since all R chondrite samples analyzed in the present study are desert finds, the depletion of Au might be caused by terrestrial weathering as suggested by Rubin and Kallemeyn (1994). Alternatively heterogenous distribution of Au bearing phases has been discussed (Kallemeyn et al., 1996), as indicated by the occurrence of rare grains rich in Au in some R chondrites (Bischoff et al., 1994; Schulze et al., 1994). However, the mobilization of Au during terrestrial weathering seems to be unlikely since NWA 753 is one of the freshest R chondrite specimens (Bischoff et al., 2001). Furthermore, Re/Os ratios of NWA 753 and NWA 978 are not fractionated relative to CI (Fig. 3.7f) and both samples plot close to the Os reference isochron in Fig. 3.2. Significant terrestrial weathering would almost certainly have caused fractionation of Re from Os, and offers the best explanation for the low Re/Os of EET 96026 and its unsupported, but chondritic $^{187}Os/^{188}Os$.

The cause for the fractionated HSE patterns of R chondrites is not well understood. Simple evaporation or condensation processes of solar or CI-like material or gas are inconsistent with the observation that volatile siderophile and chalcophile elements (Au, As, Ga, Sb, Se, Zn) are depleted relative to lithophile elements (Mn, Na, K) with similar

condensation temperatures (Kallemeyn et al., 1996). The depletion of chalcophile elements and the variability in Pt, Pd and Au abundances may have been caused by the extraction of sulphide melt due to impact induced melting (Kallemeyn et al., 1996), a model that will be discussed further below.

In summary, HSE abundances in chondrites likely record mixing and dilution of two, in the case of EL chondrites perhaps only one, HSE bearing components with a different nebular history (Figs. 3.4, 3.5, 3.6, 3.7). Thus, with the exception of Au in some carbonaceous chondrites, chemical gradients that might result from chemical or physical fractionation processes on the parent bodies such as evaporation or melting do not seem to control the HSE abundance systematics in whole rocks of chondrites. HSE abundance variations in carbonaceous chondrites are consistent with mixing of a minimum of two components – one that has unfractionated HSE abundances relative to CI and another one enriched in refractory HSE (Re, Os, Ir, Ru, Pt) and variably depleted in the more volatile HSE (Rh, Pd, Au). In the case of ordinary chondrites, linearly correlated HSE abundances (Figs. 3.4, 3.6) indicate a binary mixture of a minor, CI like or slightly Pd-Au enriched component, and a major component enriched in refractory HSE and depleted in Pd and Au. In enstatite chondrites the situation is reverse: the predominating component is enriched in Pd and Au and depleted in refractory HSE, the minor component shows similarities with CI compositions.

The mixing relationships of carrier phases with distinct HSE compositions outlined for carbonaceous, ordinary and enstatite chondrites, and constant HSE ratios for some chondrite groups, suggests, that differences in HSE compositions and $^{187}Os/^{188}Os$ between chondrite classes most likely result from early phase separation of HSE carrier phases before the accretion of chondrite parent bodies. In cases where binary mixing of unrelated phases may have occurred, such as in carbonaceous, EH and ordinary chondrites (Figs. 3.4 – 3.6 this work, Horan et al., 2009), careful interpretation of internal chondrite isochrons involving siderophile elements is required (e.g. ^{182}Hf-^{182}W, ^{107}Pd-^{107}Ag).

3.6 HSE fractionation processes in chondrite precursor materials

Processes, which may have been involved in the generation of the HSE abundance patterns in chondrites, must account for 1. the systematic differences of Re/Os and Rh/Ir in ordinary and enstatite chondrites relative to carbonaceous chondrites; 2. decreasing HSE abundances from Re to Ir and increasing abundances from Ir to Rh in ordinary and enstatite chondrites relative to CI chondrites; 3. variable depletions and enrichments of the more volatile HSE Pd and Au among different chondrite classes, and 4. the systematics and quality of linear correlations observed for HSE abundances (Figs. 3.4 to 3.6). Under reducing conditions and at high temperatures, fractionations among the HSE may be produced by a range of processes: 1. volatility controlled processes such as partial condensation or evaporation; 2. HSE partitioning during magmatic processes, possibly involving different phases such as liquid metal, solid metal, sulfides, silicate and oxides.

3.6.1 Volatility controlled processes and mixing of condensates or evaporation residues

The depletion of volatile elements in solar gas is mainly a function of condensation temperature of the elements and also depends on the local dust to gas ratio in the nebula. High dust to gas ratios can lead to locally more oxidizing conditions (Wasson and Kallemeyn, 1988). Calculated equilibrium condensation curves for siderophile elements from a gas of solar composition show that the refractory HSE are nearly completely condensed before the condensation of Pd (Fegley and Palme, 1985; Sylvester et al., 1990; Campbell et al., 2003). Only small fractions of Pt and Rh condense simultaneously with Pd and Au, which both condense into solid solution with FeNi metal. Most of these condensation calculations for siderophile elements assume ideal solid solution in the condensate. Thus partial condensation or evaporation would most likely result in HSE patterns like the ones observed typically at the carbonaceous chondrite groups other than CI, with increasing depletion of the more volatile HSE from Pt to Au (Palme et al., 1988;

Wasson and Kallemeyn, 1988; Humayun and Cassen, 2000). However, the mixing relations outlined for carbonaceous chondrites require the presence of at least two HSE bearing components with different HSE composition. Recently, Hammond et al. (2008) reported HSE concentration data for metals from the CR chondrite Renazzo. Some of the metals analyzed in that study were strongly enriched in refractory HSE relative to CI, others had CI-like refractory element abundances and were enriched in the moderately volatiles Ni, Pd and Au. These differences in HSE compositions of individual metal grains from a single meteorite strongly support the notion that bulk rock HSE data of chondrites reflect mixing of different condensation derived phases (e.g. Palme and Wlotzka, 1976; Blander et al., 1980; Eisenhour and Buseck, 1992). Recent data of Horan et al. (2009) on ordinary chondrite components show that non-magnetic fractions of ordinary chondrites contain highly refractory HSE carrier phases, depleted in Pd and characterized by low Re/Os. Horan et al. suggest that lower $^{187}Os/^{188}Os$ in carbonaceous chondrites may be explained by the presence of a higher portion of components similar to those found in the non-magnetic fractions of ordinary chondrites. Such refractory components may have been early condensates. In another recent study Berg et al. (2009) show that abundances of Os, W, Mo and Ru in refractory metal alloys recovered from the Murchison (CM2) meteorite hold direct evidence for their formation by nebular condensation processes.

It is obvious that the complex fractionated HSE abundance patterns of ordinary and enstatite chondrites cannot be explained by single phase condensation processes. These chondrites require a model which enables the formation of alloys with fractionated HSE abundances that differ in their HSE composition. Possible mechanisms to cause fractionated Re/Os of ordinary and enstatite chondrites relative to carbonaceous chondrites have been discussed in the literature (Morgan et al., 1985; Chen et al., 1998; Sylvester et al., 1990; Becker et al., 2001a; Walker et al., 2002; Horan et al., 2003). A multi phase condensation model was employed by Sylvester et al. (1990) to explain fractionated HSE ratios (Re/Os and Ir/Pt) of refractory metal nuggets from an Allende inclusion. This model assumes ideal solid solutions only between metals with the same high temperature crystal structure and requires the continuous removal of early condensed alloys in a very specific temperature interval combined with subsequent mixing of later formed alloys. Mixing of such alloys in varying proportions might account for the

fractionated HSE compositions of ordinary and enstatite chondrites relative to carbonaceous chondrites.

Recently, subtle fractionations have also been reported for refractory lithophile elements. Pack et al. (2007) observed systematically higher Y/Ho ratios in ordinary and enstatite chondrites compared to carbonaceous ones. Because Y is slightly more refractory under solar nebular conditions, they suggest that this fractionation was the result of fractional condensation combined with the addition or loss of a refractory component in the formation region of ordinary and enstatite chondrites. Pack et al. (2007) discuss the effect in the light of the addition of an ultrarefractory CAI-like component with high Y/Ho or alternatively by loss of CAIs with Group II REE patterns, which have low Y/Ho ratios compared to other CAIs. Group II CAIs analysed by Becker et al. (2001a) show mostly elevated Re/Os and more radiogenic $^{187}Os/^{188}Os$ compared to other groups of CAIs. While the removal of such a component may explain elevated Y/Ho, it fails to explain the higher Re/Os in ordinary and enstatite chondrites compared to carbonaceous chondrites.

3.6.2 Magmatic differentiation processes

Early formed differentiated bodies could have been disrupted during collisions, and differentiated material from such bodies might have contributed material to chondrules or matrix before their accretion into chondrites (Chen et al., 1998; Libourel et al., 2006; Libourel and Krot, 2007). Phases formed by very early metal-silicate, liquid metal-solid metal or liquid sulphide-solid sulphide segregation may reveal hints of associated element partitioning if preferentially incorporated into chondrites and if present in significant amounts. In the following we discuss the possible effects of different partitioning processes and their relevance for the complex fractionated HSE abundance patterns observed particularly for ordinary, enstatite and R chondrites.

3.6.2.1 Metal - silicate partitioning

Metal-silicate partitioning has played a major role during metal segregation and core formation on planets and smaller planetesimals. The process of chondrule formation also might lead to metal-silicate equilibration on a smaller scale. Experimentally determined

partition coefficients show that at low pressures HSE preferentially partition into the metal phase compared to silicates (metal-silicate partition coefficients $D^{met/sil}$ are > 10^4, e.g. O´Neill et al., 1995; Holzheid et al., 2000; Walter et al., 2000; Ertel et al., 2008). Although there are differences in the partitioning of some HSE at low and high pressure conditions (Jones and Walker, 1991; Righter et al., 1997; Li and Agee, 2001; Mann et al., 2007; Van Orman et al., 2008), during low pressure metal-silicate equilibration the HSE will be quantitatively stripped off the silicate portion of a planetesimal. Literature data on chondrite components show that the major host phase of HSE in chondrites is FeNi metal (e.g. Rambaldi et al., 1977a,b, 1978; Grossman and Wasson, 1985; Horan et al., 2009), so that any HSE contributed by silicate phases can be neglected here.

3.6.2.2 Liquid metal – solid metal partitioning

Liquid metal–solid metal fractionation takes place upon cooling of solidifying planetary or asteroidal cores and may also play a role during melting events of chondrule precursor materials or during shock melting on parent bodies. It is well established that fractional crystallization has played a major role for HSE fractionation observed in magmatic iron meteorite groups (Scott, 1972; Scott and Wasson, 1975; Kelly and Larimer, 1977). For example a possible mechanism to achieve low refractory HSE/Ni and high Pd/Ni and Au/Ni ratios, as observed in enstatite chondrites, is liquid metal-solid metal partitioning. With progressive fractional crystallization of metallic cores, the remaining liquid metal becomes enriched in Pd, Au and Ni. In contrast refractory HSE (Os, Ir, Ru, Pt and Rh) preferentially partition into solid metal (e.g. Scott, 1972). Analysis of individual FeNi metal grains from the EL3 chondrite PCA91020 show depletions in the refractory HSE Re, Os, Ir and Pt relative to Au and Pd which are interpreted to reflect injected liquid metal produced during impact melting (Van Niekerk et al., 2009). An extraneous origin of these metal grains is assumed because no complementary residual metal is observed. Further evidence supporting such a scenario is derived from analyses of metal grains from NWA 2526 which are interpreted to reflect partial melt residues of enstatite chondrite parentage (Humayun et al., 2009). Impact induced melting was also suspected to cause fractionations of refractory lithophile elements in EL chondrites (Rubin et al., 2009).

The partitioning behaviour of most HSE during fractional crystallisation of solid FeNi metal is well studied for magmatic iron meteorite groups (e.g. Jones and Malvin, 1990; Fleet et al., 1999; Chabot and Jones, 2003) and depends strongly on the minor element composition of the liquid phase, especially the content of S and C, and to a lesser extent on temperature and pressure conditions. Partition coefficients between solid metal and liquid metal ($D_{HSE}^{sm/lm}$) for most HSE increase with increasing S content of the liquid (Chabot et al., 2003; Chabot and Jones, 2003; Fleet et al., 1999; Jana and Walker, 1997). Recent studies on the Fe-Ni-C system show that Re partitions more strongly in the liquid metal as the C content of the melt increases, while other HSE partition more strongly into the solid metal (Chabot et al., 2006), hence fractionated Re/Os could be established by fractional crystallisation of a C-bearing melt. Corgne et al. (2008) observed two immiscible coexisting liquid alloys in the Fe-Ni-S-C-O system at low pressures (<5.5 GPa). One alloy was enriched in C, the other in S. Thus, especially smaller bodies may be affected by separation of two immiscible metallic liquids during metal-silicate equilibration. Because of the immiscibility of C- and S-rich metallic liquids the metal phase of chondrites could contain contributions from both metallic liquids and their corresponding solids if material in chondrites was derived from a differentiated body.

To test a possible magmatic prehistory of chondrite metals, we have employed a model for the evolution of critical HSE ratios in a metallic liquid containing varying amounts of C (0 - 3.6 wt%) during fractional crystallization of solid metal, assuming a CI like starting composition. Partition coefficients for HSE modelling in the Fe-Ni-S-C system were obtained from the literature and are given in Fig. 3.9. We have also investigated the evolution of S-rich metallic liquids (0 – 20 % S), but because of the ability to generate more fractionated Re/Os we only show the C-bearing metallic melt compositions in the diagram. In Figure 3.9a Re/Os and Pt/Ir for chondrite bulk samples from this study, Walker et al. (2002), Horan et al. (2003) and Brandon et al. (2005a,b) are compared to the evolving composition of a C-bearing metallic liquid. Additionally, data on ordinary chondrite metal grains analyzed by LA-ICP-MS (Humayun and Campbell, 2002; Campbell and Humayun, 2003) are shown for comparison.

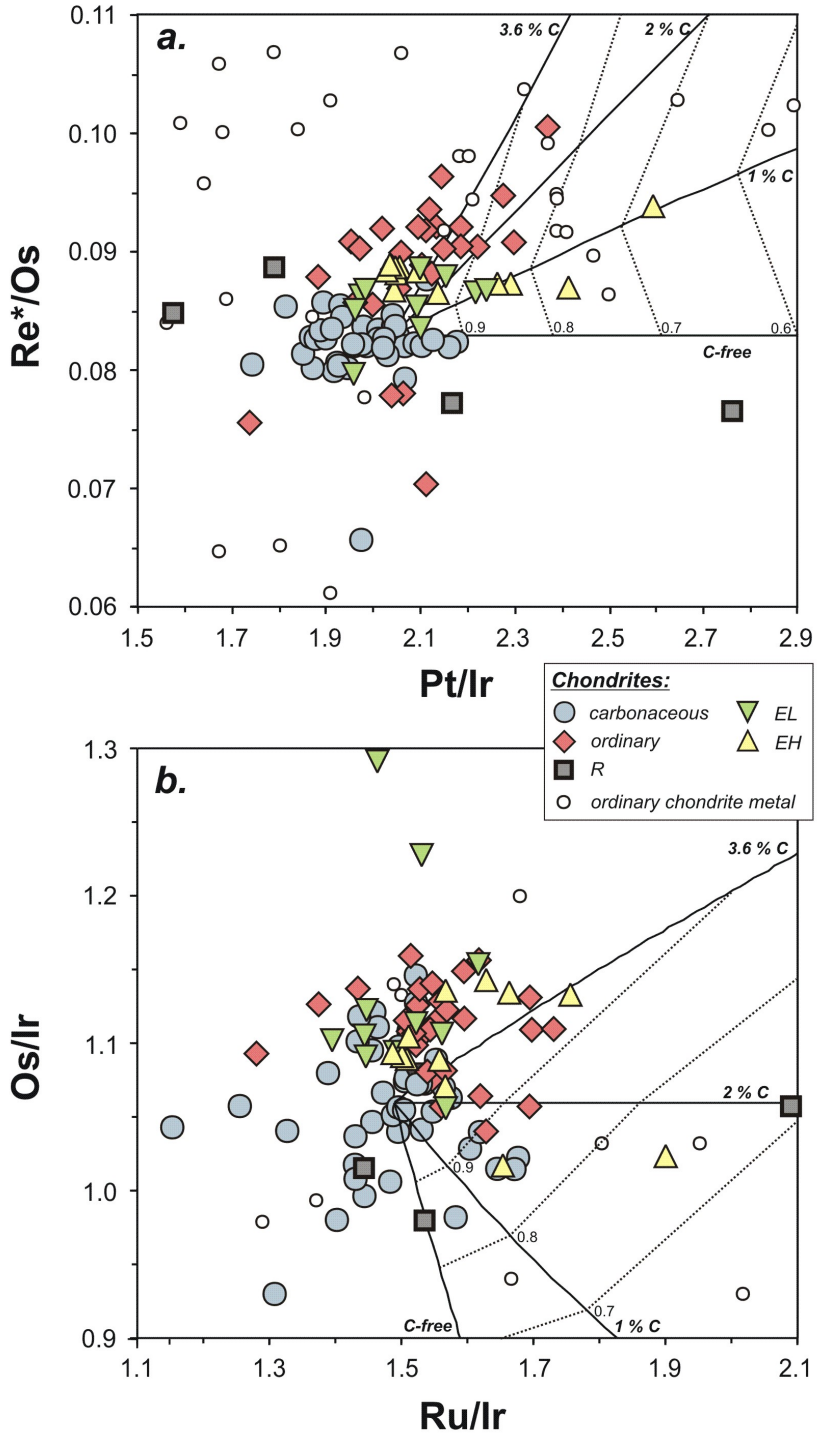

Fig. 3.9. Re*/Os vs. Pt/Ir (a) and Os/Ir vs. Ru/Ir (b) from this study, Walker et al. (2002), Horan et al. (2003) and Brandon et al. (2005a,b) for whole rocks of chondrites from different classes and groups in comparison to a Rayleigh fractionation model showing the chemical evolution of a metallic liquid with varying amounts of C (0 wt% - 3.6 wt%). The model is employed to test the possibility of a magmatic differentiation history of chondrite metals. For comparison LA-ICP-MS data from Humayun and Campell (2002) and Campbell and Humayun (2003) are shown. The model assumes a CI chondrite-like initial metal composition

(Table 3.3). Consistent sets of solid metal-liquid metal partition coefficients ($D^{sm/lm}$) from the literature were used (0 % C: D_{Re}= 2, D_{Os}= 2, D_{Ir}= 1.5, D_{Ru}= 1.3, D_{Pt}= 0.81; 1 % C: D_{Re}= 2, D_{Os}= 2.3, D_{Ir}= 1.9, D_{Ru}= 1.4, D_{Pt}= 1.3; 2 % C: D_{Re}= 1.7, D_{Os}= 2.5, D_{Ir}= 2.5, D_{Ru}= 1.5, D_{Pt}= 1.7; 3.6 % C: D_{Re}=1.4 , D_{Os}= 3.4, D_{Ir}= 4.6, D_{Ru}= 1.8, D_{Pt}= 3.4; Chabot and Jones, 2003; Walker et al., 2005; Chabot et al., 2006). Dotted lines represent the evolution of the remaining liquid in 10 % increments of increasing crystallization (1 = initial composition). Fractional crystallization from a C-bearing metallic liquid could possibly account for differences in Re/Os and Pt/Ir (a), but it fails to predict Os/Ir (b) of ordinary and enstatite chondrites relative to carbonaceous chondrites. Re* = calculated time-integrated Re abundances for chondrite whole rock data as described in the text.

Fig. 3.9b shows the same crystallization sequence compared to Os/Ir and Ru/Ir of chondrites. The evolution of a C-bearing metallic liquid during fractional crystallization can possibly explain Re/Os and Pt/Ir in some ordinary and enstatite chondrites, and ordinary chondrite metal grains, but the model fails to predict Os/Ir and Ru/Ir in ordinary and enstatite chondrites, and in the ordinary chondrite metal grains. Fractional crystallization models for S-bearing metallic melts show decreasing Os/Ir and increasing Pt/Ir ratios in the remaining liquid with increasing degree of crystallization and increasing amount of S in the initial liquid metal composition. The effect of small amounts of S on fractionation of Re/Os is less than observed for C-bearing metallic liquids. Thus, S-bearing metallic liquids also fail to explain the chondrite data. At least the present data provides no indication that chondrite precursor materials have been processed by fractional crystallization of a metallic liquid.

3.6.2.3 Monosulphide solid solution – liquid sulphide partitioning

Sulphide-rich melts could be produced during impact melting on a planetary body. Such a scenario was outlined to explain sulphide-rich shock veins in R chondrites (Kallemeyn et al., 1996). In the case of R chondrites the variability in Pt, Pd and Au abundances might be produced by monosulphide solid solution (mss)-sulphide liquid partitioning. Platinum, Pd and Au are incompatible and partition more strongly into sulphide melt compared to mss (e.g. Fleet et al., 1993; Ballhaus et al., 2006; Mungall et al., 2005). The extraction of a few percent sulphide melt from a CI starting material would cause depletions of Pt, Pd and Au and results in CI-normalized HSE abundance patterns very similar to the one observed for NWA 978 and to some extent for EET 96026 (Fig. 3.10). HSE data of NWA 753, however, are inconsistent with the model.

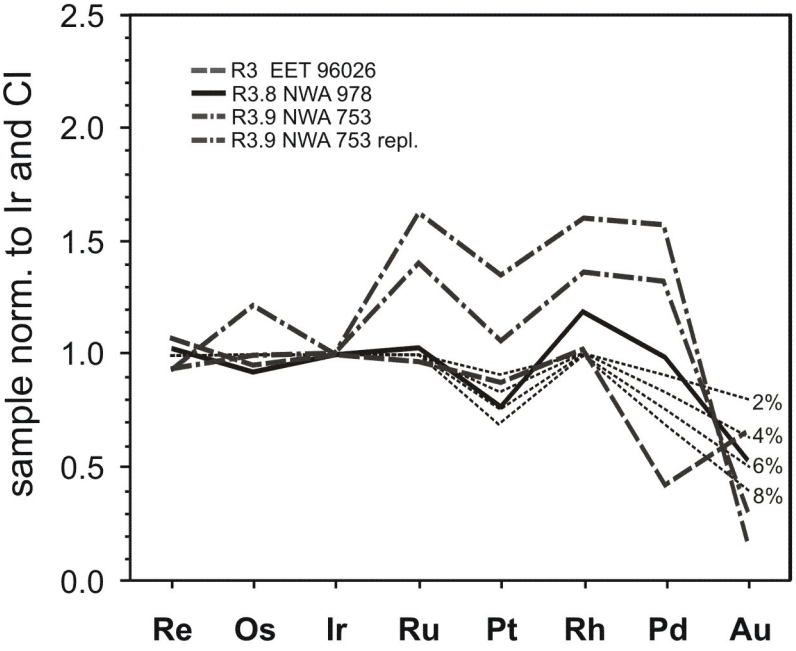

Fig. 3.10. Double-normalized (normalized to Ir and to CI Mean abundances from Table 3.3) HSE data for R chondrites in comparison with residual HSE compositions after increasing sulphide melt extraction (2 – 8%) from an assumed CI precursor composition. Dotted lines represent per cent fractions of sulphide melt extraction. Monosulphide solid solution (mss)-sulphide liquid partition coefficients ($D^{mss/sl}$) from Fleet et al. (1993) and Ballhaus et al. (2006) were used (D_{Re}= 2.4, D_{Os}= 4.4, D_{Ir}= 3.6, D_{Ru}= 4.2, D_{Pt}= 0.21, D_{Rh}= 3.0, D_{Pd}= 0.21, D_{Au}= 0.09). In the case of NWA 978 and possibly EET 96026 the model provides an acceptable fit, while HSE abundances of NWA 753 are inconsistent with the model.

3.6.2.4 Mineral-melt partitioning in silicate and oxide systems

In chondritic meteorites, metal or sulphide phases hold the lion´s share of the HSE. Experimental studies on the partitioning between sulphide and silicate melts show that all HSE partition strongly into the sulphide phase (e.g. Fleet et al., 1991, 1996; Bezmen et al., 1994; Crocket et al., 1997). Judging from their high metal-silicate partition coefficients silicates could play only a minor role in fractionating HSE in chondrites, if any. Partitioning experiments have shown that Ir, Ru and Rh are compatible in Cr-rich spinels, while Re, Pd and Au are incompatible (Righter et al., 2004). For olivine, Ir, Ru and Rh have been found to be compatible and Re, Pt, Pd and Au incompatible relative to silicate melt (Righter et al., 2004; Brenan et al., 2005). Partitioning of HSE between spinel, mafic silicates and silicate melts is considered to be an unlikely process to cause the observed HSE patterns of chondrites.

3.7 Conclusions

The new HSE data, along with previous high-precision HSE concentration data on chondrite bulk samples (Walker et al, 2002; Horan et al., 2003; Brandon et al. 2005a,b) show that chondrite classes are characterized by distinct HSE abundance patterns and ratios. Differences between chondrite classes and groups are best resolved in ratio plots of $^{187}Os/^{188}Os$ vs. Au/Ir (Fig. 3.8a) and Rh/Ir vs. Au/Ir (Fig. 3.8c).

The CI normalized HSE abundance patterns for carbonaceous chondrites other than CI are affected by depletion of the moderately volatile elements Pd and Au. HSE correlations are consistent with a CI like component and a Pd-Au depleted component, enriched in refractory siderophiles, consistent with recent data on metal grains from carbonaceous chondrites by Hammond et al. (2008). The refractory component may have formed by partial condensation (or evaporation) under solar nebular conditions (e.g. Palme and Wlotzka, 1976; Blander et al., 1980; Eisenhour and Buseck, 1992; Palme, 2008, Horan et al., 2009).

Well-defined HSE correlations for ordinary and enstatite chondrites may also reflect binary mixing, with a strongly fractionated Pd-Au rich component present as the major component in enstatite chondrites and a Pd-Au depleted, refractory HSE enriched component dominating ordinary chondrites. Subtle fractionations among refractory siderophile elements (most prominently Rh/Ir, Re/Os) within ordinary and enstatite chondrites relative to carbonaceous chondrites might be explained by fractional condensation combined with the removal of early condensates and mixing of early and late formed alloys (Sylvester et al., 1990), however, the conditions under which such phase separations may have occurred remain largely unconstrained.

The present HSE data on bulk samples of carbonaceous, ordinary and enstatite chondrites, and ordinary chondrite metal grains, provide no evidence that chondrite components or chondrite precursor materials have been processed by planetary differentiation processes. Abundances of HSE in some, but not all Rumuruti chondrites might be affected by sulphide melt extraction and monosulphide solid solution-liquid sulphide partitioning related to impact events.

Further constraints on the origin of HSE fractionation within chondrites, may require detailed study of chondrite components, especially metals and sulphides but also matrix, chondrules and calcium-aluminium-rich inclusions.

Acknowledgements

We thank T. McCoy, M. Wadhwa, F. Brandstetter, A. Greshake, D. Ebel and K. Rankenburg for supplying samples, K. Hammerschmidt for help and advice in the TIMS Lab, M. Feth for help und support in the Clean Lab and U. Wiechert for discussions. M. Fischer-Gödde thanks D. v. Acken for help and discussions. Thanks to J. & J. & I.. We appreciate reviews from Mary Horan, Munir Humayun, Herbert Palme and the editorial handling by Al Brandon. This work was supported by the Deutsche Forschungsgemeinschaft (Be 1820/3-1).

Table 3.1: Highly siderophile element abundances (in ng/g), $^{187}Os/^{188}Os$ isotope ratios and $^{187}Re/^{188}Os$ for Smithsonian Allende chondrite standard powder (USNM 3529)

	split/pos.	weight (g)	Re	Re*	Os	Ir	Ru	Pt	Rh	Pd	Au	$^{187}Os/^{188}Os$	$^{187}Re/^{188}Os$	Δ_{Os}[j]
this study														
Allende[a]	15 pos. 8	0.057	62.0	57.1	689	644	1007	1321	166	652	123	0.12624	0.4252	-25.4
Allende[b]	15 pos. 8	0.050	64.0	65.3	795	705	1073	1380	168	681	140	0.12596	0.3806	7.0
Allende[b]	16 pos. 4	0.048	58.7	60.0	732	660	997	1334	178	684	144	0.1259[#]	0.3791	7.3
Allende[b]	16 pos. 4	0.062	58.4	57.8	709	762	997	1409	183	676	152	0.12572	0.3895	-2.4
Allende[b]	16 pos. 4	0.061	58.6	58.2	703	654	991	1321	177	692	135	0.12614	0.3940	-1.7
Allende[b]	16 pos. 4	0.065	61.4	61.0	749	680	975	1379		657		0.12569	0.3872	-0.9
Mean			**60.5**	**59.9**	**729**	**684**	**1007**	**1357**	**174**	**674**	**139**	**0.12595**	**0.3926**	**-2.3**
%RSD			*3.8*	*5.1*	*5.3*	*6.4*	*3.4*	*2.7*	*4.1*	*2.3*	*7.8*	*0.18*	*4.3*	
literature data														
Allende Lit.[c]	USNM 3529		**61.2**		**763**	**700**	**1140**	**1379**		**786**		**0.12638**	**0.3860**	**7**
	16 pos. 4													
Allende Lit.[d]	USNM 3529		**63.5**		**785**	**720**	**1118**	**1421**		**682**		**0.12596**	**0.3896**	**-0.1**
Allende Lit.[e]	USNM 3529		**60.9**		**758**	**712**	**1016**	**1348**		**674**		**0.12615**	**0.3873**	**3.6**
%RSD			*2.8*		*2.4*	*1.7*		*1.4*		*2.4*		*0.11*	*0.81*	
Allende Lit.[f]	MPI		**60.2**		**746**	**730**	**843**	**1290**	**169**		**161**			
%[#]			*4.0*		*4.0*	*4.0*	*7.0*	*4.0*	*10*		*4.0*			
Allende Lit.[g]						**694**	**1058**	**1395**	**210**	**598**				
Allende Lit.[h]	USNM 3529		**68.4**		**833**	**776**				**705**	**137**			
%RSD			*7.6*		*8.8*	*5.4*				*12*	*7.1*			
Allende Lit.[i]	USNM 3529					**740**					**150**			
%RSD						*12*					*6.7*			

[a] Carius tube data at 320°C.
[b] High-pressure asher data at 320°C.
[c] Carius tube data at 345°C, Becker et al. (2006).
[d] Carius tube data at 270°C, Brandon et al. (2005a).
[e] Carius tube data at 220°C, Walker et al. (2002), Horan et al. (2003).
[f] Spark source mass spectrometry data, Jochum (1996), [#]estimated accuracy.
[g] NiS fire assay pre-concentration data, Tagle and Berlin (2008).
[h] RNAA data, Takahashi et al. (1978).
[i] recommended values from compiled NAA data, Jarosewich et al. (1987).
[j] Δ_{Os} refers to the combined deviation in the determined $^{187}Os/^{188}Os$ and $^{187}Re/^{188}Os$ for a given chondrite sample from the IIIA iron meteorite reference isochron, $\Delta_{Os} = 10^4$ ($^{187}Os/^{188}Os_{chondrite}$ – (0.09524 + 0.07887 × $^{187}Re/^{188}Os_{chondrite}$)), $^{187}Os/^{188}Os_{chondrite}$ and $^{187}Re/^{188}Os_{chondrite}$ are the values determined for chondrites, 0.09524 is the initial $^{187}Os/^{188}Os$ and 0.07887 is the slope of the IIIA iron meteorite isochron (Smoliar et al., 1996).
[#] $^{187}Os/^{188}Os$ measured with secondary electron multiplier (SEM).
Re* = calculated Re abundances as discussed in text.
USNM, U.S. National Museum of Natural History; MPI, Max Planck Institut, Mainz.

Table 3.2: Highly siderophile element abundances (in ng/g), $^{187}Os/^{188}Os$ and $^{187}Re/^{188}Os$ data for chondrites

Meteorite	Group	ID	weight (g)	Re	Re*	Os	Ir	Ru	Pt	Rh	Pd	Au	$^{187}Os/^{188}Os$	$^{187}Re/^{188}Os$	Δ_{Os} [a]
Carbonaceous chondrites															
Orgueil	CI1	MfNB	0.050	37.4	38.5	468	435	655	906	133	595	194	0.12600	0.3781	9.4
replicate			0.028	35.9	37.9	458	418	625	888	137	566	167	0.12613	0.3704	16.8
replicate			0.051				412	608	841	123	555	164	0.12604		
Ivuna	CI1	USNM 6630	0.051	38.1	36.0	438	422	630	871	131	564	116	0.12592	0.4108	-17.2
replicate			0.054	35.0	35.6	434	405	618	851	126	557	103	0.12591	0.3811	6.1
Murchison	CM2	USNM 5453	0.053	46.7	47.2	572	569	843	1127	151	642	175	0.12609	0.3857	4.3
Mighei	CM2	ME 1456	0.050	45.1	43.6	543	545	787	1061	150	605	165	0.12527	0.3927	-9.4
Nogoya	CM2	MfNB	0.053	46.3	47.1	574	548	820	1074	147	572	179	0.12594	0.3816	6.0
Kainsaz	CO3		0.052	47.8	61.1	737	660	947	1233	158	712	204	0.12622	0.3063	68.2
Ninqiang	CK3	ME 3207	0.052	57.4	57.0	695	670	959	1449	171	753	165	0.12591	0.3901	-1.0
replicate			0.056	54.2	55.5	674	662	947	1439	182	751	162	0.12604	0.3805	7.9
Karoonda	CK4	USNM 7035	0.053	49.0	46.7	791	712	1042	1432	175	730	133	0.11732	0.2930	-10.3
Bencubbin	CB	USNM 6702	0.101	47.9	45.8	577	538	826	1110	157	709	112	0.12490	0.3922	-12.8
Allende[b]	CV3	USNM 3529	*mean*	60.5	59.9	729	684	1007	1357	174	674	139	0.12594	0.3926	-2.3
Ordinary chondrites															
Dhajala	H3.8	USNM 5832	0.052	88.1	87.1	965	847	1309	1819	283	1024	280	0.12897	0.4315	-3.0
Bremervörde	H3.9	MfNB	0.052	66.6	64.8	684	595	949	1355	208	838	238	0.13064	0.4605	-9.2
Ochansk	H4		0.051	80.7	77.6	872	788	1198	1659	252	908	265	0.12848	0.4375	-12.6
Forest City	H5	USNM 1649	0.059	72.2	72.5	828	714	1080	1463	238	806	244	0.12799	0.4125	2.1
Mt.Tazerzait	L5		0.072	55.8	54.8	544	482	815	1141	181	674	185	0.13282	0.4844	-6.3
Chainpur	LL3.4	USNM 7028	0.052	32.6	33.1	366	328	523	727	114	533	152	0.12905	0.4204	6.5
Benguerir	LL6		0.051	39.9	40.0	442	394	619	861	138	531	147	0.12905	0.4262	2.0
St.Severin	LL6	USNM 6672	0.050	26.3	25.7	365	321	490	678	102	370	101	0.12158	0.3415	-5.9
Enstatite chondrites															
Sahara 97072	EH3		0.055	58.2	53.0	607	532	867	1219	179	948	348	0.12783	0.4531	-31.5
Abee	EH4	USNM 6582	0.050	50.4	50.6	540	528	1003	1371	178	1087	407	0.13029	0.4413	2.4
Indarch	EH4	USNM 3482	0.051	52.9	52.1	602	531	832	1135	172	918	398	0.12756	0.4147	-3.9
replicate			0.075		50.7	583							0.12773		
St.Marks	EH5	USNM 3027	0.055	52.6	45.1	518	458	804	1105	148	875	323	0.12776	0.4795	-53.0
replicate			0.057	50.8	48.9	561	495	823	1119	171	880	329	0.12784	0.4280	-11.6
MAC 02839	EL3	MWG JSC	0.060	49.2	46.6	555	430	629	903	139	638	223	0.12664	0.4188	-16.3
MAC 88136	EL3	MWG JSC	0.061	49.1	50.1	562	501	724	1052	164	760	279	0.12853	0.4127	7.4
Pillistfer			0.055	71.1	70.4	808	658	1008	1461	212	878	317	0.12782	0.4163	-2.6
replicate	EL6	NMW	0.055		63.5	728	632	1022	1414	217	865	298	0.12785		
Blithfield	EL6	ME 1979	0.051	34.3	33.3	387	348	530	729	108	448	155	0.12732	0.4187	-9.4
Hvittis	EL6	ME 1470	0.050	9.56	8.56	107	97.7	146	191	30.0	152	60.0	0.1252[#]	0.4227	-34.0
Rumuruti-class chondrites															
NWA 978	R3.8		0.050	40.9	43.5	513	524	805	824	178	617	89.5	0.12692	0.3771	19.4
NWA 753	R3.9		0.049	34.2	34.8	455	352	855	973	162	651	19.3	0.12385	0.3561	5.3
replicate			0.051	33.7	33.1	429	406	851	880	159	634	39.5	0.12407	0.3716	-4.8
EET 96026	R3	MWG JSC	0.053	20.2	62.3	701	690	996	1236	204	382	146	0.12843	0.1359	225

[a] see Table 3.1 footer for explanation.
[b] Allende mean data from Table 3.1.
[#] $^{187}Os/^{188}Os$ measured with secondary electron multiplier (SEM).
MfNB, Museum für Naturkunde, Berlin; USNM, U.S. National Museum of Natural History; ME, Field Museum, Chicago; NMW, Naturhistorisches Museum, Wien; MWG JSC, Meteorite Working Group, Johnson Space Center.
Re* = calculated Re abundances as discussed in text.

Table 3.3: Highly siderophile element abundances (in ng/g), $^{187}Os/^{188}Os$ isotope and HSE ratios for CI chondrites Orgueil and Ivuna in comparison to literature data and compiled values

Meteorite	Reference	Re	Os	Ir	Ru	Pt	Rh	Pd	Au	$^{187}Os/^{188}Os$	$^{187}Re/^{188}Os$	Re/Ir	Os/Ir	Ru/Ir	Pt/Ir	Rh/Ir	Pd/Ir	Au/Ir
Orgueil	FUB[a]	37.4	468	435	655	906	133	595	194	0.12600	0.3781	0.086	1.08	1.51	2.08	0.306	1.37	0.446
replicate				412	608	841	123	555	164	0.12604				1.47	2.04	0.298	1.35	0.397
replicate		35.9	458	418	625	888	137	566	167	0.12613	0.3704	0.086	1.10	1.50	2.13	0.328	1.36	0.400
Ivuna	FUB[a]	38.1	438	422	630	871	131	564	116	0.12592	0.4108	0.090	1.04	1.49	2.07	0.311	1.34	0.275
replicate		35.0	434	405	618	851	126	557	103	0.12591	0.3811	0.086	1.07	1.53	2.10	0.311	1.38	0.255
Mean		**36.6**	**450**	**418**	**627**	**872**	**130**	**567**	**149**	**0.12600**	**0.3851**	**0.087**	**1.07**	**1.50**	**2.08**	**0.311**	**1.36**	**0.355**
%RSD		*3.9*	*3.6*	*2.7*	*2.8*	*3.1*	*4.3*	*2.8*	*25*	*0.07*	*4.6*	*2.4*	*2.2*	*1.3*	*1.6*	*3.5*	*5.3*	*24*
Orgueil	UMD[b] & DTM[c]	38.0	459	456	652	858		563		0.12638	0.3990	0.083	1.01	1.43	1.88		1.24	
replicate		41.0	457	432	648	874		574				0.095	1.06	1.50	2.02		1.33	
replicate		38.3	459							0.12644	0.4025							
Ivuna	UMD[b] & DTM[c]	35.2	429	406	609	829		529		0.12654	0.3935	0.087	1.06	1.50	2.04		1.30	
replicate		37.1	450	428	636	860				0.12646	0.3970	0.087	1.05	1.49	2.01			
Mean		**37.9**	**451**	**431**	**636**	**856**		**555**		**0.12646**	**0.3980**	**0.088**	**1.05**	**1.48**	**1.99**		**1.29**	
%RSD		*6.5*	*3.1*	*4.7*	*3.0*	*2.2*		*4.2*		*0.04*	*0.94*	*5.6*	*2.3*	*2.2*	*3.6*		*3.7*	
Mean ID	FUB[a], UMD[b]	**37.3**	**450**	**424**	**631**	**864**	**130**	**563**	**149**	**0.12621**	**0.3915**	**0.088**	**1.06**	**1.49**	**2.04**	**0.311**	**1.33**	**0.355**
%RSD	& DTM[c]	*5.0*	*3.0*	*3.8*	*2.8*	*2.7*	*4.3*	*3.3*	*25*	*0.20*	*3.5*	*4.0*	*2.5*	*1.8*	*3.4*	*3.5*	*5.5*	*24*
Mean CI[d]		**40.7**	**491**	**462**	**688**	**943**	**133**	**563**	**149**	**0.12621**	**0.3915**	**0.088**	**1.06**	**1.49**	**2.04**	**0.307**	**1.22**	**0.322**
%RSD		*5.0*	*3.0*	*3.8*	*2.8*	*2.7*	*4.3*	*3.3*	*25*	*0.20*	*3.5*	*4.0*	*2.5*	*1.8*	*3.4*	*3.5*	*5.5*	*24*
CI Lit.	Jochum (1996)	**39.5**	**492**	**480**	**683**	**982**	**140**		**148**			**0.082**	**1.03**	**1.42**	**2.05**	**0.292**		**0.308**
%RSD		*4.1*	*2.0*	*4.0*	*7.0*	*3.9*	*2.9*		*4.1*									
Data compilations:																		
CI Lit.	Anders and	**36.5**	**486**	**481**	**712**	**990**	**134**	**560**	**140**			**0.076**	**1.01**	**1.48**	**2.06**	**0.279**	**1.16**	**0.291**
%RSE	Grevesse (1989)	*9.4*	*6.3*	*6.1*	*5.4*	*7.4*	*8.0*	*6.6*	*15*									
CI Lit.	Tagle and		**502**	**472**	**717**	**959**	**135**	**563**	**139**				**1.06**	**1.52**	**2.03**	**0.290**	**1.19**	**0.300**
%RSD[#]	Berlin (2008)												*3.8*	*4.6*	*7.4*	*4.8*	*8.4*	*13*
CI Lit.	Lodders (2009)	**39.3**	**493**	**469**	**686**	**947**	**139**	**558**	**146**			**0.084**	**1.05**	**1.46**	**2.02**	**0.296**	**1.19**	**0.311**
%RSE		*10*	*8.0*	*5.0*	*6.0*	*8.0*	*10*	*5.0*	*10*									

see next page for Table 3.3 footer.

[a] FUB: Freie Universität Berlin (this study), sample ID: Orgueil (MfNB, Museum für Naturkunde Berlin), Ivuna (USNM 6630, U.S. National Museum of Natural History).
[b] UMD: University of Maryland (Walker et al., 2002).
[c] DTM: Department of Terrestrial Magnetism, Carnegie Institution of Washington (Horan et al., 2003), sample ID: Orgueil (MPI-318/5, Max Planck Institut, Mainz), Ivuna (USNM 2478, U.S. National Museum of Natural History).
[d] CI values of the Mean ID data adjusted to a mean CI Ir abundance of 462 ± 38 ng/g as described in text.
[#] concentrations calculated from compiled and filtered element/Ir ratios with an average uncertainty of ~5% (RSD).

Table 3.4.

Slopes and intercepts of linear regression calculations.

Slope		±2s	Intercept		±2s
Carbonaceous chondrites					
Re/Ir	0.084	+0.007/-0.008	Re	1.3	+4.1/-3.8
Re*/Ir	0.086	+0.006/-0.006	Re*	-0.1	+3.1/-3.3
Os/Ir	1.12	+0.07/-0.08	Os	-31	+37/-36
Ru/Ir	1.35	+0.14/-0.10	Ru	72	+61/-67
Pt/Ir	1.81	+0.11/-0.15	Pt	97	+65/-62
Rh/Ir	0.155	+0.019/-0.028	Rh	65	+15/-13
Pd/Ir	0.450	+0.130/-0.100	Pd	364	+50/-71
Au/Ir	0.0	+0.140/-0.099	Au	162	+54/-110
Ordinary chondrites					
Re/Ir	0.105	+0.001/-0.001	Re	-3.3	+4.1/-5.3
Re*/Ir	0.104	+0.005/-0.008	Re*	-1.9	+2.6/-3.1
Os/Ir	1.13	+0.04/-0.04	Os	-7	+19/-14
Ru/Ir	1.52	+0.07/-0.07	Ru	10	+38/-23
Pt/Ir	2.12	+0.13/-0.11	Pt	-10	+46/-93
Rh/Ir	0.310	+0.023/-0.021	Rh	5.3	+8.2/-6.4
Pd/Ir	1.01	+0.12/-0.12	Pd	115	+50/-120
Au/Ir	0.294	+0.044/-0.052	Au	21	+22/-19
Rh/Re	3.07	+0.09/-0.24	Rh	15	+12/-7.4
Pd/Au	3.13	+0.29/-0.34	Pd	116	+53/-53
EL chondrites					
Re/Ir	0.096	+0.002/-0.037	Re	0.8	+10/-2.1
Re*/Ir	0.096	+0.007/-0.013	Re*	-0.3	+9.1/-1.9
Os/Ir	1.08	+0.04/-0.15	Os	7	+78/-12
Ru/Ir	1.54	+0.12/-0.13	Ru	-7	+18/-65
Pt/Ir	1.99	+0.20/-0.18	Pt	-1	+110/-31
Rh/Ir	0.348	+0.037/-0.023	Rh	-10	+7.9/-16
Pd/Ir	1.19	+0.16/-0.20	Pd	37	+160/-28
Au/Ir	0.450	+0.010/-0.100	Au	15	+23/-64
Rh/Re	3.18	-0.42/-0.85	Rh	2.0	+13/-77
Pd/Au	2.80	+0.30/-0.40	Pd	3.0	+89/-45
EH chondrites					
Pd/Au	2.00	+1.0/-1.2	Pd	182	+420/-360

3.8 Appendix

The first part of the appendix (3.8.1) provides a comparison of data obtained by isotope dilution (ID) and high-pressure asher digestion (HPA-S; 320°C; this study) with data obtained on the same samples using ID combined with a Carius tube digestion technique (CT; 220-240°C; Walker et al., 2002; Horan et al., 2003). The second part (3.8.2) provides a comparison of our new defined HSE data for CI chondrites with previously reported abundances. In the third part (3.8.3) some of the Figures shown in the manuscript are redrawn with a distinction between data from this study and literature data.

3.8.1 Comparison to existing high precision data

Comparison of HSE concentration data obtained by isotope dilution (ID) and high-pressure asher digestion (HPA-S; 320°C; this study) with data obtained on the same samples using ID combined with a Carius tube digestion technique (CT; 220-240°C; Walker et al., 2002; Horan et al., 2003). Concentration data obtained by both techniques compare well and show no systematic deviations (Fig 3.11). The scatter around the 1:1 reference line thus reflects a combination of random analytical biases and heterogeneities of chondrite samples on the sample scale (50 – 150 mg for digestion, and between 200 – 2000 mg for powder preparation).

In Fig. 3.12 osmium isotopic composition data ($^{187}Os/^{188}Os$) and HSE/Ir ratios from both studies are shown. The data comparison hints at small systematic shifts for HSE/Ir ratios of about 2-3 % between the data sets. According to Fig. 3.12, HSE/Ir data on chondrites from the present work appear to be systematically higher than the data from Horan et al. (2003). This may be caused by differences for Ir, which tends to be lower in this work, compared to data in Horan et al. (2003). These differences may be explained by a systematic bias between the different Ir spikes and spike calibrations used in these studies. The original calibration of the spike used in the present work was performed by H. Becker in 2003 at the University of Maryland, using a standard solution prepared by John Morgan. The Ir spike was recalibrated in 2007 in Berlin using dilutions of two

different commercial ICP standard solutions. Calibration against an AlfaAeser™ Specpure ICP Ir standard produced a spike concentration that is systematically higher by 0.70 % compared to the original calibration value. Another calibration against a Merck™ ICP Ir standard solution produced results that are on average by 1.70 % lower compared to the original calibration value.

The mean of all results of the 2007 calibration is indistinguishable from the 2003 calibration, with an uncertainty (2 standard errors) of ± 0.89 %. A recalibration of the Ru tracer used in the present study with AlfaAeser™ Specpure ICP and Merck™ ICP standard solutions agrees with the 2003 calibration within ± 0.28 %. Thus the new calibrations essentially confirm the 2003 calibration results. We note however, that resolvable differences in true vs. certified abundances of PGE in commercial standard solutions limit the reliability of such standards for spike calibrations.

Data for $^{187}Os/^{188}Os$ obtained with the Carius tube digestion technique at 220-240°C tend to be slightly higher than our data obtained by high-pressure asher digestion at 320°C. Due to sample heterogeneity and overlapping errors it is difficult to evaluate the significance of these differences.

3.8.2 Comparison of HSE abundances for CI chondrites

In Fig. 3.13 we show the Ir data considered to calculate the mean Ir CI abundance that was used to adjust the refractory HSE abundances of our new defined Mean CI abundances as discussed in section 3.3.2 of the main text. Our adjusted Mean CI abundances (Table 3.3) are compared to literature data in Fig. 3.14. Abundances of the refractory HSE (Re, Os, Ir, Ru, Pt, Rh) of the combined ID data from this study, Walker et al. (2002) and Horan et al. (2003) are ~8 % lower compared to the new defined Mean CI, while Pd and Au agree well for reasons discussed in section 3.3.2. The SSMS data of Jochum (1996) agree within < 5 %, except the 7 % lower Re/Ir ratio. Compared to data compilations our Mean CI is in very good agreement with the recent reported CI abundances of Lodders et al. (2009). Compilations of Anders and Grevesse (1989) and Tagle and Berlin (2008) compare principally well, except for particular elements and ratios.

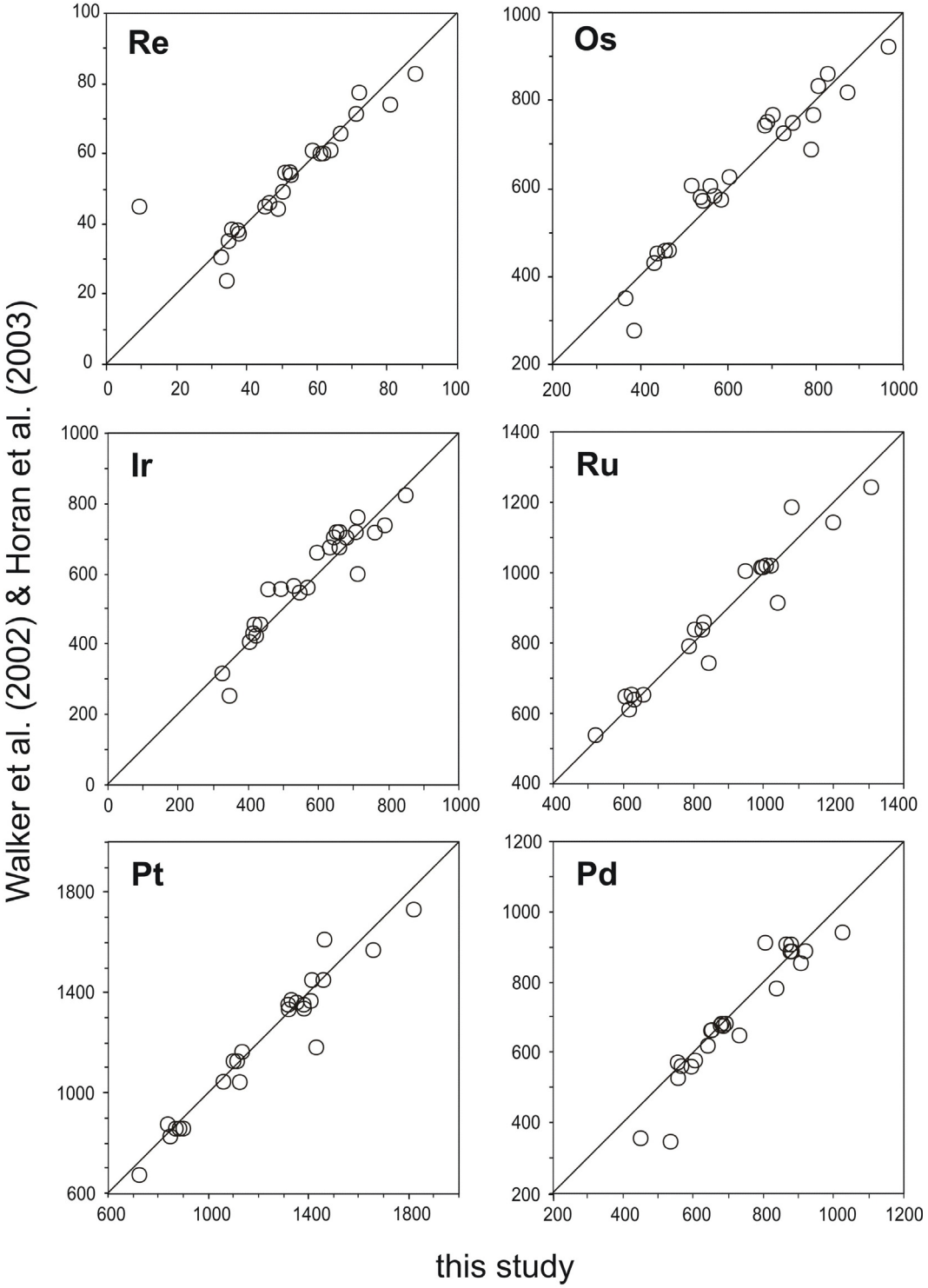

Fig. 3.11. Comparison between HSE concentration data for different aliquots from the same chondrite acquired by this study and data from Walker et al. (2002) and Horan et al. (2003). Both data sets were obtained by isotope dilution, ICP-MS and TIMS analysis. It should be noted that different enriched isotopic tracers for Ru, Ir, Pt and Pd, were used in these studies.

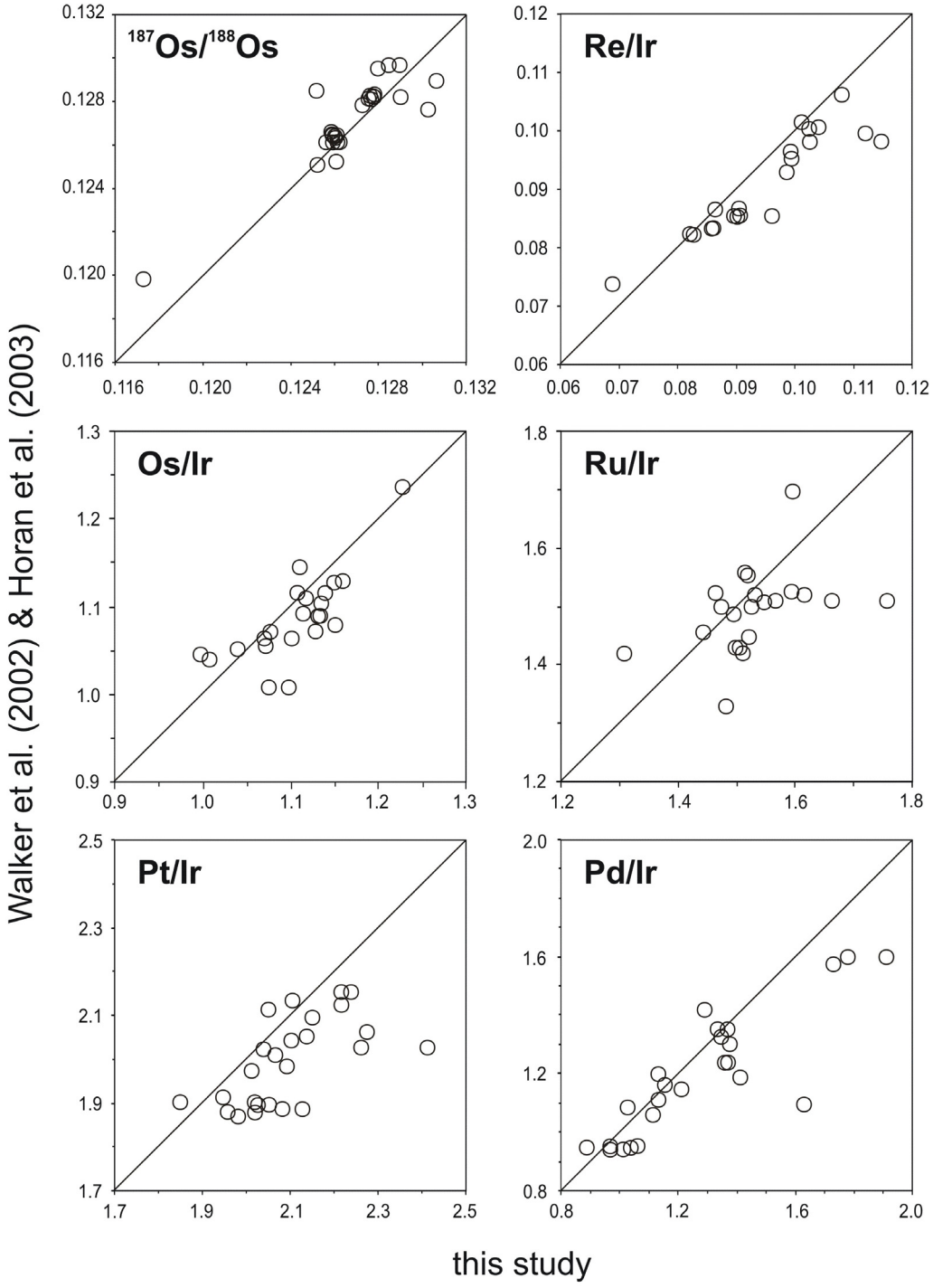

Fig. 3.12. Comparison between $^{187}Os/^{188}Os$ and HSE/Ir data for chondrite samples obtained by isotope dilution ICP-MS and TIMS analysis and data obtained by isotope dilution from Walker et al. (2002) and Horan et al. (2003). Some element ratios relative to Ir hint at a systematic difference between these data sets of ca. 2-3 %.

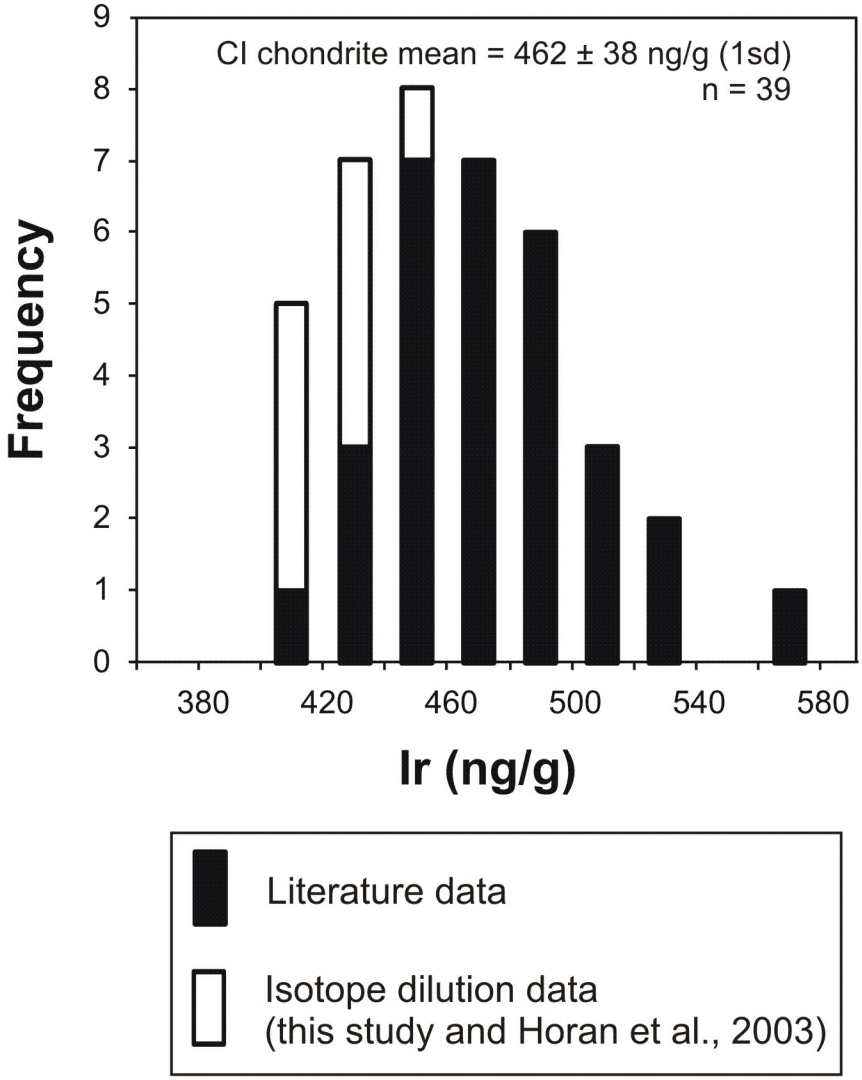

Fig. 3.13. Population density diagram showing the Ir data used to calculate the mean Ir CI abundance. Data from this study, Horan et al. (2003), the data compilation of Tagle and Berlin (2008), Hermann and Wichtl (1974), Chou et al. (1976) and Friedrich et al. (2002) are plotted. High precision isotope dilution (ID) data are shown as white bars, other data as black bars.

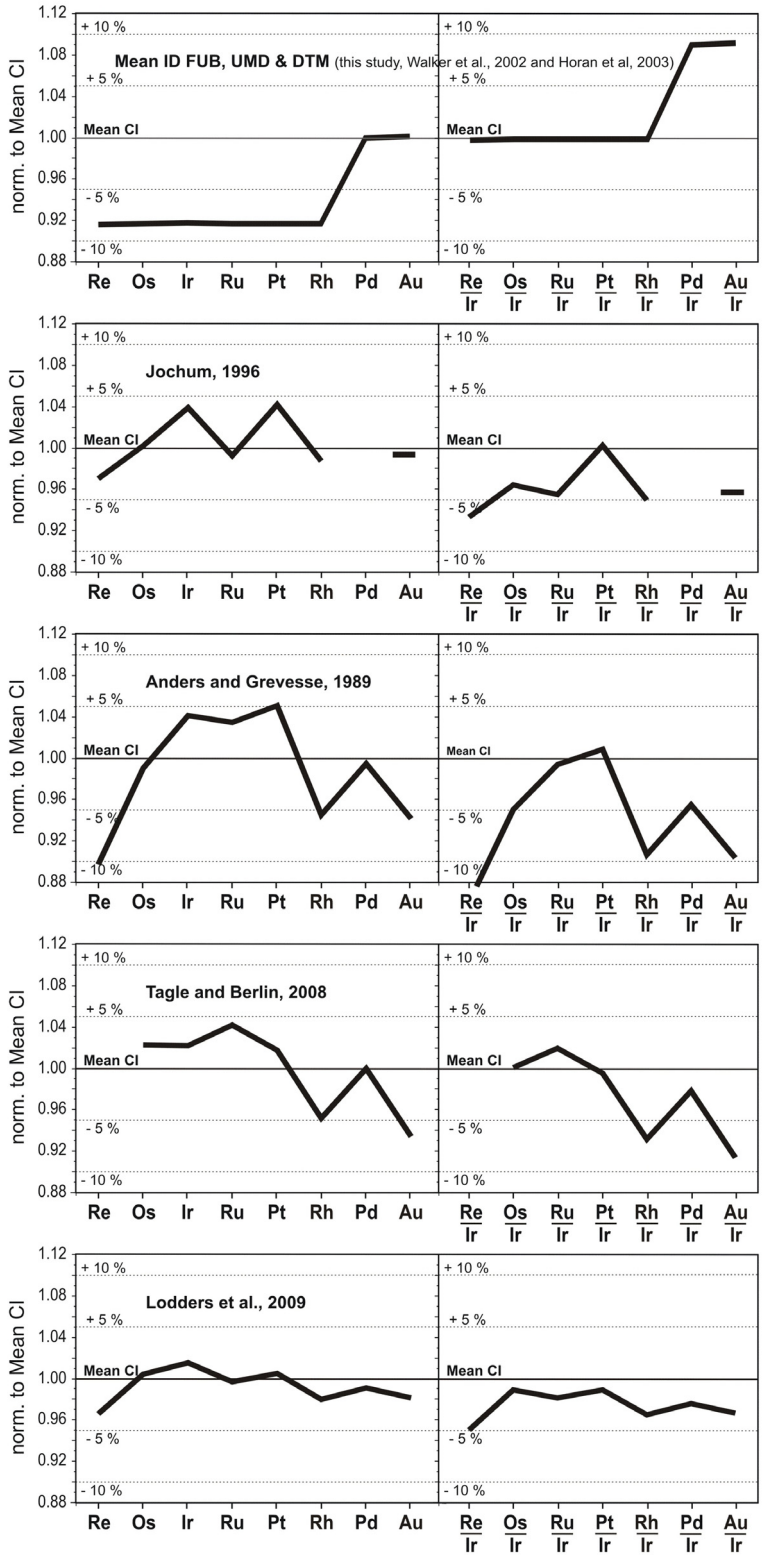

Fig. 3.14. Comparison of HSE abundances and ratios for CI chondrites. The data are normalized to our new defined Mean CI abundances (Table 3.3).

3.8.3 Identification of literature data in main text figures

In the manuscript data from this study and the literature data are shown using the same symbols. A distinction between the data from this study and literature data is provided in the following (Figures 3.15, 3.16, 3.17).

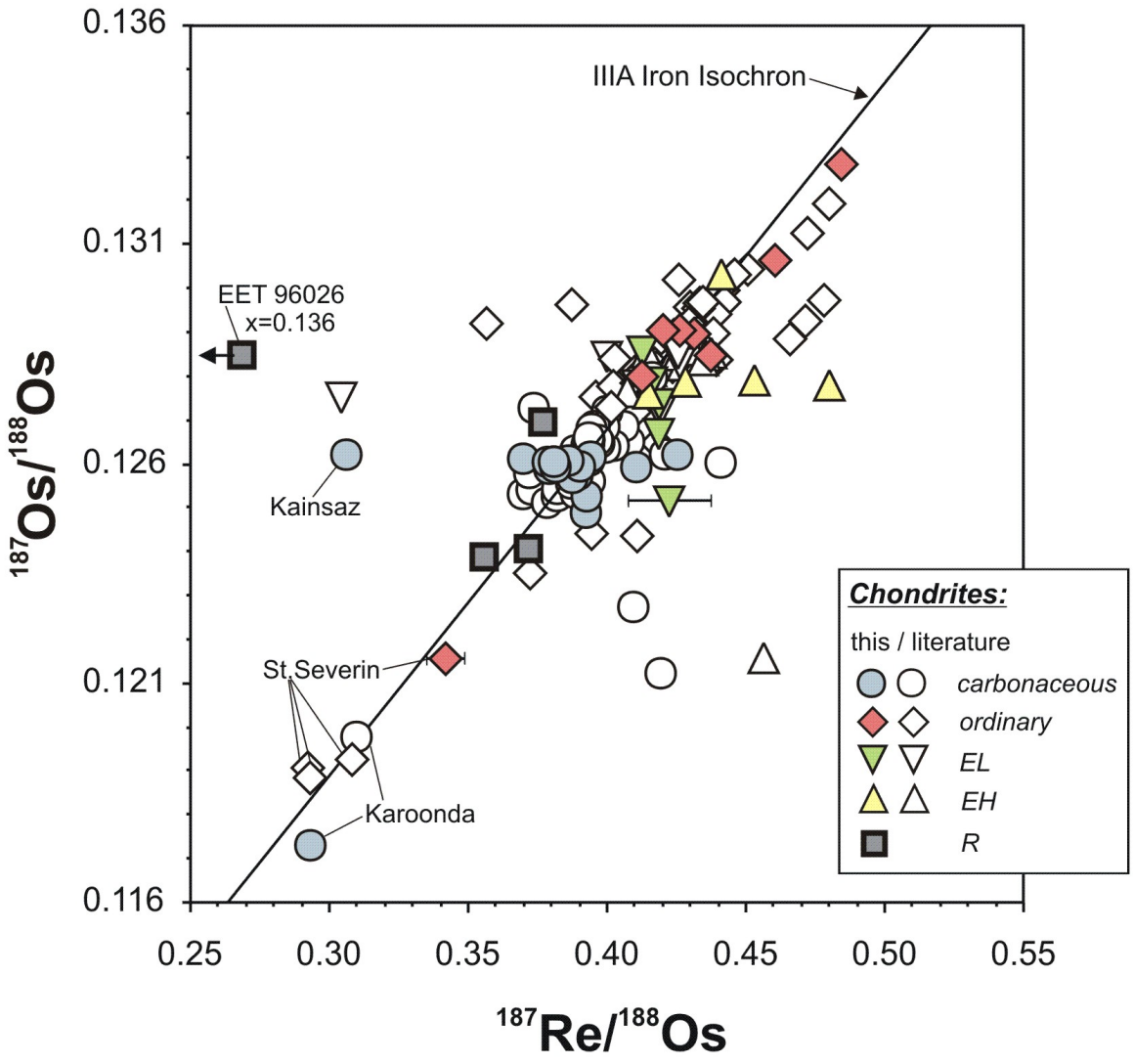

Fig. 3.15. $^{187}Re/^{188}Os$ vs. $^{187}Os/^{188}Os$ for chondrite bulk samples analysed in this study, Chen et al. (1998), Walker et al. (2002) and Brandon et al. (2005a,b). Compare with Fig. 3.2 of the main text.

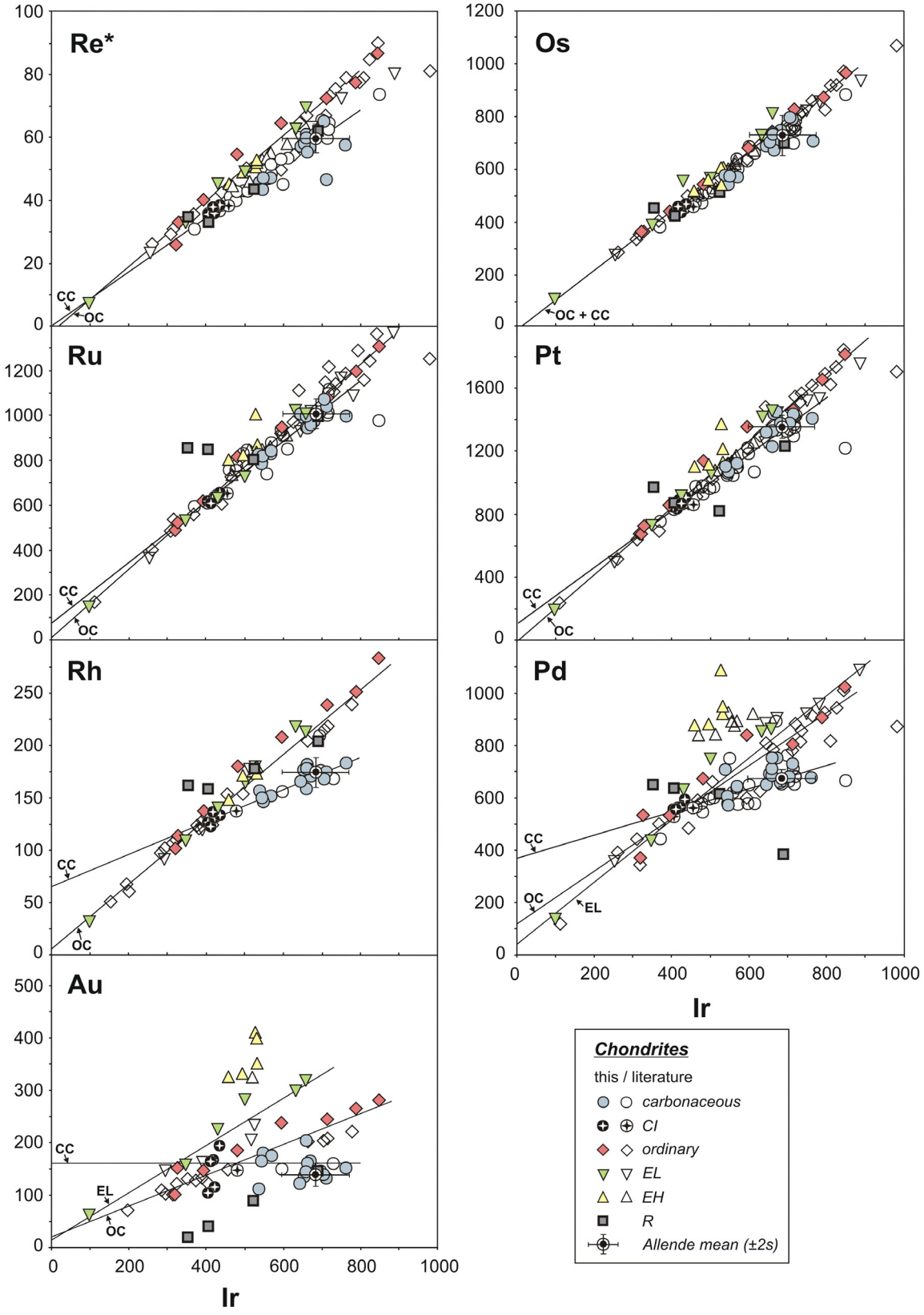
Re*
CC
OC
Os
OC + CC
Ru
CC
OC
Pt
CC
OC
Rh
CC
OC
Pd
CC
OC
EL
Au
CC
EL
OC
Ir
Ir
Chondrites
this / literature
carbonaceous
CI
ordinary
EL
EH
R
Allende mean (±2s)

Fig. 3.16. Chondrite HSE abundances plotted versus Ir (all data in ng/g). Precise ID ICP-MS data for Re*, Os, Ir, Ru, Pt, and Pd are from this study, Walker et al. (2002), Horan et al. (2003) and Brandon et al. (2005a,b). Data for Rh and Au from this study, Jochum (1996), McDonald and Russell (2001), McDonald et al. (2001) and Tagle and Berlin (2008) are plotted. Compare with Fig. 3.4 of the main text.

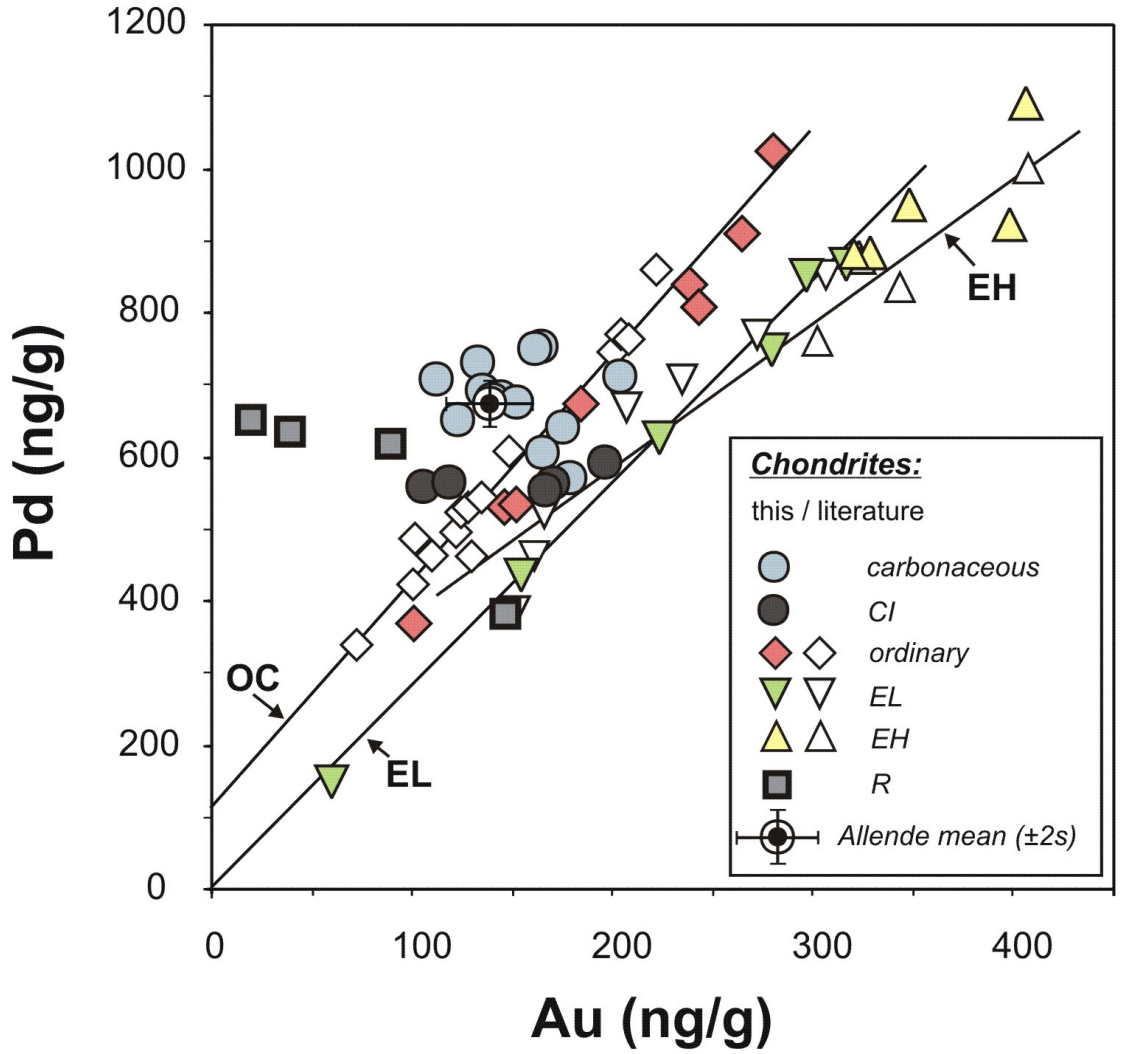

Fig. 3.17. Concentration data for Pd and Au from this study, Hertogen et al. (1983), McDonald and Russell (2001) and McDonald et al. (2001). Compare with Fig. 3.6 of the main text.

4. Rhodium, gold and other highly siderophile elements in orogenic peridotites and peridotite xenoliths

4.1 Abstract

The abundances of Rh, Au and other highly siderophile elements (HSE: Re, Os, Ir, Ru, Pt, Rh, Pd and Au), and $^{187}Os/^{188}Os$ isotope ratios have been determined for samples from peridotite massifs and xenoliths in order to further constrain HSE abundances in the Earth's mantle and to place constraints on the distributions processes accounting for observed HSE variations between fertile and depleted mantle lithologies. Concentrations of Re, Os, Ir, Ru, Pt and Pd were determined by isotope dilution ICP-MS and N-TIMS. The monoisotopic elements Rh and Au were quantified by standardization relative to the abundances of Ru and Ir, respectively, and were determined from the same digestion aliquot as other HSE. The precision of the concentration data, as inferred from repeated analyses of reference materials and sample powders, is estimated to be better than 10 % for Rh and better than 15 % for Au (1s).

Fertile lherzolites display non-systematic variation of Rh abundances and constant Rh/Ir of 0.34 ± 0.03 (1s, n=57), indicating a Rh abundance for the primitive mantle of 1.2 ± 0.2. The data also suggests that Rh behaves as a compatible element during low to moderate degrees of partial melting in the mantle, but may be depleted at higher degrees of melting. In contrast, Au concentrations and Au/Ir correlate with peridotite fertility, indicating incompatible behaviour of Au during magmatic processes in the mantle. Fertile lherzolites display Au/Ir ranging from 0.20-0.65, while residual harzburgites have Au/Ir <0.20. Abundances of Au and Re are correlated with each other and suggest similar

compatibility of both elements. The primitive mantle abundance of Au calculated from correlations displayed by Au/Ir with Al_2O_3 and Au with Re is 1.7 ± 0.5 ng/g (1s).

The depletion of Pt, Pd, Re and Au relative to Os, Ir, Ru and Rh displayed by residual harzburgites, suggests HSE fractionation during partial melting. However, the HSE abundance variations of fertile and depleted peridotites can not be explained by a single fractionation process. Correlations displayed by Pd/Ir, Re/Ir and Au/Ir with Al_2O_3 are consistent with refertilization of previously melt depleted mantle rocks due to reactive infiltration of silicate melts.

Relative abundances of Rh and Au inferred for the primitive mantle model composition are similar to values of ordinary and enstatite chondrites, but distinct from carbonaceous chondrites. The HSE pattern of the primitive mantle is inconsistent with compositions of known chondrite groups, but may be explained by late accretion of ancient meteoritic materials, or alternatively, by meteoritic materials mixed into mantle with a HSE signature inherited from core formation.

4.2 Introduction

The term highly siderophile elements (HSE: Re, Os, Ir, Ru, Pt, Rh, Pd, Au) comprises those elements characterized by very high metal-silicate partition coefficients (O'Neill et al., 1995; Holzheid et al., 2000; Walter et al., 2000; Ertel et al., 2008; Brenan and McDonough, 2009). During metal-silicate segregation the HSE will be quantitatively stripped off the silicate portion of a planet or planetesimal and concentrate in the metallic core. Contrary to their expected complete removal HSE abundances in the Earth's mantle are several orders of magnitude elevated compared to metal-silicate equilibrium. The excess siderophile abundances in the Earth's mantle are commonly explained by the addition of late accreted meteoritic materials after core formation (Chou, 1978; Jagoutz et al., 1979; Morgan, 1986; O'Neill, 1991; Schmidt et al., 2000; Meisel et al., 2001; Morgan et al., 2001; Schmidt, 2004; Becker et al., 2006). A strong argument favouring the late veneer hypothesis stems from broadly chondritic relative HSE abundances in conjunction with $^{187}Os/^{188}Os$ and $^{186}Os/^{188}Os$ similar to ordinary and enstatite chondrites deduced for fertile peridotites and mantle materials (Morgan et al., 1981; Meisel et al., 1996; Brandon

et al., 2000; Meisel et al., 2001; Walker et al., 2005a; Brandon et al., 2006). Alternative explanations invoke inefficient core formation scenarios (Arculus and Delano, 1981; Jones and Drake, 1986), contributions from outer core material (Snow and Schmidt, 1998) or decreasing partition coefficients at high pressure-temperature core formation conditions (Murthy, 1991; Righter and Drake, 1997; Righter et al., 1997; Li and Agee, 2001; Righter et al., 2008). While some specific high PT core formation scenarios may account for observed Pt, Pd and Au abundances in the mantle, abundances of other HSE like Os, Ir, Ru and Rh would still require the addition of a late meteoritic veneer (Cottrell and Walker, 2006; Righter et al., 2008; Brenan and McDonough, 2009). Thus a combination of different processes might account for the HSE abundances in the mantle (e.g. Walker, 2009).

Recent years have seen an increase of high-quality data sets of HSE abundances and $^{187}Os/^{188}Os$ in mantle peridotites using a combination of reverse aqua regia digestion, isotope dilution, ICP-MS, and TIMS based methods (e.g. Handler and Bennett, 1999; Meisel et al., 2001; Pearson et al., 2004; Becker et al., 2006; Luguet et al., 2007). These data have finally confirmed previous hints that fertile mantle, and primitive mantle models derived from such compositions, might posses resolvable suprachondritic Ru and Pd abundances relative to other HSE (e.g. Pattou et al., 1996; Schmidt et al., 2000). Deviations from chondritic HSE ratios as observed for Ru/Ir and Pd/Ir may be attributed to late accreted meteoritic materials with different chemical composition than known chondrite groups (Morgan et al., 1974; Puchtel et al., 2008) and mixing of meteoritic components with residual HSE signatures inherited from core formation (Brenan and McDonough, 2009). On the other hand, the validity of the inferred PM model composition has been challenged because some peridotites evidently have been affected by refertilization processes (e.g. Becker et al., 2001b; Saal et al., 2001; Pearson et al., 2004; Le Roux et al., 2007; Bodinier et al., 2008; van Acken et al., 2008; Lorand et al., 2009, 2010).

Most of the HSE data sets on mantle peridotites obtained by acid digestion and isotope dilution did not include abundance data for monoisotopic Rh and Au (e.g. Pearson et al., 2004; Becker et al., 2006) with the notable exception of the data by Handler and Bennett, 1999, which include Rh data. Other studies reported Rh and Au data obtained using NiS fire assay pre-concentration followed by INAA (Lorand et al., 1993; Lorand et al., 1999;

Lorand et al., 2000; Snow et al., 2000; Schmidt et al., 2003) or ICP-MS analysis (Pattou et al., 1996; Lorand et al., 1999; Luguet et al., 2003; Luguet et al., 2004). These studies suggest compatible behaviour of Rh during magmatic processes in the mantle similar to Os, Ir and Ru. Abundances of Au in fertile peridotites in some of these studies showed considerably scatter. Correlations of Au with other moderately incompatible elements like Re and Al_2O_3 in a few data sets might indicate incompatible behaviour of Au during magmatic processes (Morgan, 1986; Lorand et al., 1999).

In the present study abundances of Rh, Au and other HSE and for some samples $^{187}Os/^{188}Os$, have been determined in the same digestion aliquot of orogenic peridotites and peridotite xenoliths using isotope dilution and standardization techniques modified from those used by Meisel et al. (2003a).

The main objectives of this study are: i) to place constraints on the abundances of Rh and Au, and their ratios with other HSE, in the mantle, ii) to study their variation with other HSE and lithophile elements and the processes that control these variations, iii) to infer the relative compatibilities of Rh and Au in comparison to other HSE, and to discuss the partitioning of the HSE during magmatic processes in the mantle, and iv) to deduce Rh and Au abundances for a primitive mantle (PM) model composition, to discuss their uncertainties and to place them into the context of the HSE composition of chondritic meteorites.

4.3 Samples

The samples included in this study represent massif-type-peridotites (Pyrenees, Lanzo, Ronda, Totalp), and xenoliths (Hannuoba) that were analyzed previously for Re, Os, Ir, Ru, Pt and Pd concentrations and $^{187}Os/^{188}Os$ using isotope dilution and high-temperature Carius tube digestion (see Becker et al., 2006, and references therein). We report new sets of HSE data for lherzolites from the internal and external Ligurides (IL1, IL2, IL3, EL1), from Beni Bousera (BB3A, BB2C, BB2G), and harzburgite xenoliths from the Leyendecker pit, West Eifel volcanic field (Ley106, Ley108, LeyX1, LeyX2, LeyX3, LeyX4), which have not been studied before. The HSE data obtained for these samples will be compared and discussed along with literature data on samples from the same

localities (Snow et al., 2000; Schmidt and Snow, 2002; Schmidt et al., 2003; Luguet et al., 2004; Pearson et al., 2004). Sample descriptions and petrographic information for these samples are given below. Major and lithophile trace element data are reported in the appendix (4.8.1, Table 4.4).

For more details about samples from the Pyrenees, Lanzo, Ronda and Hannuoba such as localities, petrographic descriptions and geochemical data we refer to previous studies (Bodinier, 1988; Bodinier et al., 1988; Bodinier et al., 1991; Reisberg et al., 1991; Lorand et al., 1993; Reisberg and Lorand, 1995; Pattou et al., 1996; Lorand et al., 1999; Lorand et al., 2000; Gao et al., 2002; Rudnick et al., 2004; Becker et al., 2006; van Acken et al., 2008).

4.3.1 Beni Bousera massif peridotites

The studied Beni Bousera samples are protogranular spinel and garnet lherzolites. They consist mainly of olivine, orthopyroxene, clinopyroxene, spinel (BB3A and BB3G), and garnet (BB2C). The garnet grains are surrounded by a corona structure of kelyphite. Samples BB2C and BB2G are moderately and weakly serpentinized, whereas BB3A is relatively fresh. The latter was in direct contact with a garnet pyroxenite layer and the aliquot used for sample preparation was located a few cm away from the contact zone. All samples have fertile compositions from 3.0 - 3.9 wt.% Al_2O_3, similar to the range reported in Pearson et al. (2004). Major element systematics of peridotites from the Beni Bousera massif are very similar to the Ronda massif and both massifs have been interpreted to reflect residues after varying degrees of melt extraction (Frey et al., 1985; Gueddari et al., 1996; Pearson et al., 2004).

4.3.2 Ligurides peridotites

The Ligurian ophiolites of the Northern Apennines represent remnants of the Jurassic Tethys ocean (Rampone and Piccardo, 2000). Most of the peridotites from the Internal Ligurides (IL) ophiolite complex are clinopyroxene-poor spinel-plagioclase peridotites.

Their depleted chemical and petrographic compositions are interpreted to represent suboceanic asthenospheric mantle residues after MORB extraction (Rampone et al., 1996; Rampone and Piccardo, 2000). In contrast to the IL ophiolite, the External Ligurides (EL) ultramafic complex is interpreted to represent a part of the Proterozoic subcontinental lithospheric mantle, which was tectonically emplaced due to crustal extension (Rampone et al., 1995; Rampone and Piccardo, 2000). Peridotite samples of the EL are mostly less depleted spinel-plagioclase lherzolites as inferred from their major and trace element compositions and modal mineral abundances (Rampone et al., 1995).

The mineral assemblage of the studied samples from the Internal Ligurides (IL1, IL2, IL3) is olivine, orthopyroxene, minor clinopyroxene, minor plagioclase (IL1) and spinel. Sample IL1 is relatively fresh compared to the moderately serpentinized samples IL2 and IL3. Sample IL3 has a mylonitic texture with developed S-C foliation. Al_2O_3 contents range from 1.7 - 2.3 wt.% similar to the results of previous studies (Rampone et al., 1996). The External Ligurides sample EL1 has a protogranular texture consisting of serpentinized olivine, orthopyroxene, clinopyroxene and spinel. It is characterized by a more fertile chemical composition (3.4 wt.% Al_2O_3) similar to previously studied EL peridotites (2.9 – 4 wt.% Al_2O_3) (Rampone et al., 1995).

4.3.3 Eifel xenoliths

Mantle xenoliths from the West Eifel volcanic field are hosted by Quaternary olivine nephelinitic lavas. Samples (Ley106, Ley108, LeyX1, LeyX2, LeyX3, LeyX4) were collected from a quarry (Leyendecker) located at the Meerfelder Maar. The mineral assemblage is olivine, orthopyroxene and minor clinopyroxene, which form a protogranular texture. Most samples contain spinel. In thin sections the xenoliths display evidence for melt migration along grain boundaries. All of the studied samples are harzburgites with low Al_2O_3 contents (1.0 – 1.7 wt.%) indicating moderately high degrees of partial melting.

4.4 Analytical techniques

For sample preparation altered surfaces were cut with a rock saw and cut surfaces were abraded with corundum emery paper. Unweathered fresh looking pieces were crushed into chips using a ceramic jaw breaker. The chips were milled to a fine powder using an agate disc mill.

4.4.1 Major element and lithophile trace element analysis

Major elements, sulphur and carbon contents were determined using XRF (Panalytical^{TM} Axios Advanced) and IR-based C and S analysis (Leco^{TM} CS-225 Determinator) both at the GFZ Potsdam. Reproducibilities (2s) range from 2-3% for SiO_2, MgO and FeO, 5-8% for Al_2O_3 and CaO, 10-20% for Na_2O, TiO_2 and MnO. Accuracy of the data was monitored by the analysis of ultramafic rock standards (DTS-1, PCC-1). The detection limit for S determinations was 50 ppm. Loss on ignition (LOI) was determined gravimetrically after combustion at 1100°C.

4.4.2 Sample digestion and HSE separation

For HSE analysis powder aliquots of about 2 g were weighted into quartz glass digestion vessels and mixed ^{185}Re-^{190}Os and ^{191}Ir-^{99}Ru-^{194}Pt-^{105}Pd spike solutions were added, followed by 2.5 ml conc. HCl and 5 ml conc. HNO_3. The concentrated acids used for decomposition were two times quartz and two times teflon distilled (sub-boiling), respectively. The vessels were sealed with teflon-tape and heated to 320°C in a high-pressure asher (HPA-S, Anton Paar^{TM}) for 6 h. For comparison sample aliquots of the ultramafic reference material UB-N and some sample powders (TUR7, TUR21) were digested using both the HPA-S and a high-temperature Carius tube technique at 320°C as described by Becker et al. (2006).

Gold abundances of the UB-N reference and TUR7 sample powders were also quantified using a standard addition technique. For each respective sample four 2 g

powder aliquots were spiked for isotope dilution analysis and three out of the four aliquots were also doped with about 2 ng, 4 ng and 6 ng Au in ~100-300 µl 6 M HCl using a microbalance and a carefully diluted Alfa Aesar ICP solution. A recalibration of the diluted Au solution with the original Alfa Aesar ICP solution and an additional Merck Certipur solution resulted in differences of only 0.2% and 1.3%, respectively. The samples used for standard addition were digested using Carius tubes. After decomposition the sample solutions were transferred into Savillex beakers and further diluted with 0.5 M HCl to a total weight of 20 g. These solutions were split into two 10 g aliquots, one set of aliquots for ICP-MS analysis of Ir, Ru, Pt and Pd after chemical separation as described below. The second set of aliquots was further diluted with 0.5 M HCl to obtain a 50-fold dilution (1 g sample in 50 g solution) for standard addition analysis. The undissolved and precipitated sample matrices were removed by centrifugation and the solutions were directly analyzed for Au by ICP-MS without chemical separation.

Osmium was extracted immediately after digestion by solvent extraction from the reverse *aqua regia* into CCl_4, back extraction into HBr (Cohen and Waters, 1996), and further purification by microdistillation from a H_2SO_4-dichromate solution into a drop of HBr (Roy-Barman, 1993). For other HSE a separation technique slightly modified from to the one described in Fischer-Gödde et al. (2010a) was applied. About 2-3 ml of the *aqua regia* solution were transferred into a PFA beaker and evaporated to near dryness. To ensure that Rh and Au are completely present as their chloro complex species, the solution was taken to near dryness twice with 2 ml 8.3 M HCl and once with 1 ml 1.25 M HCl. Rhenium, Ir, Ru, Pt, Rh, Pd and Au were separated from the matrix by cation exchange chromatography using 10 ml of pre-cleaned Eichrom™ 50W-X8 (100-200 mesh) resin. The resin was equilibrated with 20 ml 0.5 M HCl-40% acetone (6 ml 0.83 M HCl + 4 ml distilled acetone). The sample solutions were adjusted to the same HCl-acetone concentration before loading onto the columns. The use of acetone prevents the formation of neutral and positive species of Rh and Au during the separation chemistry (Strelow et al., 1971). All HSE were eluted together in 14 ml 0.5 M HCl-40% acetone. Sample solutions of UB-N and a mixed HSE standard solution were used to conduct column calibrations and recovery tests. We found that Ir, Ru, Pt, Pd, Rh and Au showed parallel elution curves, while Re sometimes was slightly shifted to larger acid volumes. In order to test HSE recovery in some samples the remaining matrix elements were eluted from the

resin in 30 ml of 6 M HCl after elution of the HSE fraction. Recoveries were >95% for all HSE.

The eluted HSE fraction was split in half: one split for the analysis of Au, Re, Ir, and Pt, and the other for analysis of Rh along with Ir, Ru, Pt and Pd. Iridium and Pt were analysed in both splits. Before analysis of the Au-Re-Ir-Pt split the acetone was evaporated by placing the beakers onto a hot plate for one hour at 60 °C and for another hour at 80 °C.

Because of the use of 0.5 M HCl during the chemical separation step Cd passed simultaneously with the HSE through the column. To avoid interferences from Cd isotopes on Pd a clean-up procedure using smaller columns filled with 2 ml Eichrom 50W-X8 (100-200 mesh) resin and 0.2 M HCl as the eluting solvent was performed. The Rh-Ir-Ru-Pt-Pd cut was evaporated to near dryness and the residue was taken up in 0.5 ml 0.2 M HCl and loaded onto the column. The eluted HSE fraction was evaporated to near dryness and the residue taken up into 0.28 M HNO_3 for ICP-MS analysis.

4.4.3 Mass spectrometry

Osmium isotopic compositions were measured by negative thermal ionisation mass spectrometry using a Thermo-Finnigan™ Triton at Freie Universität Berlin. Measured ratios were corrected for isobaric OsO_3^- interferences. Mass fractionation was corrected for using $^{192}Os/^{188}Os = 3.0827$. Values and long-term reproducibility for $^{187}Os/^{188}Os$ of the UMD Os standard solution were 0.11379 ± 0.00005 (2s, n=25) on Faraday cups and 0.1138 ± 0.0003 (2s, n=8) for measurements with secondary electron multiplier. Os concentrations were determined by isotope dilution.

All other HSE were measured by sector-field inductively coupled plasma mass spectrometry using the ThermoElectron™ Element XR equipped with an ESI™ SC-autosampler at Freie Universität Berlin. Concentrations of Re, Ir, Ru, Pt and Pd were determined by isotope dilution (ID) analysis. Signals were detected on a secondary electron multiplier operating in pulse counting mode at low resolution. One analysis consists of 100 measurements (runs), each comprised of 3 scans (i.e. 300 scans in total) of the following analyte and interfering isotope masses: 99, 101, 102, 104 (Ru), 103 (Rh),

105, 106, 108, 110 (Pd), 111 (Cd), 185, 187 (Re), 189 (Os), 191, 193 (Ir), 194, 195, 196, 198 (Pt), 197 (Au), 199 (Hg). Each mass was integrated for 45 ms during each scan. The HSE spike isotopes ^{185}Re, ^{191}Ir, ^{99}Ru, ^{194}Pt and ^{105}Pd were not affected by isobaric interferences. Of the other isotopes used for concentration calculations, only ^{108}Pd was significantly affected by ^{108}Cd (^{106}Pd and ^{110}Pd are also interfered by Cd isobars, but were not involved in data reduction). Corrections for the interference on ^{108}Pd were always conducted but minor (<1%) in most cases. Internal precision of measured isotopic ratios ranged from 0.1 to 1% ($2\sigma_m$, with n=100).

The two splits derived from column chemistry were run with different sample introduction setups. The Au-Re-Ir-Pt split was analyzed from an approximately 1 M HCl solution using a glass spray chamber (either cyclonic or Scott-type). The Rh-Ir-Ru-Pt-Pd split was run with an Aridus membrane desolvator, which reduced oxide rates and increased signal intensities. While the glass spray chamber setup yielded better reproducibilities for Au and Re, the setup with the Aridus was required for precise and accurate Ru-Rh-Pd data, obviously due to reduced interferences in this mass range. Sample solutions were introduced using a Glass Expansion™ MicroMist nebulizer or an ESI™ PFA microconcentric nebulizer in self-aspirating mode. Uptake rates of the analysed solutions were 80-140 µl/min depending on the nebulizer and tubing used. Acid blank solutions were measured at the start of each measurement session and after every 3-4 sample solutions to control background intensities and memory effects. Background corrections were carried out, if the background intensities were >1% of the sample intensities. At the start, in the middle and at the end of each measurement session a Re, Ir, Ru, Pt, Rh, Pd, Au standard solution with roughly chondritic relative HSE abundances and ~1 ppb Ir was measured. Mass fractionation was determined and corrected for by the comparison of the isotope ratios measured in the standard solution with IUPAC reference values. The long-term external reproducibility of uncorrected isotopic ratios in the standard solution is <1% (1s).

For the concentration determination of the monoisotopic Rh and Au a combined internal-external standardization technique was used similar to that employed by Meisel et al. (2003a). The calculation of Rh and Au concentrations were conducted by standardisation to the ^{101}Ru and ^{193}Ir signal intensities and the Ru and Ir abundances as inferred by isotope dilution. For Au determinations calculations based on ^{193}Ir provided

the best reproducibility. For Rh calculations based on ^{101}Ru were most reproducible. The concentration of Au (or Rh in analogy) was calculated according to:

$$Au_{sample}\ [ng/g] = (Ir_{sample}\ [ng/g] / RF) \times (^{197}Au\ [cps] / {}^{193}Ir_{corrected}\ [cps])_{samplesolution} \quad (1)$$

where Au_{sample} is the Au concentration of the sample, Ir_{sample} the Ir concentration of the sample determined by isotope dilution analysis, ^{197}Au [cps] corresponds to the count rate in counts per second (cps) obtained for the sample solution from ICP-MS analysis, and $^{193}Ir_{corrected}$ [cps] represents the count rate in the sample solution corrected for the contribution from the spike added for isotope dilution analysis. The response factor RF which corresponds to the relative intensities of ^{197}Au/^{193}Ir and ^{103}Rh/^{101}Ru for a given concentration was inferred from the analysis of the external HSE standard solution with known abundances:

$$RF = (^{197}Au\ [cps] / Au\ [ng/g]) / (^{193}Ir\ [cps] / Ir\ [ng/g]) \quad (2)$$

where ^{197}Au [cps] and ^{193}Ir [cps] are the count rates (in cps) obtained for the HSE standard solution, and Au [ng/g] and Ir [ng/g] correspond to the concentrations in the standard solution.

Total chemistry blank levels for Carius tube digestions were 19±10 pg Re, 7±3 pg Os, 1±1 pg Ir, 12±1 pg Ru, 280±85 pg Pt, 45±6 pg Rh, 30±15 pg Pd, 11±6 pg Au (n = 3). For digestions using the HPA-S total chemistry blank levels were substantially reduced to 9±2 pg Re, 2±2 pg Os, 0.5±0.3 pg Ir, 2±1 pg Ru, 9±6 pg Pt, 2±2 pg Rh, 21±12 pg Pd, 7±6 pg Au (n=14). Improved chemistry blanks reflect both lower blank levels in the quartz glass HPA-S reaction vessels and improvements in the purification of reagents. Blank corrections were always applied and usually insignificant (<1%), except for some extremely depleted Eifel xenoliths, where blank corrections were <25% for Re, <15% for Au, <5% for Pd and Rh, <3% for Os and Pt, and <1% for Ir and Ru. Somewhat higher blank corrections were also necessary for Re (<8%) concentration determinations for samples digested using the Carius tube technique. Although the Carius tube digestions showed elevated Pt blank levels in comparison to the HPA-S digestions, the blank correction for Pt was still insignificant (<1%) for the samples digested using Carius tubes.

4.4.4 Data quality and comparison to literature data

4.4.4.1 Isotope dilution and standardization analysis

Accuracy and reproducibility of the method were tested using repeated analysis of the UB-N reference powder and by comparison of these data with data obtained in other studies (Table 4.1). HSE abundances of Os, Ir, Ru, Pt and Pd for UB-N determined by isotope dilution (ID) are reproducible within 3.4-7.0 % (1s). Rhenium abundances in the present study are less reproducible (within 13 %) compared to other studies. Ratios of HSE obtained for UB-N by ID in this study compare well with previously reported ID data (Table 4.1). Rhodium and Au abundances determined by combined internal-external standardization are reproducible to 10% and 17% (1s, n=11), respectively. If two unusually low Au determinations for UB-N are excluded from the mean, Au abundances are reproducible within 8 % (1s). The unusually low Au values deduced for two of our UB-N splits were confirmed by repeated chemical separation and analysis of the same digestion aliquot, which agreed within <10%. The average Au concentration for UB-N determined by standardization to Ir after chemical separation is 1.49 ± 0.26 ng/g (1s, n=11, including all Au data obtained by standardization from Table 4.1) and 1.59 ± 0.12 ng/g (1s, excluding the two unusually low Au values).

Replicate analysis of sample powders were conducted for 18 samples (Table 4.2). The reproducibilities from replicate analysis of sample powders for HSE abundances determined by ID is usually <5%, except for Re which is somewhat less reproducible within <10% (25% for TUR14). Rhodium concentrations of replicates reproduce within <8% (1s), except TA15 (17%). The reproducibility of Au is <15% (1s) for most samples, except for 71-107 (33%) and L732a (38%). Overall HSE abundances from replicate determinations of samples are in accordance with the reproducibility deduced for UB-N (Table 4.1).

For replicate samples where Au determinations displayed poor reproducibility, Au was re-analyzed from the same digestion aliquot. These repeated Au determinations in all cases confirmed the previous results within the stated reproducibility of the UB-N reference powder or better. Because of the high molarity of acids used for digestion, we consider the possibility of Au loss due to precipitation during digestion to be unlikely.

Thus, inhomogeneity of sample powders may be the most likely explanation for variable results obtained on repeat digestions of samples.

4.4.4.2 Standard addition analysis

Gold in UB-N and sample TUR 7 was also analyzed by the standard addition technique. In order to account for the drift during the standard addition analysis, Au signals were normalized to ^{193}Ir and ^{209}Bi measured in the sample solution. Normalization to Ir and Bi yielded $1.49^{+0.05}_{-0.04}$ ng/g and $1.51^{+0.11}_{-0.07}$ ng/g for UB-N, and $1.34^{+0.20}_{-0.11}$ ng/g and $1.36^{+0.13}_{-0.08}$ ng/g for TUR 7, respectively (2s, n=4). Very good correlations were obtained despite independent digestions for each aliquot, suggesting that Au/Ir and Au/Bi were homogeneous at the 2 g sample aliquot scale and that the digestion method yields reproducible results. More details about the regression calculations are provided in the appendix (4.8.2).

Within stated uncertainties, the Au abundances obtained by standard addition analysis are indistinguishable from the results obtained by standardization to Ir after chemical separation. While standard addition analysis yielded valuable data, its use for routine applications is hampered by the high matrix loading introduced to the mass spectrometer, prolonged analysis times and time consuming sample preparation.

4.4.4.3 Comparison to literature data

The Au concentration for UB-N determined in this study is most comparable to the value of 1.6 ± 0.5 ng/g (2s) reported by Korotev (1996) deduced by instrumental neutron activation (INAA), but lower by a factor of ~2 in comparison to values obtained by other groups using either neutron activation (NAA) or graphite furnace atomic adsorption spectroscopy (Table 4.1) (Bornhorst et al., 1984; Benedetti et al., 1987; Terashima, 1988; Lorand et al., 1989; Bédard and Barnes, 2002; Constantin, 2008). Our results from both the chemical separation and the standard addition analysis indicate that Au abundances and Au/Ir ratios are generally well reproducible for UB-N. The two UB-N aliquots with deviating Au abundances may reflect heterogeneity of the sample powder. Our mean Rh concentration of 1.10 ± 0.21 ng/g (2s, n=11) obtained for UB-N is in excellent agreement with the Rh value of 1.12 ± 0.12 ng/g (2s) reported by Meisel et al. (2003a) and Meisel and Moser (2004), and the value of 1.25 ± 0.30 ng/g reported by Lorand et al. (2009).

Many samples analyzed in this study were previously analyzed for $^{187}Os/^{188}Os$ and Re, Os, Ir, Ru, Pt and Pd abundances by Becker et al. (2006), using isotope dilution (ID) combined with a high-temperature Carius tube digestion technique and separation of Re, Ir, Ru, Pt and Pd by anion exchange. Because both data sets agree within a few % (appendix 4.8.3, Fig. 4.11) the values reported by Becker et al. (2006) are also included in the figures together with precise ID data obtained on samples from the same localities using high-temperature acid digestion techniques (Meisel et al., 2003a; Meisel and Moser, 2004; Pearson et al., 2004; Luguet et al., 2007; Lorand et al., 2008; Lorand et al., 2010). Some of the samples from Lanzo, Pyrenees (Lherz and Turon de Técouère) and Rhonda were previously analyzed for Rh and Au using fire assay pre-concentration techniques followed by ICP-MS or INAA analysis (Lorand et al., 1993; Pattou et al., 1996; Lorand et al., 1999; Lorand et al., 2000). A comparison between our data and data from the literature is given in the appendix (4.8.3).

4.5 Results

Whole rock major element analysis for new samples from Beni Bousera, the Ligurides and Eifel are listed in the appendix (4.8.1, Table 4.4). The Beni Bousera samples (BB3A, BB2C, BB2G) have fertile compositions ranging from 3.0 to 3.9 wt.% Al_2O_3. Good correlations are displayed among lithophile moderately incompatible elements such as Al, Ca and Ti. An unusual high sulphur abundance of 407 ppm is observed for BB2C. The samples from the internal Ligurides (IL1, IL2, IL3) have experienced moderate degrees of melt extraction indicated by their Al_2O_3 contents ranging from 1.7 to 2.3 wt%, while our sample from the external Ligurides (EL1) has a more fertile composition. The Ligurides samples show good positive correlations between Al_2O_3 and S. The Eifel xenoliths have low Al_2O_3 contents typical for harzburgitic compositions. Lithophile moderately incompatible elements correlate well with each other (e.g. Al and Ca) and are anticorrelated with Mg. The Eifel samples are further characterized by low H_2O contents and low S abundances which are below the detection limit (<50 ppm S).

In conjunction with the results of previous studies on samples from the same localities (Lorand et al., 1993; Lorand et al., 1999; Lorand et al., 2000; Snow et al., 2000; Gao et al., 2002; Schmidt et al., 2003; Luguet et al., 2004), it can be concluded that S abundances of massif-type peridotites and the Hannuoba xenolith suite are positively correlated with Al_2O_3 contents. Sulphur abundances of some Eifel xenoliths show a more scattered covariation of S and Al_2O_3 (Schmidt and Snow, 2002; Schmidt et al., 2003).

For reasons of consistency and to exclude scatter induced by less precise analytical techniques, HSE data shown in the figures are those of the present work and previous data obtained by similar techniques on samples from the same locales. In accordance with previous studies concentrations of Ir, Os and Ru correlate well with each other (not shown, e.g. Pearson et al., 2004, and references therein). Rhodium correlates positively with Ir and Pt (Fig. 4.1a,c). Samples from Lherz and the Eifel tend to plot towards lower Pt/Ir in the Pt vs. Ir diagram. These samples also show distinct trends in other variation diagrams (Fig. 4.1), which reflects lower Pd and Pt for a given Ir or Rh abundance compared to other peridotite suites. Lower Pd and Pt abundances relative to Ir and Rh are also observed for the Lherz samples analyzed by Luguet et al. (2007) and Lorand et al. (2010), but not for samples from Turon de Tecouere from the Western Pyrenees (this study, Becker et al., 2006, and references therein). Abundances and ratios of Rh, Ir, Ru and Os are neither correlated with Pd, Re and Au (e.g. Fig. 4.1d), nor with lithophile melt extraction indicators (e.g. Al_2O_3) and S contents. Fertile lherzolites display relatively constant Rh concentrations and constant Rh/Ir around 0.34 (Fig. 4.2). Samples with <2.5 wt% Al_2O_3 show slightly more variable Ru/Ir and Os/Ir than fertile samples and gradually decreasing ratios of Rh/Ir (Fig. 4.2) and Pt/Ir. Some of the Eifel xenoliths (LeyX3 and Ley106) contain very little Ir and Os, thus resulting in more strongly suprachondritic Ru/Ir and Rh/Ir than other samples. Only few samples from this study and the literature display ratios deviating from these general trends, most probably reflecting sample heterogeneity or redistribution of HSE during secondary processes (Rehkämper et al., 1999a; Becker et al., 2006). The Lanzo sample L215 is depleted in Ir relative to other HSE and for 86-V2 from Lherz an elevated Os concentration is noted (this study and Becker et al., 2006). Lanzo sample L9 has a somewhat higher Rh concentration.

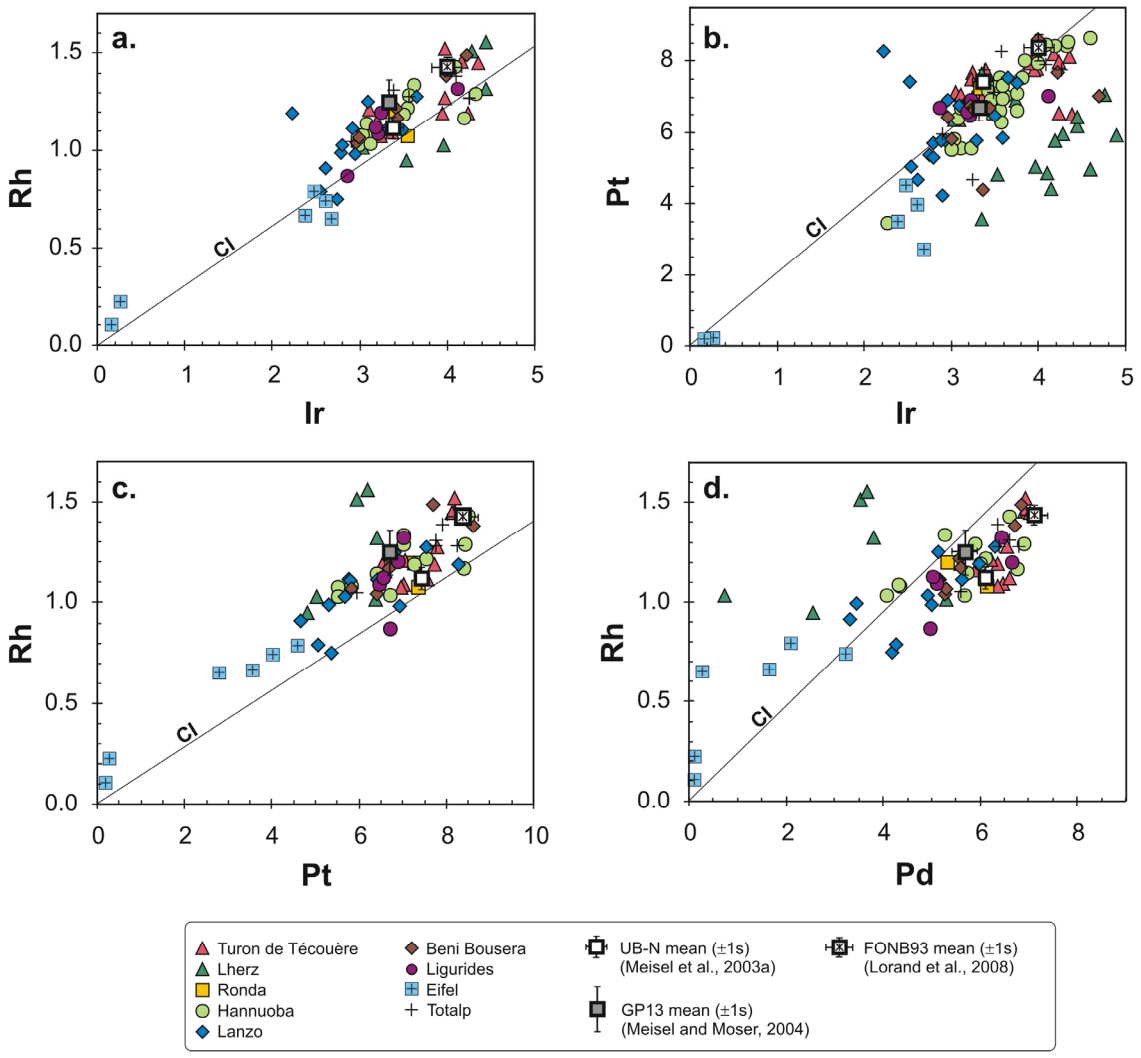

Fig. 4.1. Element variation diagrams of Rh vs. Ir, (a) Pt vs. Ir, (b) Rh vs. Pt (c), and Rh vs. Pd (d). Only data obtained by high-temperature acid digestion are displayed for samples from the same locales. Rhodium is best correlated with Ir and Pt. Platinum abundances are correlated with Ir. Compared to other peridotite suites samples from Lherz and Eifel define a different trend at lower Pt/Ir, higher Rh/Pt and Rh/Pd, and somewhat lower Rh/Ir. CI chondrite ratios (CI) are shown for reference (Fischer-Gödde et al., 2010a, and references therein). Peridotite data shown from this study, Meisel et al. (2003a), Meisel and Moser (2004), Pearson et al. (2004), Becker et al. (2006), Luguet et al. (2007) and Lorand et al. (2008). Data from this study, Pearson et al. (2004), Becker et al. (2006) and Luguet et al. (2007) for samples from the same localities are shown using the same symbols.

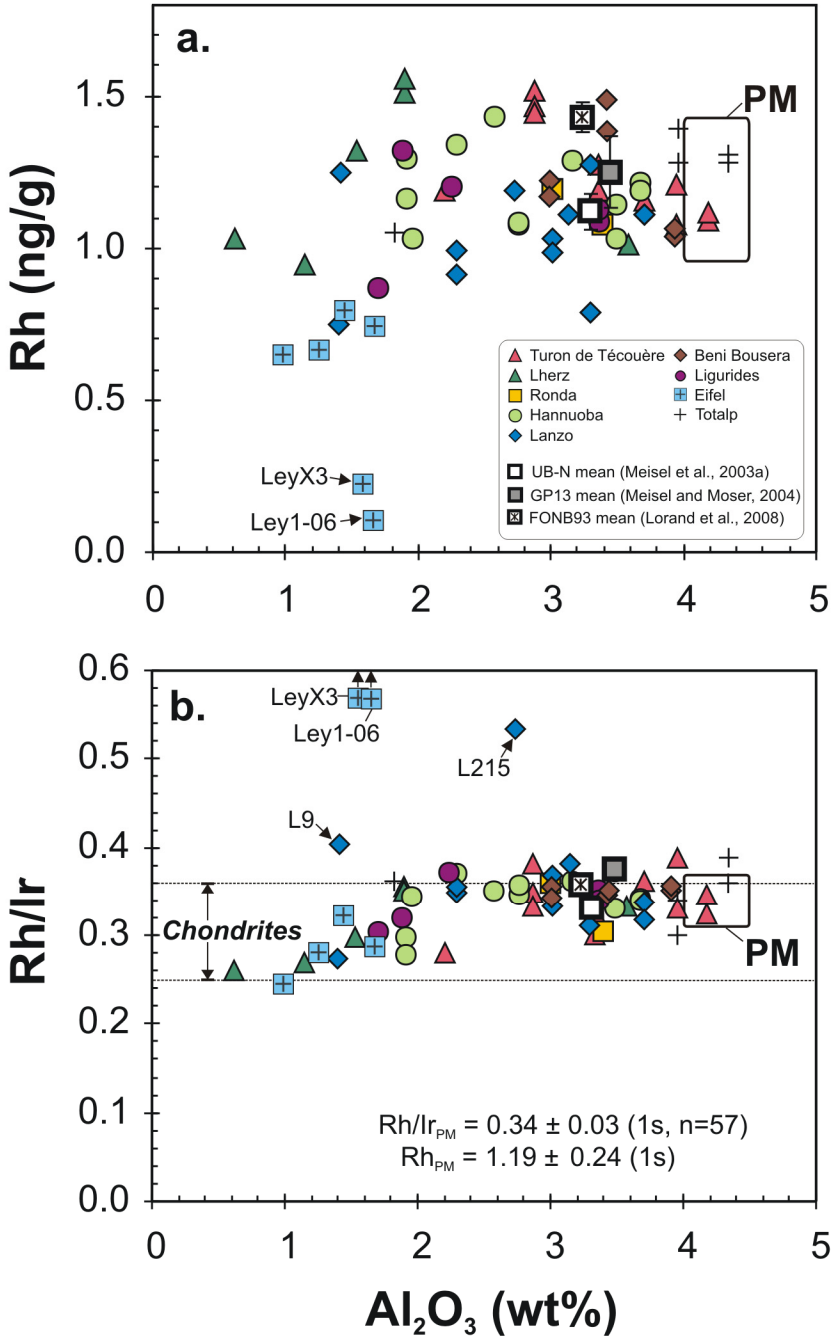

Fig. 4.2. Rh and Rh/Ir vs. Al_2O_3. Rhodium abundances and Rh/Ir are constant over a wide range of compositions and slightly decrease in melt depleted peridotites. Two of the Eifel xenoliths are extremely depleted in Ir and hence plot towards high Rh/Ir. The box delineates the inferred Rh abundance and Rh/Ir of the primitive mantle (PM). Peridotite data shown from this study, Meisel et al. (2003a), Meisel and Moser (2004) and Lorand et al. (2008). Horizontal dashed lines correspond to the range of Rh/Ir ratios observed for chondritic meteorites (Fischer-Gödde et al., 2010a).

As in previous studies (Gao et al., 2002; Pearson et al., 2004; Becker et al., 2006; Liu et al., 2009), concentrations of Pd, Re and Au, and their ratios to Ir or Os display positive correlations with Al_2O_3 and other lithophile melt extraction indicators, although afflicted with substantial scatter in some cases (Figs. 4.4 and 4.5). Ratios of Pd/Ir seem to be relatively constant for the most fertile peridotite compositions but decrease substantially with increasing degree of melt extraction for compositions <2.5wt% Al_2O_3 (Fig. 4.5c). Rhenium and ratios of Re/Ir, Re/Os and $^{187}Os/^{188}Os$ are well correlated with Al_2O_3 confirming previous data (Fig. 4.5d, Reisberg and Lorand, 1995; Meisel et al., 1996; Meisel et al., 2001; Gao et al., 2002; Pearson et al., 2004; Becker et al., 2006). Measured $^{187}Os/^{188}Os$ ratios are consistent with long-term Re depletion due to partial melt extraction at various times (Reisberg and Lorand, 1995; Meisel et al., 2001). The $^{187}Os/^{188}Os$ of Eifel xenoliths range from 0.1146 to 0.1226 and correspond to Re depletion ages (T_{RD}) between 1-2 Ga, which overlap at the lower end with the T_{RD} ages reported for Eifel xenoliths analyzed by Schmidt and Snow (2002), underscoring the heterogeneous nature of the underlying mantle domain beneath the Eifel volcanic field. Osmium isotopic compositions determined for the Ligurides samples are comparable to $^{187}Os/^{188}Os$ reported by Snow et al. (2000). Some samples from the Ligurides, Totalp and Beni Bousera display higher $^{187}Os/^{188}Os$ than expected for their Al_2O_3 content. Such samples may have been affected by addition of radiogenic Os during melt percolation processes (Chesley et al., 1999; Brandon et al., 2000; Becker et al., 2001b; Büchl et al., 2002; Becker et al., 2006; van Acken et al., 2008).

Gold concentrations and Au/Ir correlate with peridotite fertility (Fig. 4.4), but are more variable at a given Al_2O_3 content compared to Pd/Ir and Re/Ir. Fertile lherzolites display Au/Ir ranging from 0.20-0.65, while melt depleted harzburgites from Lherz and Eifel have Au/Ir <0.2. Deviations displayed by some samples in Figs. 3 and 4 are either caused due to high Au concentrations (71-107, L215) or unusually low Ir contents (Ley1-06). Gold is almost linearly correlated with Re (Fig. 4.3c, Morgan, 1986), although with substantial scatter at high concentrations. Plots of Re vs. Pd, and Au vs. Pt and Pd display non-linear positive correlations (Fig. 4.3a,b,d). HSE which are positively correlated with aluminium content also correlate with S, although with some scatter.

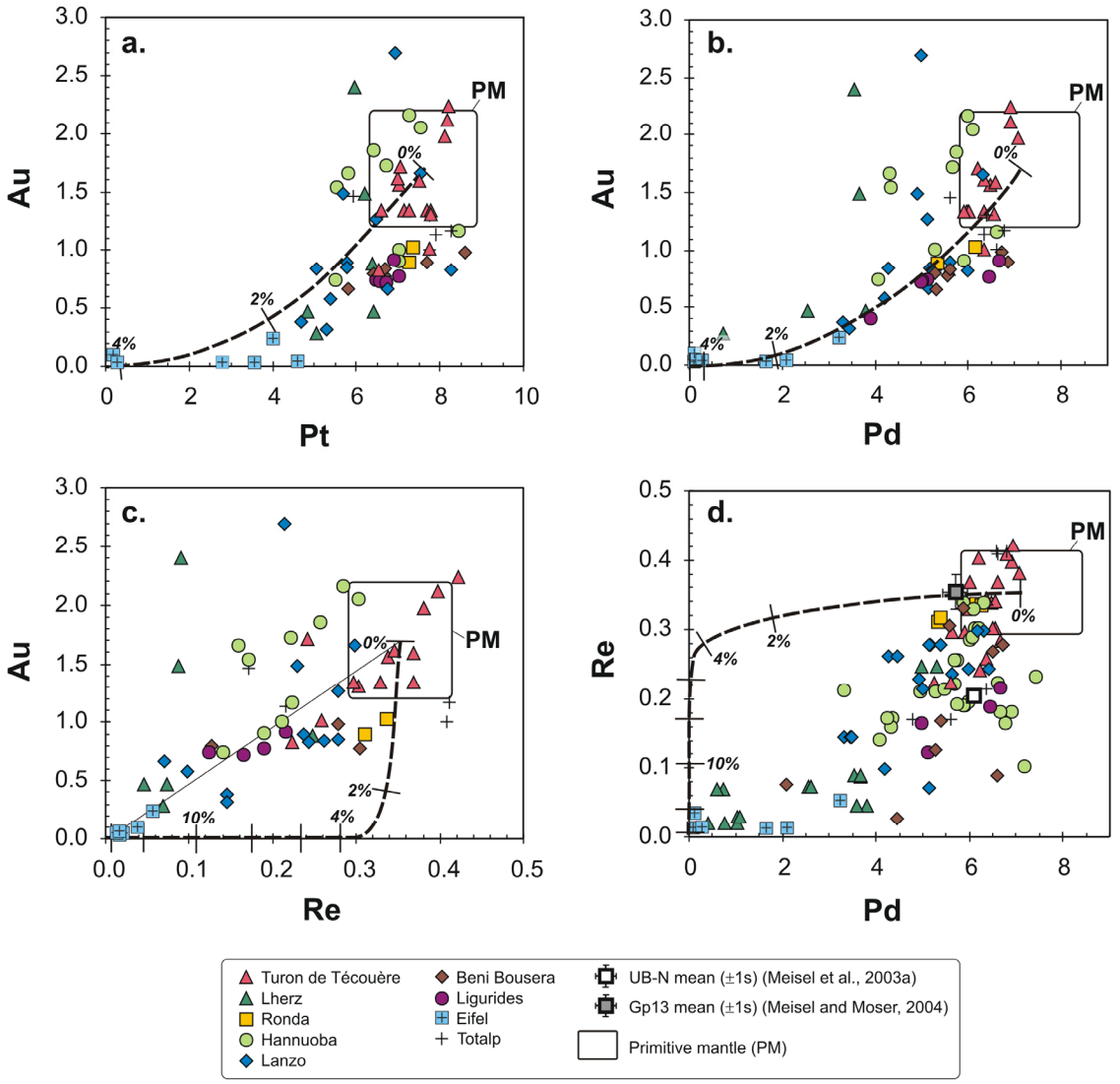

Fig. 4.3. Element variation diagrams of Au vs. Pt (a), Au vs. Pd (b), Au vs. Re (c), and Re vs. Pd (d). Gold is almost linearly correlated with Re, suggesting similar partitioning behaviour of both elements during magmatic processes in the mantle. The correlation between Re and Au is used to infer the primitive mantle (PM) model composition of Au via linear regression. Dashed lines in the diagrams refer to a fractional melting model in 2% increments from a PM initial composition as described in text. Gold, Pt, Pd and Re were modelled using monosulphide solid solution (mss)-sulphide liquid (sl) partition coefficients $D^{mss\text{-}sl}$ according to the literature (Fleet et al., 1993; Brenan, 2002; Mungall et al., 2005; Ballhaus et al., 2006). Data shown from this study, and additional Re and Pd data in d) from Meisel et al. (2003a), Meisel and Moser (2004), Pearson et al. (2004), Becker et al. (2006) and Luguet et al. (2007). Data from this study, Pearson et al. (2004), Becker et al. (2006) and Luguet et al. (2007) for samples from the same localities are shown using the same symbols.

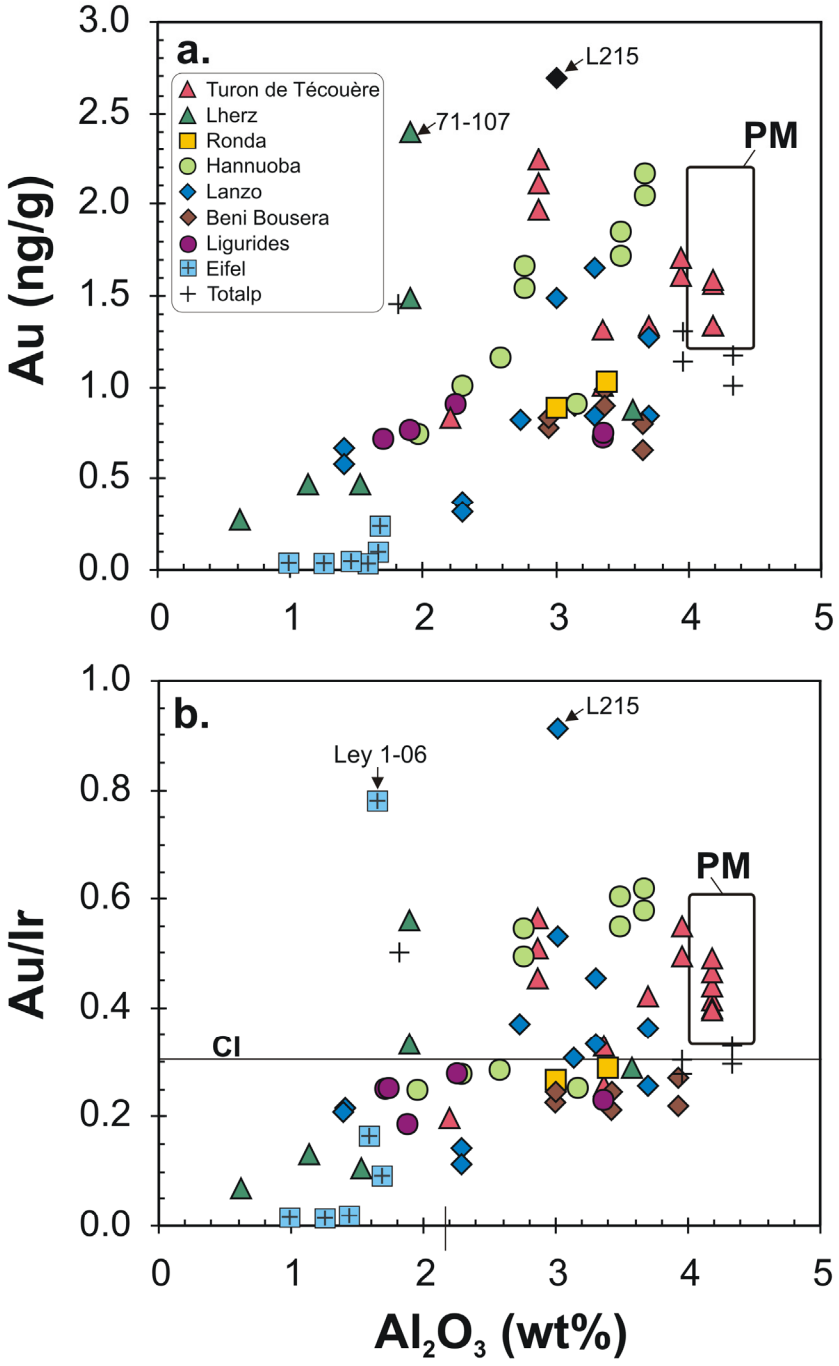

Fig. 4.4. Au and Au/Ir vs. Al_2O_3. Gold abundances and Au/Ir vary as a function of Al content, indicating incompatible behaviour in the mantle. The box delineates the inferred Au abundance and Au/Ir of the primitive mantle (PM). Horizontal line in b) corresponds to the Au/Ir ratio inferred for CI chondrite (Fischer-Gödde et al., 2010a, and references therein). The Au/Ir –Al_2O_3 trend of peridotites would be consistent with moderately incompatible behaviour of Au during fractional melting, or alternatively with refertilization models.

4.6 Discussion

4.6.1 Reproducibility and accuracy of Rh and Au determinations

In order to asses reproducibility and accuracy of the analytical methods and the homogeneity of sample powders replicate analyses were conducted for UB-N (n=11) and 18 sample powders (Tables 4.1 and 4.2). The Rh and Au concentration determinations for most samples are reproducible within 10% and 15%, respectively, while other HSE determined by ID are reproducible within <7%, except Re (<13%). The Rh abundances obtained for the UB-N ultramafic reference are in excellent agreement with the results of Meisel et al. (2003a), Meisel and Moser (2004) and Lorand et al. (2009), indicating that Rh abundances show only limited variation in the sample powder, comparable to other HSE determined by isotope dilution. A relatively homogeneous distribution of Rh within the powders is also indicated from replicate determinations for sample powders (Table 4.2). The Rh abundances and Rh/Ir obtained in this study compare well with previously reported values obtained using either combined ID and standardization ICP-MS analysis (Figs. 4.1 and 4.2, Meisel et al., 2003a; Meisel and Moser, 2004) or NiS fire-assay preconcentration combined with external standardization ICP-MS analysis (Pattou et al., 1996; Luguet et al., 2004; Lorand et al., 2009; Lorand et al., 2010). Rhodium data reported for peridotite xenoliths by Handler and Bennett (1999) are systematically higher compared to the results of other studies. Suprachondritic Rh/Ir of some mantle peridotites from previous studies using INAA (Lorand et al., 2000; Snow et al., 2000; Schmidt et al., 2003) seem to be biased by the analytical technique as discussed below and in the appendix (4.8.3) and could not be confirmed by the present work on the same or similar samples.

In the case of Au, our results for UB-N show that Au abundances are somewhat less reproducible compared to Rh and other HSE. Replicate analyses of some sample powders (71-107, L217, L732a) indicate a heterogeneous distribution of Au within those powders. A comparison between Au abundances for UB-N obtained in this study with data from the literature reveals differences of a factor about ~2, exceeding by far the reproducibility of

our method. Most of the previous studies using INAA, RNAA or atomic adsorption techniques reported a Au abundance clustering around a value of ~3 ng/g for UB-N, compared to 1.49 ± 0.26 ng/g (1s, n=11) obtained in this study. The most comparable reported Au value of 1.6 ng/g obtained by INAA (Korotev, 1996) is reproducible within 10-30%. A comprehensive study of Constantin (2008) including 70 reference materials analyzed by INAA report a reproducibility for Au determinations of 20-50% (57% in particular for 14 UB-N aliquots) for samples with Au contents <10 ng/g, while the reproducibility was usually better than 10% for samples with Au >10 ng/g. They suggested that sample heterogeneity is the most probable reason for the observed variability at a sample size of 2-3 g. The relative standard deviations for Au determinations by GF-AAS was reported to be 30% at the 0.3 to 8 ng/g level (Terashima, 1988), and the limit of determination was reported to be 3 ng/g (Benedetti et al., 1987). Less reproducible Au abundances obtained using NiS preconcentration techniques on 15 g powder aliquots combined with ICP-MS analysis were also reported by Pattou et al. (1996), Lorand et al. (1999) and Luguet et al. (2004). Because the variability for replicate Au determinations on a 2 g sample aliquot scale from this study is significantly reduced compared to the previously reported variation, we suggest that the Au abundances determined by standardization in combination with ID ICP-MS analysis produces more reliable and precise data for a concentration range <10 ng/g Au.

4.6.2 Serpentinization, hydrothermal alteration and other secondary processes

4.6.2.1 Serpentinization, hydrothermal alteration and weathering

In this study no systematic relationship between HSE abundances and the degree of serpentinization was observed. The degree of serpentinization is inferred from the H_2O content, which is estimated from the weight loss on ignition (LOI, Table 4.4 in the appendix 4.8.1). Because peridotites with variable degrees of serpentinization show relatively constant Os/Ir, Ru/Ir and Rh/Ir over a range of Al_2O_3 compositions and also display positive correlations between $^{187}Os/^{188}Os$, Re/Os, Re/Ir, Pd/Ir and Au/Ir with Al_2O_3 (Figs. 4.2, 4.4 and 4.5, Reisberg and Lorand, 1995; Meisel et al., 2001; Gao et al.,

2002; Pearson et al., 2004; Becker et al., 2006), we infer that HSE abundances are not or only weakly affected by serpentinization processes. We also find no systematic correlation between the degree of serpentinization and Au abundances, consistent with observations by Lorand et al. (1989). For example the Ligurides samples IL1, IL2 and IL3 display a range of LOI contents from 0.7-6.5 wt.% and different degrees of serpentinization in thin sections, but their average Au abundance of 0.80 ± 0.10 ng/g (1s) is relatively constant combined with a narrow range in Al_2O_3 contents (1.7-2.3 wt.%). The same observation applies to the Beni Bousera samples, which show a narrow range in Au abundances (0.83 ± 0.11 ng/g) and aluminium contents (3.0-3.9 wt.%), but are affected by different extents of serpentinization. Most previous studies have also concluded that HSE abundances and Re-Os isotope systematics are not strongly affected by serpentinization, mainly because of the prevailing reducing conditions (Snow and Schmidt, 1998; Rehkämper et al., 1999a; Büchl et al., 2002; van Acken et al., 2008). Possible effects of alteration processes under more oxidizing conditions such as weathering were inferred from studies on abyssal peridotites and seem to affect mainly Pd and Re abundances, while Os, Ir, Ru and Pt remain largely unaffected (Luguet et al., 2003; Liu et al., 2009).

In the case of Au, redistribution by hydrothermal fluids is a well known process for the generation of hydrothermal and epithermal ore deposits (e.g. Williams-Jones et al., 2009). The dissolution and precipitation of Au in hydrothermal fluids is basically controlled by HS^- and Cl^- ligands, and depends on temperature, pH, and the activities of HS^- and Cl^-, and fO_2 (Henley, 1973; Seward, 1973; Stefánsson and Seward, 2003).

Although Au and Au/Ir correlate with Al_2O_3 (Fig. 4.4) and with Re (Fig. 4.3c), we can at present not rule out that peridotite samples plotting towards higher or lower Au/Ir for a given Al_2O_3 content may have gained or lost some Au due to secondary redistribution processes. In order to asses the possibility of Au loss caused by circulating hydrothermal fluids it is instructive to study the variation of Au with other fluid-mobile elements. For example Sr abundances for most peridotite samples from Hannuoba, Ligurides and Beni Bousera plot along on a correlation line which passes through the estimated Sr/Al of the primitive mantle composition, indicating that Sr in these samples was not strongly mobilized due to aqueous solutions. Gold abundances of peridotites from the Hannuoba xenolith suite and the Internal Ligurides are well correlated with Sr abundances (Sr data from this study (Table 4.4 in the appendix 4.8.1) and for Hannuoba xenoliths from Gao et

al., 2002). In contrast lherzolite samples from Beni Bousera and the External Ligurides may have lost Au relative to Sr and also plot at lower Au/Ir ratios for a given Al_2O_3 content. Whether the covariation of Au and Sr is diagnostic is difficult to evaluate, because we do not have Sr concentration data for all of the studied samples, or reliable data for other fluid-mobile trace elements. A comparison of Au and Sr is further hampered by their different geochemical affinities.

4.6.2.2 Secondary processes affecting HSE abundances of peridotite xenoliths

In comparison to data from massif-type peridotites some peridotite xenoliths from this study and the literature show systematic deviations for abundances and ratios of some HSE. For example Eifel xenolith samples LeyX3 and Ley106 are extremely depleted in all HSE except Ru and Rh (Fig. 4.6b), and some xenoliths show low Os/Ir (LeyX2, Ley106) compared to massif peridotites. Low sulphur contents (<50 ppm) combined with lower Os/Ir as observed for Eifel xenoliths is also known from other xenolith peridotite suites and has been interpreted in some cases to reflect late stage mobility of S due to sulphide breakdown during emplacement of the host lava or sulphide weathering (Lorand, 1990; Chesley et al., 1999; Handler and Bennett, 1999; Handler et al., 1999; Pearson et al., 2004; Ackerman et al., 2009; Rudnick and Walker, 2009). Sulphide breakdown in peridotite xenoliths during emplacement and concurrent alteration of HSE abundances may be a more widespread secondary process than previously recognized, and may contribute to a possible bias of the abundances of Os and Ir towards low values in peridotite xenoliths (e.g. Pearson et al., 2004; Reisberg et al., 2005). In such cases it may be difficult to distinguish HSE compositions affected by secondary processes from primary mantle signatures. Some xenolith suites seem to be unaffected by late stage S loss, like the Hannuoba xenoliths (China) where sulphur and HSE abundances are comparable to massif-type peridotites (Gao et al., 2002; Becker et al., 2006).

4.6.3 HSE behaviour during magmatic processes in the mantle

4.6.3.1 Empirical partitioning behaviour of HSE during magmatic processes in the mantle

The relative partitioning behaviour of HSE during magmatic processes in the mantle can be deduced from their abundances in fertile and melt depleted peridotites relative to lithophile melt depletion indicators but also from their relative abundances in mantle derived sulphur undersaturated magmas such as komatiites (Morgan and Lovering, 1967; Jagoutz et al., 1979; Morgan, 1986; Brügmann et al., 1987; Puchtel and Humayun, 2000; Morgan et al., 2001; Pearson et al., 2004; Puchtel and Humayun, 2005; Becker et al., 2006; Maier et al., 2009; Puchtel et al., 2009). It is generally accepted that Os, Ir and Ru are compatible in the mantle residuum during partial melting of the mantle as indicated by their high abundances and the lack of correlation with lithophile melt extraction indicators in peridotites. Work on fertile peridotites suggests that Rh and Pt also may behave compatibly in the mantle (Figs. 4.2 and 4.5e). In some suites of peridotites Pd, Re and Au display positive correlations with Al_2O_3, indicating moderately incompatible behaviour (Figs. 4.4 and 4.5, Morgan, 1986; Lorand et al., 1999; Pearson et al., 2004; Becker et al., 2006). Element variation diagrams show significant correlations for element pairs of similar compatibility like Rh-Pt (Fig. 4.1), Pt-Pd (not shown) and Re-Au (Fig. 4.3c). Different slopes and shapes of curves in Figs. 4.1 and 4.3 reflect relative differences in compatibility during magmatic processes in the mantle. The relative partitioning behaviour indicated in Figs. 1-5 in conjunction with the results of previous studies (e.g. Pearson et al., 2004; Becker et al., 2006) yield apparent bulk peridotite-melt partition coefficients during magmatic processes in the mantle according to the following sequence: $Re \leq Au < Pd < Pt \leq Rh < Ir \leq Ru \leq Os$. This sequence is approximately consistent with the relative enrichment of these elements in basalts and komatiites. In detail, basalt data indicate that Re may be more compatible than Au, Pt more compatible than Rh, and in many cases Ir may be more compatible than Ru (e.g. Hertogen et al., 1980; Brügmann et al., 1987; Hauri and Hart, 1997; Rehkämper et al., 1999b; Puchtel and Humayun, 2000; Bézos et al., 2005; Puchtel and Humayun, 2005; Dale et al., 2008; Maier et al., 2009; Puchtel et al., 2009).

4.6.3.2 Partial melting or refertilization and metasomatism?

Based on the observed correlations displayed by Pd, Re, Au and $^{187}Os/^{188}Os$ with Al_2O_3 and other lithophile melt extraction indicators in mantle peridotites, the relatively high abundances of Os, Ir, Ru and Rh in such rocks, and the relative enrichment of Pd, Re and Au relative to Os, Ir and Ru in basalts and komatiites, it was inferred that extraction of partial melts from fertile mantle compositions should be the predominant process controlling HSE variations in mantle peridotites (e.g. Morgan and Lovering, 1967; Hertogen et al., 1980; Morgan, 1986; Brügmann et al., 1987; Meisel et al., 2001). For Pt the case is less clear, as it shows a less incompatible behaviour during low degrees of partial melting, but an increasing degree of depletion during increasing melt extraction (Lorand et al., 1999; Pearson et al., 2004; Becker et al., 2006; Luguet et al., 2007).

More recent studies found growing evidence that some of the fertile lherzolites were influenced by melt-rock interaction or metasomatic processes and therefore their HSE compositions are inconsistent with a simple melt extraction history (Pattou et al., 1996; Rehkämper et al., 1999a; Alard et al., 2000; Luguet et al., 2001; Büchl et al., 2002; Büchl et al., 2004; Chesley et al., 2004; Le Roux et al., 2007; Bodinier et al., 2008; van Acken et al., 2008; Lorand et al., 2009; Lorand et al., 2010). The addition of radiogenic Os and also Re from percolating silicate melts was reported by a number of studies (Chesley et al., 1999; Becker et al., 2001b; Büchl et al., 2002; Büchl et al., 2004; Pearson et al., 2004; van Acken et al., 2008). Detailed petrographic studies and in situ LA-ICP-MS analysis reveal the presence of different sulphide generations contained in mantle rocks indicating redistribution processes affecting sulphide phases (Alard et al., 2000; Lorand and Alard, 2001; Luguet et al., 2001). The occurrence of two different generations of sulphides has been interpreted to reflect metasomatic addition and/or coprecipitation of Cu-Pd-Pt-Re-Au-rich sulphides from silicate melts along silicate grain boundaries, while residual sulphides included in silicate grains survived partial melt extraction and concentrate compatible HSE like Os, Ir, Ru and Rh (Burton et al., 1999; Chesley et al., 1999; Alard et al., 2000; Lorand and Alard, 2001; Luguet et al., 2001; Alard et al., 2002; Luguet et al., 2003; Alard et al., 2005; van Acken et al., 2008; Lorand et al., 2009). The residual sulphides have subchondritic Re/Os and unradiogenic $^{187}Os/^{188}Os$, while the sulphides located on grain boundaries tend to have suprachondritic Re/Os and Os isotopic

compositions (Burton et al., 1999; Alard et al., 2000; Alard et al., 2002), indicating redistribution of Re and radiogenic Os between sulphide phases. In summary, these various observations lead to the conclusion that linear trends of whole rock compositions of at least some suites of peridotites in diagrams of Re/Os, Re/Ir, Pd/Ir and Au/Ir with Al_2O_3 may likely reflect reactive infiltration processes in the mantle leading to mixing of depleted peridotites with precipitates from mafic silicate melts. Such complex histories of mantle peridotites warrant a better characterization of the relevant partitioning processes and their controlling factors, in particular because of possible implications for models of the HSE composition of the primitive mantle.

In the following sections we discuss HSE data obtained on peridotite bulk rock samples and sulphides in the light of possible distribution processes for which experimental partitioning data is available. Although the behaviour of most HSE during metal-silicate, sulphide-silicate and solid sulphide-liquid sulphide partitioning is now well constrained from laboratory experiments, the detailed distribution process accounting for HSE compositions in peridotites and mantle-derived magmas currently remains poorly understood. Experimentally determined partitioning data often explain some of the HSE characteristics of peridotites and basalts, but it has been difficult to establish coherent models that account for the variation of all HSE in natural samples (e.g. Ballhaus et al., 2006; Mallmann and O'Neill, 2007; Brenan, 2008).

4.6.3.3 Sulphide-silicate partitioning during partial melt extraction

With the possible exception of Re (see below), HSE abundances in the Earth's upper mantle should be mainly controlled by sulphide phases and platinum-group element minerals (PGM) (Jagoutz et al., 1979; Mitchell and Keays, 1981; Hart and Ravizza, 1996; Pattou et al., 1996; Handler and Bennett, 1999; Handler et al., 1999; Burton et al., 2000; Lorand and Alard, 2001; Luguet et al., 2007; Fonseca et al., 2007; Brenan, 2008). In the past, abundance variations observed in variably melt depleted peridotites were commonly interpreted to be caused by sulphide-silicate partitioning during melt extraction. Meanwhile several studies on natural samples and the results of laboratory partitioning experiments have shown that relative HSE abundance variations observed between fertile and melt depleted peridotites (Fig. 4.6a,b, e.g. Re/Os and Pd/Ir) are inconsistent with sulphide-silicate partitioning during melt extraction (e.g. Handler and Bennett, 1999;

Lorand et al., 1999; Rehkämper et al., 1999a; Pearson et al., 2004; Luguet et al., 2007; Liu et al., 2009). Sulphide-silicate partitioning is also inconsistent with the empirical compatibility sequence of HSE during magmatic processes in the mantle. Experimentally determined partition coefficients for HSE (D_{HSE}) between sulphide and silicate melts are, with the exception of Re, typically $>10^4$ (Peach et al., 1990; Fleet and Stone, 1991; Fleet et al., 1991; Bezmen et al., 1994; Peach et al., 1994; Fleet et al., 1996; Crocket et al., 1997; Sattari et al., 2002). Consequently, fractionation of the platinum group elements and Au due to sulphide-silicate partitioning during partial melt extraction is considered to be unlikely, as long as there is any sulphide in the system. Assuming a less chalcophile behaviour for Re as indicated by recent work (Mallmann and O'Neill, 2007; Brenan, 2008) may explain the fractionation of Re and Os in basalts, but not the fractionation among other HSE observed in basalts and moderately depleted to fertile peridotites.

4.6.3.4 HSE distribution between sulphide phases

The experimentally determined partitioning behaviour of HSE during partial melting of sulphides indicates that Cu-Ni-rich sulphide melts enriched in Pt, Pd and Au may coexist with residual monosulphide solid solution (mss) enriched in Re, Os, Ir and Ru (Fleet et al., 1993; Li et al., 1996; Fleet et al., 1999; Barnes et al., 2001; Brenan, 2002; Bockrath et al., 2004; Mungall et al., 2005; Ballhaus et al., 2006). In Fig. 4.3 (a-d) we compare the Pt, Pd, Re and Au abundances of peridotites with a fractional melting model assuming that HSE abundances are controlled by monosulphide solid solution (mss)-sulphide liquid (sl) partitioning during melt extraction from a PM starting composition. Experimentally determined mss-liquid sulphide partition coefficients ($D_{HSE}^{mss\text{-}sl}$) were obtained from the literature (Fleet et al., 1993; Brenan et al., 2002; Bockrath et al., 2004; Ballhaus et al., 2006; Mungall et al., 2005) and are given in Table 4.3 together with other model parameters. Partition coefficients were scaled according to the mass fraction of sulphides assuming a primitive mantle source containing 280 ppm S and assuming a mass fraction of ~35% S in 100% sulphide. The amount of S left after extraction of a given melt increment was calculated assuming a sulphur solubility of 1000 ppm for the generated partial melt fraction (Mavrogenes and O'Neill, 1999). Evolution trends for residual mss after sulphide melt extraction are broadly consistent with the data in the Au-Pt and Au-Pd diagrams (Fig. 4.3a,b).

Solid sulphide-liquid sulphide partitioning models also fail to account for data trends in the Au-Re and Re-Pd diagrams, as long as Re is assumed to be compatible in mss (Fig. 4.3c,d and Fig. 4.5d). In contrast, the peridotite data in Fig. 4.3c,d would be consistent with a model that assumes incompatible behaviour of Re during sulphide melt extraction using a partition coefficient $D_{Re}^{mss\text{-}sl}$ of 0.1. Clearly, Re behaves like a moderately incompatible element in the mantle as is indicated by the correlations between $^{187}Os/^{188}Os$, Re/Os, Re/Ir and Al_2O_3 (Fig. 4.5d, Reisberg and Lorand, 1995; Meisel et al., 2001; Gao et al., 2002; Pearson et al., 2004; Becker et al., 2006), the enrichment of Re along with Pd in sulphides precipitated from silicate melts migrating in the mantle (Alard et al., 2002; van Acken et al., 2010), and because of the enrichment of Re in mantle derived melts (Morgan and Lovering, 1967; Hertogen et al., 1980; Hauri and Hart, 1997; Dale et al., 2008). Recent studies of Mallmann and O´Neill (2007), Fonseca et al. (2007) and Brenan (2008) have revealed that the partitioning behaviour and the oxidation state of Re is strongly dependant on oxygen and sulphur fugacities. While Re is considered to be a chalcophile element in most f_{O2} environments of the upper mantle (Roy-Barman et al., 1998; Sattari et al., 2002; Fonseca et al., 2007; Mallmann and O'Neill, 2007), it may also be compatible in garnet and clinopyroxene (Righter and Hauri, 1998; Mallmann and O'Neill, 2007; Brenan, 2008), and under S-undersaturated and more oxidizing conditions in spinel (Righter et al., 1998; Righter and Downs, 2001).

In Fig. 4.5 the peridotite data for Rh/Ir, Au/Ir, Pd/Ir, Pd/Pt and Re/Ir are compared to a partial melting model using the same parameters as described above. The fractional melting model employs $D_{HSE}^{mss\text{-}sl}$ according to the literatue and melt extraction model parameters for Al_2O_3 as defined by Niu (1997). The model seems to be broadly consistent for the compatible elements Ir, Rh and Re (Figs. 4.5a, d). For Au/Ir the fractional melting model could not account for the abundance variations of peridotites, as for low Pd/Ir ratios of residual harzburgites (Fig. 4.5b,c). An increasing mismatch is observed between modelled and measured Pt and Pd abundances for increasingly melt depleted peridotite compositions (Fig. 4.5e). All available partitioning studies obtain almost identical or very similar $D^{mss\text{-}sl}$ values < 1 for Pt and Pd, indicating similar incompatible behaviour in the mss structure. In contrast, both in moderately depleted peridotites and in basalts, Rh, Pt and Pd tend to be substantially fractionated (Figs. 4.1-4.3, 4.5, and Rehkämper et al., 1999b; Bezos et al., 2005).

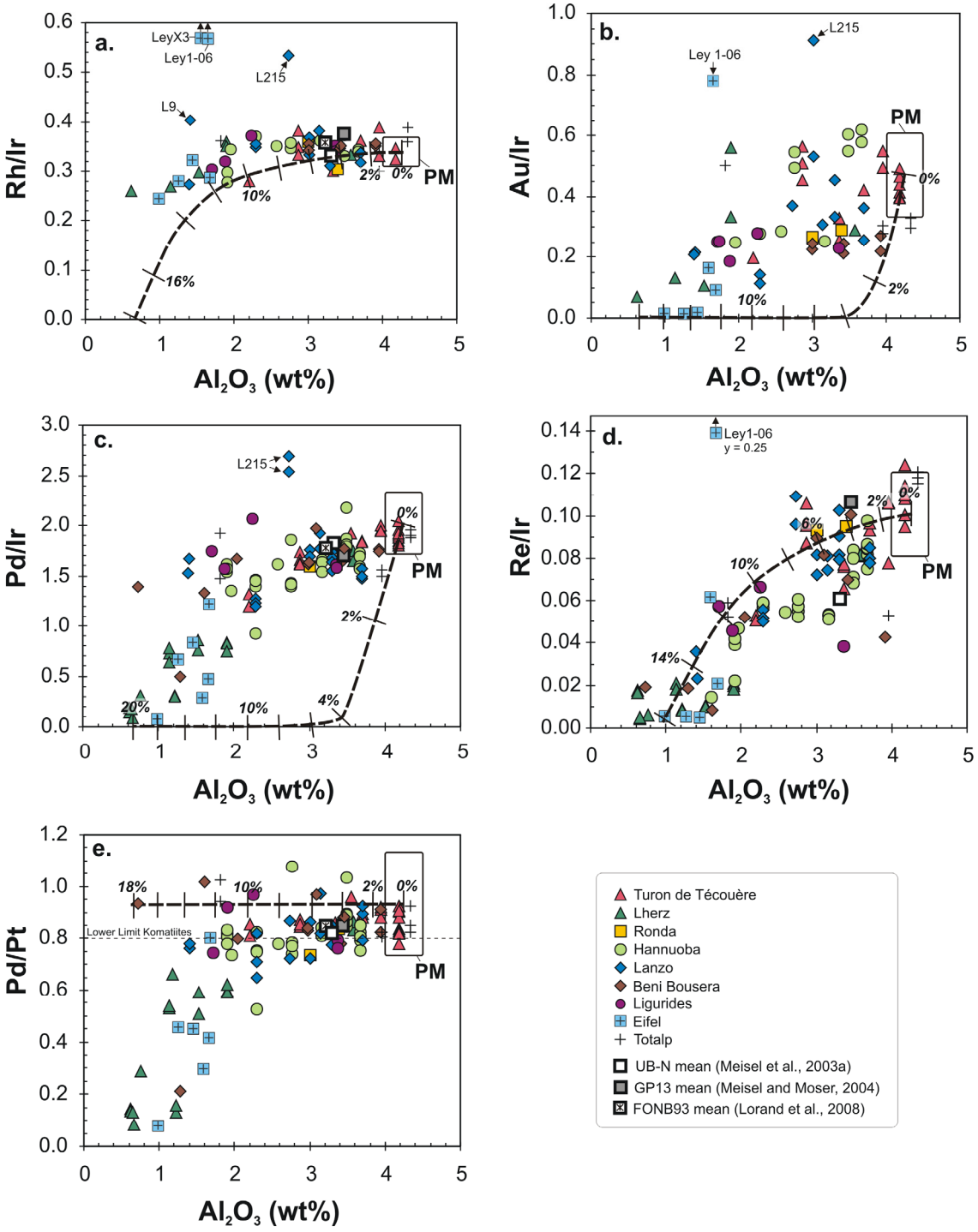

Fig. 4.5. Rh/Ir, Au/Ir, Pd/Ir, Re/Ir and Pd/Pt vs. Al_2O_3. Ratios of Pd/Ir and Pd/Pt are relatively constant for fertile lherzolites and display an increasing depletion with decreasing Al_2O_3 content. Re/Ir is almost linearly correlated with Al_2O_3. The boxes in the diagrams indicate the inferred HSE ratios for the primitive mantle (PM) model composition (Becker et al., 2006). Horizontal dashed line in c) corresponds to the lower limit of Pd/Pt observed for komatiites (Puchtel et al., 2004; Puchtel and Humayun, 2005; Maier et al., 2009; Puchtel et al., 2009). Bold dashed lines correspond to a fractional melting model as described in Fig. 4.4 and in the text. Peridotite data shown are high-temperature acid digestion and isotope dilution data from

this study, Meisel et al. (2003a), Meisel and Moser (2004), Pearson et al. (2004), Becker et al. (2006), Luguet et al. (2007), Lorand et al. (2008) and Lorand et al. (2010). Data from this study, Pearson et al. (2004), Becker et al. (2006), Luguet et al. (2007) and Lorand et al. (2010) for samples from the same localities are shown using the same symbols.

The Pd/Pt ratios of komatiites range from 0.8-1.3 (Puchtel et al., 2004b; Puchtel and Humayun, 2005; Maier et al., 2009) and are comparable to lherzolites, suggesting that at higher degrees of mantle melting Pd and Pt behave more similar. In order to explain the change in Pd/Pt ratios in Fig. 4.5e the relative $D^{mss/sl}$ values of Pt and Pd would have to change from $D_{Pd}/D_{Pt} \approx 1$ to a value <1 during increasing partial melt extraction (see also discussions in Becker et al., 2006 and Luguet et al., 2007).

In summary, solid sulphide-liquid sulphide partitioning is not fully consistent with abundances and the fractionation of the HSE in peridotites and mantle derived magmas. The abundance systematics of Rh, Pt, Pd, and particularly Re in the upper mantle must be controlled by additional processes.

4.6.3.5 Refertilization of depleted peridotites

As noted before some evidence suggests that correlations displayed by incompatible HSE with Al_2O_3 may reflect melt-rock interaction processes. In this case these correlations must reflect mixing between depleted mantle domains that have undergone melt extraction in the past and contributions from migrating silicate melts. Besides mixing, the shape of these trends would be influenced by partition coefficients, the relevant partitioning process and the physicochemical conditions controlling mineral precipitation. During the precipitation of sulphide liquid from silicate melt in the mantle, the HSE are likely controlled by sulphide-silicate partitioning, but additional control of Re abundances by precipitation of clinopyroxene or garnet may play a role as well (Mallmann and O'Neill, 2007; Brenan, 2008). Precipitation of sulphide is only possible if mantle melts are sulphur saturated. Because the sulphur solubility of a basaltic melt increases with decreasing pressure (Mavrogenes and O'Neill, 1999), the process which forces re-enrichment of melt depleted mantle may be restricted to a certain depth in the mantle, probably the asthenosphere-lithosphere transition (Le Roux et al., 2007; van Acken et al., 2008). Another possible mechanism to achieve S oversaturation in the melt

would be substantial crystallization of silicates or decreasing temperatures (Mavrogenes and O'Neill, 1999).

Bockrath et al. (2004) and Ballhaus et al. (2006) suggested a model where HSE abundances in mantle rocks are controlled by partitioning between monosulphide solid solution (mss) and coexisting sulphide melt. The sulphide melt could be drained by infiltration of silicate melt and subsequent melt extraction. Hence, incompatible HSE that preferentially partition into sulphide melt become associated with silicate melts. In detail similar problems appear in explaining the behaviour of Re and the relative fractionation of Pd, Pt and Rh in peridotites, pyroxenites and mantle-derived magmas as for the partial melting model outlined in the previous section.

While more detailed studies are necessary to understand the role of melt migration and sulphide precipitation in peridotites, HSE abundances in whole rocks and sulphides from mantle pyroxenites hint that sulphide saturation and sulphide-silicate partitioning may play a critical role in redistribution of HSE in the mantle (Büchl et al., 2002; Becker et al., 2006; Luguet et al., 2008; van Acken et al., 2010).

4.6.4 Primitive mantle estimates for Rh and Au

In a previous study Becker et al. (2006) calculated HSE abundances for a hypothetical primitive mantle model HSE composition based on abundance data for fertile lherzolites (Fig. 4.6a) and covariations observed for incompatible HSE and melt extraction indicators (Al_2O_3), assuming that the primitive mantle has a composition similar to fertile lherzolite (McDonough and Sun, 1995, and references therein). These data and most other literature data on mantle peridotites and komatiites (Pattou et al., 1996; Lorand et al., 1999; Rehkämper et al., 1999a,b; Schmidt et al., 2000; Puchtel et al., 2004a; Puchtel et al., 2004b; Puchtel and Humayun, 2005; Puchtel et al., 2007; Liu et al., 2009; Maier et al., 2009) and Os isotopic data (Meisel et al., 1996; Brandon et al., 2000; Meisel et al., 2001; Walker et al., 2005a; Brandon et al., 2006) are consistent with chondritic values for some HSE ratios in the primitive mantle (e.g. Re/Os, Os/Ir, Pt/Ir, Pt/Os), while other ratios are suprachondritic (Ru/Ir, Pd/Ir). It should be noted though that not all fertile lherzolites posess suprachondritic Pd/Ir (Rehkämper et al., 1997; Morgan et al., 2001). New data on

fertile peridotites from the present study essentially confirms results from previous studies. Becker et al. (2006) did not analyze Rh and Au, but they provided estimates of Rh and Au abundances for the fertile mantle based on ICP-MS and INAA data from Lorand et al. (1993, 1999, 2000). New data from the present study indicate Rh/Ir and Au/Ir in fertile lherzolites are above CI chondrite values, similar to values in enstatite (EL) and ordinary chondrites (Figs. 4.7 and 4.8).

Because Rh/Ir does not show systematic variation with Al_2O_3 in lherzolites, and apparently shows compatible behaviour at low to moderate degrees of melting (Fig. 4.2), Rh/Ir and the Rh abundance in the primitive mantle can be obtained from lherzolite compositions with Al_2O_3 >2.5wt%. The mean Rh/Ir ratio of lherzolites from this study and literature data (Meisel et al., 2003a; Meisel and Moser, 2004; Lorand et al., 2008) is 0.34 ± 0.03 (1s, n=57), which is similar to the previous estimate of 0.32 ± 0.03 reported by Becker et al. (2006) based on literature data from Lorand et al. (1993, 1999, 2000). In conjunction with an Ir_{PM} of 3.5 ± 0.4 ng/g (Becker et al., 2006) this would yield a Rh abundance of 1.2 ± 0.2 ng/g (1s) for the PM composition. For the calculation of the average Rh/Ir only data obtained by high-temperature acid digestion and isotope dilution ICP-MS analysis in combination with internal standardization techniques for the quantification of Rh were considered. We did not include some previous data on peridotite xenoliths where erratic variations of Rh/Ir may reflect partial Ir or Rh loss due to secondary sulphide breakdown or metasomatism (Handler and Bennett, 1999; Handler et al., 1999; Lorand and Alard, 2001; Lorand et al., 2003).

The calculation of a mean Au/Ir for the primitive mantle is more difficult. While Au abundances and Au/Ir are broadly correlated with Al_2O_3, these correlations are not well defined. In particular fertile lherzolites show relatively large variations (Fig. 4.5) with Au/Ir ranging from 0.20 to 0.65. A gold abundance for the PM composition was calculated via linear regression from the correlation displayed by Au/Ir with Al_2O_3 yielding Au/Ir_{PM} = 0.47 ± 0.10 (1s), most similar to values observed for ordinary and EL enstatite chondrites. With a Ir_{PM} abundance of 3.5 ± 0.4 ng/g this value yields Au_{PM} = 1.7 ± 0.5 ng/g (1s). Abundances of Re and Au are positively correlated, indicating similar compatibilities of both elements during mantle processes (Fig. 4.3c). The Au abundance of the PM was also calculated via linear regression from the Re vs. Au diagram. With Re_{PM} of 0.35 ± 0.06 ng/g (Meisel et al., 2001; Becker et al., 2006) this would yield Au_{PM}

of 1.7 ± 0.5 ng/g (1s), indistinguishable from the result of the Au/Ir vs. Al_2O_3 regression. As discussed in the case of Rh above we did not include Au data from most peridotite xenoliths, except for Hannuoba. Previously reported Au data obtained using NiS pre-concentration techniques were also not considered for calculation for reasons discussed above and in the appendix (4.8.3).

4.6.5 Reliability of the primitive mantle model HSE composition

In the light of the evidence for a complex depletion and re-enrichment history now recognized in many peridotites, the validity of primitive mantle model compositions for the HSE has been recently challenged (Alard et al., 2000; Lorand et al., 2008, 2009, 2010). In the case of the compatible HSE Os, Ir, Ru and Rh their relative abundances are not easily affected by melt-rock interaction processes, and thus their ratios in lherzolites should be representative of PM values. While correlations of Pd/Ir or Re/Os with Al_2O_3 for fertile peridotites may be generated by refertilization, suprachondritic Ru/Ir are difficult to explain by such processes, as are the chondritic Os/Ir of lherzolites, particularly since melts tend to display fractionated Os/Ir and Ru/Ir. The proposition that suprachondritic Ru/Ir in peridotites might reflect addition of Ru from percolating melt is not very attractive, because significant mantle reservoirs that display chondritic or subchondritic Ru/Ir have not been identified.

It has been known for a long time that fertile peridotite compositions may reach values around 4 wt.% Al_2O_3, which for cosmochemical (e.g. roughly chondritic Al/Ti, Ca/Al of PM) and geophysical reasons is considered a reasonable estimate for the Al_2O_3 content of the primitive mantle (McDonough and Sun, 1995; Palme and O'Neill, 2003). While it is now recognized that some correlations of lithophile incompatible elements in peridotites with MgO may reflect re-enrichment processes, this does not invalidate the derivation of model compositions for the bulk mantle from such data. A similar reasoning applies to ratios such as Re/Os (or $^{187}Os/^{188}Os$) and Pd/Ir. These ratios correlate with Al_2O_3 and other moderately incompatible lithophile elements in peridotite suites from various regions suggesting reproducible processes that represent a feature of chemical geodynamics of the mantle. HSE data on ancient Al undepleted komatiites provide

additional evidence that larger domains of the mantle are characterized by compositions similar to PM, i.e. roughly chondritic Re/Os, suprachondritic Pd/Pt near 1, and chondritic ratios of lithophile incompatible elements (e.g. Jochum et al., 1991; Puchtel et al., 2004b; Puchtel and Humayun, 2005; Maier et al., 2009).

4.6.6 Implications for late accretion processes in the Earth-Moon system

The new data on Rh and Au for peridotites show that Rh/Ir_{PM} and Au/Ir_{PM} are similar to values in ordinary and EL enstatite chondrites (Fig. 4.7), in agreement with previous Re-Os work (Meisel et al., 1996; Brandon et al., 2000; Meisel et al., 2001; Walker et al., 2005a; Brandon et al.,, 2006). However, a comparison of the HSE composition inferred for the PM (this study and Becker et al., 2006) with the compositions of primitive meteorite groups (Walker et al., 2002; Horan et al., 2003; Fischer-Gödde et al., 2010a) reveals that none of the chondrite groups provides a good match for the PM (Figs. 4.7 and 4.8). Recent data on ancient lunar impact melt rocks indicate that some of the meteoritic components accreted to the lunar surface prior to 3.8 Ga may have had a HSE composition different from known chondrite groups (e.g. Morgan et al., 1974; Hertogen et al., 1977; Puchtel et al., 2008; Fischer-Gödde et al., 2010b). Some meteoritic components contained in ancient lunar impact melt rocks bear evidence for the late accretion of meteoritic material with elevated Pd/Ir and Ru/Ir which extent beyond the suprachondritic ratios inferred for the PM model HSE composition (Norman et al., 2002; Puchtel et al., 2008; Fischer-Gödde et al., 2010b). Thus, one intriguing option to explain the suprachondritic Ru/Ir and Pd/Ir of the Earth's primitive mantle would be late accretion of meteoritic material with a HSE composition different from the known chondrite groups, mixed with chondritic materials. Alternatively, the Earth's mantle HSE signature may reflect contributions inherited from early metal-silicate segregation mixed with additions from late accretion (e.g. Righter et al., 2008; Brenan and McDonough, 2009; Walker, 2009, and references therein).

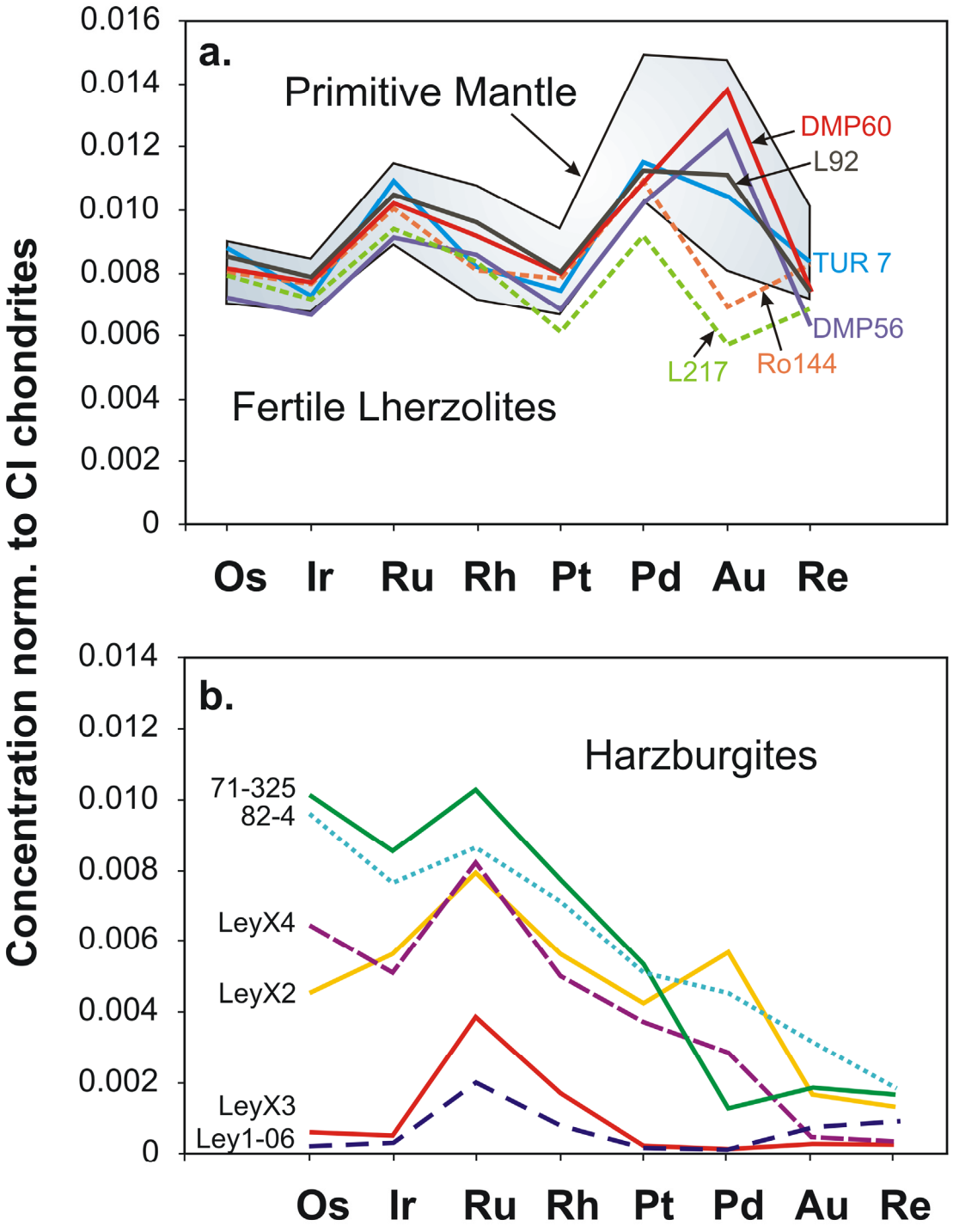

Fig. 4.6. Normalized concentration diagrams of selected lherzolites (a) and harzburgites (b) analyzed in this study. CI chondrite values of HSE from Fischer-Gödde et al. (2010a). Elements listed in the order of increasing incompatible behaviour from left to right. Harzburgites are depleted in Pt, Pd, Re and Au compared to more compatible HSE. Some of the Eifel xenoliths (LeyX3, Ley1-06) are depleted in all HSE except Ru and Rh or show low Os/Ir (LeyX2) compared to other harzburgites. Their HSE abundances most probably reflect late stage mobility of sulphide or sulphide break down during emplacement.

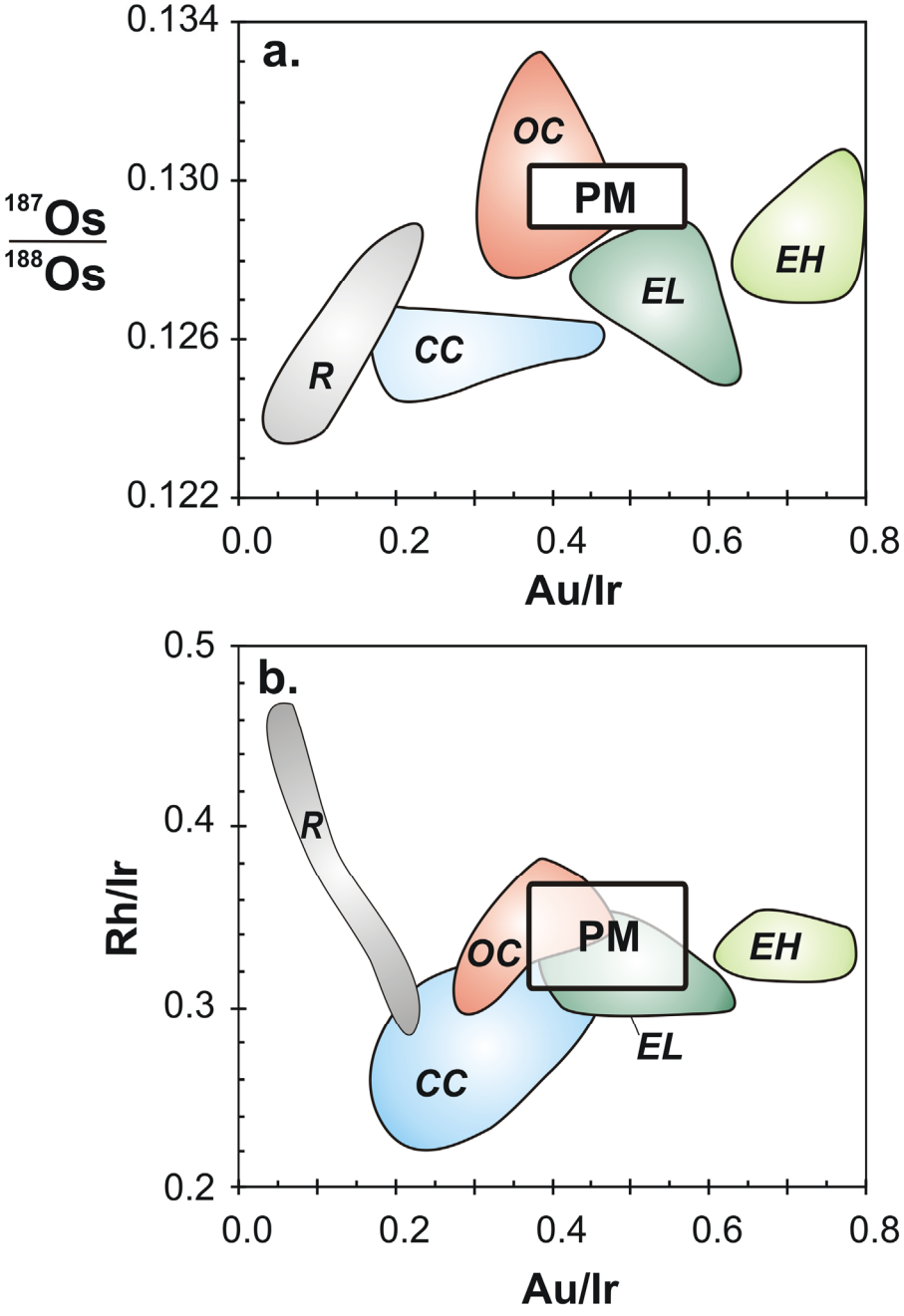

Fig. 4.7. Ratio diagrams of Au/Ir vs. $^{187}Os/^{188}Os$ (a) and Au/Ir vs. Rh/Ir (b) for HSE ratios inferred for the primitive mantle (PM) in comparison to different chondrite classes and groups. The inferred HSE composition for the PM model is more similar to ordinary (OC) and enstatite (EL) chondrites, but distinct from the fields of carbonaceous (CC) and Rumuruti (R) chondrites. Primitive mantle ratios according to this study, Meisel et al. (2001) and Becker et al. (2006). Chondrite fields based on data from Fischer-Gödde et al. (2010a).

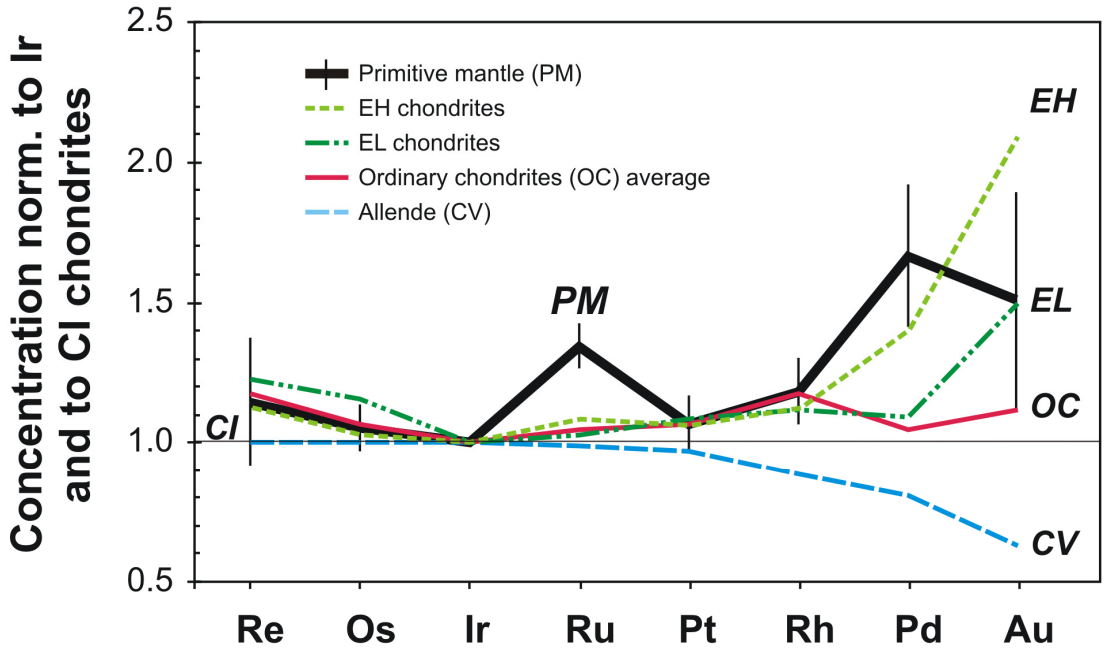

Fig. 4.8. Double normalized HSE abundance diagram (normalized to Ir and CI chondrite values, CI values from Fischer-Gödde et al., 2010a) showing the primitive mantle (PM) model composition in comparison to representative HSE patterns of chondrites from different classes and groups (Walker et al., 2002; Horan et al., 2003; Fischer-Gödde et al., 2010a). None of the chondrite groups provides a good match for the PM abundance pattern.

4.7 Conclusions

A new technique that permits obtaining a complete set of HSE data on the same digestion aliquot of peridotites yields a compatibility sequence of Re ≤ Au < Pd < Pt ≤ Rh < Ir ≤ Ru ≤ Os during magmatic processes in the mantle. Rhodium and Pt behave as compatible elements during low degrees of partial melt extraction, indicated by constant Rh/Ir of 0.34 ± 0.03 and Pt/Ir of 2.07 ± 0.16 displayed by fertile lherzolites. Residual peridotite compositions <2.5wt% Al_2O_3 show decreasing Rh/Ir, and more pronounced Pt/Ir, most probably caused by the consumption of HSE host phases during increasing degree of partial melt extraction. The Rh abundance of the primitive mantle model composition calculated from Rh/Ir of fertile lherzolites is 1.2 ± 0.2 ng/g (1s).

Palladium, Re and Au behave as moderately incompatible elements, indicated by scattered correlations with lithophile melt extraction indicators (e.g. Al, Ca, Ti). Gold is

almost linearly correlated with Re, suggesting a similar compatibility for both elements during magmatic processes, although data on basalts indicates that Re may be somewhat more incompatible than Au. Fertile peridotites display Au/Ir ranging from 0.20-0.65, while harzburgites show decreasing Au/Ir < 0.20 with increasing depletion. The abundance of Au for a primitive mantle model composition calculated via linear regression from the correlations displayed by Au with Re and Au/Ir with Al_2O_3 is 1.7 ± 0.5 ng/g (1s).

Abundance variations and some HSE ratios, notably Pd/Ir, Pd/Pt, Re/Ir and Au/Ir, are difficult to explain by solid sulphide-sulphide melt partitioning during partial melt extraction. Refertilization of residual harzburgite due to infiltration of sulphide and silicate melt from mafic mantle melts may be a viable option if an incompatible behaviour of Re during partial melting is assumed.

Rh/Ir and Au/Ir for the primitive mantle model composition are most similar to ordinary and EL enstatite chondrites, but unlike carbonaceous chondrites. In conjunction with the previously inferred primitive mantle model composition (Becker et al., 2006) the new Rh and Au data reveals a HSE composition for the primitive mantle model that is unlike any known group of chondrites, but may be explained by contributions from meteoritic components identified in ancient lunar impact melt rocks.

Acknowledgements

We thank Jean-Pierre Lorand and Shan Gao for providing samples for this study. We acknowledge Corinna Wutzke, Marc Weynell and Linda Caroline Meier for assistance during sample preparation, digestion and chemical separation procedures. Konrad Hammerschmidt is acknowledged for help and advice in the TIMS lab and Monika Feth for help and support in the clean lab. We thank Rudolph Naumann and Andrea Gottsche for XRF analysis and S determination at the GFZ. We appreciate discussions with Chris Ballhaus, Ambre Luguet, Thomas Meisel, Herbert Palme and David van Acken. This work was supported by the Deutsche Forschungsgemeinschaft (Be 1820/3-1).

Table 4.1. Highly siderophile element concentrations (in ng/g), $^{187}Re/^{188}Os$ and $^{187}Os/^{188}Os$ for the UB-N reference powder.

Nr.	Batch	Digestion[a]	Os	Ir	Ru	Rh	Pt	Pd	Re	Au	2sd[c]	$^{187}Re/^{188}Os$	$^{187}Os/^{188}Os$
This study:													
1	a	CT	3.99	3.24	6.02		7.23	5.75					0.1268
2	a	CT	3.29	3.08	6.13		10.4[d]	5.54					0.12740
3	a	CT	3.65	3.42	6.22		7.43	5.67					0.12692
4	a	CT	3.88	3.56	7.26		8.33	5.77					0.12702
5	a	CT[b]		3.29	6.52		7.57	5.97		1.49[b]			
6	a	CT[b]		3.41	6.57		7.47	5.97	0.215	1.49[b]			
7	a	CT[b]		3.34	6.73		7.19	6.13	0.194	1.49[b]			
8	a	CT[b]		3.45	6.73		7.60	6.02	0.195	1.49[b]			
9	a	HPAS	3.55	3.19	6.62	1.12	7.14	5.95	0.189	0.99[c]	0.10[c]	0.256	0.12727
10	b	HPAS	3.43	3.04	6.11	1.16	7.31	5.92	0.221	1.67		0.310	0.12754
11	b	HPAS	3.68	3.18	6.77	1.24	7.48	6.05	0.204	1.75		0.267	0.12739
12	b	HPAS	3.23	2.96	6.34	1.15	7.14	5.95	0.151	1.62		0.225	0.12751
13	b	HPAS	3.63	3.28	6.65	1.17	7.14	6.10	0.211	1.66		0.281	0.1275
14	b	HPAS	3.84	3.05	6.98	0.91	6.52	5.53	0.155	1.42		0.194	0.12673
15	c	HPAS	3.25	2.78	6.01	0.97	6.84	5.56	0.153	1.54		0.228	0.12754
16	c	HPAS	3.27	2.88	5.74	1.02	6.71	5.55	0.165	1.66		0.243	0.12710
17	c	HPAS	3.50	2.98	6.31	1.01	7.21	5.96	0.182	1.03[c]	0.14[c]	0.250	0.12735
18	c	HPAS	3.39	2.97	6.26	1.19	6.94	5.96	0.203	1.41		0.288	0.12729
19	c	HPAS	3.30	2.88	6.17	1.17	8.29	5.91	0.194	1.59		0.283	0.12701
		Mean	**3.53**	**3.16**	**6.43**	**1.10**	**7.31**	**5.85**	**0.188**	**1.49**		**0.257**	**0.12722**
		sd	0.25	0.22	0.38	0.10	0.47	0.20	0.024	0.26		0.033	0.00028
		%rsd	7.0	7.0	5.9	9.5	6.4	3.4	13	17		13	0.22
		n	15	19	19	11	18	19	14	11		11	15

[a] CT high temperature (320°C) Carius tube digestion as described in Becker et al. (2006); HPAS high pressure asher digestion at 320°C (Meisel et al., 2003a).
[b] digestion aliquot used for standard addition analysis of Au, other HSE determined by isotope dilution.
[c] average concentration (± 2sd) calculated from repeated analysis of the same digestion aliquot.
[d] erratic value excluded for calculation of the mean.

Table 4.1. continued. Highly siderophile element concentrations (in ng/g), $^{187}Re/^{188}Os$ and $^{187}Os/^{188}Os$ for the UB-N reference powder.

	Method[e]	Os	Ir	Ru	Rh	Pt	Pd	Re	Au	2sd	$^{187}Re/^{188}Os$	$^{187}Os/^{188}Os$
Literature:												
Becker et al. 2006	ID ICP-MS	3.51	3.26	6.51		7	5.85	0.205			0.282	0.12737
	%rsd	3.5	3.9	5		3.3	4.5	1.9			5.2	0.2
Meisel et al. 2003a,b &	ID ICP-MS	3.71	3.38	6.3	1.12	7.42	6.11	0.206				0.1278
Meisel & Moser 2004	%rsd	7.1	6.4	4.6	7.9	4	2.9	2.4				0.16
Puchtel & Humayun 2005	ID ICP-MS	3.64	3.52	7.24		7.48	6.1	0.197				
	%rsd	9	8	8		3	3	10				
Luguet et al. 2007	ID ICP-MS	3.66	3.24	6.48		8.07	6.17	0.205				0.1279
	%rsd	4.1	9.6	4.5		14.5	4.1	3.4				0.39
Puchtel et al. 2007, 2008	ID ICP-MS	3.85	3.58	6.93		7.47	5.7	0.213				0.12722
	%rsd	8.3	11	6.8		2.1	2.1	5.2				0.3
Lorand et al. 2009	ICP-MS	3.28	3	6.5	1.25	6.78	6					
	%rsd	6.1	6.7	5.5	24	5.3	0.83					
Bornhorst et al. 1984	RNAA								3.30	0.33		
Benedetti et al. 1987	GF-AAS								2.92	0.20		
Terashima 1988	GF-AAS								3.49	0.09		
Lorand et al. 1989	INAA								3.1	0.8		
	RNAA								3.3	0.5		
Korotev 1996	INAA		3.4						1.6	0.5		
Bédard and Barnes 2002	INAA		3.52						3.8	0.7		
Constantin 2008	INAA		3.56						2.7	1.6		

[e] ID ICP-MS isotope dilution inductively coupled plasma mass spectrometry analysis combined with Carius tube or high pressure asher digestion technique; NiS ICP-MS inductively coupled plasma mass spectrometry analysis after NiS fire assay preconcentration; GF-AAS graphite furnace atomic absorption spectrometry; RNAA radiochemical neutron activation analysis; INAA instrumental neutron activation analysis.

Table 4.2. Highly siderophile element concentrations (in ng/g), $^{187}Os/^{188}Os$, Al_2O_3 (in wt.%) and S (in µg/g) for peridotites.

Sample	Digestion[a]	Os[b]	Ir	Ru	Rh	Pt	Pd	Re[b]	Au	2sd[e]	$^{187}Re/^{188}Os$[b]	$^{187}Os/^{188}Os$[b]	Al_2O_3[c]	S[c]
Turon de Técouère (Western Pyrenees, France)														
TUR 7[d]	CT		3.25	6.79		7.69	5.98		1.34[d]				4.18	270
TUR 7[d]	CT		3.05	6.14		7.14	5.97	0.329	1.34[d]				4.18	270
TUR 7[d]	CT		3.35	6.63		7.26	6.01	0.368	1.34[d]				4.18	270
TUR 7[d]	CT		3.39	6.65		7.77	6.35		1.34[d]				4.18	270
TUR 7	CT	3.76	3.25	6.62		6.88	6.19	0.403			0.517	0.12961	4.18	270
Replicate	HPAS	4.31	3.37	7.50	1.09	7.02	6.48	0.338	1.56		0.378	0.12898	4.18	270
Replicate	HPAS	3.73	3.23	6.56	1.12	7.51	6.60	0.368	1.59		0.476	0.12960	4.18	270
TUR 11	HPAS	4.32	3.94	7.89	1.19	7.74	6.35	0.259	1.01[e]	0.03[e]	0.289	0.12566	3.36	190
Replicate	HPAS	*4.25*	3.97	8.02	1.27	7.78	6.56	*0.302*	1.31[e]	0.11[e]	*0.342*	*0.12590*	3.36	190
TUR 14	HPAS	3.45	3.11	6.37	1.21	7.06	6.22	0.242	1.71		0.338	0.12839	3.95	240
Replicate	HPAS	*3.66*	3.24	6.73	1.08	6.98	6.35	*0.345*	1.61		*0.454*	*0.12852*	3.95	240
TUR 16	HPAS	*4.93*	4.23	8.96	1.19	6.55	5.59	*0.223*	0.83		*0.218*	*0.12009*	2.2	140
TUR 21	CT	4.43	3.98	7.62	1.52	8.20	6.93	0.422	2.24		0.459	0.1266	2.87	155
Replicate	HPAS	4.83	4.17	8.16	1.46	8.19	6.91	0.398	2.12		0.398	0.12649	2.87	155
Replicate	HPAS	5.16	4.36	9.15	1.45	8.12	7.08	0.381	1.97		0.356	0.12643	2.87	155
TUR 23	HPAS	*3.58*	3.19	6.44	1.16	6.60	5.91	*0.297*	1.34		*0.399*	*0.12883*	3.7	220
Lherz (Eastern Pyrennes, France)														
71-325	HPAS	*4.98*	3.96	7.07	1.03	5.04	0.72	*0.069*	0.28		*0.0671*	*0.11536*	0.62	5
71-107	HPAS	4.88	4.45	7.48	1.56	6.19	3.67	0.088	1.49[e]	0.01[e]	0.0866	0.11565	1.9	158
Replicate	HPAS	*5.58*	4.27	7.57	1.51	5.95	3.55	*0.090*	2.40[e]	0.01[e]	*0.0777*	*0.11570*	1.9	158
71-322	HPAS	*4.03*	4.45	7.82	1.32	6.42	3.80	*0.046*	0.47		*0.0544*	*0.12325*	1.53	56
86-V2	HPAS	*5.85*	3.04	6.31	1.01	6.37	5.30	*0.247*	0.88		*0.203*	*0.12773*	3.58	250
82-4	HPAS	*4.72*	3.53	5.96	0.95	4.82	2.55	*0.074*	0.47		*0.0755*	*0.11410*	1.14	
Ronda (Betic Cordillera, Spain)														
Ro126	*HPAS*	*3.91*	3.34	6.65	1.20	7.25	5.33	*0.311*	0.89		*0.383*	*0.12669*	3	160
Ro144	*HPAS*	*3.94*	3.54	6.93	1.08	7.35	6.15	*0.337*	1.03		*0.412*	*0.12779*	3.39	240

Table 4.2 continued. Highly siderophile element concentrations (in ng/g), $^{187}Os/^{188}Os$, Al_2O_3 (in wt.%) and S (in µg/g) for peridotites.

Sample	Digestion[a]	Os[b]	Ir	Ru	Rh	Pt	Pd	Re[b]	Au	2sd[e]	$^{187}Re/^{188}Os$[b]	$^{187}Os/^{188}Os$[b]	Al_2O_3[c]	S[c]
Hannuoba (China)														
DMP04	HPAS	*3.76*	3.62	7.15	1.34	7.02	5.29	*0.211*	1.01		*0.271*	*0.12289*	2.29	73
DMP19	HPAS	3.90	4.19	8.56	1.17	8.41	6.78	0.164	5.77[e]	0.33[e]	0.203	0.11999	1.91	91
Replicate	HPAS	*4.13*	4.33	8.77	1.29	8.43	6.90	*0.181*	6.82[e]	0.75[e]	*0.211*	*0.11998*	1.91	91
DMP41	HPAS	2.86	3.03	5.86	1.08	5.82	4.32	0.159	1.66		0.268	0.12322	2.76	110
Replicate	HPAS	*2.91*	3.12	5.97	1.08	5.54	4.35	*0.172*	1.54		*0.285*	*0.12327*	2.76	110
DMP 51	HPAS	3.16	3.00	6.50	1.03	5.51	4.07	0.141	0.74		0.215	0.12317	1.96	130
DMP 56	HPAS	*3.55*	3.08	6.28	1.14	6.41	5.74	*0.257*	1.86		*0.350*	*0.12748*	3.49	260
Replicate	HPAS		3.13	6.33	1.03	6.71	5.68	0.222	1.72			0.12765	3.49	260
DMP58	HPAS	*3.78*	3.57	7.08	1.29	7.03	5.90	*0.190*	0.91		*0.242*	*0.12539*	3.16	230
DMP 59	HPAS	4.45	4.09	7.98	1.43	8.46	6.60	0.224	1.16		0.242	0.12331	2.58	200
DMP60	HPAS	3.79	3.50	6.79	1.19	7.27	6.00	0.285	2.16		0.363	0.12623	3.67	320
Replicate	HPAS	*4.00*	3.55	7.01	1.22	7.53	6.11	*0.303*	2.05		*0.365*	*0.12628*	3.67	320
Lanzo (Italian Alps)														
L9	HPAS	3.39	3.09	6.90	1.25	6.75	5.15	0.071	0.67		0.101	0.12291	1.41	52
L52	HPAS	3.65	2.75	6.56	0.75	5.38	4.20	0.098	0.58		0.129	0.11932	1.4	80
L66	HPAS	*3.61*	2.92	6.12	1.11	5.77	5.62	*0.237*	0.90		*0.316*	*0.12619*	3.14	168
L92	HPAS	*4.19*	3.65	7.22	1.28	7.54	6.32	*0.298*	1.66		*0.343*	*0.12550*	3.3	142
L213	HPAS	*3.25*	2.54	5.00	0.79	5.05	4.28	*0.261*	0.84		*0.387*	*0.12680*	3.3	200
L215	HPAS	*3.67*	2.23	5.85	1.19	8.27	5.99	*0.243*	0.83		*0.318*	*0.12220*	2.73	215
L216	HPAS	*3.41*	2.61	5.63	0.91	4.67	3.32	*0.145*	0.38		*0.205*	*0.12020*	2.29	100
Replicate	HPAS	*3.41*	2.79	5.57	0.99	5.30	3.44	*0.145*	0.31		*0.205*	*0.12020*	2.29	100
L217	HPAS	*3.90*	3.29	6.48	1.11	5.79	5.18	*0.279*	0.85[e]	0.15[e]	*0.344*	*0.12325*	3.7	210
Replicate	HPAS	*3.90*	3.50	6.40	1.11	6.48	5.14	*0.279*	1.26		*0.344*	*0.12325*	3.7	210
L 732a	HPAS	3.12	2.80	5.58	1.03	5.69	4.91	0.229	1.49[e]	0.20[e]	0.353	0.1270	3.01	163
Replicate	HPAS	3.15	2.95	5.74	0.98	6.92	4.99	0.214	2.69		0.328	0.12644	3.01	163

Table 4.2 continued. Highly siderophile element concentrations (in ng/g), $^{187}Os/^{188}Os$, Al_2O_3 (in wt.%) and S (in µg/g) for peridotites.

Sample	Digestion[a]	Os[b]	Ir	Ru	Rh	Pt	Pd	Re[b]	Au	2sd[e]	$^{187}Re/^{188}Os$[b]	$^{187}Os/^{188}Os$[b]	Al_2O_3[c]	S[c]
Totalp (Swiss Alps)														
TA-15	HPAS	*3.93*	3.57	7.09	1.28	8.26	6.79	*0.412*	1.17[e]	0.14[e]	*0.505*	*0.13103*	4.34	
Replicate	HPAS	*4.02*	3.39	6.91	1.31	7.76	6.61	*0.409*	1.00		*0.490*	*0.13110*	4.34	
TA-22-A2	HPAS	*3.41*	2.90	7.39	1.05	5.94	5.60	*0.171*	1.46[e]	0.18[e]	*0.242*	*0.12283*	1.82	
TA-31	HPAS	4.55	4.08	8.15	1.39	7.90	6.35	0.215	1.13[e]	0.05[e]	0.228	0.12613	3.96	
Replicate	HPAS		4.27	8.44	1.28	7.76	6.39		1.30				3.96	
Beni Bousera (Morocco)														
BB3A	HPAS	3.90	3.42	7.10	1.22	6.69	5.56	0.305	0.78		0.377	0.12302	3.00	99
Replicate	HPAS		3.43	7.15	1.17	6.69	5.60		0.84				3.00	99
BB2C	HPAS	3.28	2.96	5.97	1.04	6.42	5.28	0.126	0.80		0.185	0.12792	3.92	407
Replicate	HPAS		3.00	5.79	1.07	5.82	5.30		0.66				3.92	407
BB2G	HPAS	4.49	3.99	8.02	1.38	8.62	6.72	0.278	0.99		0.298	0.12468	3.43	114
Replicate	HPAS		4.22	8.21	1.49	7.69	6.86		0.90				3.43	114
Ligurian ophiolites (Northern Apennines, Italy)														
EL1	HPAS	3.66	3.21	6.51	1.09	6.47	5.13	0.123	0.74		0.163	0.12482	3.37	315
Replicate	HPAS		3.18	6.14	1.12	6.57	5.02		0.73				3.37	315
IL 1	HPAS	4.83	4.12	8.68	1.32	7.01	6.45	0.189	0.77		0.189	0.12132	1.91	88
IL 2	HPAS	3.23	2.86	5.87	0.87	6.70	4.99	0.165	0.72		0.245	0.12551	1.71	104
IL 3	HPAS	4.00	3.23	7.17	1.20	6.89	6.66	0.216	0.91		0.259	0.12535	2.25	228
West Eifel xenoliths (Germany)														
Ley1-08	HPAS	3.26	2.67	6.74	0.66	2.75	0.23	0.016	0.046		0.0239	0.11591	0.98	<50
Ley1-06	HPAS	0.11	0.14	1.39	0.11	0.16	0.07	0.036	0.113		1.519	0.1226	1.66	<50
LeyX1	HPAS	3.13	2.46	5.58	0.80	4.57	2.07	0.014	0.050		0.0214	0.11471	1.44	<50
LeyX2	HPAS	2.25	2.60	5.45	0.75	3.99	3.21	0.055	0.251		0.119	0.11827	1.68	<50
LeyX3	HPAS	0.30	0.25	2.66	0.23	0.25	0.07	0.016	0.042		0.245	0.1192	1.59	<50
LeyX4	HPAS	3.16	2.37	5.66	0.67	3.52	1.62	0.015	0.039		0.0224	0.11460	1.25	<50

[a] see Table 4.1 footer for description.
[b] italicized values given for Re, Os, $^{187}Re/^{188}Os$ and $^{187}Os/^{188}Os$ from Becker et al. (2006).
[c] Al_2O_3 and S for Beni Bousera, Ligurian and Eifel samples from this study, all other from the literature as described in text.
[d] digestion aliquot used for standard addition analysis of Au, other HSE determined by isotope dilution.

[e] average concentration (± 2sd) calculated from repeated analysis of the same digestion aliquot.
Replicate = replicate digestion of the same sample powder.

Table 4.3.

Model parameters. HSE abundances in ng/g, Al_2O_3 in wt.%, S in µg/g, and monosulphide solid solution (mss)-sulphide liquid (sl) partition coefficients ($D_{HSE}^{mss\text{-}sl}$).

	Ir	Rh	Pt	Pd	Re	Au	Al_2O_3	S
Primitive Mantle[a]	3.5	1.2	7.6	7.1	0.35	1.7	4.25	280
$D_{HSE}^{mss\text{-}sl}$	3.6	3.0	0.2	0.2	2.5	0.1		

[a]Primitive mantle model composition according to McDonough and Sun (1995), Becker et al. (2006) and this study.

4.8 Appendix

4.8.1 Major element data

Major element data for peridotite samples from the Ligurides, Beni Bousera and West Eifel xenoliths were recalculated to 100% volatile free compositions and are listed in Table 4.4. Uncorrected measured whole rock major element compositions are listed in Table 4.5.

4.8.2 Standard addition analysis

Gold abundances of the UB-N serpentine reference and the TUR7 sample powders were determined by standard addition analysis. The results of the regression calculations are shown in Figs. 4.9 and 4.10. For both samples Au signals were normalized to ^{193}Ir and ^{209}Bi, respectively, in order to account for the drift during the measurement.

Table 4.4. Whole rock major elements in wt.% recalculated to 100% volatile free, and Sr (μg/g).

	SiO_2	TiO_2	Al_2O_3	FeO[a]	MnO	MgO	CaO	Na_2O	K_2O	P_2O_5	Cr_2O_3	NiO	LOI[b]	Sr
West Eifel xenoliths														
LeyX1	44.3	0.03	1.44	7.06	0.12	45.5	0.69	0.17	0.02	0.02	0.39	0.28	0.16	20
LeyX2	43.4	0.06	1.68	8.46	0.13	44.1	1.07	0.38	0.04	0.03	0.40	0.27	0.15	15
LeyX3	43.2	0.02	1.59	7.77	0.13	44.0	1.32	1.30	0.02	0.02	0.36	0.29	0.14	19
LeyX4	43.8	0.02	1.25	7.14	0.12	46.2	0.61	0.16	0.01	0.02	0.36	0.29	0.17	15
Ley1-06	43.4	0.05	1.66	8.42	0.15	43.8	1.33	0.37	0.09	0.03	0.43	0.28	0.27	39
Ley1-08	44.6	0.02	0.98	7.01	0.12	45.8	0.49	0.19	0.02	0.04	0.38	0.30	0.22	21
Ligurian ophiolites (Northern Apennines, Italy)														
IL1	43.8	0.04	1.91	7.99	0.13	43.3	2.00	0.15	0.01	0.01	0.33	0.28	0.72	3
IL2	43.7	0.06	1.71	8.30	0.14	42.7	2.33	0.42	0.01	0.01	0.42	0.27	2.13	2
IL3	44.0	0.05	2.25	7.91	0.13	42.6	2.28	0.14	0.01	0.01	0.39	0.28	6.46	3
EL1	44.5	0.13	3.37	7.91	0.13	40.0	3.09	0.25	0.01	0.01	0.35	0.26	5.40	13
Beni Bousera (Morocco)														
BB3A	44.6	0.11	3.00	8.22	0.13	40.1	2.79	0.43	0.01	0.01	0.38	0.26	0.77	24
BB2C	44.3	0.16	3.92	8.22	0.14	38.9	3.21	0.47	0.01	0.02	0.38	0.25	5.87	16
BB2G	45.5	0.11	3.43	7.57	0.13	39.2	3.01	0.34	0.01	0.01	0.39	0.25	0.98	13

[a]Total Fe content reported as FeO.
[b]Loss On Ignition (LOI).

Table 4.5. Measured whole rock major elements in wt.%, except Cr and Ni (μg/g).

	SiO_2	TiO_2	Al_2O_3	Fe_2O_3[a]	MnO	MgO	CaO	Na_2O	K_2O	P_2O_5	Cr	Ni	LOI[b]	Total
West Eifel xenoliths														
LeyX1	43.9	0.03	1.43	7.77	0.12	45.1	0.68	0.17	0.02	0.02	2622	2216	0.16	99.84
LeyX2	42.9	0.06	1.66	9.29	0.13	43.6	1.06	0.38	0.04	0.03	2677	2082	0.15	99.76
LeyX3	42.6	0.02	1.57	8.52	0.13	43.4	1.30	1.28	0.02	0.02	2443	2231	0.14	99.48
LeyX4	43.5	0.02	1.24	7.86	0.12	45.8	0.60	0.16	0.01	0.02	2457	2262	0.17	99.87
Ley1-06	42.9	0.05	1.64	9.25	0.15	43.2	1.31	0.37	0.09	0.03	2927	2192	0.27	99.83
Ley1-08	44.2	0.02	0.97	7.72	0.12	45.4	0.49	0.19	0.02	0.04	2545	2300	0.22	99.86
Ligurian ophiolites (Northern Apennines, Italy)														
IL1	43.1	0.04	1.88	8.73	0.13	42.6	1.97	0.15	0.01	0.01	2191	2175	0.72	99.75
IL2	42.2	0.05	1.65	8.93	0.14	41.3	2.25	0.41	0.01	0.01	2812	2074	2.13	99.60
IL3	40.7	0.04	2.08	8.14	0.12	39.4	2.11	0.13	0.01	0.01	2497	2018	6.46	99.67
EL1	41.7	0.12	3.16	8.23	0.13	37.5	2.89	0.23	0.01	0.01	2273	1912	5.40	99.73
Beni Bousera (Morocco)														
BB3A	43.8	0.10	2.95	8.98	0.13	39.4	2.74	0.42	0.01	0.01	2535	2028	0.77	99.79
BB2C	41.3	0.15	3.65	8.50	0.13	36.2	2.99	0.44	0.01	0.02	2399	1810	5.87	99.61
BB2G	44.7	0.11	3.37	8.26	0.13	38.5	2.95	0.33	0.01	0.01	2595	1894	0.98	99.78

[a]Total Fe content reported as Fe_2O_3.
[b]Loss On Ignition (LOI).

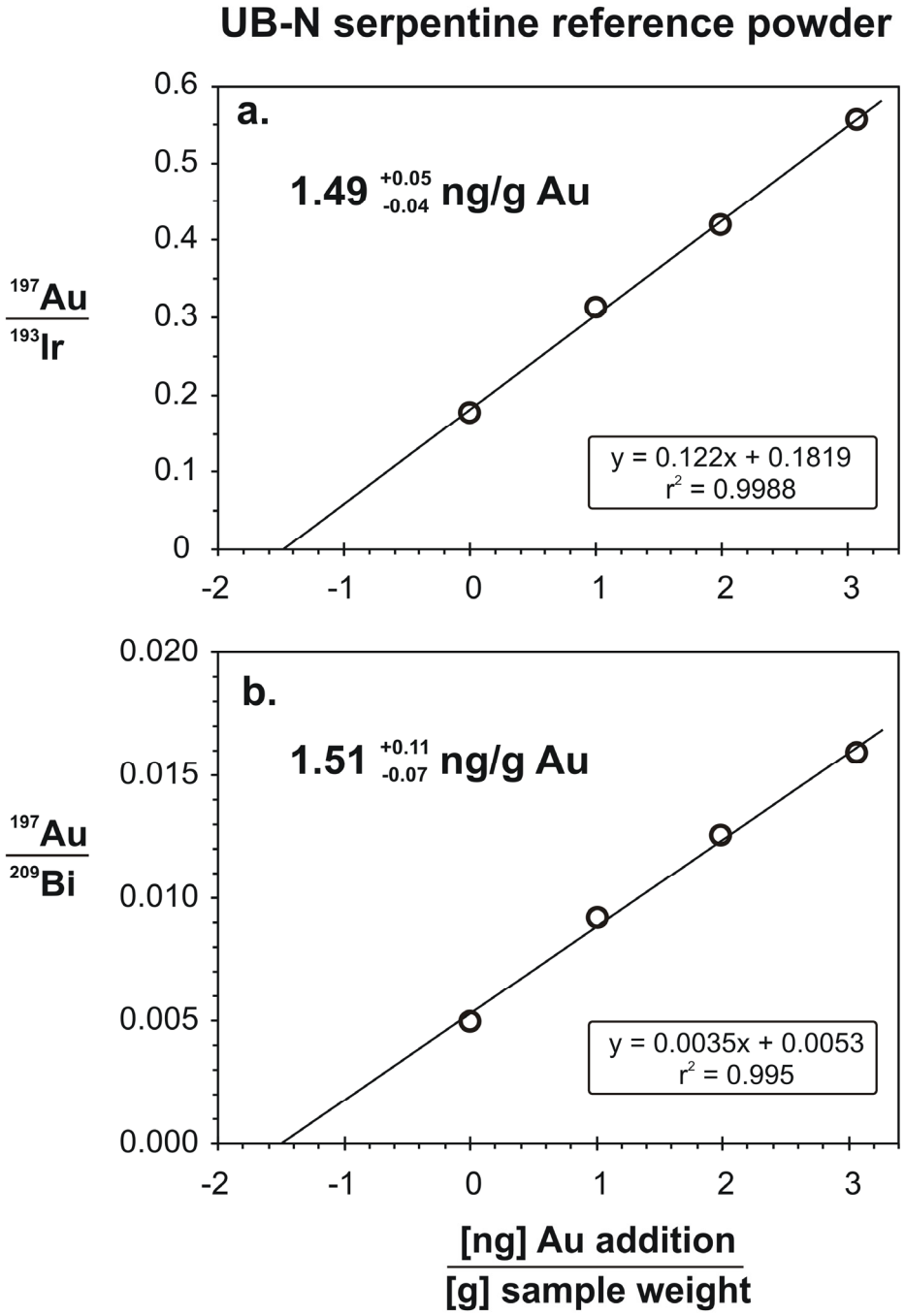

Fig. 4.9. Gold abundances and linear regression results of standard addition analysis for the UB-N ultramafic reference powder. a) ^{193}Ir of the sample solution used for drift correction, b) ^{209}Bi of the sample solution used for drift correction.

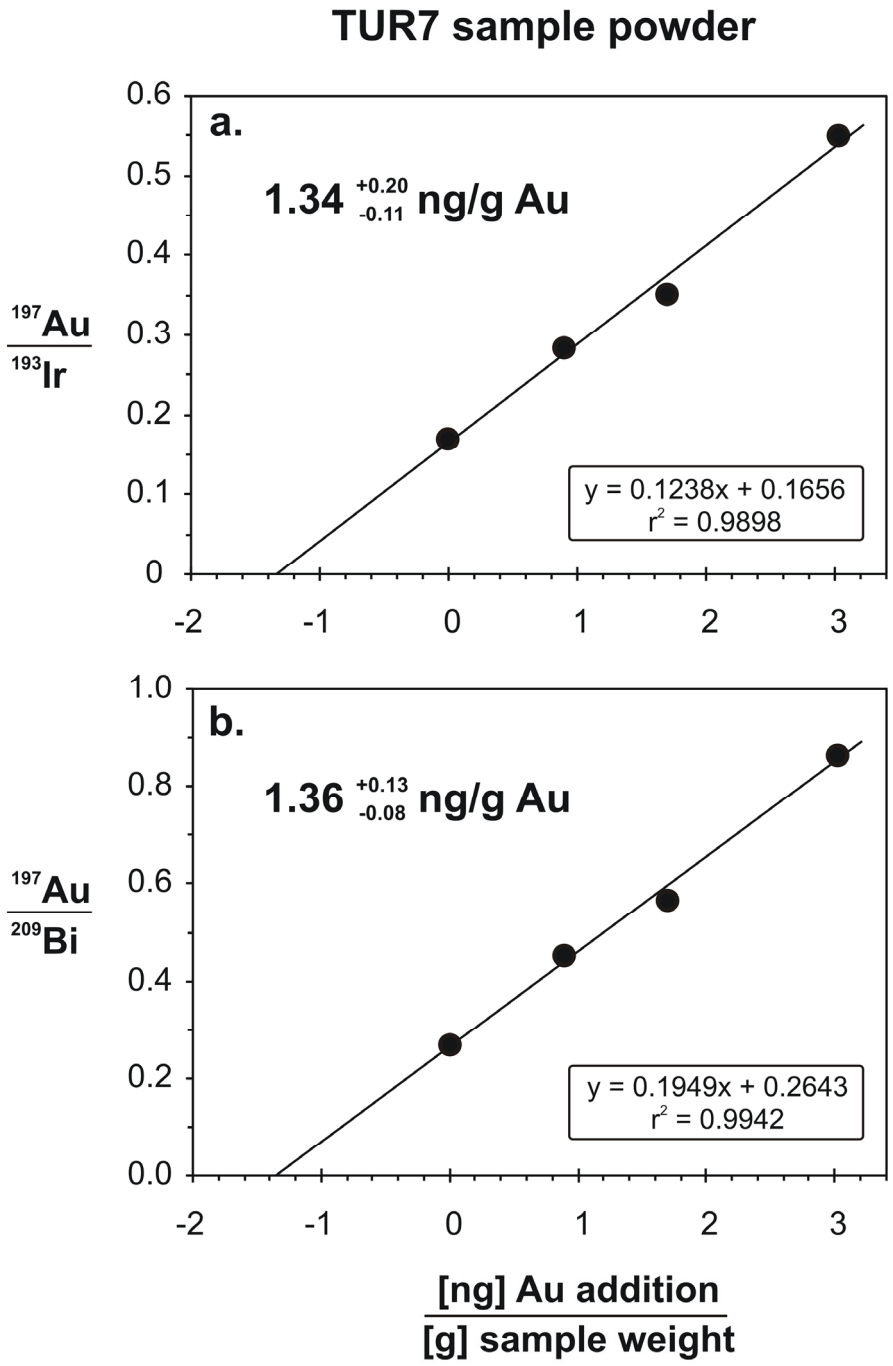

Fig. 4.10. Gold abundances and linear regression results of standard addition analysis for the TUR7 sample powder. a) ^{193}Ir of the sample solution used for drift correction, b) ^{209}Bi of the sample solution used for drift correction.

4.8.3 Comparison of Ir, Rh and Au abundances with literature data

Some of the samples included in this study have previously been analyzed for Ir, Rh and Au (and other HSE) using somewhat different analytical techniques. Iridium abundances determined by high-temperature Carius tube digestion combined with isotope dilution (ID) ICP-MS analysis reported by Becker et al. (2006) agree within <5% with data obtained in this study (Fig. 4.11a). A comparison of Ir concentrations reported in this study with literature data obtained using NiS fire assay pre-concentration techniques followed by INAA and ICP-MS analysis (Lorand et al., 1993; Pattou et al., 1996; Lorand et al., 1999; Lorand et al., 2000) reveals that Ir abundances determined by INAA (Lorand et al., 1993; Lorand et al., 2000) show systematic deviations both towards lower and higher Ir abundances (Fig. 4.11b). Iridium concentrations determined by NiS and ICP-MS analysis (Pattou et al., 1996; Lorand et al., 1999) are most comparable to ID ICP-MS analysis, although some of the Ir values reported in Lorand et al. (1999) tend to be slightly lower in comparison to the ID data.

Rhodium concentration data reported by Pattou et al. (1996) and Lorand et al. (1999) are comparable to the values reported in this study, except some Rh values reported by Lorand et al. (1999) which tend to be somewhat lower in comparison to Rh data from this study (Fig. 4.12a). The Rh/Ir values obtained using NiS fire assay pre-concentration followed by ICP-MS analysis (Pattou et al., 1996; Lorand et al., 1999) compare well with our new data, while most of the NiS INAA data reported by Lorand et al. (2000) show higher Rh/Ir caused mainly due to lower Ir and also higher Rh concentrations compared to this study and to Ir data from Becker et al. (2006) (Figs. 4.11 and 4.12b).

In the case of Au replicate digestions of the same sample powders occasionally yield Au concentrations that differ about 30% and even the UB-N reference powder shows some variability (Tables 4.1 and 4.2 in the main text). A pronounced variability of Au in sample powder of the same sample has also been noted in previous studies (e.g. Lorand et al., 1999; Luguet et al., 2004), and hence, a direct comparison to data obtained using different analytical techniques is somewhat more complicated. Gold concentrations and Au/Ir from Pattou et al. (1996) and Lorand et al. (1999) obtained by NiS collection combined with ICP-MS analysis seem to be most comparable to our data (Fig. 4.13a,b). Other data from Lorand et al. (1993, 2000) obtained by INAA after NiS collection in most

cases yielded much higher Au concentrations and Au/Ir in comparison to this study. Lorand et al. (1999) used both ICP-MS and NAA techniques for determination of Au, and the difference between both techniques was up to 50% for particular samples. As discussed in Lorand et al. (1999) Au determinations using NiS collection seem to be governed by non-quantitative Au yields, lower precision and reproducibility, and elevated blank levels (Pattou et al., 1996; Luguet et al., 2004).

A comparison of PGE abundances obtained on komatiites by NiS fire-assay collection combined with ID ICP-MS in comparison to data obtained by Carius tube digestion and ID ICP-MS reveals that both analytical methods show the same general trends, but absolute HSE abundances were underestimated using the NiS digestion method by 17-42% for Os, Ir, Ru, Pt and Pd, probably because spinel phases were not dissolved by the NiS method (Puchtel et al., 2004). Furthermore (Lorand et al., 2008) observed that Os, Ir and Pt abundances determined after NiS fire assay collection were underestimated by 10-20% in comparison to ID ICP-MS analysis after high temperature acid digestion, while Ru, Rh and Pd abundances were reproducible to the same values using both methods.

As noted earlier the scatter displayed by HSE data obtained using NiS fire assay pre-concentration techniques has been larger than the scatter of data obtained from HPA-S and CT digestion techniques combined with ID ICP-MS analysis (Fig. 4.11a,b), despite the sample weights used for NiS fire assay pre-concentration are typically much larger (10-15 g) compared to HPA-S and CT digestions (2-3 g). Thus, sample heterogeneity is considered to be unlikely to account for the larger scatter observed for data obtained by NiS digestion (see discussions in (Meisel and Moser, 2004; Becker et al., 2006).

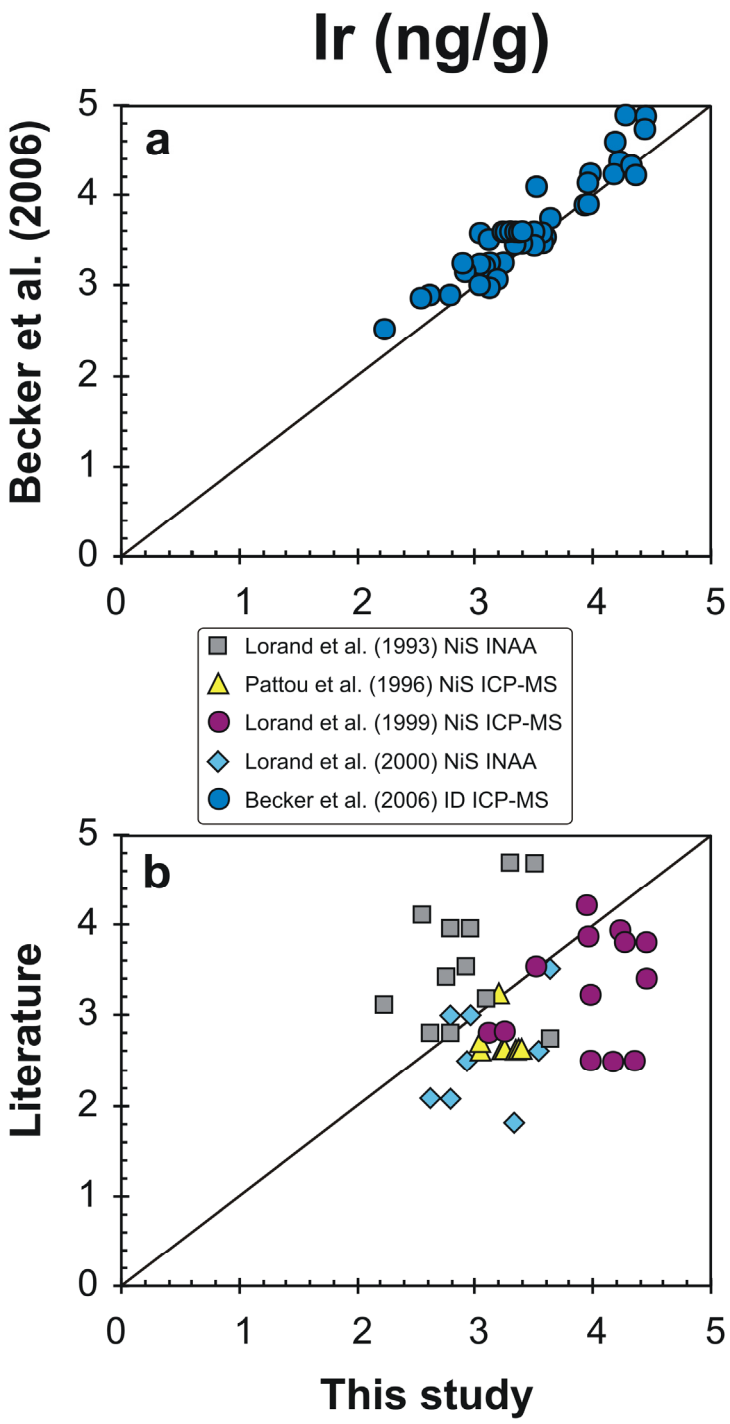

Fig. 4.11. Iridium abundances from this study obtained after high-temperature acid digestion followed by ID ICP-MS analysis in comparison to literature values for the same samples from Becker et al. (2006) (a), and Lorand et al. (1993), Pattou et al. (1996) and Lorand et al. (1999, 2000) (b).

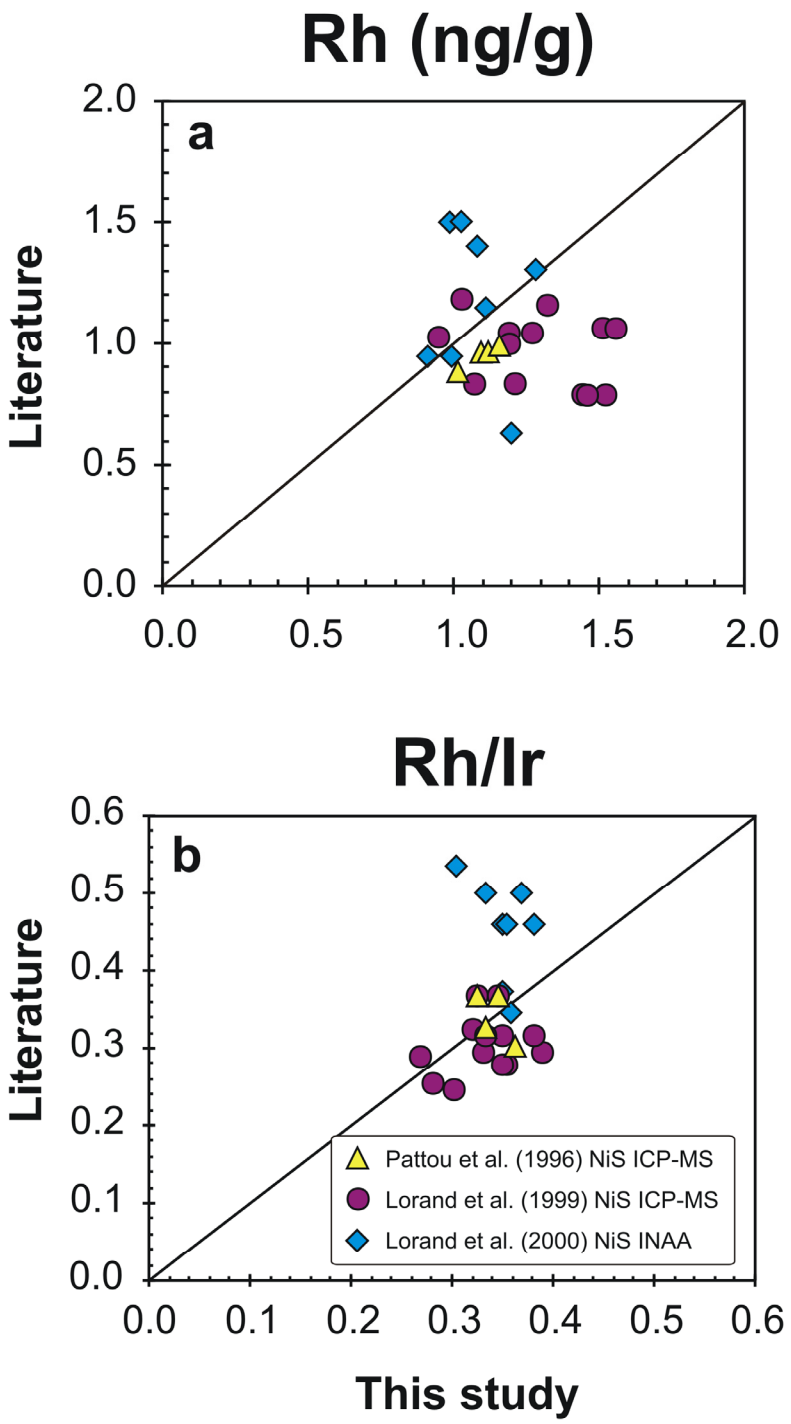

Fig. 4.12. Rhodium concentration data and Rh/Ir from this study obtained after high-temperature acid digestion followed by ICP-MS analysis in comparison to literature values from Pattou et al. (1996) and Lorand et al. (1999, 2000) for the same samples.

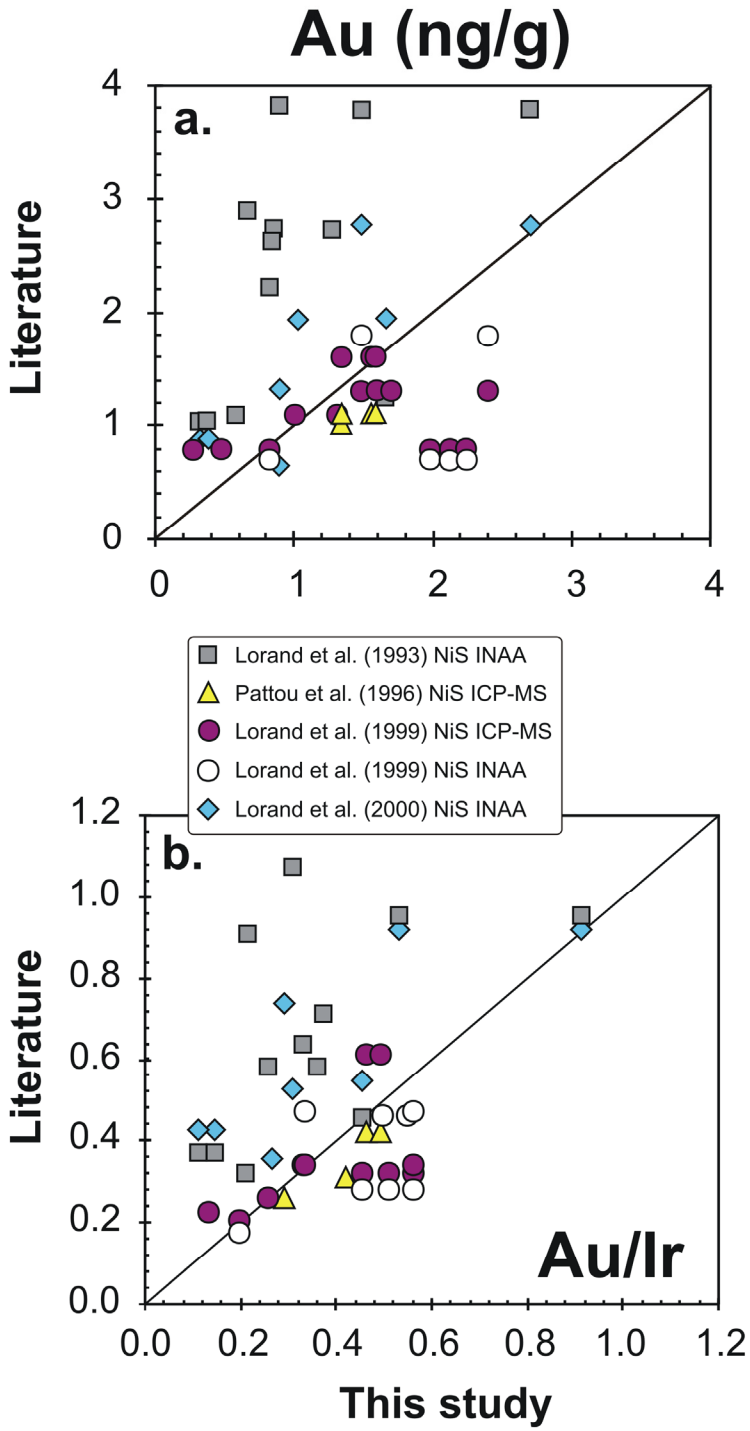

Fig. 4.13. Gold concentration data and Au/Ir from this study obtained after high-temperature acid digestion followed by ICP-MS analysis in comparison to literature values from Lorand et al. (1993), Pattou et al. (1996) and Lorand et al. (1999, 2000) for the same samples.

5. Highly siderophile element abundances and $^{187}Os/^{188}Os$ in ancient lunar impact melt rocks

5.1 Abstract

The abundances of highly siderophile elements (HSE: Re, Os, Ir, Ru, Pt, Rh, Pd, Au) and $^{187}Os/^{188}Os$ isotope compositions have been determined for 57 subsamples of five lunar impact melt breccias from Apollo 14 (14310), 16 (60315, 67935, 67955), 17 (79215), and the lunar meteorite DaG400. Concentrations of Re, Os, Ir, Ru, Pt and Pd were determined by isotope dilution ICP-MS and N-TIMS. The monoisotopic elements Rh and Au were quantified relative to the abundance of Ir. The new data allow further constraints to be placed on the compositions of meteoritic materials accreted to the early Earth-Moon system.

We report the first Re-Os age obtained for a lunar impact melt rock. ^{187}Re-^{187}Os isotope systematics for Apollo 16 sample 67935 define an isochron age of 4.11 ± 0.12 Ga, which is interpreted to reflect localized solid metal-liquid metal separation in the impact melt, and thus the impact that produced the melt. This particular impact event may have produced the Nectaris basin.

Excellent linear correlations displayed by subsamples of a given impact melt rock in plots of HSE vs. Ir are explained by dilution processes or binary mixing between a high HSE end-member composition and a low HSE end-member composition. The high HSE component corresponds to the meteoritic impactor composition, whereas the low HSE component represents HSE components in the lunar target rocks. Linear regression calculations yield zero intercept values for true binary mixtures between meteoritic impactor material and pristine lunar crustal target rocks. Intercept values statistically resolvable from zero indicate contributions from the lunar target rocks, or may reflect mixing of different HSE-rich impactor materials within the same rock.

Slope-derived HSE compositions and $^{187}Os/^{188}Os$ of the high HSE end-member in granulitic impact melt rocks from Apollo 16 and 17 are similar to chondritic meteorites and resemble the composition inferred for Apollo 17 aphanitic melt rocks. Suprachondritic ratios of Ru/Ir, Pt/Ir, Rh/Ir, and Pd/Ir for Apollo 14 basaltic impact melt rock are similar to ratios observed for other Apollo 14 samples and Apollo 17 poikilitic impact melt breccias. Apollo 16 poikilitic and basaltic impact melt rocks show subchondritic Os/Ir and pronounced suprachondritic ratios of $^{187}Os/^{188}Os$, Re/Ir, Ru/Ir, Pt/Ir, Rh/Ir, Pd/Ir and Au/Ir out of the chondritic range. Their strongly fractionated HSE abundance patterns are similar to IVA iron meteorites and indicate a possible iron meteorite impactor. Despite the similarities to chondritic meteorites observed for the granulitic impact melt rocks and the possible match with iron meteorites inferred for Apollo 16 impactites, suprachondritic ratios observed for some impact melt rocks can not be related to known chondrite groups. As discussed earlier these compositions may reflect ancient meteoritic material with distinct chemical compositions not recognized in the present meteoritic record or differentiated meteoritic material.

5.2. Introduction

The surface of the Moon is characterized by large impact basins, which may have formed 4 billion years ago during a period of intense bombardment in the inner solar system (e.g. Hartmann et al., 2000; Ryder, 2002). Basin forming impact events generate large volumes of impact melt rocks and breccias (here collectively referred to as ancient lunar impact rocks). These rocks provide important information on the nature and origin of the projectiles and on the timing of the early impact flux to the Moon and by inference to the early Earth and other terrestrial planets. More specifically, the compositional record of ancient lunar impact rocks may provide constraints for understanding the excess siderophile element abundances observed of the Earth's mantle, commonly explained by late accretion of meteoritic materials after core formation (Chou, 1978; Jagoutz et al., 1979; Morgan, 1986; O'Neill, 1991; Schmidt et al., 2000; Meisel et al., 2001; Morgan et al., 2001; Schmidt, 2004; Becker et al., 2006).

High abundances of siderophile elements in ancient lunar impact rocks were added by the meteoritic impactors and are entirely the result of late accretion processes (Anders et al., 1973; Morgan et al., 1974). Because the pristine lunar crustal target rocks have very low HSE concentrations (Gros et al., 1976; Hertogen et al., 1977; Warren and Wasson, 1977; Ebihara et al., 1992; Day et al., 2010), absolute and relative HSE abundances in ancient lunar impact rocks are dominated by the impacting bodies (Korotev et al., 1994; Puchtel et al., 2008).

Early work on samples collected from the Apollo landing sites revealed differences in relative abundances of refractory and volatile siderophile elements (e.g. Ir, Au, Re, Sb, Ge) for ancient lunar impact rocks from different landing sites. These data were used for impactor discrimination and to relate distinct siderophile element compositions to specific impact basins on the lunar surface (Morgan et al., 1972; Anders et al., 1973; Morgan et al., 1974; Higuchi and Morgan, 1975; Morgan et al., 1975a,b; Wasson et al., 1975; Gros et al., 1976; Morgan et al., 1976; Hertogen et al., 1977; Morgan and Petrie, 1979). These studies revealed that some of the impacting bodies were similar to chondritic meteorites, while other compositions could not be related to known chondrite groups. It was suggested that the latter compositions reflect ancient meteoritic impactor populations (Morgan et al., 1974; Hertogen et al., 1977; Morgan et al., 1977), or may reflect compositions of evolved chondritic metal probably derived from iron meteorites (Ganapathy et al., 1972; Morgan et al., 1972; Korotev, 1987a,b; James, 1995; 1996; 2002).

Precise highly siderophile element (HSE: Re, Os, Ir, Ru, Pt, Rh, Pd, Au) abundance and $^{187}Os/^{188}Os$ data sets obtained using modern analytical techniques also show that some of the meteoritic components accreted to the lunar surface may have had a HSE composition different from the known chondrite groups. In particular, some meteoritic components contained in these rocks bear evidence for the late accretion of meteoritic material with elevated Pd/Ir and Ru/Ir, which extend beyond the suprachondritic ratios, similar to values inferred for the Earth's primitive mantle (Norman et al., 2002; Becker et al., 2006; Puchtel et al., 2008; Fischer-Gödde et al., 2010c).

The goal of the present work is to increase the HSE data base on ancient lunar impact rocks and to include lithologies and locales for which no comprehensive HSE data set has been available. Constraining the impactor compositions and evaluating mixing between

putative impactor compositions and indigenous or multiple meteoritic components in the target rock requires analysis of multiple aliquots of a single rock sample (e.g. Korotev, 1994; McDonald et al., 2001; Tagle and Claeys, 2005; Puchtel et al., 2008). We report new HSE concentration data for Re, Os, Ir, Ru, Pt, Rh, Pd, Au and $^{187}Os/^{188}Os$ data obtained on subsamples of five lunar impact melt rocks from Apollo 14 (14310), Apollo 16 (60315, 67935, 67955), Apollo 17 (79215), and the lunar meteorite DaG400. The new data will be discussed along with previous precise HSE data sets obtained on lunar impact melt rocks in order to relate specific impactor compositions

5.3. Samples

Apollo samples were selected based on their sampling sites and abundances of diagnostic siderophile elements (Ir, Re, Au) determined by previous studies that utilized neutron activation analysis (NAA), indicating meteoritic contributions contained within the rocks.

5.3.1 Apollo 14 basaltic impact melt rock

The Apollo 14 landing site is located on the Fra Mauro Formation north of the Fra Mauro crater and about 550 km south of the Imbrium basin rim crest (Stöffler and Ryder, 2001; Hiesinger and Head, 2006). It was chosen primarily to sample the Fra Mauro Formation which has been interpreted to represent a part of the continuous Imbrium ejecta blanket (Stöffler and Ryder, 2001), or a mixture between Imbrium and locally derived material (Oberbeck, 1975; Wilhelms 1987; Haskin et al., 2002).

Sample 14310 has been collected during the second extravehicular activity (EVA) as a separate sample on the lunar surface at station G. It could have been a clast within the Fra Mauro Formation or not. The sample is described as a fine-grained feldspathic basalt consisting of ~68% plagioclase, ~31% pyroxene, ~0.5% opaque assemblages, trace metals and about ~0.5% mesostasis (LSPET, 1972). Plagioclase laths build a randomly orientated intersertal texture with interstitial pyroxene. Some large plagioclase phenocrysts are also

observed. Interstitial ilmenite is the most abundant opaque phase and is intergrown with pyroxene. Other opaque phases are troilite, ulvöspinel and Fe-Ni metal. Occasional breccia clasts surrounded by crystalline melt indicate an impact rather than a magmatic origin. Further evidence for an impact origin comes from high siderophile element abundances (8.5 - 10.5 ng/g Ir and 4.31 ng/g Au, Baedecker et al., 1972; Morgan et al., 1972). Ar-Ar and Rb-Sr ages range from 3.79 to 3.88 Ga (Papanastassiou and Wasserburg 1971, York et al. 1972, Turner et al. 1972). We received a 1.062 g chip of subsample 14310, 35. Under the binocular microscope the rock showed a typical basaltic texture consisting mainly of plagioclase and pyroxene, and minor ilmenite and troilite. No visible clasts were observed.

5.3.2 Apollo 16 impact melts

The purpose of the Apollo 16 mission was primarily to study the lunar anorthositic highland crust. At the Apollo 16 landing site two dominant geologic formations occur: the Cayley Formation and the Descartes Formation (Hiesinger and Head, 2006). Numerous subdued craters are located near the landing site, e.g. North Ray crater. The landing site was located on the Cayley Formation, which is interpreted to be emplaced as a part of the discontinuous ejecta of the Imbrium impact event, while the Descartes Formation is suggested to be related to the Nectaris ejecta blanket (James, 1981; Stöffler et al., 1981; Stöffler and Ryder, 2001). The landing site most probably consists of ejecta depositions contributed from Imbrium, Nectaris and Serenitatis basins (Muehlberger et al., 1980; Haskin et al., 2002).

Sample 60315 was collected 5 m north of the lunar landing module. It is a greenish-grey coherent rock and was classified as a poikilitic melt breccia (McKinley et al., 1984). The sample is holocrystalline and dense. It has a poikilitic texture with large oikocrysts of pyroxene enclosing smaller plagioclase and olivine grains (Simonds et al., 1973). Siderophile element abundances in one aliquot are 11.0 ng/g Ir, 18.3 ng/g Au and 1.36 ng/g Re (Ganapathy et al., 1974). The sample was dated with Ar-Ar (3.87 – 4.03 Ga, Kirsten et al., 1973; Husain & Schaeffer, 1973; Schaeffer et al., 1976; Norman et al., 2006) and Pb-Pb (3.99 Ga, Nunes et al., 1973). The sample used for the present work is a

1.020 g chip derived from the interior of subsample 60315, 46. Under the binocular microscope the sample comprises of mainly plagioclase, pyroxene and minor olivine. Visible minor components were Fe-Ni metal and troilite. One corner of the chip showed a mm-sized metal globule contained in a vesicle. The weight of the metal globule was about ~9 mg, and it was analyzed as a separate subsample. During break-up of the sample several tiny sub-millimeter sized metal globules were observed.

Samples 67935 and 67955 were collected from "Outhouse Rock" a large boulder located on the rim of the North Ray crater at Station 11. Both samples were located only a few cm away from each other within in the same boulder. The material excavated by the North Ray crater projectile is thought to be derived from the Descartes formation which is supposed to be related to formation of the Nectaris basin (Stöffler et al., 1981; Stöffler and Ryder, 2001). 67935 is described as a moderately coherent, light gray, fine grained basaltic impact melt. It consists of coarser-grained areas with a subophitic texture and finer grained areas with a poikilitic texture. The sample contains Fe-metal/troilite intergrowths which are randomly distributed. Stöffler at al. (1985) classified this sample as a subophitic intersertal impact melt breccia. Siderophile element abundances in one aliquot are 12.9 ng/g Ir, 13.9 ng/g Os, 12.3 ng/g Au and 1.37 ng/g Re (Hertogen et al., 1977). To our knowledge 67935 has not been dated before. Argon ages determined for impact melt breccias and regolith clasts from the same location show ages between 3.9 - 4.1 Ga with maximum ages as old as 4.2 Ga (Schaeffer and Husain, 1973; Maurer et al., 1978; Norman et al., 2006, 2007, 2010). It is highly debated whether these old age populations may represent the Nectaris impact event or a pre-Nectaris impact event (e.g. James, 1981; Norman et al., 2010). We received two chips from subsample 67935, 1 with a total weight of 1.144 g. A description of Apollo 16 sample 67955 is given in the following section.

5.3.3 Lunar Granulites

Samples 67955 and 79215 belong to a group of highland rocks with metamorphic textures, the so called granulitic impactite suite (Warner et al., 1977; Lindstrom and Lindstrom, 1986). The granulitic rocks are thought to originate from the early lunar crust

before it was reworked by later lunar bombardment (Warner et al., 1977). Ar-Ar ages and Sm-Nd model ages ≥4.0 Ga (Turner and Cadogan, 1975; Jessberger et al., 1976; Norman et al., 2007; Hudgins et al., 2008) and the occurrence of granulitic clasts in subsequent 3.9 Ga old impact melt rocks indicate that the lunar granulites were formed and metamorphosed before the 3.9-3.8 impact events (Warner et al., 1977). The granulites consist of a ferroan and a magnesian group and are most probably derived from anorthositic and noritic precursor rocks (Lindstrom and Lindstrom, 1986). Both of our sample aliquots are members of the magnesian group. Three different textural types of lunar granulites can be distinguished: poikilitic, poikilitic-granoblastic and granoblastic breccias, which all have similar equilibration temperatures of 1100 ± 50 °C according to the two-pyroxene thermometer (Cushing et al., 1999). Cushing et al. (1999) suggested that the granoblastic textures (e.g. 79215) were generated during metamorphism, whereas the poikilitic textures (e.g. 67955) are suggested to represent the result of impact induced melting.

Apollo 16 sample 67955 is a coarse grained grey noritic anorthosite. The rock texture is poikiloblastic and the sample was classified as a feldspathic granulite and as a poikilitic magnesian granulite (Warner et al., 1977; Lindstrom and Lindstrom, 1986). The mineral assemblage is 78.5 % plagioclase, 14.5 % pyroxene, 6 % olivine and 1 % opaque phases. Plagioclase and olivine grain shapes are euhedral to subhedral, surrounded by pyroxene oikocrysts (Hollister et al., 1973). The sample contains 5.56 - 11 ng/g Ir, 1.6 – 2.2 ng/g Au and 0.572 ng/g Re (Ganapathy et al., 1974; Boynton et al., 1976; Wasson et al., 1977; Palme et al., 1978; Lindstrom et al., 1986) and has a chondritic Ni/Co ratio (Ostertag et al., 1984). A Sm/Nd crystallization age of 4.20 Ga was reported by Norman et al. (2007). We were allocated a 1.180 g chip subsample of 67955, 87. Under the binocular microscope the chip shows a granoblastic texture of plagioclase, olivine, with larger grains of pyroxene. It has a brecciated appearance with brittle fracture planes. It consists of grey and white colored zones, the latter appear to be finer grained than the grey parts. Dark oxide phases are contained mainly in the white parts.

Apollo 17 sample 79215 was classified as a magnesian granulitic impactite (Lindstrom & Lindstrom, 1986). It is a holocrystalline feldspar-rich rock, characterized by a granoblastic matrix of equant plagioclase grains (McGee et al., 1971; Neal and Taylor, 1993). The plagioclase grain boundaries are equilibrated show 120° triple junctions with

intersertal grains of olivine, pyroxene and opaque minerals (Bickel et al., 1976; McGee et al., 1978). The average mineralogical composition of the sample is about 80 % plagioclase, 10 % olivine and 8 % pyroxene (Bickel et al., 1976; McGee et al., 1978). The rock contains assemblages of opaque minerals consisting of spinel, ilmenite, troilite, rutile and metallic iron, which are surrounded by a corona of plagioclase and olivine (McGee et al., 1978). Three subsamples of this granulite contain 6.95 - 28.8 ng/g Ir, 1.67 - 15.6 ng/g Au, 0.495 - 2.10 ng/g Re (Higuchi & Morgan, 1975). Hudgins et al. (2008) reported abundances of Ir (6.0 – 6.6 ng/g) and Au (1.1 – 5 ng/g). Ar-Ar age determinations range from 3.87 to 4.03 Ga (MacGee et al., 1978; Oberli et al., 1979; Hudgins et al., 2008). A peak metamorphic Ar-Ar age of 3.9 ± 0.1 Ga was inferred by Hudgins et al. (2008), which is supposed to reflect the time when 79215 was excavated from depth by a large basin forming impact event. This age may also correlate with the age of the Serenitatis impact basin (Stöffler et al., 2006). We were allocated five chips of subsample 79215, 2 weighting 1.154 g. Under the binocular the chips showed a granoblastic texture consisting of mainly plagioclase and minor olivine and pyroxene. It also contains visible opaque phases (troilite and ilmenite).

5.3.4 Lunar meteorite DaG400

The lunar meteorite Dar al Garni (Dag) 400 was recovered from the Libyan Desert. A detailed classification and description of the meteorite is given in Zipfel et al. (1998). According to that study the meteorite consists of a fine grained matrix containing mostly subophitic clasts of impact melt breccias, granulitic fragments, recrystallized anorthositic clasts, and other mineral fragments. The meteorite contains visible melt spherules and impact melt veins. Its major and trace element composition is similar to other lunar highland meteorites (Zipfel et al., 1998; Korotev et al., 2003; Cahill et al., 2004). Siderophile element abundance ranges are 4.0 - 5.3 ng/g Ir and 2.3 - 26 ng/g Au (Zipfel et al., 1998; Korotev et al., 2003). We were allocated a subsample of ~300 mg. Fresh looking parts of the sample were grey and dense. Terrestrial alteration was indicated by visible carbonate veins and some rusty spots on the surface and in the interior.

5.4 Analytical techniques

The samples were crushed into coarse grained chips using an alumina ceramic mortar. Of gram sized Apollo impact melt rock samples about 10 subsample aliquots weighting ~100 mg, and 7 subsample aliquots from the lunar meteorite DaG400 weighting ~40 mg, were weighted into quartz glass digestion vessels. Mixed ^{185}Re-^{190}Os and ^{191}Ir-^{99}Ru-^{194}Pt-^{105}Pd spike solutions were added, followed by 2.5 ml conc. HCl and 5 ml conc. HNO_3. The vessels were sealed with teflon-tape and heated in a high-pressure asher (HPA-S, Anton Paar™) for 16 h at 320°C.

Osmium was extracted immediately after digestion by solvent extraction from the reverse aqua regia into CCl_4, back extraction into HBr (Cohen and Waters, 1996), and further purification by microdistillation from a H_2SO_4-dichromate solution into a drop of HBr (Roy-Barman, 1993). The remaining aqua regia solution was transferred into a PFA beaker, evaporated to near dryness and afterwards taken to near dryness twice with 2 ml 8.3 M HCl and once with 1 ml 1.25 M HCl. Rhenium, Ir, Ru, Pt, Rh, Pd and Au were separated from the matrix by cation exchange chromatography using 10 ml of pre-cleaned Eichrom™ 50W-X8 (100-200 mesh) resin and a 0.5 M HCl-60 % acetone mixture (4 ml 1.25 M HCl + 6 ml ultrapure acetone) as the eluting solvent. The resin and the sample solutions were adjusted to the same HCl-acetone concentration before loading onto the column. All HSE were eluted together in 14 ml 0.5 M HCl-60 % acetone. A detailed description of the chemical separation procedure is provided in Fischer-Gödde et al. (2010).

For ICP-MS analysis of Re, Ir, Pt and Au the acetone content of the eluted HSE fraction was evaporated so that the solution introduced into the ICP-MS instrument was ~1 M HCl. After analysis the remaining solution was taken to near dryness and taken up into 0.28 M HNO_3 for analysis of Rh, Ru (along with Ir and Pt). In order to avoid interferences from Cd isotopes on Pd a clean-up procedure using smaller columns filled with 2 ml Eichrom 50W-X8 resin (100-200 mesh) and 0.2 M HCl was performed with the remaining solution after analysis of the Rh-Ru-Ir-Pt cut. The 0.2 M HCl solution was evaporated to near dryness and taken up into 0.28 M HNO_3 for ICP-MS analysis of Pd.

Osmium isotopic compositions were measured by negative thermal ionisation mass spectrometry using a Thermo-Finnigan^{TM} Triton at the FU Berlin. Osmium concentrations were determined by isotope dilution. Signals were detected on Faraday cups in static mode or on a secondary electron multiplier (SEM) operating in pulse counting mode. Measured ratios were corrected for isobaric OsO_3^- interferences using $^{16}O/^{18}O$ and $^{17}O/^{18}O$ of 0.00204 and 0.00037, respectively. Mass fractionation was corrected using a linear law and $^{192}Os/^{188}Os$ = 3.08271 (Shirey and Walker, 1998). Values and long-term reproducibility for $^{187}Os/^{188}Os$ of the UMD Os standard solution were 0.11380 ± 0.00003 (2s, n = 43) on Faraday cups and 0.1141 ± 0.0003 (2s, n = 19) for measurements on the SEM.

All other HSE were measured by sector-field inductively coupled plasma mass spectrometry using the ThermoElectron^{TM} Element XR equipped with an ESI^{TM} SC-autosampler at FU Berlin. Concentrations of Re, Ir, Ru, Pt and Pd were determined by isotope dilution. The monoisotopic elements Rh and Au were quantified using a combined internal/external standardization technique (Fischer-Gödde et al., 2010a,b). Signals were detected in low resolution by a secondary electron multiplier operating in pulse counting mode. Internal precision of measured isotopic ratios ranged from 0.1 to 1 % ($2s_m$, with n = 100). For analysis of Re, Ir, Pt and Au in ~1 M HCl media a glass spray chamber (either cyclonic or Scott-type) was used. The Rh-Ru-Ir-Pt cut and the Pd clean-up fraction were analyzed in 0.28 M HNO_3 media using an Aridus membrane desolvator, which reduced oxide interferences and increased signal intensities. While the glass spray chamber setup yielded better reproducibilities for Au and Re, the setup with the Aridus was required for precise and accurate Ru-Rh-Pd data, obviously due to suppressed interferences in this mass range (Fischer-Gödde et al., 2010a). Acid blank solutions were measured at the start of each measurement session and after every 3-4 sample solutions to monitor background intensities and memory effects. Background corrections were carried out, if the background intensities were > 1 % of the sample intensities. At the start, in the middle and at the end of each measurement session a Re, Ir, Ru, Pt, Rh, Pd, Au standard solution with roughly chondritic HSE ratios and ~1 ppb Ir was measured. Mass fractionation was determined and corrected for by the comparison of the ratios measured in the standard solution with IUPAC reference values. The long-term external reproducibility of isotopic compositions in the standard solution is < 1 % (1s).

Total chemistry blank levels for HPA-S digestions were 7 ± 2 pg Re, 2 ± 1 pg Os, 0.7 ± 0.6 pg Ir, 2 ± 1 pg Ru, 3 ± 2 pg Pt, 3 ± 2 pg Rh, 18 ± 13 pg Pd, 13 ± 7 pg Au (n=12). Average blank contributions for Apollo samples are less than 0.5% for Os, Ir, Ru and Pt, 2% for Rh, 5% for Pd, and less than 10% for Re and Au. The precision of the HSE concentration data estimated based on blank contribution and variation in the blank is conservatively estimated to be better than 1% for Os, 2% for Ir, Ru and Pt, 5% for Pd, Re. The precision for Rh and Au concentrations is estimated to be better than 10% and 15%, respectively. For the lunar meteorite DaG400 the precision might be somewhat less because of the smaller sample weights used for digestion and higher blank contributions of less than 2% for Os, Ir, Ru and Pt, 5% for Rh, 20% for Pd and Au, and less than 35% for Re.

Accuracy and reproducibility of the analytical technique can be assessed from the results obtained for the Smithsonian Allende reference powder (Table 3.1, p. 61, Fischer-Gödde et al., 2010a) and the UB-N ultramafic reference powder (Table 4.1, p. 114, Fischer-Gödde et al., 2010b) in comparison to results obtained in other laboratories.

5.5 Results

5.5.1 Re/Os and osmium isotope compositions

Rhenium, Os, $^{187}Re/^{188}Os$ and $^{187}Os/^{188}Os$ data are provided in Table 5.1. Concentrations of Re and Os obtained on the subsample aliquots span a total range from 0.343 to 146 ng/g and 2.92 to 1295 ng/g, respectively. Lowest concentrations for Re and Os were obtained for subsamples from the lunar meteorite DaG400, and highest for a metal spherule subsample from 60315 (#10). In the case of Apollo 14 sample 14310 no Re and Os data could have been obtained because a wrong Re-Os spike solution was added. Subsamples of a given impact melt rock commonly display only limited variation in Re/Os and $^{187}Os/^{188}Os$ (Table 5.1 and Puchtel et al., 2008). Because of the ß-decay of ^{187}Re to ^{187}Os measured $^{187}Os/^{188}Os$ ratios should reflect the time-integrated Re/Os ratio of the meteoritic materials contained in lunar impact melt rocks, provided that the Re/Os

ratio was not disturbed before or during the accretion to the lunar surface. Average $^{187}Os/^{188}Os$ of Apollo 14 basaltic impact melt rock 14310 and the lunar meteorite DaG400 are 0.1312 ± 3 and 0.1295 ± 14, respectively. Both Apollo 16 poikilitic and basaltic impact melt rocks 60315 and 67935 are characterized by the most radiogenic average $^{187}Os/^{188}Os$ of 0.1398 ± 6 and 0.1362 ± 42 obtained for lunar impact melt rocks so far. These samples also have corresponding Re/Os, which are higher than the most radiogenic chondrites, and more similar to values observed for some magmatic iron meteorites (e.g. Smoliar et al., 1996; Cook et al., 2004; Walker et al., 2005). Measured $^{187}Os/^{188}Os$ for subsamples of 67935 display a relatively large variation from 0.1258 – 0.1412, compared to other lunar impact melts analyzed in this study and Puchtel et al. (2008). The Apollo 16 and 17 granulitic breccias show average $^{187}Os/^{188}Os$ of 0.1277 ± 4 (67955) and 0.1277 ± 8 (79215), similar to chondrites and consistent with their Re/Os. Average ratios of $^{187}Os/^{188}Os$ for 14310, 67955, 79215 and DaG400 are within the range of chondritic meteorites (0.1173 – 0.1328, Chen et al., 1998; Walker et al., 2002; Brandon et al., 2005a,b; Fischer-Gödde et al., 2010a). The lunar meteorite DaG400 shows highly variable $^{187}Re/^{188}Os$ ranging from 0.41 to 1.01.

Re-Os isotope systematics for subsample aliquots of Apollo 16 sample 67935 yield a well defined internal isochron corresponding to an age of 4.11 ± 0.12 Ga and initial $^{187}Os/^{188}Os$ of 0.099 ± 0.001 (MSWD = 0.93) (Fig 5.1a). Back-calculation of the measured isotopic compositions for the subsamples to an age of 4.558 Ga, the likely closure age of IIIA iron meteorites, yields an average initial $^{187}Os/^{188}Os$ indistinguishable from the chondritic initial solar system $^{187}Os/^{188}Os$ of 0.09531 obtained for IIIA irons. Assuming a two step evolution, the calculation of the stage-1 Re/Os of the precursor material corresponding to an age of 4.558 Ga yields a $^{187}Re/^{188}Os$ of 0.475 ± 0.013, which overlaps with the highest $^{187}Re/^{188}Os$ observed for enstatite and ordinary chondrites (Walker et al., 2002; Brandon et al., 2005a,b; Fischer-Gödde et al., 2010), but also with ratios of magmatic iron meteorites (Shen et al., 1996; Smoliar et al., 1996; Horan et al., 1998; Cook et al., 2004; Walker et al., 2005).

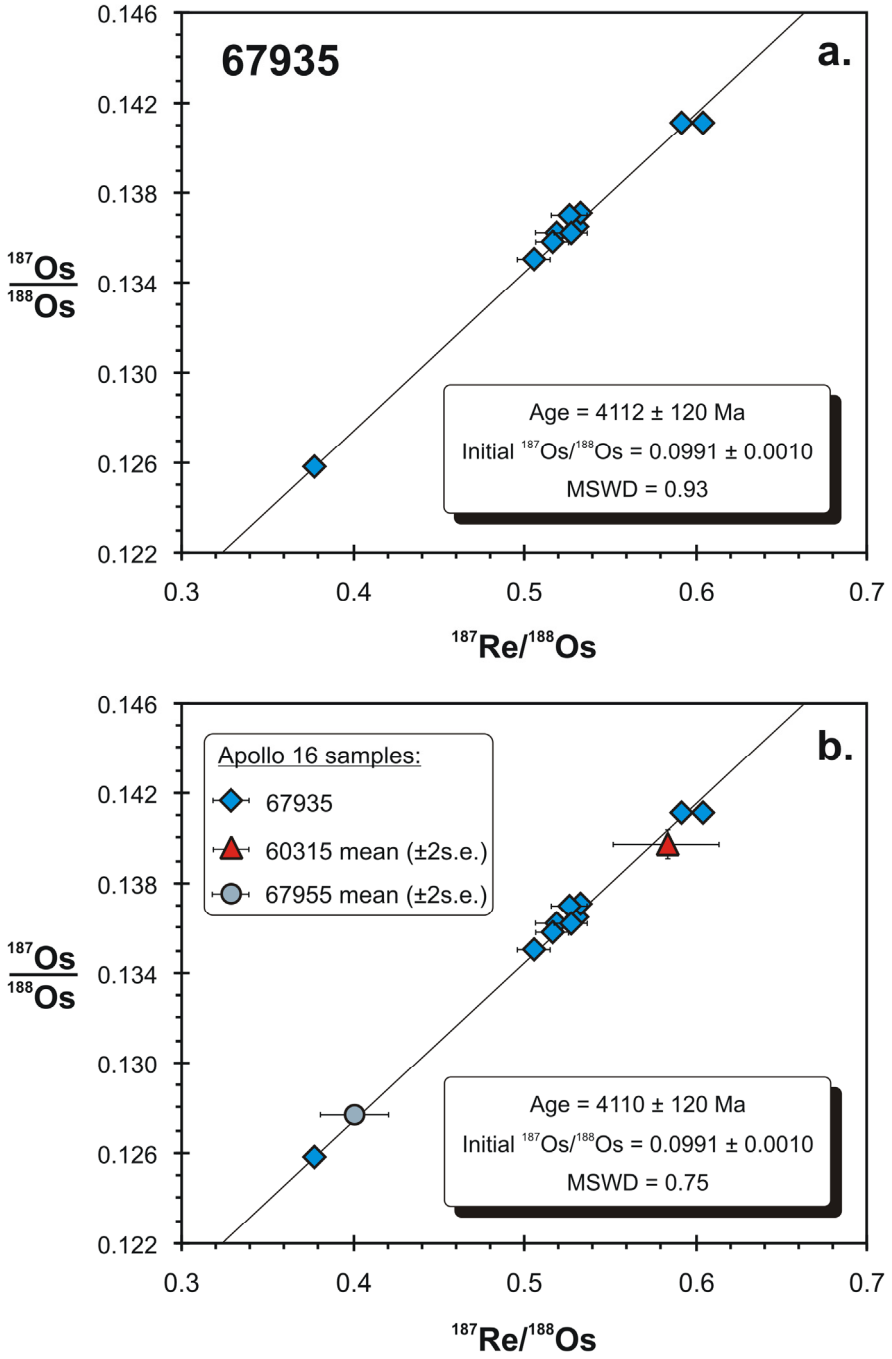

Fig. 5.1. $^{187}Os/^{188}Os$ versus $^{187}Re/^{188}Os$ for subsamples of Apollo 16 sample 67935 (a), and calculated average $^{187}Os/^{188}Os$ and $^{187}Re/^{188}Os$ ratios for 60315 and 67955 in comparison to subsamples of 67935 (b). Age regressions shown in (a) and (b) yield essentially the same age of 4.1 Ga. Uncertainties for $^{187}Os/^{188}Os$ and $^{187}Re/^{188}Os$ are 2σ for subsamples of 67935 and $2\sigma_m$ for calculated averages of 60315 and 67955.

Because of limited variation in $^{187}Os/^{188}Os$ and $^{187}Re/^{188}Os$, other Apollo 16 samples (67955, 60315) do not yield reliable isochronous relationships. However, subsample aliquots of these samples plot close to the 4.1 Ga isochron defined by 67935. Calculated average $^{187}Re/^{188}Os$ and $^{187}Os/^{188}Os$ for 67955 and 60315 plot within uncertainties on the isochron. In Fig. 5.1b the calculated averages for 67955 and 60315 are included into the age regression together with subsample aliquots of 67935, yielding essentially the same age. In a plot of 1/Os vs. $^{187}Os/^{188}Os$ (not shown) for subsamples of 67935, 60315 and 67955 no systematic relationship between Os isotopic composition and Os concentration exists, thus eliminating mixing processes to account for the observed variation.

Because of significant blank corrections, Re abundances were also calculated based on the measured Os concentrations and Os isotopic compositions assuming the samples evolved from an initial solar system $^{187}Os/^{188}Os$ of 0.09531 at 4.56 Ga and $\lambda = 1.666 \times 10^{-11}$ yr^{-1} (Shirey and Walker, 1998). Measured Re concentrations and calculated Re* concentrations for subsamples of Apollo 16 samples 60315 and 67935 generally agree within <5%. Only three subsamples of 60315 (#4, #5, #7) show somewhat larger deviations of 8-14%. Mass weighted average concentrations of Re and Re* for 60315 and 67935 are indistinguishable. Measured and calculated Re abundances of the granulitic impact melt rocks 67955 and 79215 display deviations of up to 12% for particular subsamples (e.g. 67955 #8 and 79215 #3), while mass weighted average concentrations deviate around 4% for 67955 and 9% for 79215. Significant differences between Re and Re* observed for subsamples of the lunar meteorite DaG400 most likely reflect mobilisation of Re due to terrestrial weathering.

5.5.2 Highly siderophile element variation in lunar impact melt rocks

The HSE concentration data for Re, Re*, Os, Ru, Pt, Rh, Pd, and Au (Table 5.1) from different subsamples of a given impact melt are generally well correlated with Ir (Fig. 5.2). Abundance data for a few subsamples from Apollo 16 samples 60315, 67935 and 67955 deviate significantly from the correlation lines. In the case of DaG400 Re and Au abundances are not correlated with Ir. Slope derived HSE/Ir ratios were calculated from the correlations displayed by plots of HSE vs. Ir using ISOPLOT (Ludwig, 2003). Fully

fledged regression calculations were conducted using the analytical uncertainties of the concentration determinations as stated above. The regression results are provided in Table 5.2 together with representative HSE ratios for chondrites from different classes and groups, and ratios inferred for the Earth's primitive mantle (PM). HSE abundances of subsamples from Apollo 16 samples 60315, 67935 and 67955 that deviate significantly from the correlation lines, were excluded from the regression calculations.

5.6 Discussion

5.6.1 Data quality and comparison to previous studies

A comparison to concentration data obtained by previous NAA studies is somewhat complicated, because most previous studies did not analyze several subsamples of the same sample. As shown in Fig. 5.2 absolute abundances of HSE for different subsamples of a given impact melt can show large variations (e.g. 60315 and 67935).

Relative HSE abundances for subsamples of a given sample are much more reproducible than absolute values. Ratios of refractory HSE (Re, Os, Ir, Ru, Pt, Rh) to Ir for subsamples of 14310, 60315, 67955 and 79215 reproduce within <10%, and within <20% for 67935. Correlations involving the more volatile siderophiles Pd and Au in some cases are less well defined and show more scatter for some samples (Fig. 5.2). Consequently, ratios of Pd/Ir and Au/Ir for subsamples of the same rock show somewhat more variation compared to refractory HSE ratios.

Generally, the range of HSE abundances and ratios determined for subsamples of a given impact rock overlap with the values reported in previous studies (Baedecker et al., 1972; Morgan et al., 1972; Ganapathy et al., 1974; Higuchi and Morgan, 1975; Wänke et al., 1976; Hertogen et al., 1977; Palme et al., 1978; Wasson et al., 1978; Lindstrom and Lindstrom, 1986; Zipfel et al., 1998; Korotev et al., 2003; Warren et al., 2005; Hudgins et al., 2008).

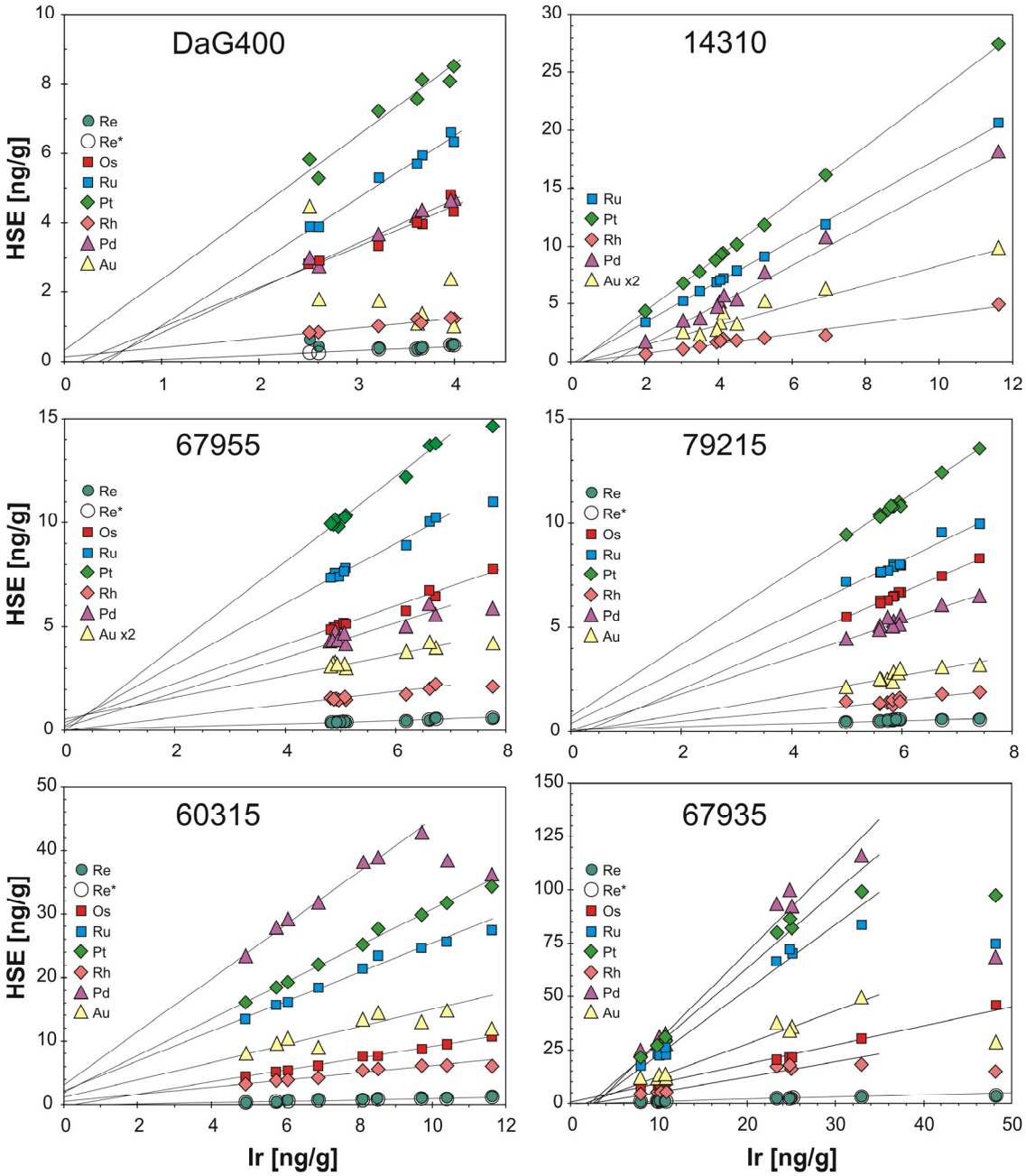

Fig. 5.2. Linear regressions of Ir vs. Re, Re*, Os, Ru, Pt, Rh, Pd and Au for lunar impact melt rocks from Apollo 14, 16 and 17, and the lunar meteorite DaG400. HSE concentration data for different subsamples of a given impact melt are generally well correlated. The slopes of the regression lines represent the HSE/Ir ratios of the meteoritic high HSE end-member composition. Re* corresponds to the time-integrated Re/Os required for the evolution from the solar system initial $^{187}Os/^{188}Os$ to measured $^{187}Os/^{188}Os$ as described in text. Sample 60315 #10 is not displayed because the high HSE concentrations in this subsample are two orders of magnitude higher than in other subsamples (see Table 5.1).

5.6.2 HSE compositions of impact melt rocks

In previous studies, well-defined linear correlations displayed among subsamples of a given lunar impact melt rock, or a suite of related rocks, have been interpreted as mixing or dilution lines between a high HSE meteoritic impactor end-member composition and a low HSE end-member composition, which corresponds to the pre-existing lunar crust (Norman et al., 2002; Puchtel et al., 2008). HSE concentrations of pristine lunar crustal rocks are very low (e.g. Morgan et al., 1972, 1973; Ganapathy et al., 1973; Warren and Wasson, 1977, 1978). Pristine ferroan anorthosites, the predominant and most ancient lunar crustal rocks, are characterized by HSE abundances of only about 0.00002 × CI (Day et al., 2010). Thus, in a true binary mixture between HSE-rich meteoritic impactor material and ferroan anorthosite, contributions from the latter can be neglected.

As shown in previous studies, regression calculated HSE/Ir ratios are very close to the high HSE end-member composition of the meteoritic impactor component (Korotev et al., 1987a,b; McDonald et al., 2001; Tagle and Claeys, 2005; Puchtel et al., 2008). However regression calculations could be biased for samples that may contain contributions from more than one meteoritic impactor, or samples that contain contributions from the lunar target rocks. Possible mixing of different meteoritic impact compositions and/or contributions from target rocks are indicated by statistically resolvable positive or negative intercept values of the regression calculations (Table 5.2), or by individual subsamples which plot off the correlation lines in Fig. 5.2.

In the case of 14310 a statistically resolvable negative intercept value for Pd indicates the presence of a HSE-poor end-member composition with lower Pd/Ir, compared to the HSE-rich component. Ratios of Ru/Ir, Pt/Ir and Rh/Ir for the metal spherule subsample #10 from 60315 are 20-40% lower, while Pd/Ir and Au/Ir are about a factor of ~2 lower, compared to ratios of other subsamples. A similar observation applies to subsample aliquot #7 from 67935, where Ru/Ir, Pt/Ir, Rh/Ir, Pd/Ir and Au/Ir are between 1.5 to 2 times lower than ratios of other subsamples. These deviations in combination with statistically resolvable intercept values for some HSE, and a relatively large uncertainty in intercept values for Pd and Au (Table 5.2) possibly reflect the presence of two or more meteoritic end-member compositions in these rocks.

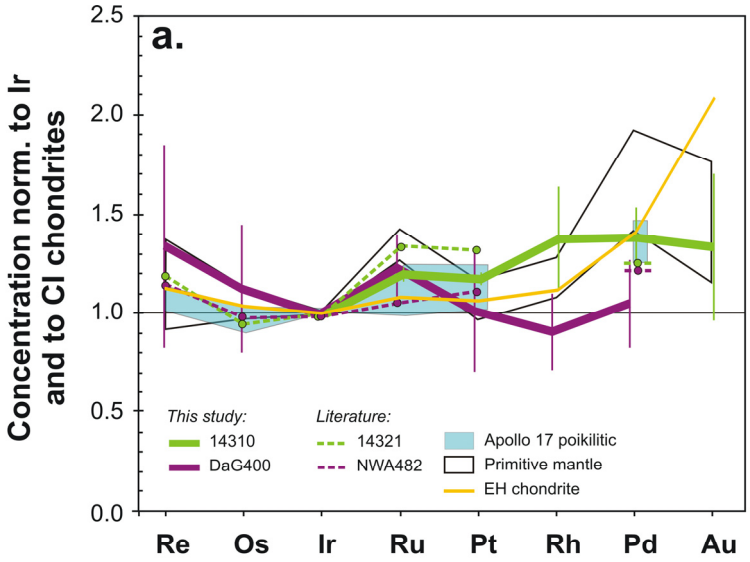
a.
Concentration norm. to Ir and to CI chondrites
2.5
2.0
1.5
1.0
0.5
0.0
This study:
14310
DaG400
Literature:
14321
NWA482
Apollo 17 poikilitic
Primitive mantle
EH chondrite
Re
Os
Ir
Ru
Pt
Rh
Pd
Au

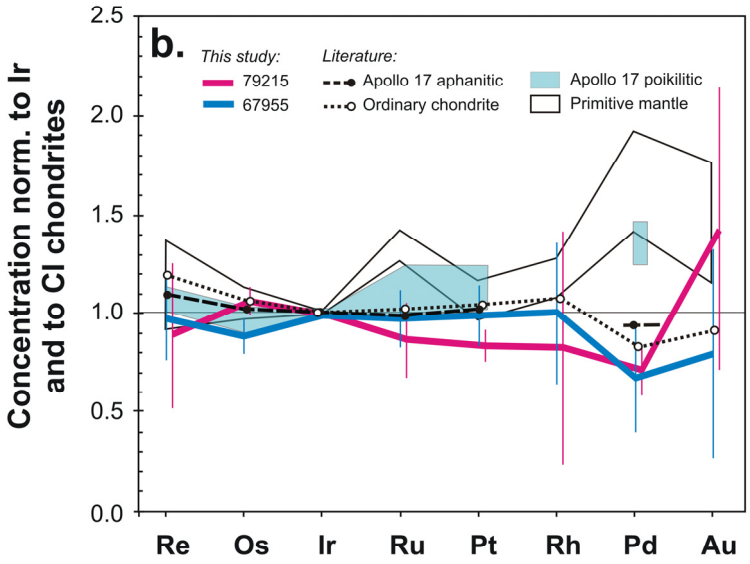
b.
Concentration norm. to Ir and to CI chondrites
2.5
2.0
1.5
1.0
0.5
0.0
This study:
79215
67955
Literature:
Apollo 17 aphanitic
Ordinary chondrite
Apollo 17 poikilitic
Primitive mantle
Re
Os
Ir
Ru
Pt
Rh
Pd
Au

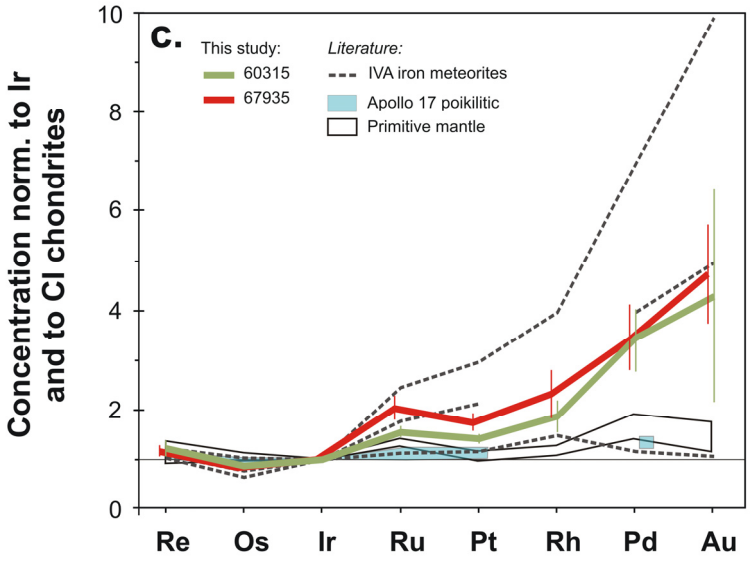
c.
Concentration norm. to Ir and to CI chondrites
10
8
6
4
2
0
This study:
60315
67935
Literature:
IVA iron meteorites
Apollo 17 poikilitic
Primitive mantle
Re
Os
Ir
Ru
Pt
Rh
Pd
Au

Fig. 5.3. Double normalized HSE abundance diagram (normalized to Ir and CI chondrite values, CI values from Fischer-Gödde et al., 2010a) showing the slope derived HSE compositions of the high HSE impactor components in comparison to the compositions obtained on lunar impact melt rocks in previous studies (Norman et al., 2002; Puchtel et al., 2008). In addition, the primitive mantle (PM) model HSE composition (Becker et al., 2006, Rh and Au from Fischer-Gödde et al., 2010b), and the HSE compositions of selected chondrite classes and groups, as well as members of the IVA iron meteorite group are shown for comparison (Walker et al., 2002; Horan et al., 2003; Walker et al., 2005b; Fischer-Gödde et al., 2010a). Relative abundances of Ru and Pd inferred for the PM composition are clearly out of the range defined by chondritic meteorites. A good match can be observed between the PM and HSE patterns of Apollo 17 poikilitic lunar impact melt rocks, which also display Ru and Pd enhancements.

Positive intercept values of Ru, Pt, Rh, Pd, and Au obtained for 60315 indicate the presence of a minor component with elevated Ru/Ir, Pt/Ir, Rh/Ir, Pd/Ir, and Au/Ir compared to the main component. In contrast, negative intercept values of Ru, Pt, Rh, Pd, and Au obtained for 67935 reflect a HSE composition with lower Ru/Ir, Pt/Ir, Rh/Ir, Pd/Ir, and Au/Ir ratios relative to the main HSE-rich end-member composition. An alternative explanation for the deviating subsamples would be fractionation of HSE between solid metal and liquid sulphur-rich metal upon cooling of the impact melt, as discussed in the next section.

In Fig. 5.3 slope-derived HSE/Ir ratios of the high HSE impactor compositions of lunar impact melt rocks were normalized to CI chondrite abundance ratios (CI values from Fischer-Gödde et al., 2010a). Compositions derived from ancient lunar impact rocks from this study, Norman et al. (2002) and Puchtel et al. (2008) are shown in comparison to the inferred HSE composition of the primitive mantle (Becker et al., 2006; Fischer-Gödde et al., 2010b), and the composition of chondrites (Walker et al., 2002; Horan et al., 2003; Brandon et al., 2005a,b; Fischer-Gödde et al., 2010), and also IVA iron meteorites (Walker et al., 2005).

Slightly suprachondritic Ru/Ir, Pt/Ir and Rh/Ir are observed for the high HSE end-member of Apollo 14 basaltic impact melt rock 14310, while Pd/Ir, Au/Ir and $^{187}Os/^{188}Os$ are in the range of chondritic meteorites (Figs. 5.3a, 5.4). The HSE composition of 14310 is very similar to the compositions previously reported for Apollo 17 poikilitic impact melt rocks, the Apollo 14 sample 14321, and the lunar meteorite NWA482 (Fig. 5.3a, Puchtel et al., 2008). It is also similar to the HSE composition of the Earth's primitive mantle (PM) (Becker et al., 2006; Fischer-Gödde et al., 2010b).

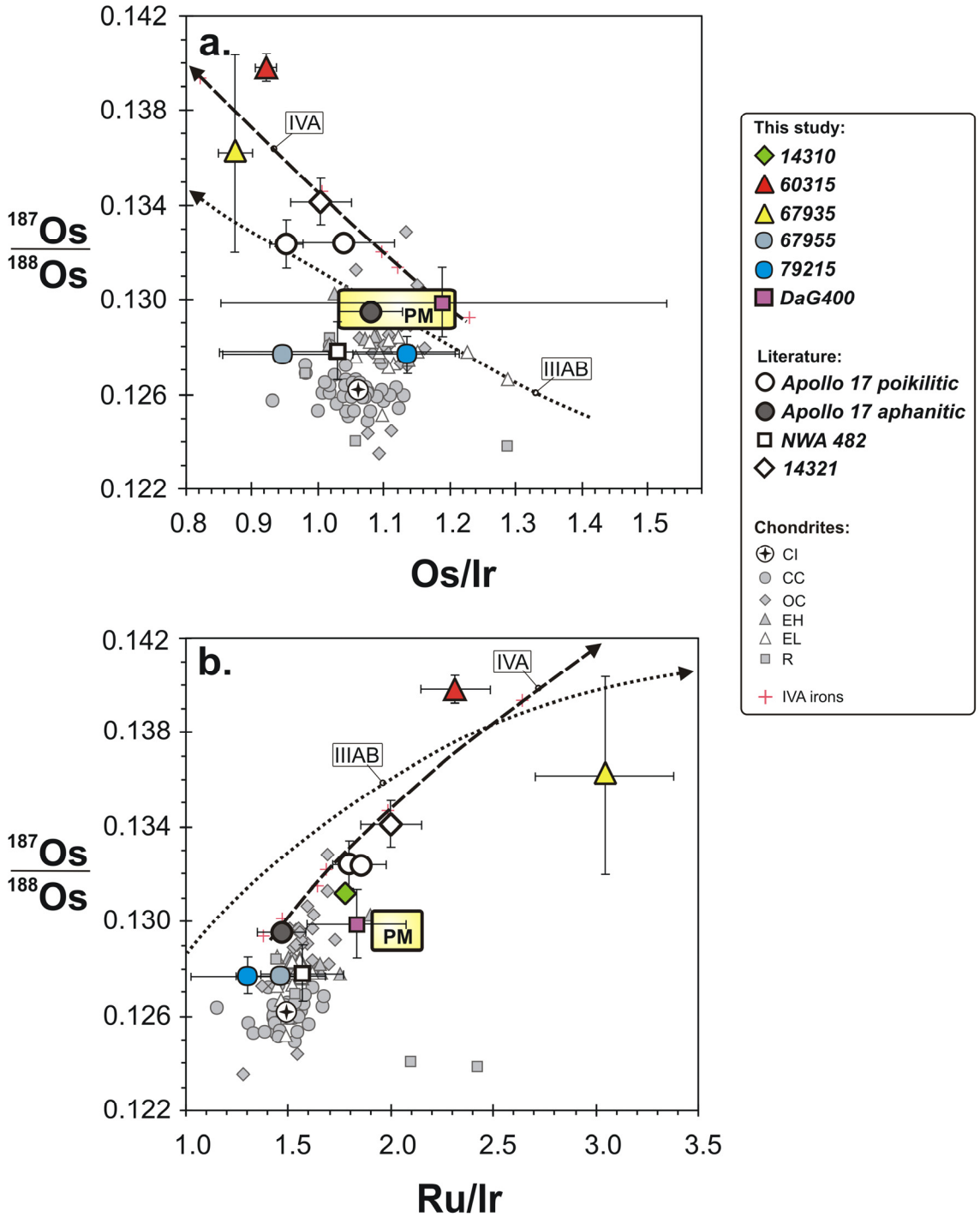

Fig. 5.4. $^{187}Os/^{188}Os$ versus ratios of Os/Ir (a), Ru/Ir (b), Pd/Ir (c), and Au/Ir (d). Average $^{187}Os/^{188}Os$ and slope derived HSE/Ir ratios of the high HSE impactor component in comparison to ratios of chondrites, the Earth's primitive mantle (PM), and magmatic differentiation trends defined by IIIAB and IVA iron meteorites. Errors for $^{187}Os/^{188}Os$ of the impactor component are quoted at $2\sigma_m$, while errors for elemental ratios reflect 2σ uncertainty of the concentration determination used for the regression calculations.

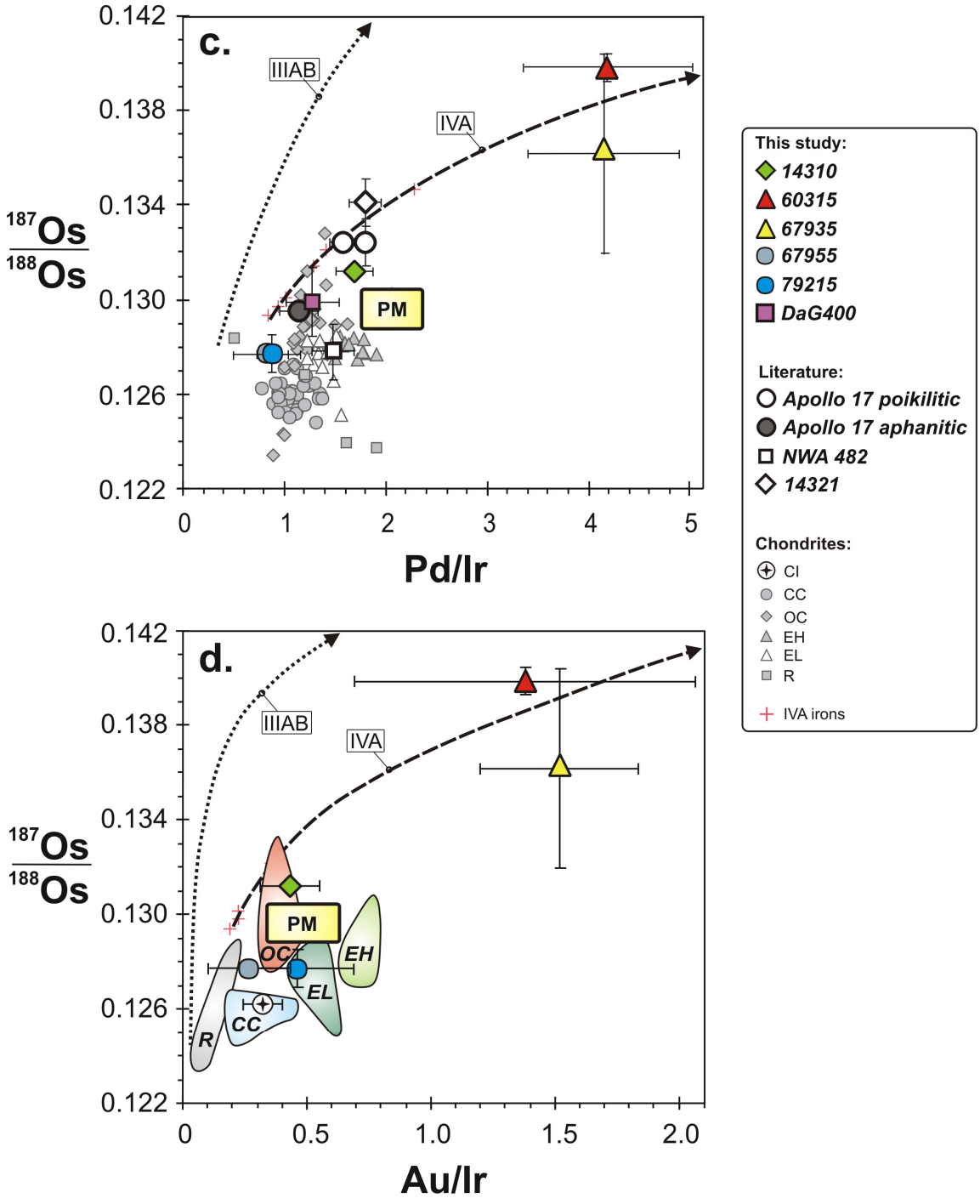

Data for chondrites are from Walker et al. (2002), Horan et al. (2003), Brandon et al. (2005a,b) and Fischer-Gödde et al. (2010a). Primitive mantle values are from Becker et al. (2006) with Au/Ir from Fischer-Gödde et al. (2010b). Data for IVA and IIIAB iron meteorites are from Pernicka and Wasson (1987), Smoliar et al. (1996), Wasson and Richardson (2001), Cook et al. (2004), and Walker et al. (2005b).

The lunar meteorite DaG400 shows slightly suprachondritic Ru/Ir while other HSE ratios are in the range of chondritic meteorites (Fig. 5.3a). Refractory HSE ratios of DaG400 are similar to ratios inferred for the Earth's primitive mantle, while relative abundances of Rh and Pd do not match the PM composition.

Granulites 67955 and 79215 are characterized by Re/Ir, Os/Ir, Ru/Ir, Pt/Ir and Rh/Ir ratios similar to or slightly lower than HSE ratios of CI and ordinary chondrites (Fig. 5.3b). Ratios of Pd/Ir for both samples and Au/Ir for 67955 are more similar to ordinary chondrites or volatile depleted carbonaceous chondrites, while Au/Ir for 79215 hints at a higher value but also shows a larger uncertainty. The HSE composition inferred for the granulitic breccias is comparable to Apollo 17 aphanitic melt breccias 73215 and 73255 (Puchtel et al., 2008). HSE abundances of the latter are assumed to reflect partially or entirely the HSE composition of granulitic clasts contained in these breccias.

The regression-derived HSE compositions of 60315 and 67935 yield suprachondritic Ru/Ir, Pt/Ir, Rh/Ir, Pd/Ir and Au/Ir ratios combined with chondritic Re/Ir and subchondritic Os/Ir (Figs. 5.3c, 5.4). Suprachondritic HSE ratios inferred for the high HSE end-member composition of these samples are similar, but plot far away from ratios observed for chondritic meteorites. In HSE-rich planetary materials such fractionated relative HSE abundances are only known from some magmatic iron meteorites. More specifically, HSE compositions of 60315 and 67935 are very similar to some members of the IVA iron meteorite group (Figs. 5.3c, 5.4, 5.5), either suggesting an iron meteorite projectile, or alternatively, HSE fractionation during impact in a similar manner as observed for solid metal-liquid metal partitioning systems.

5.6.3 Age constraints from Apollo 16 impact melt rocks

The Re-Os isochron age obtained for 67935 most probably represents the age of the impact on the lunar surface. Possible processes to establish fractionated Re/Os during impact are centimetre-scale partitioning processes between solid metal and C and S bearing metallic liquids during cooling of the impact melt sheets. Such partitioning processes require that the impactor contained sufficient quantities of sulphur and FeNi

metal. The observation of FeNi metal and troilite intergrowths within 67935 hints at metal-sulphide fractionation upon cooling of impact generated melt. Possible Re/Os fractionation by volatility controlled processes during impact like vaporization seem less likely, because both Re and Os should behave as refractory elements under reducing conditions.

The Re-Os age of 67935 is resolvable older than more precise Ar-Ar ages obtained for the majority of Apollo 16 samples, which typically range from 3.75 – 3.96 Ga (e.g. Norman et al., 2006). Ages >4.0 Ga were also reported for melt breccia clasts contained in fragmental breccias from the North Ray Crater at the Apollo 16 landing site (Maurer et al., 1978; Stöffler et al., 1985; Duncan and Norman, 2005; Norman et al., 2006). Most of these old ages cluster around a value of 4.1 Ga, which has been assumed to be related to the Nectaris impact event or an older pre-Nectaris impact event (James, 1981; Korotev et al., 2002; Warren, 2003). Alternatively, such old Ar-Ar ages may have been caused due to incomplete degassing of clastic debris within the melt rocks, and/or slow diffusion in the highly aluminous melt rocks (Norman et al., 2006).

For Apollo 16 poikilitic granulite 67955 Norman et al. (2007) reported a Sm-Nd crystallization age of 4.20 ± 0.07 Ga. Because of the metamorphic rock texture and the inferred slow cooling rate for this rock type (0.5 to 50°C/year, Cushing et al., 1999), this age was interpreted by Norman et al. (2007) to date a large basin forming impact event. Sample 67955 was collected from the same boulder as 67935 near the North Ray Crater at the Apollo 16 landing site. The boulder was apparently excavated by the North Ray crater projectile and is assumed to represent a part of the Descartes formation which probably derives from the Nectaris impact (James, 1981; Stöffler et al., 1981; Stöffler and Ryder, 2001). Slope-derived HSE abundance patterns for 67955 and 67935 differ vastly (Fig. 5.3b,c), suggesting that both samples reflect a different impactor composition related to different impact events. Both, the Re-Os age of 4.11 ± 0.12 Ga obtained for 67935 in this study and the metamorphic recrystallization age of 4.20 ± 0.07 Ga for 67955 (Norman et al., 2007) bear further evidence for large basin forming impact events, in the present case likely related to Nectaris, occurring significantly before 3.9 Ga. Moreover, the first time it may be possible to relate the age of an impact event to a specific impactor composition, i.e. IVA iron like material.

The majority of ages obtained by previous geochronological studies on lunar impact melt rocks mostly fall within a restricted range of 3.75 to 3.95 Ga (e.g. Jessberger et al., 1974; Turner and Cadogan, 1975; Norman et al., 2006). Because of the narrow time interval defined by these ages and the scarcity of ages older than 4.0 Ga, it is commonly believed that there was a pronounced spike in the flux of large impacting bodies in the inner solar system around 3.9 Ga (Late Heavy Bombardment, e.g. Stöffler and Ryder, 2001; Ryder, 2002). Possible mechanisms to cause such a pronounced spike in the flux of impacting bodies during that time may have been late perturbations of materials within the asteroid belt or the late migration of Uranus and Neptune (Morbidelli et al., 2001; Levinson et al., 2001; Gomes et al., 2005). However, the sharpness of this age spike is largely anchored by the age of 3.92 Ga inferred for the Nectaris basin (Stöffler and Ryder, 2001). Assuming an age of 4.2 Ga for the Nectaris impact event would significantly affect the cratering curve and weaken the final cataclysm hypothesis (Norman, 2009).

5.6.4 Evidence for differentiated meteoritic metal phases in Apollo 16 melt breccias

Strongly fractionated HSE patterns observed for the meteoritic component recorded in Apollo 16 impact melt rocks 60315 and 67935 may have been established during the impact event, or alternatively may reflect a HSE composition different from the known chondrite groups and similar to magmatic iron meteorites, or both. The systematics of refractory HSE abundances and ratios of 60315 and 67935 (e.g. Os/Ir, Pt/Ir, Ru/Ir) cannot be explained by volatility-controlled fractionation processes during impact (Table 5.2, Fig. 5.4a). Subchondritic Os/Ir and suprachondritic $^{187}Os/^{188}Os$, Re/Ir, Ru/Ir, Pt/Ir, Rh/Ir, Pd/Ir and Au/Ir of these samples are similar to the composition of residual liquid metal phases after crystallization of solid metal.

If the impactor was a magmatic iron meteorite, the fractionated HSE compositions recorded in samples 67935 and 60315 could have been generated during solid metal-liquid metal partitioning on the parent body before the impact on the Moon. Similar fractionated HSE abundance patterns observed for 67935, 60315 and IVA iron meteorites hint at a possible magmatic prehistory of the meteoritic material contained in Apollo 16 impact melt rocks. During progressive fractional crystallization of a planetary core the

composition of residual liquid metal evolves towards increasing suprachondritic ratios from Re/Os, Ru/Ir, Pt/Ir, Rh/Ir, Pd/Ir to Au/Ir, and subchondritic Os/Ir (e.g. Scott, 1972; Chabot and Jones, 2003; Chabot et al., 2006).

To test a possible magmatic prehistory slope derived HSE/Ir ratios of lunar impact melt rocks are compared to the compositional evolution of magmatic trends defined by IIIAB and IVA iron meteorites (Figs. 5.4 and 5.5). These iron meteorite groups were chosen, because their ranges in $^{187}Os/^{188}Os$, $^{187}Re/^{188}Os$ and HSE/Ir ratios are most comparable to the ones observed for lunar impact melt breccias. While the trend defined by the IIIAB group is somewhat different, because it evolves towards higher $^{187}Os/^{188}Os$ for a given Pd/Ir and Au/Ir (Fig. 5.4c,d), the trend for the IVA irons in nearly all cases evolves towards $^{187}Os/^{188}Os$ and HSE/Ir ratios observed for 60315 and 67935 (Figs. 5.4 and 5.5). Given these constraints, it seems likely, that the high HSE end-member component recorded in 60315 and 67935 reflects the composition of evolved meteoritic metal phases, similar to the composition of members from the group IVA iron meteorites.

In order to test whether the meteoritic component in Apollo 16 impact melt rocks is derived from IVA iron meteorites, FeNi metal phases contained in the breccias should be analysed for Ni and Ga abundances. The IVA iron meteorites are characterized by lower Ga contents compared to most other iron meteorite groups (e.g. Kelly and Larimer, 1977). Only the volatile depleted IVB iron meteorites show lower Ga, but higher Ni contents than the IVA irons.

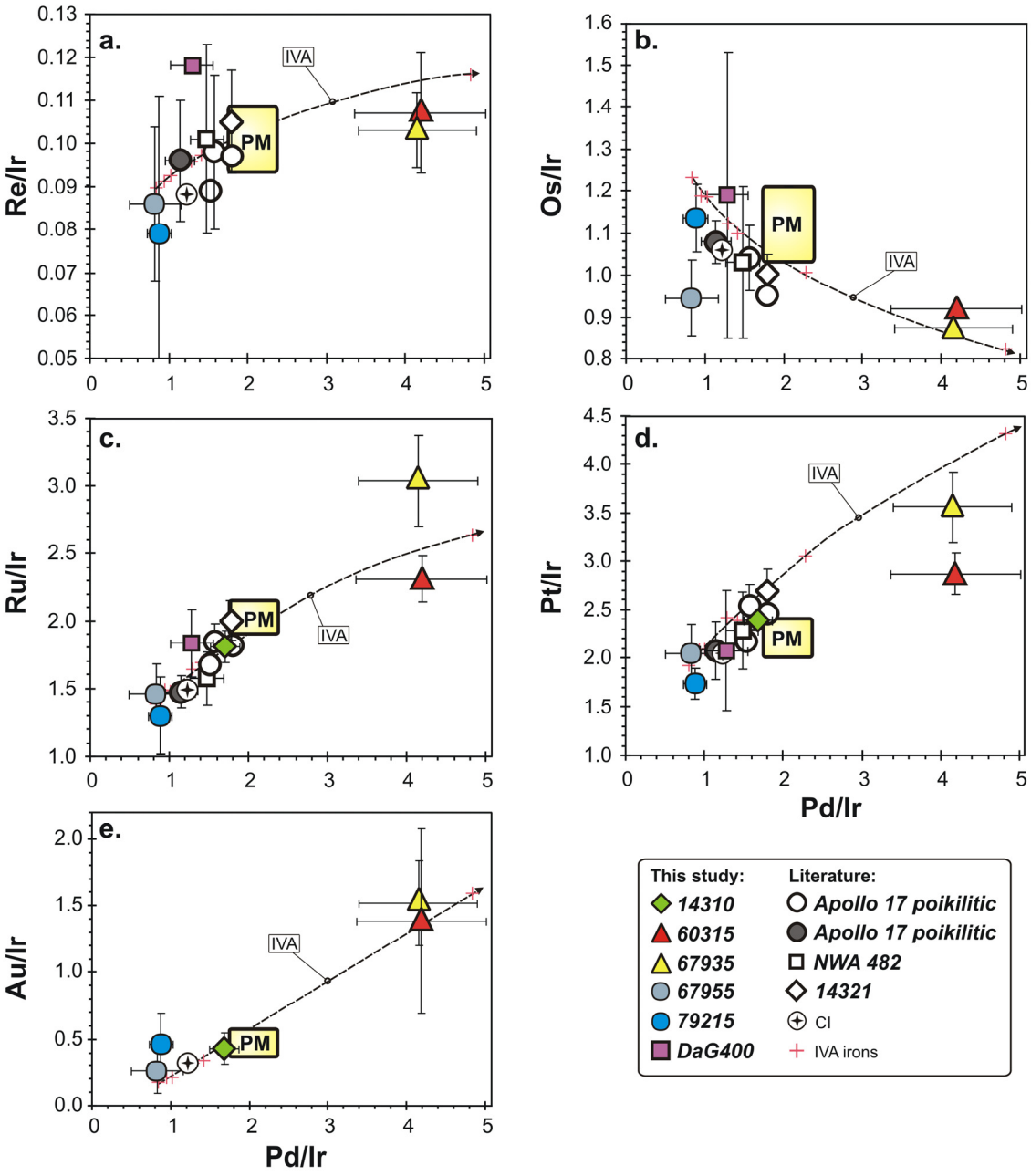

Fig. 5.5. Ratios of Re/Ir (a), Os/Ir (b), Ru/Ir (c), Pt/Ir (d), and Au/Ir (e) versus Pd/Ir. Slope derived HSE/Ir ratios of the high HSE impactor component in comparison to ratios of the Earth's primitive upper mantle (PUM) and magmatic differentiation trends defined by IVA iron meteorites. Errors for elemental ratios of the impactor components reflect 2σ uncertainties of the concentrations used for the regression calculations. Primitive mantle values are from Becker et al. (2006) with Au/Ir from Fischer-Gödde et al. (2010b). Data for IVA iron meteorites are from Wasson and Richardson (2001) and Walker et al. (2005b).

5.7 Conclusions

The results of this study in conjunction with previous precise HSE and $^{187}Os/^{188}Os$ data (Norman et al., 2002; Puchtel et al., 2008) indicate that ancient lunar impact rocks contain a minimum of three different meteoritic components. HSE abundance patterns and $^{187}Os/^{188}Os$ of granulitic breccias 67955 and 79215 are most similar to carbonaceous or ordinary chondrites, and to compositions observed for Apollo 17 aphanitic impact melt rocks (Puchtel et al., 2008). Apollo 14 impact melt rock 14310 is similar in HSE composition to 14321, the lunar meteorite DaG400 and Apollo 17 poikilitic impact melt rocks reported by Norman et al. (2002) and Puchtel et al. (2008). Collectively, the high-HSE meteoritic end-member in these samples displays suprachondritic Re/Os, Ru/Ir and Pd/Ir. Apollo 16 samples 60315 and 67935 display strongly fractionated HSE compositions and $^{187}Os/^{188}Os$ far out of the range observed for chondritic meteorites. The impactor composition recorded in these rocks is similar to IVA iron meteorites and suggests an origin from a differentiated planetary body. Subchondritic Os/Ir and suprachondritic Re/Ir, Ru/Ir, Pt/Ir, Rh/Ir, Pd/Ir and Au/Ir resemble the composition of residual liquid metal phases after crystallization of solid metal.

In this study the first sufficiently precise Re-Os isochron for a lunar impact melt rock was obtained. The small scale Re-Os fractionation among subsamples of 67935 is interpreted to reflect localized solid metal-liquid metal separation in the impact melt. Consequently, the age of 4.11 ± 0.12 Ga records the impact event. Sample 67935 is believed to derive from the Descartes formation which was related to the Nectaris impact event (Stöffler and Ryder, 2001). Thus, the inferred age supports previous notions that the Nectaris basin may be as old as 4.1 Ga (Korotev et al., 2002; Warren, 2003). These inferences are consistent with recent Sm-Nd age constraints on associated granulites (Norman et al., 2007).

The range of different HSE compositions observed for lunar impact melt rocks, suggests that the HSE composition of the Earth's mantle also may reflect a mixture of different meteoritic impactor compositions. The admixture of differentiated meteoritic metal components seems to be a viable option to generate suprachondritic ratios of certain HSE in the Earth's mantle. The HSE composition of the Earth's mantle may be explained

by a binary mixture of chondritic material with some fractionated HSE component similar to that found in 67935 and 60315 (Figs. 5.4 and 5.5). A combination of a fractionated HSE signature inherited from core segregation and addition of a late veneer component may be an alternative solution to explain the excess abundances of HSE and their relative abundances in the Earth's mantle.

Acknowledgements

Generous supply of Apollo samples by CAPTEM and the lunar sample curator (G. Lofgren) is gratefully acknowledged. We thank Jutta Zipfel for supplying a sample of the lunar meteorite DaG400. Konrad Hammerschmidt is acknowledged for help and advice in the TIMS lab and Monika Feth for help and support in the clean lab. We thank Marc Weynell for assistance during sample preparation, digestion and chemical separation procedures. We appreciate discussions with Richard Walker, Al Brandon, Igor Puchtel, Kai Rankenburg, Odette James, Thomas Meisel and Herbert Palme. This work was supported by the Deutsche Forschungsgemeinschaft (Be 1820/6-1).

Table 5.1. Highly siderophile element abundances (in ng/g), $^{187}Os/^{188}Os$ and $^{187}Re/^{188}Os$ data for Apollo 14, 16 and 17 impact melt rocks, and lunar meteorite DaG400.

	weight	Re	Re*	Os	Ir	Ru	Pt	Rh	Pd	Au	$^{187}Os/^{188}Os$	$^{187}Re/^{188}Os$
Apollo 14 basaltic impact melt rock												
14310 #1	0.101				6.92	11.9	16.1	2.26	10.7	3.13	0.1304 ± 3	
14310 #2	0.091				2.02	3.39	4.30	0.68	1.69	0.79	0.1306 ± 6	
14310 #3	0.090				4.51	7.85	10.1	1.79	5.28	1.60	0.1313 ± 3	
14310 #4	0.097				3.51	6.05	7.84	1.30	3.62	1.12	0.1313 ± 3	
14310 #5	0.101				5.26	9.08	11.9	2.01	7.63	2.57	0.1311 ± 3	
14310 #6	0.098				11.6	20.7	27.4	4.89	18.1	4.89	0.1321 ± 3	
14310 #7	0.102				3.04	5.23	6.82	1.12	3.44	1.25	0.1311 ± 3	
14310 #8	0.105				4.06	7.10	9.24	1.74	5.05	1.62	0.1314 ± 4	
14310 #9	0.100				3.96	6.84	8.90	1.63	4.73	1.33	0.1314 ± 4	
14310 #10	0.162				4.14	7.24	9.43	1.96	5.56	2.06	0.1313 ± 3	
Average[a]					4.87	8.47	11.1	1.94	6.54	2.05	0.1312 ± 3	
Apollo 16 poikilitic impact melt breccia												
60315 #1	0.105	0.504	0.523	4.40	4.94	13.4	16.0	3.31	23.2	7.94	0.1397 ± 4	0.553 ± 21
60315 #2	0.099	1.05	1.10	9.36	10.4	25.8	31.6	6.11	38.3	14.6	0.1392 ± 4	0.540 ± 10
60315 #3	0.098	0.586	0.620	5.15	5.76	15.6	18.5	3.81	27.7	9.43	0.1402 ± 4	0.549 ± 19
60315 #4	0.103	0.809	0.876	7.44	8.12	21.5	25.2	5.41	38.0	13.2	0.1392 ± 4	0.525 ± 13
60315 #5	0.095	0.745	0.656	5.34	6.07	16.0	19.3	3.90	29.0	10.4	0.1411 ± 4	0.673 ± 19
60315 #6	0.102	1.30	1.25	10.5	11.6	27.5	34.3	5.95	35.9	11.7	0.1397 ± 4	0.597 ± 9
60315 #7	0.103	1.01	0.93	7.57	8.53	23.5	27.7	5.60	38.8	14.2	0.1410 ± 4	0.643 ± 12
60315 #8	0.098	0.775	0.744	6.08	6.92	18.5	22.1	4.24	31.7	8.84	0.1409 ± 4	0.615 ± 16
60315 #9	0.103	1.07	1.02	8.71	9.71	24.7	29.9	6.06	42.7	12.8	0.1392 ± 4	0.591 ± 11
60315 #10	0.009	146	148	1295	1401	2816	3767	613	2651	1151	0.1379 ± 4	0.543 ± 1
Average[a]		2.22	2.23	19.1	21.0	46.7	59.8	10.6	58.3	22.0	0.1398 ± 6	0.588 ± 31

Table 5.1. continued. Highly siderophile element abundances (in ng/g), $^{187}Os/^{188}Os$ and $^{187}Re/^{188}Os$ data for Apollo 14, 16 and 17 impact melt rocks, and lunar meteorite DaG400.

	weight	Re	Re*	Os	Ir	Ru	Pt	Rh	Pd	Au	$^{187}Os/^{188}Os$	$^{187}Re/^{188}Os$
Apollo 16 basaltic impact melt rock												
67935 #1	0.100	2.37	2.35	21.6	25.1	70.2	82.0	16.2	92.0	35.3	0.13653 ± 4	0.530 ± 4
67935 #2	0.101	1.10	1.09	10.3	10.8	22.8	29.1	5.16	27.1	11.8	0.13589 ± 7	0.516 ± 9
67935 #3	0.100	2.66	2.64	21.8	24.8	72.1	86.7	17.9	99.4	33.5	0.14118 ± 4	0.591 ± 4
67935 #4	0.101	0.810	0.794	7.54	7.98	17.7	21.8	4.18	24.5	11.7	0.1362 ± 1	0.518 ± 13
67935 #5	0.101	3.33	3.35	30.2	32.9	83.8	99.1	18.0	116	49.2	0.13718 ± 4	0.533 ± 3
67935 #6	0.101	1.02	1.01	9.36	10.0	22.4	27.8	5.27	30.6	13.8	0.13705 ± 8	0.525 ± 10
67935 #7	0.103	3.62	3.74	46.2	48.2	75.1	97.3	14.9	68.2	28.1	0.12584 ± 4	0.378 ± 2
67935 #8	0.101	1.04	1.00	9.50	9.84	22.7	27.1	5.57	28.0	11.4	0.13628 ± 4	0.527 ± 9
67935 #9	0.101	1.06	1.04	10.1	10.8	26.0	30.9	6.04	32.1	13.7	0.13508 ± 4	0.505 ± 9
67935 #10	0.109	2.57	2.52	20.6	23.3	66.6	80.0	17.4	93.1	37.1	0.14123 ± 4	0.603 ± 4
Average[a]		1.96	1.96	18.7	20.4	48.1	58.3	11.1	61.2	24.6	0.1362 ± 27	0.514 ± 38
Apollo 16 poikilitic magnesian granulite												
67955 #1	0.101	0.374	0.418	4.87	6.19	8.93	12.2	1.79	4.95	1.88	0.1273 ± 3	0.370 ± 20
67955 #2	0.102	0.393	0.436	4.97	4.91	7.56	10.2	1.56	4.69	1.64	0.1281 ± 3	0.382 ± 19
67955 #3	0.100	0.628	0.662	7.83	7.76	11.0	14.6	2.15	5.80	2.09	0.12686 ± 6	0.387 ± 12
67955 #4	0.103	0.552	0.597	6.69	6.62	10.0	13.7	2.01	6.04	2.11	0.1286 ± 3	0.398 ± 14
67955 #5	0.102	0.402	0.453	5.19	5.07	7.66	10.3	1.68	4.63	1.60	0.12781 ± 9	0.373 ± 18
67955 #6	0.104	0.390	0.436	5.03	4.87	7.38	9.90	1.51	4.27	1.60	0.12762 ± 9	0.374 ± 18
67955 #7	0.102	0.438	0.434	5.12	4.97	7.36	9.82	1.49	4.29	1.58	0.12688 ± 9	0.412 ± 19
67955 #8	0.101	0.639	0.570	6.48	6.73	10.3	13.8	2.23	5.53	1.97	0.12813 ± 7	0.475 ± 15
67955 #9	0.103	0.444	0.453	5.16	5.10	7.81	10.4	1.53	4.11	1.48	0.12804 ± 9	0.415 ± 18
67955 #10	0.104	0.430	0.426	4.90	4.83	7.33	9.96	1.58	4.25	1.54	0.12770 ± 9	0.422 ± 19
Average[a]		0.469	0.488	5.62	5.70	8.53	11.5	1.75	4.85	1.75	0.1277 ± 4	0.398 ± 20

Table 5.1. continued. Highly siderophile element abundances (in ng/g), $^{187}Os/^{188}Os$ and $^{187}Re/^{188}Os$ data for Apollo 14, 16 and 17 impact melt rocks, and lunar meteorite DaG400.

	weight	Re	Re*	Os	Ir	Ru	Pt	Rh	Pd	Au	$^{187}Os/^{188}Os$	$^{187}Re/^{188}Os$
Apollo 17 granoblastic magnesian granulite												
79215 #1	0.100	0.718	0.666	8.27	7.41	9.96	13.6	1.96	6.43	3.16	0.1254 ± 3	0.418 ± 12
79215 #2	0.100	0.612	0.562	6.64	5.95	8.03	11.0	1.65	5.10	2.80	0.1269 ± 3	0.444 ± 14
79215 #3	0.103	0.573	0.513	5.53	4.99	7.21	9.46	1.48	4.40	2.14	0.1299 ± 3	0.500 ± 17
79215 #4	0.100	0.607	0.562	6.51	5.84	8.02	10.8	1.56	5.03	2.34	0.1275 ± 3	0.450 ± 15
79215 #5	0.105	0.699	0.647	7.44	6.73	9.58	12.4	1.84	6.05	3.05	0.1278 ± 3	0.453 ± 12
79215 #6	0.100	0.604	0.550	6.52	5.85	7.91	10.8	1.27	5.26	2.86	0.1268 ± 3	0.446 ± 15
79215 #7	0.100	0.626	0.588	6.65	5.98	7.94	10.8	1.47	5.49	3.02	0.1283 ± 3	0.454 ± 15
79215 #8	0.101	0.596	0.555	6.13	5.61	7.63	10.4	1.40	4.83	2.49	0.1291 ± 3	0.469 ± 16
79215 #9	0.102	0.582	0.533	6.31	5.74	7.75	10.6	1.43	5.42	2.53	0.1268 ± 3	0.445 ± 15
79215 #10	0.102	0.613	0.559	6.25	5.61	7.58	10.3	1.39	5.04	2.57	0.1287 ± 3	0.472 ± 15
Average[a]		0.623	0.574	6.62	5.97	8.16	11.0	1.55	5.31	2.69	0.1277 ± 8	0.453 ± 14
Lunar highland meteorite												
DaG 400 #1	0.041	0.468	0.455	4.82	3.96	6.61	8.09	1.22	4.60	2.35	0.1305 ± 3	0.47 ± 12
DaG 400 #2	0.038	0.346	0.329	3.36	3.22	5.29	7.22	1.02	3.63	1.75	0.1319 ± 4	0.50 ± 19
DaG 400 #3	0.040	0.377	0.387	4.08	3.67	5.95	8.14	1.07	4.34	1.33	0.1307 ± 3	0.45 ± 15
DaG 400 #4	0.045	0.343	0.354	4.00	3.61	5.69	7.59	1.21	4.17	1.06	0.1283 ± 3	0.41 ± 13
DaG 400 #5	0.045	0.477	0.394	4.52	3.99	6.34	8.52	1.22	4.67	0.97	0.1278 ± 3	0.51 ± 12
DaG 400 #6	0.052	0.415	0.246	2.92	2.61	3.86	5.29	0.83	2.72	1.76	0.1267 ± 3	0.69 ± 16
DaG 400 #7	0.032	0.619	0.277	2.94	2.52	3.90	5.84	0.83	2.98	4.45	0.1305 ± 3	1.01 ± 25
Average[a]		0.429	0.348	3.81	3.38	5.38	7.23	1.06	3.87	1.85	0.1295 ± 14	0.50 ± 16

[a] Mass-weighted average concentration data, and simple averages ($\pm 2\sigma_m$) for $^{187}Os/^{188}Os$ and $^{187}Re/^{188}Os$.
Re* corresponds to calculated Re abundances as discussed in text.
Estimated uncertainties for concentration data are better than 1% for Os, 2 % for Ir, Ru and Pt, 5% for Pd, Re, 10% for Rh, and 15% for Au.

Table 5.2. Slopes and intercepts for linear regression calculations of HSE/Ir data.

	14310 basaltic impact melt rock	**60315** poikilitic impact melt rock	**67935** basaltic impact melt rock	**67955** magnesian granulite	**79215** magnesian granulite	**DaG400** Lunar meteorite
Intercept values (ng/g)						
Re		0.03 ± 0.11	-0.01 ± 0.11	-0.027 ± 0.099	0.10 ± 0.19	
Re*		0.006 ± 0.014	0.0 ± 0.1	0.031 ± 0.046	0.13 ± 0.12	-0.05 ± 0.15
Os		-0.20 ± 0.12	0.64 ± 0.35	0.37 ± 0.49	-0.15 ± 0.47	-0.2 ± 1.1
Ru	-0.19 ± 0.15	2.3 ± 1.2	-7.5 ± 4.1	0.2 ± 1.2	0.4 ± 1.7	-0.80 ± 0.79
Pt	-0.51 ± 0.19	2.0 ± 1.5	-7.6 ± 4.4	-0.1 ± 1.6	0.72 ± 0.94	0.3 ± 2.0
Rh	-0.14 ± 0.29	0.48 ± 0.68	-1.8 ± 1.7	0.03 ± 0.57	0.0 ± 1.0	0.12 ± 0.19
Pd	-1.81 ± 0.60	3.0 ± 5.6	-12.1 ± 8.7	0.2 ± 1.8	0.0 ± 1.0	-0.45 ± 0.86
Au	-0.15 ± 0.43	1.1 ± 5.4	-2.5 ± 3.9	0.28 ± 0.89	-0.1 ± 1.4	
Slope						
Re/Ir		0.107 ± 0.014	0.103 ± 0.009	0.086 ± 0.018	0.079 ± 0.032	
Re*/Ir		0.106 ± 0.002	0.104 ± 0.009	0.082 ± 0.009	0.074 ± 0.020	0.118 ± 0.045
Os/Ir		0.921 ± 0.016	0.875 ± 0.027	0.945 ± 0.091	1.134 ± 0.080	1.19 ± 0.34
Ru/Ir	1.78 ± 0.04	2.31 ± 0.17	3.04 ± 0.34	1.46 ± 0.22	1.30 ± 0.28	1.83 ± 0.25
Pt/Ir	2.39 ± 0.05	2.87 ± 0.21	3.56 ± 0.37	2.04 ± 0.31	1.73 ± 0.16	2.07 ± 0.62
Rh/Ir	0.423 ± 0.081	0.571 ± 0.097	0.71 ± 0.15	0.31 ± 0.11	0.26 ± 0.18	0.278 ± 0.059
Pd/Ir	1.69 ± 0.18	4.19 ± 0.83	4.15 ± 0.75	0.83 ± 0.33	0.88 ± 0.15	1.28 ± 0.27
Au/Ir	0.43 ± 0.12	1.38 ± 0.69	1.52 ± 0.32	0.26 ± 0.17	0.46 ± 0.23	
HSE/Ir ratios for chondrite groups (CI, CV, OC, EC, EH) and Earth's primitive mantle (PM)						
	CI	**CV**	**OC**	**EL**	**EH**	**PM**
Re/Ir	0.088	0.088	0.105	0.096	0.099	0.101
Os/Ir	1.06	1.07	1.13	1.08	1.09	1.12
Ru/Ir	1.49	1.47	1.52	1.54	1.61	2.03
Pt/Ir	2.04	1.98	2.12	1.99	2.17	2.17
Rh/Ir	0.307	0.255	0.310	0.348	0.321	0.349
Pd/Ir	1.22	0.985	1.01	1.19	1.71	2.06
Au/Ir	0.322	0.203	0.294	0.450	0.669	0.47

Uncertainties for slope and intercept values are 2σ. Errors used for regression calculations were 1% for Os, 2 % for Ir, Ru and Pt, 5% for Pd, Re, 10% for Rh, and 15% for Au.
HSE/Ir ratios for chondrites from different classes and groups (CI and CV carbonaceous chondrites, average ordinary chondrite (OC), EL and EH enstatite chondrites) and for the Earth's primitive mantle (PM) are shown for comparison. Chondrite data from Walker et al. (2002), Horan et al. (2003), Brandon et al. (2005a,b), Fischer-Gödde et al. (2010a). Data for the Earth's primitive mantle from Becker et al. (2006) and Fischer-Gödde et al. (2010b).

6. Conclusions

The major goal of this study was to place constraints on the origin of the HSE composition in the Earth's mantle and the lunar crust with the help of precise HSE abundance data and $^{187}Os/^{188}Os$ for primitive meteorites, terrestrial peridotites and lunar impact melt rocks. For this purpose an analytical technique that permits the precise and accurate measurement of *all* HSE, including precise concentration data for monoisotopic Rh and Au, in the same digestion aliquot was developed. Concentrations of Re, Os, Ir, Ru, Pt and Pd can be determined to an analytical precision <5% using isotope dilution techniques. The precision for the concentrations of the monoisotopic Rh and Au, determined using a standardization technique, is <10% for Rh and <15% for Au.

6.1 Chondrites

The study on chondrites provides new precise highly siderophile element abundance data and $^{187}Os/^{188}Os$ isotope ratios for a set of carbonaceous, ordinary, enstatite and Rumuruti chondrites. This study reports the first comprehensive data set for all HSE in the same aliquot of chondrite samples, including precise concentration data for monoisotopic Rh and Au. Differences in the HSE abundance patterns and ratios such as Re/Os, $^{187}Os/^{188}Os$, Pd/Ir, Rh/Ir and Au/Ir of chondrite classes are further substantiated with new data, and additional Rh and Au data, including new data for CI chondrites and Rumuruti chondrites.

The CI normalized HSE abundance patterns for carbonaceous chondrites other than CI are affected by depletion of the moderately volatile elements Pd and Au. HSE correlations are consistent with a CI like component and a Pd-Au depleted component, enriched in refractory siderophiles, consistent with recent data on metal grains from carbonaceous chondrites by Hammond et al. (2008). The refractory component may have formed by partial condensation (or evaporation) under solar nebular conditions (e.g. Palme and Wlotzka, 1976; Blander et al., 1980; Eisenhour and Buseck, 1992; Palme, 2008, Horan et al., 2009).

Well-defined HSE correlations for ordinary and enstatite chondrites may also reflect binary mixing, with a strongly fractionated Pd-Au rich component present as the major component in enstatite chondrites and a Pd-Au depleted, refractory HSE enriched component dominating ordinary chondrites. Subtle fractionations among refractory siderophile elements (most prominently Rh/Ir, Re/Os) within ordinary and enstatite chondrites relative to carbonaceous chondrites might be explained by fractional condensation combined with the removal of early condensates and mixing of early and late formed alloys (Sylvester et al., 1990), however, the conditions under which such phase separations may have occurred remain largely unconstrained.

The present HSE data on bulk samples of carbonaceous, ordinary and enstatite chondrites, and ordinary chondrite metal grains provide no evidence that chondrite components or chondrite precursor materials have been processed by planetary differentiation processes, except R chondrites which might have been affected by sulphide melt extraction and monosulphide solid solution-liquid sulphide partitioning related to impact events.

6.2 Peridotites

Applying improved analytical techniques the abundances of the highly siderophile elements (HSE) Re, Os, Ir, Ru, Pt, Rh, Pd and Au, and $^{187}Os/^{188}Os$ isotope ratios have been determined for a comprehensive set of terrestrial peridotite samples from ultramafic massifs, ophiolites and peridotite xenoliths. The data places new constraints on i) the relative HSE abundances in Earth's fertile mantle, ii) the distribution processes accounting for observed HSE variations between fertile and melt depleted mantle lithologies, and iii) potential meteoritic source materials for the late veneer.

For Rh and Au this is the most comprehensive peridotite data set reported so far. The data indicates that Rh behaves as a compatible element during low to moderate degrees of partial mantle melting. Fertile lherzolites with $Al_2O_3 > 2.5$ wt% display relatively constant Rh abundances and constant Rh/Ir of 0.34 ± 0.03 (1s) (Fig. 1). In conjunction with an Ir abundance of 3.5 ± 0.4 ng/g inferred previously (Becker et al., 2006) this value recasts into a Rh abundance for the fertile mantle of 1.2 ± 0.2. In contrast Au concentrations and

Au/Ir are related to peridotite fertility, indicating an incompatible behaviour of Au during partial melt extraction. Fertile lherzolites display Au/Ir ranging from 0.20-0.65, while residual harzburgites have Au/Ir <0.20 (Fig. 2). Abundances of Au and Re are well correlated with each other and suggest a similar compatibility. The primitive mantle abundance of Au calculated from the correlations displayed by Au/Ir with Al_2O_3 and Au with Re is 1.7 ± 0.5 (1s).

The new HSE data on peridotites reported here is consistent with the results of previous studies (Pearson et al., 2004; Becker et al., 2006; Luguet et al., 2007) and yields a compatibility sequence of Re ≤ Au < Pd < Pt ≤ Rh < Ir < Ru ≤ Os during magmatic processes in the mantle. The depletion of Pt, Pd, Re and Au relative to Os, Ir, Ru and Rh displayed by residual harzburgites, suggests HSE fractionation during partial melting. However, the HSE abundance variations of fertile and depleted peridotites cannot be explained by a single fractionation process. Correlations displayed by Pd/Ir, Re/Ir and Au/Ir with Al_2O_3 are consistent with refertilization of previously melt depleted mantle rocks due to reactive infiltration of silicate melts.

Relative abundances of Rh and Au inferred for the primitive mantle model composition are similar to values of ordinary and enstatite chondrites, but distinct from carbonaceous chondrites. The HSE pattern of the primitive mantle is inconsistent with compositions of known chondritic materials, but may be explained by mixtures of ancient meteoritic components identified in lunar impact melt rocks.

6.3 Lunar impact melt rocks

Ancient lunar impact melt rocks have been studied to constrain the nature and origin of impacting bodies during the late accretion period in the Earth-Moon system. Well-defined linear correlations displayed among HSE abundances of subsamples from a given lunar impact melt rock were used to infer the HSE composition of the meteoritic impactor component. In conjunction with previously reported precise HSE abundance and $^{187}Os/^{188}Os$ data a minimum of three different impactor end-member compositions are recorded in lunar impact rocks from Apollo 14, 16 and 17.

The HSE abundance pattern and $^{187}Os/^{188}Os$ of the meteoritic impactor component in granulitic breccias 67955 and 79215 is most similar to carbonaceous and ordinary chondrites, and to compositions observed for Apollo 17 aphanitic impact melt rocks. Because of the presence of granulitic clasts in 3.9 Ga old impact melts, the HSE abundances of theses samples may represent an older generation of impacting bodies. This inference is also consistent with a recently reported Sm-Nd crystallisation age of 4.2 Ga for 67955 (Norman et al., 2007).

HSE abundance patterns for Apollo 14 impact melt rock 14310 and the lunar meteorite DaG400 are similar to literature data for 14321 and Apollo 17 poikilitic impact melt rocks reported by Norman et al. (2002) and Puchtel et al. (2008). The high-HSE meteoritic end-member composition of these samples displays suprachondritic Re/Os, Ru/Ir and Pd/Ir. The suprachondritic ratios inferred for the meteoritic end-member composition of these rocks cannot be related to known chondrite groups. As discussed earlier these compositions may reflect ancient meteoritic material with distinct chemical compositions not recognized in the meteoritic record.

The third meteoritic end-member component is represented by strongly fractionated HSE abundance patterns observed for Apollo 16 impact melt rocks 60315 and 67935. The HSE signature of theses samples is far out of the range of chondritic meteorites and similar to compositions of IVA iron meteorites. Because both samples derive from the Descartes formation, which is most probably related to the Nectaris impact event, the Nectaris projectile may have been an IVA iron meteorite.

6.4 Late accretion in the Earth-Moon system

The range of different HSE compositions observed for lunar impact melt rocks, suggests that the HSE composition of the Earth's mantle also may reflect a mixture of different meteoritic impactor compositions. The admixture of differentiated meteoritic metal components seems to be a viable option to generate suprachondritic ratios of certain HSE in the Earth's mantle. Assuming that similar meteoritic material has been delivered to Earth and Moon during their late accretionary history, the excess HSE abundances of the Earth's mantle and suprachondritic Pd/Ir and Ru/Ir inferred for the primitive mantle

may be explained by a binary mixture of chondritic material with some fractionated HSE component similar to that found in Apollo 16 impact melt rocks 67935 and 60315. A combination of a fractionated HSE signature inherited from core segregation and addition of a late veneer component may be an alternative solution to explain the excess abundances of HSE and their relative abundances in the Earth's mantle.

6.5 Outlook

Future work on chondritic meteorites should focus on constraining the origin of HSE fractionation within chondrites. Because the results of this study revealed the presence of different HSE carrier phases with distinct HSE abundance patterns, this will require a detailed analysis of chondrite components, especially metals and sulphides, but also matrix, chondrules and calcium-aluminium-rich inclusions (CAIs). Additional constraints on fractionation processes and the prevailing conditions in the solar nebula may be obtained from precise abundance data for chalcophile and lithophile elements on chondrite bulk samples and chondrite components.

At present the detailed distribution process accounting for HSE abundance variations in the Earth's mantle remains poorly constrained and should be the subject of future studies. While some of the observed HSE variations for peridotites seem to be consistent with partitioning between sulphide phases, especially the partitioning behaviour of Re remains an unresolved issue. The incompatible behaviour of Re during magmatic processes in the mantle cannot be explained by experimentally determined partitioning studies between solid sulphide and sulphide melt, and thus requires an alternative and so far largely unconstrained distribution process. The HSE data obtained on peridotites also show that Pt behaves more compatible at low to moderate degrees of melt extraction compared to Pd. According to laboratory partitioning studies between solid sulphide and sulphide melt Pt and Pd should behave very similar.

The characterization of the late accreted meteoritic materials to the early Earth-Moon system should be substantiated by further studies on lunar impact melt rocks from the Apollo landing sites. These studies should also include lunar soils, because they may represent an integrated average composition of late accreted meteoritic materials. Additional HSE data on pristine lunar rocks may help to estimate indigenous HSE contributions from the lunar target rocks.

As demonstrated in this study, ^{187}Re-^{187}Os isotope systematics of lunar impact melt rocks may be used to obtain additional chronological information on the timing and frequency of the late influx in the inner solar system. Re-Os isotope systematics may be less susceptible to re-equilibration processes caused by subsequent impact events. Thus Re-Os model ages may retain age information related to older impact events, even if the Ar-Ar system of the same sample may have been reset through disturbances by younger impact events.

7. References

Ackerman, L., Walker, R. J., Puchtel, I. S., Pitcher, L., Jelínek, E., and Strnad, L. (2009). Effects of melt percolation on highly siderophile elements and Os isotopes in subcontinental lithospheric mantle: A study of the upper mantle profile beneath Central Europe. *Geochimica et Cosmochimica Acta* **73**, 2400-2414.

Alard, O., Griffin, W. L., Lorand, J. P., Jackson, S. E., and O'Reilly, S. Y. (2000). Non-chondritic distribution of the highly siderophile elements in mantle sulphides. *Nature* **407**, 891-894.

Alard, O., Griffin, W. L., Pearson, N. J., Lorand, J.-P., and O'Reilly, S. Y. (2002). New insights into the Re-Os systematics of sub-continental lithospheric mantle from in situ analysis of sulphides. *Earth and Planetary Science Letters* **203**, 651-663.

Alard, O., Luguet, A., Pearson, N. J., Griffin, W. L., Lorand, J.-P., Gannoun, A., Burton, K. W., and O'Reilly, S. Y. (2005). In situ Os isotopes in abyssal peridotites bridge the isotopic gap between MORBs and their source mantle. *Nature* **436**, 1005-1008.

Albarède, F. (2009). Volatile accretion history of the terrestrial planets and dynamic implications. *Nature* **461**, 1227-1233.

Allègre, C. J. and Luck, J.-M. (1980). Osmium isotopes as petrogenetic and geological tracers. *Earth and Planetary Science Letters* **48**, 148-154.

Anders, E., Ganapathy, R., Krähenbühl, U., and Morgan, J. W. (1973). Meteoritic material on the Moon. *The Moon* **8**, 3-24.

Anders, E. and Grevesse, N. (1989). Abundances of the elements: meteoritic and solar. *Geochimica et Cosmochimica Acta* **53**, 197-214.

Arculus, R. J. and Delano, J. W. (1981). Siderophile element abundances in the upper mantle: evidence for a sulfide signature and equilibrium with the core. *Geochimica et Cosmochimica Acta* **45**, 1331-1343.

Baedecker, P. A., Chou, C. L., Kimberlin, J., and Wasson, J. T. (1972). Trace element studies of lunar rocks and soils. *Lunar Planet. Sci. Conf.* **III**, 35-37.

Baedecker, P. A. and Wasson, J. T. (1975). Elemental fractionations among enstatite chondrites. *Geochimica et Cosmochimica Acta* **39**, 735-765.

Baker, J. A., Bizzarro, M., Wittig, N., Connelly, J., and Haack, H. (2005). Early planetesimal melting from an age of 4.5662 Gyr for differentiated meteorites. *Nature* **436**, 1127-1131.

Ballhaus, C., Bockrath, C., Wohlgemuth-Ueberwasser, C., Laurenz, V., and Berndt, J. (2006). Fractionation of the noble metals by physical processes. *Contrib. Mineral. Petrol.* **152**, 667-684.

Barnes, S. J., van Achterbergh, E., Makovicky, E., and Li, C. (2001). Proton microprobe results for the partitioning of platinum-group elements between monosulfide solid solution and sulphide liquid. *South African Journal of Geology* **104**, 275-286.

Becker, H., Horan, M. F., Walker, R. J., Gao, S., Lorand, J.-P., and Rudnick, R. L. (2006). Highly siderophile element composition of the Earth's primitive upper mantle: Constraints from new data on peridotite massifs and xenoliths. *Geochimica et Cosmochimica Acta* **70**, 4528-4550.

Becker, H., Morgan, J. W., Walker, R. J., MacPherson, G. J., and Grossman, J. N. (2001a). Rhenium-osmium systematics of calcium-aluminium-rich inclusions in carbonaceous chondrites. *Geochimica et Cosmochimica Acta* **65**, 3379-3390.

Becker, H., Shirey, S. B., and Carlson, R. W. (2001b). Effects of melt percolation on the Re-Os systematics of peridotites from a Paleozoic convergent plate margin. *Earth and Planetary Science Letters* **188**, 107-121.

Bédard, L. P. and Barnes, S. J. (2002). A comparison of N-type semi-planar and coaxial INAA detectors for 33 geochemical reference samples. *Journal of Radioanalytical and Nuclear Chemistry* **254**, 485-497.

Benedetti, M. F., De Kersabiec, A. M., and Boulegue, J. (1987). Determination of Gold in Twenty Geochemical Reference Samples by Flameless Atomic Absorption Spectrometry. *Geostandards and Geoanalytical Research* **11**, 127-129.

Berg, T., Marosits, J., Maul, J., Schönhense, G., Hoppe, P., Ott, U., and Palme, H. (2009). Evidence for nebular condensation of sub-micron refractory metal alloys. *Lunar Planet. Sci. Conf.* **XXXX**, 1585.

Bezmen, N. I., Asif, M., Brügmann, G. E., Romanenko, I. M., and Naldrett, A. J. (1994). Distribution of Pd, Rh, Ru, Ir, Os, and Au between sulfide and silicate metals. *Geochimica et Cosmochimica Acta* **58**, 1251-1260.

Bézos, A., Lorand, J. P., Humler, E., and Gros, M. (2005). Platinum-group element systematics in Mid-Oceanic Ridge basaltic glasses from the Pacific, Atlantic, and Indian Oceans. *Geochimica et Cosmochimica Acta* **69**, 2613-2627.

Bickel, C. E., Warner, J. L., and Phinney, W. C. (1976). Petrology of 79215: Brecciation of a lunar cumulate. *Proc. Lunar Sci. Conf.* **7**, 1793-1819.

Bischoff, A., Geiger, T., Palme, H., Spettel, B., Schultz, L., Scherer, P., Loeken, T., Bland, P., Clayton, R. N., Mayeda, T. K., Herpers, U., Meltzow, B., Michel, R., and Dittrich-Hannen, B. (1994). Acfer 217-A new member of the Rumuruti chondrite group (R). *Meteoritics* **29**, 263-274.

Bischoff, A. and Palme, H. (1987). Composition and mineralogy of refractory-metal-rich assemblages from a Ca,Al-rich inclusion in the Allende meteorite. *Geochimica et Cosmochimica Acta* **51**, 2733-2748.

Bischoff, A., Sokol, A., Palme, H., Schultz, L., Weber, H. W., and Wolf, D. (2001). Mineralogy, chemistry, and noble gases of the unpaired Rumuruti-chondrites NWA 753 and NWA 755. *Meteorit. Planet. Sci.* **36**, A21.

Bizzarro, M., Baker, J. A., and Haack, H. (2004). Mg isotope evidence for contemporaneous formation of chondrules and refractory inclusions. *Nature* **431**, 275-278.

Blander, M., Fuchs, L. H., Horowitz, C., and Land, R. (1980). Primordial refractory metal particles in the Allende meteorite. *Geochimica et Cosmochimica Acta* **44**, 217-219, 221-223.

Bockrath, C., Ballhaus, C., and Holzheid, A. (2004). Fractionation of the platinum-group elements during mantle melting. *Science* **305**, 1951-1953.

Bodinier, J. L. (1988). Geochemistry and petrogenesis of the Lanzo peridotite body, western Alps. *Tectonophysics* **149**, 67-88.

Bodinier, J. L., Dupuy, C., and Dostal, J. (1988). Geochemistry and petrogenesis of Eastern Pyrenean peridotites. *Geochimica et Cosmochimica Acta* **52**, 2893-2907.

Bodinier, J. L., Guiraud, M., Fabriés, J., Dostal, J., and Dupuy, C. (1987). Petrogenesis of layered pyroxenites from the Lherz, Freychinéde and Prades ultramafic bodies (Ariége, French Pyrénées). *Geochimica et Cosmochimica Acta* **51**, 279-290.

Bodinier, J. L., Menzies, M. A., and Thirlwall, M. F. (1991). Continental to oceanic mantle transition-REE and Sr-Nd isotopic geochemistry of the Lanzo massif. *Journal of Petrology Spec. Lherzolite Issue*, 191-210.

Bodinier, J.-L., Garrido, C. J., Chanefo, I., Bruguier, O., and Gervilla, F. (2008). Origin of Pyroxenite-Peridotite Veined Mantle by Refertilization Reactions: Evidence from the Ronda Peridotite (Southern Spain). *J. Petrology* **49**, 999-1025.

Borisov, A. and Palme, H. (1995). The solubility of iridium in silicate melts: New data from experiments with Ir10Pt90 alloys. *Geochimica et Cosmochimica Acta* **59**, 481-485.

Bornhorst, T. J., Rose, W. I., Wolfe, S. P., and Hoffman, E. L. (1984). Gold Content of Eleven French Geochemical Reference Samples. *Geostandards and Geoanalytical Research* **8**, 1-2.

Boynton, W. V., Chou, C. L., Robinson, K. L., Warren, P. H., and Wasson, J. T. (1976). Lithophiles, siderophiles and volatiles in Apollo 16 soils and rocks. *Proc. Lunar Sci. Conf.* **7**, 727-742.

Brandon, A. D. and Walker, R. J. (2005). The debate over core-mantle interaction. *Earth and Planetary Science Letters* **232**, 211-225.

Brandon, A. D., Humayun, M., Puchtel, I. S., Leya, I., and Zolensky, M. (2005b). Osmium Isotope Evidence for an s-Process Carrier in Primitive Chondrites. *Science* **309**, 1233-1236.

Brandon, A. D., Humayun, M., Puchtel, I. S., and Zolensky, M. E. (2005a). Re-Os isotopic systematics and platinum group element composition of the Tagish Lake carbonaceous chondrite. *Geochimica et Cosmochimica Acta* **69**, 1619-1631.

Brandon, A. D., Norman, M. D., Walker, R. J., and Morgan, J. W. (1999). ^{186}Os-^{187}Os systematics of Hawaiian picrites. *Earth and Planetary Science Letters* **174**, 25-42.

Brandon, A. D., Snow, J. E., Walker, R. J., Morgan, J. W., and Mock, T. D. (2000). ^{190}Pt-^{186}Os and ^{187}Re-^{187}Os systematics of abyssal peridotites. *Earth and Planetary Science Letters* **177**, 319-335.

Brandon, A. D., Walker, R. J., and Puchtel, I. S. (2006). Platinum-osmium isotope evolution of the Earth's mantle: Constraints from chondrites and Os-rich alloys. *Geochimica et Cosmochimica Acta* **70**, 2093-2103.

Brearley, A. J. and Jones, R. H. (1998). Chondritic meteorites. In: Papike, J. J. (Ed.), *Planetary Materials*. Mineralogical Society of America, Washington, DC.

Brenan, J. M. (2002). Re-Os fractionation in magmatic sulfide melt by monosulfide solid solution. *Earth and Planetary Science Letters* **199**, 257-268.

Brenan, J. M. (2008). Re-Os fractionation by sulfide melt-silicate melt partitioning: A new spin. *Chemical Geology* **248**, 140-165.

Brenan, J. M. and McDonough, W. F. (2009). Core formation and metal-silicate fractionation of osmium and iridium from gold. *Nature Geoscience* **2**, 798-801.

Brenan, J. M., McDonough, W. F., and Ash, R. (2005). An experimental study of the solubility and partitioning of iridium, osmium and gold between olivine and silicate melt. *Earth and Planetary Science Letters* **237**, 855-872.

Brügmann, G. E., Arndt, N. T., and Hofmann, A. W. (1987). Platinum-group element abundances in komatiitic basalts and komatiites. *Terra Cognita* **5**, 288-289.

Büchl, A., Brügmann, G., Batanova, V. G., Münker, C., and Hofmann, A. W. (2002). Melt percolation monitored by Os isotopes and HSE abundances: a case study from the mantle section of the Troodos Ophiolite. *Earth and Planetary Science Letters* **204**, 385-402.

Büchl, A., Brügmann, G. E., Batanova, V. G., and Hofmann, A. W. (2004). Os mobilization during melt percolation: The evolution of Os isotope heterogeneities in the mantle sequence of the Troodos ophiolite, Cyprus. *Geochimica et Cosmochimica Acta* **68**, 3397-3408.

Burton, K. W., Schiano, P., Birck, J. L., Allegre, C. J., Rehkamper, M., Halliday, A. N., and Dawson, J. B. (2000). The distribution and behaviour of rhenium and osmium amongst mantle minerals and the age of the lithospheric mantle beneath Tanzania. *Earth and Planetary Science Letters* **183**, 93-106.

Burton, K. W., Schiano, P., Birck, J.-L., and Allègre, C. J. (1999). Osmium isotope disequilibrium between mantle minerals in a spinel-lherzolite. *Earth and Planetary Science Letters* **172**, 311-322.

Cahill, J. T., Floss, C., Anand, M., Taylor, L. A., Nazarov, M. A., and Cohen, B. A. (2004). Petrogenesis of lunar highlands meteorites: Dhofar 025, Dhofar 081, Dar al Gani 262, and Dar al Garni 400. *Meteorit. Planet. Sci.* **39**, 503-530.

Campbell, A. J. and Humayun, M. (2003). Formation of metal in Grosvenor Mountains 95551 and comparison to ordinary chondrites. *Geochimica et Cosmochimica Acta* **67**, 2481-2495.

Campbell, A. J., Humayun, M., and Weisberg, M. K. (2002). Siderophile element constraints on the formation of metal in the metal-rich chondrites Bencubbin, Weatherford, and Gujba. *Geochimica et Cosmochimica Acta* **66**, 647-660.

Campbell, A. J., Simon, S. B., Humayun, M., and Grossman, L. (2003). Chemical evolution of metal in refractory inclusions in CV3 chondrites. *Geochimica et Cosmochimica Acta* **67**, 3119-3134.

Chabot, N. L., Campbell, A. J., Jones, J. H., Humayun, M., and Agee, C. B. (2003). An experimental test of Henry´s Law in solid metal-liquid metal systems with implications for iron meteorites. *Meteorit. Planet. Sci.* **38**, 181-196.

Chabot, N. L., Campbell, A. J., Jones, J. H., Humayun, M., and Lauer, J. H. V. (2006). The influence of carbon on trace element partitioning behaviour. *Geochimica et Cosmochimica Acta* **70**, 1322-1335.

Chabot, N. L. and Jones, J. H. (2003). The parameterization of solid metal-liquid metal partitioning of siderophile elements. *Meteorit. Planet. Sci.* **38**, 1425-1436.

Chen, J. H. and Wasserburg, G. J. (1996). Live ^{107}Pd in the early solar system and implications for planetary evolution. In: Basu, A. and Hart, S. R. Eds., *Earth Processes: Reading the isotopic code*. AGU, Washington.

Chen, J. H., Papanastassiou, D. A., and Wasserburg, G. J. (1998). Re-Os systematics in chondrites and the fractionation of the platinum group elements in the early solar system. *Geochimica et Cosmochimica Acta* **62**, 3379-3392.

Chesley, J., Righter, K., and Ruiz, J. (2004). Large-scale mantle metasomatism: a Re-Os perspective. *Earth and Planetary Science Letters* **219**, 49-60.

Chesley, J. T., Rudnick, R. L., and Lee, C.-T. (1999). Re-Os systematics of mantle xenoliths from the East African Rift: age, structure, and history of the Tanzanian craton. *Geochimica et Cosmochimica Acta* **63**, 1203-1217.

Choi, B.-G. and Wasson, J. T. (2003). Microscale oxygen isotopic exchange and magnetite formation in the Ningqiang anomalous carbonaceous chondrite. *Geochimica et Cosmochimica Acta* **67**, 4655-4660.

Chou, C. L. (1978). Fractionation of siderophile elements in the Earth/'s upper mantle. *Proc. Lunar Planet. Sci. Conf.* **9**, 219-230.

Chou, C.-L., Baedecker, P. A., and Wasson, J. T. (1976). Allende inclusions: volatile-element distribution and evidence for incomplete volatilization of presolar solids. *Geochimica et Cosmochimica Acta* **40**, 85-94.

Cohen, A. S. and Waters, F. G. (1996). Separation of osmium from geological materials by solvent extraction for analysis by thermal ionisation mass spectrometry. *Anal. Chim. Acta* **332**, 269-275.

Constantin, M. (2008). Trace element data for gold, iridium and silver in seventy geochemical reference materials. *Geostandards and Geoanalytical Research* **33**, 115-132.

Cook, D. L., Walker, R. J., Horan, M. F., Wasson, J. T., and Morgan, J. W. (2004). Pt-Re-Os systematics of group IIAB and IIIAB iron meteorites. *Geochimica et Cosmochimica Acta* **68**, 1413-1431.

Corgne, A., Wood, B. J., and Fei, Y. (2008). C- and S-rich molten alloy immiscibility and core formation of planetesimals. *Geochimica et Cosmochimica Acta* **72**, 2409-2416.

Cottrell, E. and Walker, D. (2006). Constraints on core formation from Pt partitioning in mafic silicate liquids at high temperatures. *Geochimica et Cosmochimica Acta* **70**, 1565-1580.

Crocket, J. H., Fleet, M. E., and S, W. E. (1997). Implications of composition for experimental partitioning of platinum-group elements and gold between sulfide liquid and basalt melt: The significance of nickel content. *Geochimica et Cosmochimica Acta* **61**, 4139-4149.

Cushing, J. A., Taylor, G. J., Norman, M. D., and Keil, K. (1999). The granulitic impact suite: Impact melts and metamorphic breccias of the early lunar crust. *Meteorit. Planet. Sci.* **34**, 185-195.

Dale, C. W., Luguet, A., Macpherson, C. G., Pearson, D. G., and Hickey-Vargas, R. (2008). Extreme platinum-group element fractionation and variable Os isotope compositions in Philippine Sea Plate basalts: Tracing mantle source heterogeneity. *Chemical Geology* **248**, 213-238.

Danielson, L. R., Sharp, T. G., and Hervig, R. L. (2005). Implications for core formation of the Earth from high pressure temperature Au partitioning experiments. *Lunar Planet. Sci. Conf.* **XXXVI**, 1955.

Day, J. M. D., Walker, R. J., James, O. B., and Puchtel, I. S. (2010). Osmium isotope and highly siderophile element systematics of the lunar crust. *Earth and Planetary Science Letters* **289**, 595-605.

Ebihara, M., Wolf, R., and Anders, E. (1982). Are C1 chondrites chemically fractionated? a trace element study. *Geochimica et Cosmochimica Acta* **46**, 1849-1861.

Ebihara, M., Wolf, R., Warren, P. H., and Anders, E. (1992). Trace elements in 59 mostly highland Moon rocks. *Proc. Lunar Planet. Sci.* **22**, 417-426.

Ehmann, W. D., Baedecker, P. A., and McKown, D. M. (1970). Gold and iridium in meteorites and some selected rocks. *Geochimica et Cosmochimica Acta* **34**, 493-507.

Eisenhour, D. D. and Buseck, P. R. (1992). Transmission electron microscopy of RMNs: Implications for single-phase condensation of the refractory siderophile elements. *Meteoritics* **27**, 217-218.

Ertel, W., Dingwell, D. B., and Sylvester, P. J. (2008). Siderophile elements in silicate melts -- A review of the mechanically assisted equilibration technique and the nanonugget issue. *Chemical Geology* **248**, 119-139.

Ertel, W., O'Neill, H. S. C., Sylvester, P. J., and Dingwell, D. B. (1999). Solubilities of Pt and Rh in a haplobasaltic silicate melt at 1300°C. *Geochimica et Cosmochimica Acta* **63**, 2439-2449.

Ertel, W., O'Neill, H. S. C., Sylvester, P. J., Dingwell, D. B., and Spettel, B. (2001). The solubility of rhenium in silicate melts: Implications for the geochemical properties of rhenium at high temperatures. *Geochimica et Cosmochimica Acta* **65**, 2161-2170.

Ertel, W., Walter, M. J., Drake, M. J., and Sylvester, P. J. (2006). Experimental study of platinum solubility in silicate melt to 14 GPa and 2273 K: Implications for accretion and core formation in Earth. *Geochimica et Cosmochimica Acta* **70**, 2591-2602.

Fegley Jr, B. and Palme, H. (1985). Evidence for oxidizing conditions in the solar nebula from Mo and W depletions in refractory inclusions in carbonaceous chondrites. *Earth and Planetary Science Letters* **72**, 311-326.

Fischer-Gödde, M., Becker, H., and Wombacher, F. (2010c). Highly Siderophile Element Abundances and $^{187}Os/^{188}Os$ in Lunar Impact Melt Rocks: Implications for Late Accretion Processes in the Earth-Moon System. *Lunar Planet. Sci. Conf.* **41**.

Fischer-Gödde, M., Becker, H., and Wombacher, F. (2010a). Rhodium, gold and other highly siderophile element abundances in chondritic meteorites. *Geochimica et Cosmochimica Acta* **74**, 356-379.

Fischer-Gödde, M., Becker, H., and Wombacher, F. (2010b). Rhodium, gold and other highly siderophile elements in orogenic peridotites and peridotite xenoliths. *Chem. Geol.*, in review.

Fischer-Gödde, M., Wombacher, F., and Becker, H. (2007). Rhodium, gold and other highly siderophile elements in chondrites. *Lunar Planet. Sci. Conf.* **XXXVIII**, 1625.

Fleet, M. E., Chryssoulis, S. L., Stone, W. E., and Weisener, C. G. (1993). Partitioning of platinum-group elements and Au in the Fe-Ni-Cu-S system: experiments on the fractional crystallization of sulfide melt. *Contrib. Mineral. Petrol.* **115**, 36-44.

Fleet, M. E., Crocket, J. H., and Stone, W. E. (1996). Partitioning of platinum-group elements (Os, Ir, Ru, Pt, Pd) and gold between sulfide liquid and basalt melt. *Geochimica et Cosmochimica Acta* **60**, 2397-2412.

Fleet, M. E., Liu, M., and Crocket, J. H. (1999). Laboratory partitioning of platinum-group elements (PGE) and gold with application to magmatic sulfide-PGE deposits. *Lithos* **47**, 127-142.

Fleet, M. E., Liu, M., and Crocket, J. H. (1999). Partitioning of trace amounts of highly siderophile elements in the Fe-Ni-S system and their fractionation in nature. *Geochimica et Cosmochimica Acta* **63**, 2611-2622.

Fleet, M. E. and Stone, W. E. (1991). Partitioning of platinum-group elements in the Fe-Ni-S system and their fractionation in nature. *Geochimica et Cosmochimica Acta* **55**, 245-253.

Fleet, M. E., Stone, W. E., and Crocket, J. H. (1991). Partitioning of palladium, iridium, and platinum between sulfide liquid and basalt melt: Effects of melt composition, concentration, and oxygen fugacity. *Geochimica et Cosmochimica Acta* **55**, 2545-2554.

Fonseca, R. O. C., Mallmann, G., St.C.O'Neill, H., and Campbell, I. H. (2007). How chalcophile is rhenium? An experimental study of the solubility of Re in sulphide mattes. *Earth and Planetary Science Letters* **260**, 537-548.

Fortenfant, S. S., Günther, D., Dingwell, D. B., and Rubie, D. C. (2003). Temperature dependence of Pt and Rh solubilities in a haplobasaltic melt. *Geochimica et Cosmochimica Acta* **67**, 123-131.

Frey, F. A., John Suen, C., and Stockman, H. W. (1985). The Ronda high temperature peridotite: Geochemistry and petrogenesis. *Geochimica et Cosmochimica Acta* **49**, 2469-2491.

Friedrich, J. M., Wang, M.-S., and Lipschutz, M. E. (2002). Comparison of the trace element composition of Tagish Lake with other primitive carbonaceous chondrites. *Meteorit. Planet. Sci.* **37**, 677-686.

Ganapathy, R., Laul, J. C., Morgan, J. W., and Anders, E. (1972). Moon: possible nature of the body that produced the Imbrian basin, and the composition of Apollo 14 samples. *Science* **175**, 55-59.

Ganapathy, R., Morgan, J. W., Higuchi, H., and Anders, E. (1974). Meteoritic and volatile elements in Apollo 16 rocks and in separated phases from 14306. *Proc. Lunar Sci. Conf.* **5**, 1659-1683.

Ganapathy, R., Morgan, J. W., Krähenbühl, U., and Anders, E. (1973). Ancient meteoritic components in lunar highland rocks: clues from trace elements in Apollo 15 and 16 samples. *Proc. Lunar Sci. Conf.* **4**, 1239-1261.

Gao, S., Rudnick, R. L., Carlson, R. W., McDonough, W. F., and Liu, Y.-S. (2002). Re-Os evidence for replacement of ancient mantle lithosphere beneath the North China craton. *Earth and Planetary Science Letters* **198**, 307-322.

Geiger, T. and Bischoff, A. (1989). (Os,Ru,Ir)S2 and other refractory siderophile element-rich particles in the metamorphosed carbonaceous chondrites Karoonda, Mulga (West) and PCA82500. *Lunar Planet. Sci. Conf.* **XX**, 335-336.

Geiger, T. and Bischoff, A. (1995). Formation of opaque minerals in CK chondrites. Planet. Space Sci. 43, 485-498.

Gomes, R., Levinson, H. F., Tsiganis, K., and Morbidelli, A. (2005). Origin of the cataclysmic late heavy bombardment period of the terrestrial planets. *Nature* **435**, 466-470.

Grossman, J. N. and Wasson, J. T. (1985). The origin and history of the metal and sulfide components of chondrules. *Geochimica et Cosmochimica Acta* **49**, 925-939.

Grossman, L. and Ganapathy, R. (1976). Trace elements in the Allende meteorite--I. Coarse-grained, Ca-rich inclusions. *Geochimica et Cosmochimica Acta* **40**, 331-344.

Gueddari, K., Piboule, M., and Amossé, J. (1996). Differentiation of platinum-group elements (PGE) and of gold during partial melting of peridotites in the lherzolitic massifs of the Betico-Rifean range (Ronda and Beni Bousera). *Chemical Geology* **134**, 181-197.

Hammond, S. J., Rogers, N. W., and Bland, P. A. (2008). Laser ablation analysis of metal grains in carbonaceous chondrites. *Geochimica et Cosmochimica Acta* **72**, A346.

Handler, M. R. and Bennett, V. C. (1999). Behaviour of Platinum-group elements in the subcontinental mantle of eastern Australia during variable metasomatism and melt depletion. *Geochimica et Cosmochimica Acta* **63**, 3597-3618.

Handler, M. R., Bennett, V. C., and Dreibus, G. (1999). Evidence from correlated Ir/Os and Cu/S for late stage Os mobility in peridotite xenoliths: implications for Re-Os systematics. *Geology* **27**, 75-78.

Hart, S. R. and Ravizza, G. E. (1996). Os partitioning between phases in lherzolite and basalt. In: Basu, A. and Hart, S. R. Eds.), *Earth processes. Reading the isotopic code*. American Geophysical Union, Washington D.C.

Hartmann, W. K., Ryder, G., Dones, L., and Grinspoon, D. (2000). The time-dependent intense bombardment of the primordial Earth/Moon system. In: Canup, R. M. and Righter, K. Eds.), *Origin of the Earth and Moon*. University of Arizona Press.

Haskin, L. A., Korotev, R. L., Gillis, J. J., and Jolliff, B. L. (2002). Stratigraphies of Apollo and Luna highland landing sites and provenances of materials from the perspective of basin impact ejecta modelling. *Lunar Planet. Sci. Conf.* **XXXIII**, 1364.

Hauri, E. H. and Hart, S. R. (1997). Rhenium abundances and systematics in oceanic basalts. *Chemical Geology* **139**, 185-205.

Henley, R. W. (1973). Solubility of gold in hydrothermal chloride solutions. *Chemical Geology* **11**, 73-87.

Hermann, F. and Wichtl, M. (1974). Neutronenaktivierungsanalytische Bestimmung von Spurenelementen in Meteoriten der Vatikanischen Sammlung. In: Kiesl, W. and Malissa, H. Eds.), *Analyse extraterrestrischen Materials*. Springer Verlag, Wien.

Hertogen, J., Janssens, M. J., and Palme, H. (1980). Trace elements in ocean ridge basalt glasses: implications for fractionations during mantle evolution and petrogenesis. *Geochimica et Cosmochimica Acta* **44**, 2125-2143.

Hertogen, J., Janssens, M. J., Takahashi, H., Palme, H., and Anders, E. (1977). Lunar basins and craters: evidence for systematic compositional change of bombarding population. *Proc. Lunar Sci. Conf.* **8**, 17-45.

Hertogen, J., Janssens, M.-J., Takahashi, H., Morgan, J. W., and Anders, E. (1983). Enstatite chondrites: Trace element clues to their origin. *Geochimica et Cosmochimica Acta* **47**, 2241-2255.

Hiesinger, H. and Head, J. W. (2006). New views of lunar geoscience: An introduction and overview. In: Jolliff, L. J., Wieczorek, M. A., Shearer, C. K., and Neal, C. R. Eds.), *New views of the Moon*. Mineralogical Society of America, Geochemical Society, Chantilly.

Higuchi, H. and Morgan, J. W. (1975). Ancient meteoritic component in Apollo 17 boulders. *Proc. Lunar Sci. Conf.* **6**, 1625-1651.

Hollister, L. S. (1973). Sample 67955: A description and a problem. *Proc. Lunar Sci. Conf.* **4**, 633-641.

Holzheid, A., Sylvester, P., O´Neill, H. S. C., Rubie, D. C., and Palme, H. (2000). Evidence for a late chondritic veneer in the Earth's mantle from high-pressure partitioning of palladium and platinum. *Nature* **406**, 396-399.

Horan, M. F., Alexander, C. M. O. D., and Walker, R. J. (2008). An evaluation of evidence for early solar system processes preserved in the highly siderophile elements of chondrite components. *Lunar Planet. Sci. Conf.* **XXXIX**, 1448.

Horan, M. F., Alexander, C. M. O. D., and Walker, R. J. (2009). Highly siderophile element evidence for early solar system processes in components from ordinary chondrites. *Geochimica et Cosmochimica Acta* **73**, 6984-6997.

Horan, M. F., Smoliar, M. I., and Walker, R. J. (1998). ^{182}W and ^{187}Re-^{187}Os systematics of iron meteorites: Chronology for melting, differentiation, and crystallization in asteroids. *Geochimica et Cosmochimica Acta* **62**, 545-554.

Horan, M. F., Walker, R. J., Morgan, J. W., Grossman, J. N., and Rubin, A. E. (2003). Highly siderophile elements in chondrites. *Chemical Geology* **196**, 5-20.

Hudgins, J. A., Spray, J. G., Kelley, S. P., Korotev, R. L., and Sherlock, S. C. (2008). A laser probe 40Ar/39Ar and INAA investigation of four Apollo granulitic breccias. *Geochimica et Cosmochimica Acta* **72**, 5781-5798.

Humayun, M. and Campbell, A. J. (2002). The duration of ordinary chondrite metamorphism inferred from tungsten microdistribution in metal. *Earth and Planetary Science Letters* **198**, 225-243.

Humayun, M. and Cassen, P. (2000). Processes Determining the Volatile Abundances of the Meteorites and Terrestrial Planets. In: Canup, R. M. and Righter, K. Eds.), *Origin of the Earth and Moon*. University of Arizona Press.

Humayun, M., Keil, K., and Bischoff, A. (2009). Siderophile elements in metal from Northwest Africa 2526, an enstatite chondrite partial melt residue. *Lunar Planet. Sci. Conf.* **XXXX**, 1744.

Husain, L. and Schaeffer, G. A. (1973). ^{40}Ar-^{39}Ar crystallization ages and 38Ar-37Ar cosmic ray exposure ages of samples from the vicinity of Apollo 16 landing site. *Lunar Planet. Sci. Conf.* **IV**, 406-408.

Jagoutz, E., Palme, H., Baddenhausen, H., Blum, K., Cendales, M., Dreibus, G., Spettel, B., Lorenz, V., and Wänke, H. (1979). The abundances of major, minor and trace elements in the Earth's mantle as derived from primitive ultramafic nodules. *Proc. Lunar Planet. Sci. Conf.* **10**, 2031-2050.

James, O. B. (1981). Petrologic and age relations of the Apollo 16 rocks: Implications for subsurface geology and the age of the Nectaris Basin. *Proc. Lunar Planet. Sci.* **12B**, 209-233.

James, O. B. (1995). Siderophile elements in lunar impact melts: nature of the impactors. *Lunar Planet. Sci. Conf.* **XXVI**, 671-672.

James, O. B. (1996). Siderophile elements in lunar impact melts define nature of the impactors. *Lunar Planet. Sci. Conf.* **XXVII**, 603-604.

James, O. B. (2002). Distinctive meteoritic components in lunar "cataclysm" impact melt breccias. *Lunar Planet. Sci. Conf.* **XXXIII**, 1210.

Jana, D. and Walker, D. (1997). The impact of carbon on element distribution during core formation. *Geochimica et Cosmochimica Acta* **61**, 2759-2763.

Jarosewich, E., Clarke, R. S., and Barrows, J. N. (1987). The Allende meteorite reference sample. *Smithson. Contrib. Earth Sci.* **27**, 1-49.

Jochum, K. P. (1996). Rhodium and other platinum-group elements in carbonaceous chondrites. *Geochimica et Cosmochimica Acta* **60**, 3353-3357.

Jochum, K. P., Arndt, N. T., and Hofmann, A. W. (1991). Nb-Th-La in komatiites and basalts: constraints on komatiite petrogenesis and mantle evolution. *Earth and Planetary Science Letters* **107**, 272-289.

Jones, J. and Drake, M. (1986). Core formation and Earth's late accretionary history. *Nature* **323**, 470.

Jones, J. H. and Malvin, D. J. (1990). A non-metal interaction model for the segregation of trace metals during solidification of Fe-Ni-S, Fe-Ni-P, and Fe-Ni-S-P alloys. *Metallurgical and Materials Transactions B* **21B**, 697-706.

Jones, J. H. and Walker, D. (1991). Partitioning of siderophile elements in the FeNiS system: 1 bar to 80 kbar. *Earth and Planetary Science Letters* **105**, 127-133.

Kallemeyn, G. W., Boynton, W. V., Willis, J., and Wasson, J. T. (1978). Formation of the Bencubbin polymict meteoritic breccia. *Geochimica et Cosmochimica Acta* **42**, 507-515.

Kallemeyn, G. W., Rubin, A. E., Wang, D., and Wasson, J. T. (1989). Ordinary chondrites: Bulk compositions, classification, lithophile-element fractionations and composition-petrographic type relationships. *Geochimica et Cosmochimica Acta* **53**, 2747-2767.

Kallemeyn, G. W., Rubin, A. E., and Wasson, J. T. (1991). The compositional classification of chondrites: V. The Karoonda (CK) group of carbonaceous chondrites. *Geochimica et Cosmochimica Acta* **55**, 881-892.

Kallemeyn, G. W., Rubin, A. E., and Wasson, J. T. (1996). The compositional classification of chondrites: VII. The R chondrite group. *Geochimica et Cosmochimica Acta* **60**, 2243-2256.

Kallemeyn, G. W. and Wasson, J. T. (1981). The compositional classification of chondrites--I. The carbonaceous chondrite groups. *Geochimica et Cosmochimica Acta* **45**, 1217-1230.

Kallemeyn, G. W. and Wasson, J. T. (1986). Compositions of enstatite (EH3, EH4,5 and EL6) chondrites: Implications regarding their formation. *Geochimica et Cosmochimica Acta* **50**, 2153-2164.

Kelly, W. R. and Larimer, J. W. (1977). Chemical fractionations in meteorites--VIII. Iron meteorites and the cosmochemical history of the metal phase. *Geochimica et Cosmochimica Acta* **41**, 93-111.

Kimura, K., Lewis, R. S., and Anders, E. (1974). Distribution of gold and rhenium between nickel-iron and silicate melts: implications for the abundance of siderophile elements on the Earth and Moon. *Geochimica et Cosmochimica Acta* **38**, 683-701.

Kirsten, T., Horn, P., and Kiko, J. (1973). ^{39}Ar-^{40}Ar dating and rare gas analysis of Apollo 16 rocks and soils. Proc. Lunar Science Conference. *Geochim. Cosmochim. Acta* **2**, 1757-1784.

Kleine, T., Mezger, K., Palme, H., Scherer, E., and Münker, C. (2005). Early core formation in asteroids and late accretion of chondrite parent bodies: Evidence from ^{182}Hf-^{182}W in CAIs, metal-rich chondrites, and iron meteorites. *Geochimica et Cosmochimica Acta* **69**, 5805-5818.

Kong, P. and Ebihara, M. (1996). Metal phases of L chondrites: Their formation and evolution in the nebular and in the parent body. *Geochimica et Cosmochimica Acta* **60**, 2667-2680.

Kong, P. and Ebihara, M. (1997). The origin and nebular history of the metal phase of ordinary chondrites. *Geochimica et Cosmochimica Acta* **61**, 2317-2329.

Kong, P. and Palme, H. (1999). Compositional and genetic relationship between chondrules, chondrule rims, metal, and matrix in the Renazzo chondrite. *Geochimica et Cosmochimica Acta* **63**, 3673-3682.

Korotev, R. L. (1987a). The meteoritic component of Apollo 16 noritic impact melt breccias. Proc. Lunar Planet. Sci. Conf. 17. *J. Geophys. Res.* **92**, E491-E512.

Korotev, R. L. (1987b). The nature of the meteoritic components of Apollo 16 soil, as inferred from correlations of iron, cobalt, iridium, and gold with nickel. Proc. Lunar Plnet. Sci. Conf. 17. *J. Geophys. Res.* **92**, E447-E461.

Korotev, R. L. (1994). Compositional variation in Apollo 16 impact-melt breccias and inferences for the geology and bombardment history of the Central Highlands of the Moon. *Geochimica et Cosmochimica Acta* **58**, 3931-3969.

Korotev, R. L. (1996). A self-consistent compilation of elemental concentration data for 93 geochemical reference samples. *Geostandards and Geoanalytical Research* **20**, 217-245.

Korotev, R. L., Jolliff, B. L., Zeigler, R. A., Gillis, J. J., and Haskin, L. A. (2003). Feldspathic lunar meteorites and their implications for compositional remote sensing of the lunar surface and the composition of the lunar crust. *Geochimica et Cosmochimica Acta* **67**, 4895-4923.

Larimer, J. W. and Anders, E. (1970). Chemical fractionations in meteorites--III. Major element fractionations in chondrites. *Geochimica et Cosmochimica Acta* **34**, 367-387.

Le Roux, V., Bodinier, J. L., Tommasi, A., Alard, O., Dautria, J. M., Vauchez, A., and Riches, A. J. V. (2007). The Lherz spinel lherzolite: Refertilized rather than pristine mantle. *Earth and Planetary Science Letters* **259**, 599-612.

Levinson, H. F., Dones, L., Chapman, C. R., Stern, S. A., Duncan, M. J., and Zahnle, K. (2001). Could the lunar late heavy bombardment have been triggered by the formation of Uranus and Neptune? *Icarus* **151**, 286-306.

Li, C., Barnes, S. J., Makovicky, E., Rose-Hansen, J., and Makovicky, M. (1996). Partitioning of nickel, copper, iridium, rhenium, platinum, and palladium between monosulfide solid solution and sulfide liquid: Effects of composition and temperature. *Geochimica et Cosmochimica Acta* **60**, 1231-1238.

Li, J. and Agee, C. B. (2001). The effect of pressure, temperature, oxygen fugacity and composition on partitioning of nickel and cobalt between liquid Fe-Ni-S alloy and liquid silicate: implications for the earth's core formation. *Geochimica et Cosmochimica Acta* **65**, 1821-1832.

Libourel, G. and Krot, A. N. (2007). Evidence for the presence of planetesimal material among the precursors of magnesian chondrules of nebular origin. *Earth and Planetary Science Letters* **254**, 1-8.

Libourel, G., Krot, A. N., and Chaussidon, M. (2006). Presence of planetesimal material among the precursors of magnesian chondrules. *Geochimica et Cosmochimica Acta* **70**, A356-A356.

Lindstrom, M. M. and Lindstrom, D. J. (1986). Lunar granulites and their precursor anorthositic norites of the early lunar crust. Proc. Lun. Planet. Sci. Conf. 16. *J. Geophys. Res.* **91**, D263-D276.

Liu, C.-Z., Snow, J. E., Brügmann, G., Hellebrand, E., and Hofmann, A. W. (2009). Non-chondritic HSE budget in Earth's upper mantle evidenced by abyssal peridotites from Gakkel ridge (Arctic Ocean). *Earth and Planetary Science Letters* **283**, 122-132.

Lodders, K. (2003). Solar system abundances and condensation temperatures of the elements. *The Astrophysical Journal* **591**, 1220-1247.

Lodders, K., Palme, H., and Gail, H. P. (2009). Abundances of the elements in the solar system. In: Trümper, J. E. (Ed.), *Landolt-Börnstein, New Series, Vol VI/4B*. Springer, Berlin, Heidelberg, New York.

Lorand, J. P. (1990). Are spinel Iherzolite xenoliths representative of the abundance of sulfur in the upper mantle? *Geochimica et Cosmochimica Acta* **54**, 1487-1492.

Lorand, J. P., Alard, O., and Godard, M. (2009). Platinum-group element signature of the primitive mantle rejuvenated by melt-rock reactions: evidence from Sumail peridotites (Oman Ophiolite). *Terra Nova* **21**, 35-40.

Lorand, J. P., Bodinier, J. L., Dupuy, C., and Dostal, J. (1989). Abundance and distribution of gold in the orogenic-type spinel peridotites from Ariège (Northeastern Pyrenees, France). *Geochimica et Cosmochimica Acta* **53**, 3085-3090.

Lorand, J. P., Keays, R. R., and Bodinier, J. L. (1993). Copper and Noble Metal Enrichments Across the Lithosphere--Asthenosphere Boundary of Mantle Diapirs: Evidence from the Lanzo Lherzolite Massif. *J. Petrology* **34**, 1111-1140.

Lorand, J.-P. and Alard, O. (2001). Platinum-group element abundances in the upper mantle: new constraints from in situ and whole-rock analyses of Massif Central xenoliths (France). *Geochimica et Cosmochimica Acta* **65**, 2789-2806.

Lorand, J.-P., Alard, O., and Luguet, A. (2010). Platinum-group element micronuggets and refertilization process in Lherz orogenic peridotite (northeastern Pyrenees, France). *Earth and Planetary Science Letters* **289**, 298-310.

Lorand, J.-P., Luguet, A., Alard, O., Bezos, A., and Meisel, T. (2008). Abundance and distribution of platinum-group elements in orogenic lherzolites; a case study in a Fontete Rouge lherzolite (French Pyrénées). *Chemical Geology* **248**, 174-194.

Lorand, J.-P., Pattou, L., and Gros, M. (1999). Fractionation of platinum-group elements and gold in the upper mantle: a detailed study in Pyrenean orogenic lherzolites. *Journal of Petrology* **40**, 957-981.

Lorand, J.-P., Reisberg, L., and Bedini, R. M. (2003). Platinum-group elements and melt percolation processes in Sidamo spinel peridotite xenoliths, Ethiopia, East African Rift. *Chemical Geology* **196**, 57-75.

Lorand, J.-P., Schmidt, G., Palme, H., and Kratz, K.-L. (2000). Highly siderophile element geochemistry of the Earth's mantle: new data for the Lanzo (Italy) and Ronda (Spain) orogenic peridotite bodies. *Lithos* **53**, 149-164.

LSPET (1971). Preliminary examination of lunar samples from Apollo 14. *Science* **173**, 681-693.

Luck, J.-M. and Allègre, C. J. (1984). ^{187}Re-^{187}Os investigation in sulfide from Cape Smith komatiite. *Earth and Planetary Science Letters* **68**, 205-208.

Ludwig, K. R. (2003). ISOPLOT 3.00. A geochronological toolkit for Mikrosoft Excel. *Berkeley Geochronological Center Spec. Publ. No.* **4**, 70 pp.

Luguet, A., Alard, O., Lorand, J. P., Pearson, N. J., Ryan, C., and O'Reilly, S. Y. (2001). Laser-ablation microprobe (LAM)-ICPMS unravels the highly siderophile element geochemistry of the oceanic mantle. *Earth and Planetary Science Letters* **189**, 285-294.

Luguet, A., Lorand, J.-P., Alard, O., and Cottin, J.-Y. (2004). A multi-technique study of platinum group element systematic in some Ligurian ophiolitic peridotites, Italy. *Chemical Geology* **208**, 175-194.

Luguet, A., Lorand, J.-P., and Seyler, M. (2003). Sulfide petrology and highly siderophile element geochemistry of abyssal peridotites: a coupled study of samples from the Kane Fracture Zone (45°W 23°20N, MARK area, Atlantic Ocean). *Geochimica et Cosmochimica Acta* **67**, 1553-1570.

Luguet, A., Pearson, D. G., Nowell, G. N., Dreher, S. T., Coggon, J. A., Spetsius, Z. V., and Parman, S. W. (2008). Enriched Pt-Re-Os isotope systematics in plume lavas explained by metasomatic sulfides. *Science* **319**, 453-456.

Luguet, A., Shirey, S. B., Lorand, J.-P., Horan, M. F., and Carlson, R. W. (2007). Residual platinum-group minerals from highly depleted harzburgites of the Lherz massif (France) and their role in HSE fractionation of the mantle. *Geochimica et Cosmochimica Acta* **71**, 3082-3097.

Maier, W. D., Barnes, S. J., Campbell, I. H., Fiorentini, M. L., Peltonen, P., Barnes, S.-J., and Smithies, R. H. (2009). Progressive mixing of meteoritic veneer into the early Earth/'s deep mantle. *Nature* **460**, 620-623.

Mallmann, G. and O'Neill, H. S. C. (2007). The effect of oxygen fugacity on the partitioning of Re between crystals and silicate melt during mantle melting. *Geochimica et Cosmochimica Acta* **71**, 2837-2857.

Mann, U., Frost, D. J., Becker, H., Rubie, D. C., Shearer, C. K., and Agee, C. B. (2007). Effect of pressure on the partitioning of highly siderophile elements between liquid Fe-alloy and peridotitic liquid. *Lunar Planet. Sci. Conf.* **XXXVIII**, 1544.

Mason, B. and Taylor, S. R. (1982). Inclusions in the Allende meteorite. *Smithson. Contrib. Earth Sci.* **25**, 1-30.

Maurer, P., Eberhardt, P., Geiss, J., Grögler, N., Stettler, A., Brown, G. M., Peckett, A., and Krähenbühl, U. (1978). Pre-Imbrian craters and basins: ages, compositions and excavation depths of Apollo 16 breccias. *Geochimica et Cosmochimica Acta* **42**, 1687-1720.

Mavrogenes, J. A. and O'Neill, H. S. C. (1999). The relative effects of pressure, temperature and oxygen fugacity on the solubility of sulfide in mafic magmas. *Geochim. Cosmochim. Acta* **63**, 1173-1180.

McDonald, I., Andreoli, M. A. G., Hart, R. J., and Tredoux, M. (2001). Platinum-group elements in the Morokweng impact structure, South Africa: Evidence for the impact of a large ordinary chondrite projectile at the Jurassic-Cretaceous boundary. *Geochimica et Cosmochimica Acta* **65**, 299-309.

McDonald, I. and Russell, S. S. (2001). Platinum-group elements in enstatite chondrites and enstatite achondrites. *Meteorit. Planet. Sci.* **36**, A128-A129.

McDonough, W. F. and Sun, S. s. (1995). The composition of the Earth. *Chemical Geology* **120**, 223-253.

McGee, J. J., Bence, A. E., Eichhorn, G., and Schaeffer, O. A. (1978). Feldspathic granulite 79215: Limitations on T-fO2 conditions and time of metamorphism. *Proc. Lunar Planet. Sci. Conf.* **9**, 743-772.

McKinley, J. P., Taylor, G. J., Keil, K., Ma, M.-S., and Schmitt, R. A. (1984). Apollo 16: impact melt sheets, contrasting nature of the Cayley plains and Descartes mountains, and geologic history. *J. Geophys. Res.* **89**, B513-B524.

Meisel, T., Fellner, N., and Moser, J. (2003a). A simple procedure for the determination of platinum group elements and rhenium (Ru, Rh, Pd, Re, Os, Ir, and Pt) using ID-ICP-MS with an inexpensive on-line matrix separation in geological and environmental materials. *J. Anal. Atomic Spectr.* **18**, 720-726.

Meisel, T. and Moser, J. (2004). Reference materials for geochemical PGE analysis: new analytical data for Ru, Rh, Pd, Os, Ir, Pt and Re by isotope dilution ICP-MS in 11 geological reference materials. *Chemical Geology* **208**, 319-338.

Meisel, T., Reisberg, L., Moser, J., Carignan, J., Melcher, F., and Brügmann, G. (2003b). Re-Os systematics of UB-N, a serpentinized peridotite reference material. *Chemical Geology* **201**, 161-179.

Meisel, T., Walker, R. J., Irving, A. J., and Lorand, J.-P. (2001). Osmium isotopic compositions of mantle xenoliths: a global perspective. *Geochimica et Cosmochimica Acta* **65**, 1311-1323.

Meisel, T., Walker, R. J., and Morgan, J. W. (1996). The osmium isotopic composition of the Earth's primitive upper mantle. *Nature* **383**, 517-520.

Mitchell, R. H. and Keays, R. R. (1981). Abundance and distribution of gold, palladium and iridium in some spinel and garnet lherzolites: implications for the nature and origin of precious metal-rich intergranular components in the upper mantle. *Geochimica et Cosmochimica Acta* **45**, 2425-2433, 2435-2442.

Morbidelli, A., Petit, J.-M., Gladman, B., and Chambers, J. E. (2001). A plausible cause of the late heavy bombardment. *Meteorit. Planet. Sci.* **36**, 371-380.

Morgan, J. W. (1986). Ultramafic xenoliths: Clues to Earth's late accretionary history. *Journal of Geophysical Research* **91**, 12,375-12,387.

Morgan, J. W., Ganapath.R, Higuchi, H., and Anders, E. (1974). Lunar, terrestrial, and meteoritic anorthosites - Abundances of volatile and siderophile elements. *Transactions-American Geophysical Union* **55**, 325-326.

Morgan, J. W., Ganapathy, R., Higuchi, H., and Anders, E. (1977). Meteoritic material on the Moon. In: Pomeroy, J. H. and Hubbard, N. J. Eds.)*The Soviet-American Conference on Cosmochemistry of the Moon and Planets*. U.S. Govt. Priniting Office, Washington, D.C.

Morgan, J. W., Ganapathy, R., Higuchi, H., Krähenbühl, U., and Anders, E. (1974). Lunar basins: tentative characterization of projectiles, from meteoritic elements in Apollo 17 boulders. *Proc. Lunar Sci. Conf.* **5**, 1703-1736.

Morgan, J. W., Ganapathy, R., and Krähenbühl, U. (1975). Meteoritic trace elements in lunar rock 14321, 184. *Geochimica et Cosmochimica Acta* **39**, 261-264.

Morgan, J. W., Gros, M., Takahashi, H., and Hertogen, J. (1976). Lunar breccia 73215: siderophile and volatile trace elements. *Proc. Lunar Sci. Conf.* **7**, 2189-2199.

Morgan, J. W., Higuchi, H., and Anders, E. (1975). Meteoritic materials in a boulder from the Apollo 17 site: implications for its origin. *The Moon* **14**, 373-383.

Morgan, J. W., Janssens, M.-J., Takahashi, H., Hertogen, J., and Anders, E. (1985). H-chondrites: Trace element clues to their origin. *Geochimica et Cosmochimica Acta* **49**, 247-259.

Morgan, J. W., Krähenbühl, U., Ganapathy, R., Anders, E., and Marvin, U. B. (1973). Trace elements in separates from Apollo 15 soils. *Proc. Lunar Sci. Conf.* **4**, 1379-1398.

Morgan, J. W., Laul, J. C., Krähenbühl, U., Ganapathy, R., and Anders, E. (1972). Major impacts on the Moon: characterization from trace elements in Apollo 12 and 14 samples. *Proc. Lunar Sci. Conf.* **3**, 1377-1395.

Morgan, J. W. and Lovering, J. F. (1967). Rhenium and osmium abundances in some igneous and metamorphic rocks. *Earth and Planetary Science Letters* **3**, 219-224.

Morgan, J. W. and Petrie, R. K. (1979). Breccias 73215 and 73255: siderophile and volatile trace elements. *Proc. Lunar Planet. Sci. Conf.* **10**, 789-801.

Morgan, J. W., Walker, R. J., Brandon, A. D., and Horan, M. F. (2001). Siderophile elements in the Earth's upper mantle and lunar breccias: data synthesis suggests manifestations of the same late influx. *Meteorit. Planet. Sci.* **36**, 1257-1275.

Morgan, J. W., Wandless, G. A., Petrie, R. K., and Irving, A. J. (1981). Composition of the Earth's upper mantle-I. Siderophile trace elements in ultramafic nodules. *Tectonophysics* **75**, 47-67.

Muehlberger, W. R., Hörz, F., Sevier, J. R., and Ulrich, G. E. (1980). Mission objectives for geological exploration of the Apollo 16 landing site. In: Papike, J. J. and Merrill, R. B. (Eds.), *Proc. Lunar Highlands Crust*. Pergamon Press.

Mungall, J. E., Andrews, D. R. A., Cabri, L. J., Sylvester, P. J., and Tubrett, M. (2005). Partitioning of Cu, Ni, Au, and platinum-group elements between monosulfide solid solution and sulfide melt under controlled oxygen and sulfur fugacities. *Geochimica et Cosmochimica Acta* **69**, 4349-4360.

Murthy, V. R. (1991). Early Differentiation of the Earth and the problem of mantle siderophile elements: a new approach. *Science* **253**, 303-306.

Neal, C. and Taylor, L. A. (1993). Catalog of Apollo 17 rocks. Vol 3 - Central Valley, Part 2. *JSC 26088*.

Niu, Y. (1997). Mantle melting and melt extraction processes beneath ocean ridges: Evidence from abyssal peridotites. *Journal of Petrology* **38**, 1047-1074.

Norman, M. D. (2009). The lunar cataclysm: Reality or "mythconception". *Elements* **5**, 23-28.

Norman, M. D., Bennett, V. C., and Ryder, G. (2002). Targeting the impactors: siderophile element signatures of lunar impact melts from Serenitatis. *Earth and Planetary Science Letters* **202**, 217-228.

Norman, M. D., Duncan, R. A., and Huard, J. J. (2006). Identifying impact events within the lunar cataclysm from 40Ar-39Ar ages and compositions of Apollo 16 impact melt rocks. *Geochimica et Cosmochimica Acta* **70**, 6032-6049.

Norman, M. D., Duncan, R. A., and Huard, J. J. (2010). Imbrium provenance for the Apollo 16 Descartes terrain: Argon ages and geochemistry of lunar breccias 67016 and 67455. *Geochimica et Cosmochimica Acta* **74**, 763-783.

Norman, M. D., Shih, C.-Y., Nyquist, L. E., Bogard, D. D., and Taylor, L. A. (2007). Early impacts on the Moon: Crystallization ages of Apollo 16 melt breccias. *Lunar Planet. Sci. Conf.* **XXXVIII**, 1991.

Oberbeck, V. R. (1975). The role of ballistic erosion and sedimentation in lunar stratigraphy. *Rev. Geophys. Space Phys.* **13**, 337-362.

Oberli, F., Huneke, J. C., and Wasserburg, G. J. (1979). U-Pb and K-Ar systematics of cataclysm and precataclysm lunar impactites. *Lunar Planet. Sci. Conf.* **X**, 940-942.

Ohtani, E. and Yurimoto, H. (1996). Element partitioning between metallic liquid , magnesiowustite and silicate liquid at 20 GPa and 2500°C: A secondary ion mass spectrometric study. *Geophys. Res. Lett.* **23**, 1993-1996.

O'Neill, H. S. C. (1991). The origin of the moon and the early history of the earth--A chemical model. Part 2: The earth. *Geochimica et Cosmochimica Acta* **55**, 1159-1172.

O'Neill, H. S. C., Dingwell, D. B., Borisov, A., Spettel, B., and Palme, H. (1995). Experimental petrochemistry of some highly siderophile elements at high temperatures, and some implications for core formation and the mantle's early history. *Chemical Geology* **120**, 255-273.

Ostertag, R., Palme, H., Borchardt, R., and Stöffler, D. (1984). Modal, textural, and chemical characteristics of Apollo 16, Station 11 granulites. *Lunar Planet. Sci. Conf.* **XV**, 621-622.

Pack, A., Russell, S. S., Shelley, J. M. G., and van Zuilen, M. (2007). Geo- and cosmochemistry of the twin elements yttrium and holmium. *Geochimica et Cosmochimica Acta* **71**, 4592-4608.

Palme, H. (2000). Are there chemical gradients in the inner solar system? *Space Science Reviews* **192**, 237-262.

Palme, H. (2008). Platinum-group elements in cosmochemistry. *Elements* **4**, 233-238.

Palme, H., Baddenhausen, H., Blum, K., Cendales, M., Dreibus, G., Hofmeister, H., Kruse, H., Palme, C., Spettel, B., Vilcsek, E., Wänke, H., and Kurat, G. (1978). New data on lunar samples and achondrites and a comparison of the least fractionated samples from the earth, the moon, and the eucrite parent body. *Proc. Lunar Planet. Sci. Conf.* **9**, 25-57.

Palme, H., Borisov, A., and Wulf, A. V. (1998). Experimental determination of the oxidation sequence of refractory metals. *Lunar Planet. Sci. Conf.* **XXIX**, 1611.

Palme, H., Hutcheon, I. D., and Spettel, B. (1994). Composition and origin of refractory-metal-rich assemblages in a Ca,Al-rich Allende inclusion. *Geochimica et Cosmochimica Acta* **58**, 495-513.

Palme, H., Larimer, J. W., and Lipschutz, M. E. (1988). Moderately volatile elements. In: Kerridge, J. F. and Matthews, M. S. (Eds.), *Meteorites and the Early Solar System*. Univ. of Arizona, Tucson, Tucson.

Palme, H. and O'Neill, H. S. C. (2003). Cosmochemical estimates of mantle composition. In: Carlson, R. W. (Ed.), *Treatise of geochemistry*. Elsevier, Amsterdam.

Palme, H. and Wlotzka, F. (1976). A metal particle from a Ca,Al-rich inclusion from the meteorite Allende, and the condensation of refractory siderophile elements. *Earth and Planetary Science Letters* **33**, 45-60.

Papanastassiou, D. A. and Wasserburg, G. J. (1971). RbSr ages of igneous rocks from the Apollo 14 mission and the age of the Fra Mauro formation. *Earth and Planetary Science Letters* **12**, 36-48.

Pattou, L., Lorand, J.-P., and Gros, M. (1996). Non-chondritic platinum-group element ratios in the Earth's mantle. *Nature* **379**, 712-715.

Peach, C. L., Mathez, E. A., and Keays, R. R. (1990). Sulfide melt-silicate melt distribution coefficients for noble metals and other chalcophile elements as deduced from MORB: Implications for partial melting. *Geochimica et Cosmochimica Acta* **54**, 3379-3389.

Peach, C. L., Mathez, E. A., Keays, R. R., and Reeves, S. J. (1994). Experimentally determined sulfide melt-silicate melt partition coefficients for iridium and palladium. *Chemical Geology* **117**, 361-377.

Pearson, D. G., Irvine, G. J., Ionov, D. A., Boyd, F. R., and Dreibus, G. E. (2004). Re-Os isotope systematics and platinum group element fractionation during mantle melt extraction: a study of massif and xenolith peridotite suites. *Chemical Geology* **208**, 29-59.

Pernicka, E. and Wasson, J. T. (1987). Ru, Re, Os, Pt and Au in iron meteorites. *Geochimica et Cosmochimica Acta* **51**, 1717-1726.

Puchtel, I. and Humayun, M. (2000). Platinum group elements in Kostomuksha komatiites and basalts: implications for oceanic crust recycling and core-mantle interaction. *Geochimica et Cosmochimica Acta* **64**, 4227-4242.

Puchtel, I. S., Brandon, A. D., and Humayun, M. (2004a). Precise Pt-Re-Os isotope systematics of the mantle from 2.7-Ga komatiites. *Earth Planet. Sci. Lett.* **224**, 157-174.

Puchtel, I. S. and Humayun, M. (2005). Highly siderophile element geochemistry of 187Os-enriched 2.8 Ga Kostomuksha komatiites, Baltic Shield. *Geochimica et Cosmochimica Acta* **69**, 1607-1618.

Puchtel, I. S., Humayun, M., Campbell, A. J., Sproule, R. A., and Lesher, C. M. (2004b). Platinum group element geochemistry of komatiites from the Alexo and Pyke Hill areas, Ontario, Canada. *Geochimica et Cosmochimica Acta* **68**, 1361-1383.

Puchtel, I. S., Humayun, M., and Walker, R. J. (2007). Os-Pb-Nd isotope and highly siderophile and lithophile trace element systematics of komatiitic rocks from the Volotsk suite, SE Baltic Shield. *Precambrian Research* **158**, 119-137.

Puchtel, I. S., Walker, R. J., Brandon, A. D., and Nisbet, E. G. (2009). Pt-Re-Os and Sm-Nd isotope and HSE and REE systematics of the 2.7 Ga Belingwe and Abitibi komatiites. *Geochimica et Cosmochimica Acta* **73**, 6367-6389.

Puchtel, I. S., Walker, R. J., James, O. B., and Kring, D. A. (2008). Osmium isotope and highly siderophile element systematics of lunar impact melt breccias: Implications for the late accretion history of the Moon and Earth. *Geochimica et Cosmochimica Acta* **72**, 3022-3042.

Rambaldi, E. R. (1977). The content of Sb, Ge and refractory siderophile elements in metals of L-group chondrites. *Earth and Planetary Science Letters* **33**, 407-419.

Rambaldi, E. R. (1977). Trace element content of metals from H- and LL-group chondrites. *Earth and Planetary Science Letters* **36**, 347-358.

Rambaldi, E. R., Cendales, M., and Thacker, R. (1978). Trace element distribution between magnetic and non-magnetic portions of ordinary chondrites. *Earth and Planetary Science Letters* **40**, 175-186.

Rampone, E., Hofmann, A., Piccardo, G. B., Vannucci, R., Botazzi, P., and Ottolini, L. (1995). Petrology, mineral and isotope geochemistry of the external liguride peridotites (Northern Apennines, Italy). *Journal of Petrology* **36**, 81-105.

Rampone, E., Hofmann, A., Piccardo, G. B., Vannucci, R., Botazzi, P., and Ottolini, L. (1996). Trace element and isotope geochemistry of depleted peridotites from an N-Morb type ophiolite (Internal Liguride, N. Italy). *Contrib. Mineral. Petrol.* **123**, 61-76.

Rampone, E. and Piccardo, G. B. (2000). The ophiolite-oceanic lithosphere analogue: new insights from the Nothern Apennines (Italy). In: Dilek, Y., Moores, E. M., Elthon, D., and Nicolas, A. Eds.), *Ophiolites and oceanic crust: new insights from field studies and the Ocean Drilling Program*. Colorado Spec. Paper - Geol. Soc. Am., Boulder.

Rankenburg, K., Brandon, A. D., and Humayun, M. (2007). Osmium isotope systematics of ureilites. *Geochimica et Cosmochimica Acta* **71**, 2402-2413.

Rehkämper, M., Halliday, A. N., Alt, J., Fitton, J. G., Zipfel, J., and Takazawa, E. (1999a). Non-chondritic platinum-group element ratios in oceanic mantle lithosphere: petrogenetic signature of melt percolation? *Earth and Planetary Science Letters* **172**, 65-81.

Rehkämper, M., Halliday, A. N., Barfod, D., Fitton, J. G., and Dawson, J. B. (1997). Platinum-group element abundance patterns in different mantle environments. *Science* **278**, 1595-1598.

Rehkämper, M., Halliday, A. N., Fitton, J. G., Lee, D. C., Wieneke, M., and Arndt, N. T. (1999b). Ir, Ru, Pt, and Pd in basalts and komatiites: new constraints for the geochemical behaviour of the platinum-group elements in the mantle. *Geochimica et Cosmochimica Acta* **63**, 3915-3934.

Reisberg, L., Dauphas, N., Luguet, A., Pearson, D. G., Gallino, R., and Zimmermann, C. (2009). Nucleosynthetic osmium isotope anomalies in acid leachates of the Murchison meteorite. *Earth and Planetary Science Letters* **277**, 334-344.

Reisberg, L. and Lorand, J. P. (1995). Longevity of sub-continental mantle lithosphere from osmium isotope systematics in orogenic peridotite massifs. *Nature* **376**, 159-162.

Reisberg, L., Zhi, X., Lorand, J.-P., Wagner, C., Peng, Z., and Zimmermann, C. (2005). Re-Os and S systematics of spinel peridotite xenoliths from east central China: Evidence for contrasting effects of melt percolation. *Earth and Planetary Science Letters* **239**, 286-308.

Reisberg, L. C., Allègre, C. J., and Luck, J.-M. (1991). The ReOs systematics of the Ronda Ultramafic Complex of southern Spain. *Earth and Planetary Science Letters* **105**, 196-213.

Righter, K., Campbell, A. J., Humayun, M., and Hervig, R. L. (2004). Partitioning of Ru, Rh, Pd, Re, Ir, and Au between Cr-bearing spinel, olivine, pyroxene and silicate melts. *Geochimica et Cosmochimica Acta* **68**, 867-880.

Righter, K., Chesley, J. T., Geist, D., and Ruiz, J. (1998). Behaviour of Re during Magma Fractionation: an Example from Volcan Alcedo, Galapagos. *J. Petrology* **39**, 785-795.

Righter, K. and Downs, R. T. (2001). The Crystal Structures of Synthetic Re- and PGE-Bearing Magnesioferrite Spinels: Implications for Impacts, Accretion and the Mantle. *Geophys. Res. Lett.* **28**, 619-622.

Righter, K., Drake, M., and Yaxley, G. (1997). Prediction of siderophile element metal/silicate partition coefficients to 20 GPa and 2800°C: The effects of pressure, temperature, oxygen fugacity, and silicate and metallic melt compositions. *Physics of the Earth and Planetary Interiors* **100**, 115-134.

Righter, K. and Drake, M. J. (1997). Metal-silicate equilibrium in a homogeneously accreting earth: new results for Re. *Earth and Planetary Science Letters* **146**, 541-553.

Righter, K. and Hauri, E. H. (1998). Compatibility of Rhenium in Garnet During Mantle Melting and Magma Genesis. *Science* **280**, 1737-1741.

Righter, K., Humayun, M., and Danielson, L. (2008). Partitioning of palladium at high pressures and temperatures during core formation. *Nature Geoscience* **1**, 321-323.

Roy-Barman, M. (1993). Mesure du rapport $^{187}Os/^{186}Os$ dans les basalts et les péridotites: Contribution à la systématique ^{187}Re-^{187}Os dans le manteau. Ph.D., University of Paris.

Roy-Barman, M., Wasserburg, G. J., Papanastassiou, D. A., and Chaussidon, M. (1998). Osmium isotopic compositions and Re-Os concentrations in sulfide globules from basaltic glasses. *Earth and Planetary Science Letters* **154**, 331-347.

Rubin, A. E. (1993). Magnetite-sulfide chondrules and nodules in CK carbonaceous chondrites: implications for the timing of CK oxidation. *Meteoritics* **28**, 130-135.

Rubin, A. E., Huber, H., and Wasson, J. T. (2009). Possible impact-induced refractory-lithophile fractionations in EL chondrites. *Geochimica et Cosmochimica Acta* **73**, 1523-1537.

Rubin, A. E. and Kallemeyn, G. W. (1994). Pecora Escarpment 91002: A member of the new Rumuruti (R) chondrite group. *Meteoritics* **29**, 255-264.

Rudnick, R. L., Gao, S., Ling, W.-l., Liu, Y.-s., and McDonough, W. F. (2004). Petrology and geochemistry of spinel peridotite xenoliths from Hannuoba and Qixia, North China craton. *Lithos* **77**, 609-637.

Rudnick, R. L. and Walker, R. J. (2009). Interpreting ages from Re-Os isotopes in peridotites. *Lithos* **112**, 1083-1095.

Ryder, G. (2002). Mass flux in the ancient Earth-Moon system and benign implications for the origin of life on Earth. *J. Geophys. Res.* **107**, 6-1 - 6-13.

Saal, A. E., Takazawa, E., Frey, F. A., Shimizu, N., and Hart, S. R. (2001). Re-Os Isotopes in the Horoman Peridotite: Evidence for Refertilization? *J. Petrology* **42**, 25-37.

Sattari, P., Brenan, J. M., Horn, I., and McDonough, W. F. (2002). Experimental Constraints on the sulfide- and chromite-silicate melt partitioning behaviour of rhenium and platinum-group-elements. *Economic Geology* **97**, 385-398.

Schaeffer, O. A., Husain, L., and Schaeffer, G. A. (1976). Ages of highland rocks: The chronology of lunar basin formation revisited. *Proc. Lunar Sci. Conf.* **7**, 2067-2092.

Schmidt, G. (2004). Are high-temperature fractionations in the solar nebular preserved in highly siderophile element systematics of the Earth's mantle? *Meteorit. Planet. Sci.* **39**, 1995-2007.

Schmidt, G., Palme, H., Kratz, K.-L., and Kurat, G. (2000). Are highly siderophile elements (PGE, Re and Au) fractionated in the upper mantle of the earth? New results on peridotites from Zabargad. *Chemical Geology* **163**, 167-188.

Schmidt, G. and Snow, J. E. (2002). Os isotopes in mantle xenoliths from the Eifel volcanic field and the Vogelsberg (Germany): age constraints on the lithospheric mantle. *Contrib. Mineral. Petrol.* **143**, 694-705.

Schmidt, G., Witt-Eickschen, G., Palme, H., Seck, H., Spettel, B., and Kratz, K.-L. (2003). Highly siderophile elements (PGE, Re and Au) in mantle xenoliths from the West Eifel volcanic field (Germany). *Chemical Geology* **196**, 77-105.

Schönbächler, M., Carlson, R. W., Horan, M. F., Mock, T. D., and Hauri, E. H. (2008). Silver isotope variations in chondrites: Volatile depletion and the initial 107Pd abundance of the solar system. *Geochimica et Cosmochimica Acta* **72**, 5330-5341.

Schulze, H., Bischoff, A., Palme, H., Spettel, B., Dreibus, G., and Otto, J. (1994). Mineralogy and chemistry of Rumuruti: The first meteorite fall of the new R chondrite group. *Meteoritics* **29**, 275-286.

Scott, E. R. D. (1972). Chemical fractionation in iron meteorites and its interpretation. *Geochimica et Cosmochimica Acta* **36**, 1205-1236.

Scott, E. R. D. and Wasson, J. T. (1975). Classification and properties of iron meteorites. *Rev. Geophys. Space Phys.* **13**, 527-546.

Sears, D. W., Kallemeyn, G. W., and Wasson, J. T. (1983). Composition and origin of clasts and inclusions in the Abee enstatite chondrite breccia. *Earth and Planetary Science Letters* **62**, 180-192.

Seward, T. M. (1973). Thio complexes of gold and the transport of gold in hydrothermal ore solutions. *Geochimica et Cosmochimica Acta* **37**, 379-399.

Shirey, S. B. and Walker, R. J. (1998). The Re-Os isotope system in cosmochemistry and high-temperature geochemistry. *Annu. Rev. Earth Planet. Sci.* **26**, 423-500.

Simonds, C. H., Phinney, W. C., Warner, J. L., McGee, P. E., Geeslin, J., Brown, R. W., and Rhodes, J. M. (1977). Apollo 14 revisited, or breccias aren't so bad after all. *Proc. Lunar Sci. Conf.* **8**, 1869-1893.

Simonds, C. H., Warner, J. L., and Phinney, W. C. (1973). Petrology of Apollo 16 poikilitic rocks. Proc. Lunar Sci. Conf. 4. *Proc. Lunar Sci. Conf.* **4**, 613-632.

Smoliar, M. I., Walker, R. J., and Morgan, J. W. (1996). Re-Os ages of group IIA, IIIA, IVA, and IVB iron meteorites. *Science* **271**, 1099-1102.

Snow, J. E. and Schmidt, G. (1998). Constraints on Earth accretion deduced from noble metals in the oceanic mantle. *Nature* **391**, 166-169.

Snow, J. E., Schmidt, G., and Rampone, E. (2000). Os isotopes and highly siderophile elements (HSE) in the Ligurian ophiolites, Italy. *Earth and Planetary Science Letters* **175**, 119-132.

Stefánsson, A. and Seward, T. M. (2003). Stability of chloridogold(I) complexes in aqueous solutions from 300 to 600°C and from 500 to 1800 bar. *Geochimica et Cosmochimica Acta* **67**, 4559-4576.

Stöffler, D., Bischoff, A., Borchardt, R., Burghele, A., Deutsch, A., Jessberger, E. K., Ostertag, R., Palme, H., Spettel, B., Reimold, W. U., Wacker, K., and Wänke, H. (1985). Composition and evolution of the lunar crust in the Descartes highlands. Proc. 15th Lunar Planet. Sci. Conf. *J. Geophys. Res.* **90**, C449-C506.

Stöffler, D., Keil, K., and Edward R.D, S. (1991). Shock metamorphism of ordinary chondrites. *Geochimica et Cosmochimica Acta* **55**, 3845-3867.

Stöffler, D., Ostertag, R., Reimold, W. U., Borchardt, R., Malley, J., and Rehfeldt, A. (1981). Distribution and provenance of lunar highland rock types at North Ray Crater, Apollo 16. *Proc. Lunar Planet. Sci. Conf.* **12**, 185-207.

Stöffler, D. and Ryder, G. (2001). Stratigraphy and isotope ages of lunar geologic units: chronological standard for the inner solar system. *Space Science Reviews* **96**, 9-54.

Stöffler, D., Ryder, G., Ivanov, B. A., Artemieva, N. A., Cintala, M. J., and Grieve, R. A. F. (2006). Cratering history and lunar chronology. In: Jolliff, L. J., Wieczorek, M. A., Shearer, C. K., and Neal, C. R. Eds.), *New views of the Moon*. Mineralogical Society of America, Geochemical Society, Chantilly.

Strelow, F. W. E., Victor, A. H., van Zyl, C. R., and Eloff, C. (1971). Distribution coefficients and cation exchange behaviour of elements in hydrochloric acid-acetone. *Analytical Chemistry* **43**, 870-876.

Sylvester, P. J., Simon, S. B., and Grossman, L. (1993). Refractory inclusions from the Leoville, Efremovka, and Vigarano C3V chondrites: Major element differences between types A and B, and extraordinary refractory siderophile element compositions. *Geochimica et Cosmochimica Acta* **57**, 3763-3784.

Sylvester, P. J., Ward, B. J., Grossman, L., and Hutcheon, I. D. (1990). Chemical compositions of siderophile element-rich opaque assemblages in an Allende inclusion. *Geochimica et Cosmochimica Acta* **54**, 3491-3508.

Tagle, R. and Berlin, J. (2008). A database of chondrite analysis including platinum group elements, Ni, Co, Au, and Cr: Implications for the identification of chondritic projectiles. *Meteoritics & Planetary Science* **43**, 1-19.

Tagle, R. and Claeys, P. (2005). An ordinary chondrite impactor for the Popigai crater, Siberia. *Geochim. Cosmochim. Acta* **69**, 2877-2889.

Takahashi, H., Janssens, M.-J., Morgan, J. W., and Anders, E. (1978). Further studies of trace elements in C3 chondrites. *Geochimica et Cosmochimica Acta* **42**, 97-106.

Terashima, S. (1988). Determination of Gold in Sixty Geochemical Reference Samples by Flameless Atomic Absorption Spectrometry. *Geostandards and Geoanalytical Research* **12**, 57-60.

Turner, G. and Cadogan, P. H. (1975). The history of lunar bombardment inferred from ^{40}Ar-^{39}Ar dating of highland rocks. *Proc. Lunar Sci. Conf.* **6**, 1509-1538.

Turner, G., Huneke, J. C., Podosek, F. A., and Wasserburg, G. J. (1972). Ar40-39 systematics in rocks and separated minerals from Apollo 14. *Proc. Lunar Sci. Conf.* **3**, 1589-1612.

van Acken, D., Becker, H., and Walker, R. J. (2008). Refertilization of Jurassic oceanic peridotites from the Tethys Ocean -- Implications for the Re-Os systematics of the upper mantle. *Earth and Planetary Science Letters* **268**, 171-181.

van Acken, D., Becker, H., Walker, R. J., McDonough, W. F., Wombacher, F., Ash, R. D., and Piccoli, P. M. (2010). Formation of pyroxenite layers in the Totalp ultramafic massif (Swiss Alps) - Insights from highly siderophile elements and Os isotopes. *Geochimica et Cosmochimica Acta* **74**, 661-683.

Van Niekerk, D., Humayun, M., and Keil, K. (2009). In situ determination of siderophile trace elements in EL3 meteorites. *Lunar Planet. Sci. Conf.* **XXXX**, 2049.

Van Orman, J. A., Keshav, S., and Fei, Y. (2008). High-pressure solid/liquid partitioning of Os, Re and Pt in the Fe-S system. *Earth and Planetary Science Letters* **274**, 250-257.

Walker, R. J. (2009). Highly siderophile elements in the Earth, Moon and Mars: Update and implications for planetary accretion and differentiation. *Chemie der Erde - Geochemistry* **69**, 101-125.

Walker, R. J., Brandon, A. D., Bird, J. M., Piccoli, P. M., McDonough, W. F., and Ash, R. D. (2005). ^{187}Os-^{186}Os systematics of Os-Ir-Ru alloy grains from southwestern Oregon. *Earth and Planetary Science Letters* **230**, 211-226.

Walker, R. J., Horan, M. F., Morgan, J. W., Becker, H., Grossman, J. N., and Rubin, A. E. (2002). Comparative ^{187}Re-^{187}Os systematics of chondrites: Implications regarding early solar system processes. *Geochimica et Cosmochimica Acta* **66**, 4187-4201.

Walker, R. J., McCoy, T. J., Schulte, R. F., McDonough, W. F., and Ash, R. D. (2005). ^{187}Re-^{188}Os, ^{190}Pt-^{186}Os isotopic and highly siderophile element systematics of group IVA irons. *Lunar Planet. Sci. Conf.* **XXXVI**, 1313.

Walker, R. J., Morgan, J. W., Beary, E. S., Smoliar, M. I., Czamanske, G. K., and Horan, M. F. (1997). Applications of the ^{190}Pt-^{186}Os isotope system to geochemistry and cosmochemistry. *Geochimica et Cosmochimica Acta* **61**, 4799-4807.

Walker, R. J., Carlson, R. W., Shirey, S. B., and F.R, B. (1989). Os, Sr, Nd, and Pb isotope systematics of southern African peridotite xenoliths: Implications for the chemical evolution of subcontinental mantle. *Geochimica et Cosmochimica Acta* **53**, 1583-1595.

Walter, M. J., Newsome, H. E., Ertel, W., and Holzheid, A. (2000). Siderophile elements in the Earth and Moon: metal/silicate partitioning and implications for core formation. In: Canup, R. and Righter, K. Eds.), *Origin of the Earth and Moon*. University of Arizona Press, Tucson.

Wänke, H., Palme, H., Kruse, H., Baddenhausen, H., Cendales, M., Dreibus, G., Hofmeister, H., Jagoutz, E., Palme, C., Spettel, B., and Thacker, R. (1976). Chemistry of lunar highland rocks: A refined evaluation of the composition of the primary matter. *Proc. Lunar Sci. Conf.* **7**, 3479-3499.

Warner, J. L., Phinney, W. C., Bickel, C. E., and Simonds, C. H. (1977). Feldspathic granulitic impactities and pre-final bombardment lunar evolution. *Proc. Lunar Sci. Conf.* **8**, 2051-2066.

Warren, P. H. (2003). The Moon. In: Davis, M. (Ed.), *Meteorites, comets, and planets*. Elsevier, Amsterdam.

Warren, P. H., Ulff-Moller, F., and Kallemeyn, G. W. (2005). "New" lunar meteorites: Impact melt and regolith breccias and large-scale heterogeneities of the upper lunar crust. *Meteorit. Planet. Sci.* **40**, 989-1014.

Warren, P. H. and Wasson, J. T. (1977). Pristine nonmare rocks and the nature of the lunar crust. *Proc. Lunar Sci. Conf.* **8**, 2215-2235.

Warren, P. H. and Wasson, J. T. (1978). Compositional-petrographic investigation of pristine nonmare rocks. *Proc. Lunar Planet. Sci. Conf.* **9**, 185-217.

Wasson, J. T. (1985). *Meteorites*. Springer, Berlin.

Wasson, J. T., Boynton, W. V., Chou, C. L., and Baedecker, P. A. (1975). Compositional evidence regarding the influx of interplanetary materials onto the lunar surface. *The Moon* **13**, 121-141.

Wasson, J. T. and Kallemeyn, G. W. (1988). Compositions of chondrites. *Phil. Trans. R. Soc. Lond.* **A 325**, 535-544.

Wasson, J. T. and Richardson, J. W. (2001). Fractionation trends among IVA iron meteorites: contrasts with IIIAB trends. *Geochimica et Cosmochimica Acta* **65**, 951-970.

Weisberg, M. K., Prinz, M., Kojima, H., Yanai, K., Clayton, R. N., and Mayeda, T. K. (1991). The Carlisle Lakes-type chondrites: A new grouplet with high Delta^{17}O and evidence for nebular oxidation. *Geochimica et Cosmochimica Acta* **55**, 2657-2669.

Widom, E., Rubin, A. E., and Wasson, J. T. (1986). Composition and formation of metal nodules and veins in ordinary chondrites. *Geochimica et Cosmochimica Acta* **50**, 1989-1995.

Wilhelms, D. E. (1987). The geologic history of the Moon. *U.S. Geol. Surv. Prof. Pap.* **1348**, pp. 302.

Williams-Jones, A. E., Bowell, R. J., and Artashes, A. M. (2009). Gold in Solution. *Elements* **5**, 281-287.

Wilshire, H. G. and Jackson, E. D. (1972). Petrology and stratigraphy of the Fra Mauro Formation at the Apollo 14 site. *U.S. Geol. Surv. Prof. Pap.* **785**.

Wolf, R., Richter, G. R., Woodrow, A. B., and Anders, E. (1980). Chemical fractionations in meteorites--XI. C2 chondrites. *Geochimica et Cosmochimica Acta* **44**, 711-717.

Yokoyama, T., Rai, V. K., Alexander, C. M. O., Lewis, R. S., Carlson, R. W., Shirey, S. B., Thiemens, M. H., and Walker, R. J. (2007). Osmium isotope evidence for uniform distribution of *s*- and *r*-process components in the early solar system. *Earth and Planetary Science Letters* **259**, 567-580.

York, D., Kenyon, W. J., and Doyle, R. J. (1972). ^{40}Ar-^{39}Ar ages of Apollo 14 and 15 samples. *Proc. Lunar Sci. Conf.* **3**, 1613-1622.

Zipfel, J., Spettel, B., Palme, H., Wolf, D., Franchi, I., Sexton, A. S., Pillinger, C. T., and Bischoff, A. (1998). Dar al Gani 400: Chemistry and petrology of the largest lunar meteorite. *Meteorit. Planet. Sci.* **33**, A171.

Curriculum Vitae

For reasons of data protection not available in online Version

Publications

Peer-review Publications

Fischer-Gödde, M., Becker, H. and Wombacher, F. (2010): Rhodium, gold and other highly siderophile element abundances in chondritic meteorites. *Geochimica et Cosmochimica Acta,* 74, 356-379.

Manuscripts in Review:

Fischer-Gödde, M., Becker, H. and Wombacher, F. (2010): Rhodium, gold and other highly siderophile elements in orogenic peridotites and peridotite xenoliths. *Chemical Geology,* in review.

Kleinhanns, I.C., Fischer-Gödde, M., Hansen, B.T. (2010): Sr-Nd isotope systematics and geochemical characterization of the metasiliciclastic units of the Västervik Formation (Baltic Shield, SE Sweden). *International Journal of Earth Sciences,* in review.

Manuscript in Preparation:

Fischer-Gödde, M., Becker, H., Wombacher, F. (2010): Highly siderophile element abundances and $^{187}Os/^{188}Os$ in ancient lunar impact melt rocks. *in prep.*

Abstracts

Fischer-Gödde, M., Becker, H. and Wombacher, F. (2010): Highly siderophile element abundances and $^{187}Os/^{188}Os$ in lunar impact melt rocks: Implications for late accretion processes in the Earth-Moon system. 41st Lunar and Planetary Science Conference, 2262. (poster)

Becker, H., van Acken, D. and Fischer-Gödde, M. (2009): Highly Siderophile Element Fractionation During Magma Transport in the Mantle. *Fall AGU*.

Fischer-Gödde, M., Becker, H. and Wombacher, F. (2009): Highly siderophile element abundances and $^{187}Os/^{188}Os$ in lunar impact melt rocks: Implications for late accretion processes in the Earth-Moon system. *"Earth Control on Planetary Life and Environment" 99th Annual Meeting of the Geologische Vereinigung e.V. (GV), Göttingen, Germany*. (oral)

Fischer-Gödde, M., Becker, H. and Wombacher, F. (2009): Highly siderophile element abundances and $^{187}Os/^{188}Os$ in lunar impact melt breccias. *Geochim. Cosmochim. Acta* 73, Supplement 1, A381. (oral)

Becker, H., van Acken, D., Fischer-Gödde, M. and Wombacher, F. (2009): Constraints from mantle pyroxenites on highly siderophile element fractionation during melt transport in the mantle. *Geochim. Cosmochim. Acta* 73, Supplement 1, A100.

Fischer-Gödde, M., Becker, H. and Wombacher, F. (2008): Fractionation of refractory highly siderophile elements in the early solar system. *Paneth Kolloquium, Nördlingen, Germany*. (oral)

Fischer-Gödde, M., Becker, H., Wombacher, F., Gao, S. and Lorand, J.P. (2008): Chondrites do not match the highly siderophile element composition of the Earth´s mantle – constraints from new Rh/Ir and Au/Ir data on peridotites. *Jahrestagung der Deutschen Mineralogischen Gesellschaft, Berlin, Germany*. (oral)

Fischer-Gödde, M., Becker, H., Wombacher, F. and Lorand, J. P. (2008): Rhodium, gold and other highly siderophile element abundances in terrestrial peridotites. *Geochim. Cosmochim. Acta* 72, Supplement 1, A273. (poster)

Fischer-Gödde, M., Becker, H. and Wombacher, F. (2008): Fingerprinting Late Accretion: Highly siderophile elements in chondrites and terrestrial peridotites. *DFG Priority Programme SPP 1115 "Mars and the terrestrial planets" 5th Colloquium, Münster, Germany*. (oral)

Meier, L.C., van Acken, D., Fischer-Gödde, M., Wombacher, F. and Becker, H. (2007): Determination of siderophile and chalcophile elements in peridotites by sector-field ICP-MS. *Geochim. Cosmochim. Acta* **71**, Supplement 1, A649.

Fischer-Gödde, M., Wombacher, F. and Becker, H. (2007): Rhodium, gold and other highly siderophile elements in chondrites. *Geochim. Cosmochim. Acta* **71**, Supplement 1, A282. (poster)

Fischer-Gödde, M., Wombacher, F. and Becker, H. (2007): Rhodium, gold and other highly siderophile elements in chondrites. *38th Lunar and Planetary Science Conference*, 1625. (poster)

Fischer-Gödde, M., Wombacher, F. and Becker, H. (2007): Rhodium, gold and other highly siderophile elements in chondrites. *DFG Priority Programme SPP 1115 "Mars and the terrestrial planets" Colloquium, Berlin, Germany*. (oral)

Fischer, M., Hansen, B.T., Kleinhanns, I.C. (2006): Geochemische Klassifikation und Sm-Nd Isotopensystematik proterozoischer Metasedimente des Baltischen Schildes (Västervik Region, SE Schweden). In: Phillipp, S.L., Leiss, B., Vollbrecht, A., Tanner, D. & Gudmundsson, A. (Hrsg.): *11. Symposium Tektonik, Struktur- und Kristallingeologie, Göttingen*, S. 56-58. (poster)

Theses (unpublished)

Fischer, M. (2005): Sm-Nd Systematik und geochemische Klassifikation der felsischen Einheiten der Västervik-Formation, SE-Schweden. *Diploma Thesis*

Fischer, M. (2005): Paläoproterozoische Metamorphite und Magmatite der Trans-skandinavischen Magmatischen Zone im Bereich der Schärenküste E`Blankaholm Västervik-Gebiet, SE-Schweden. *Diploma Mapping Thesis*

Fischer, M. (2003): Geochemische Untersuchungen an Seesedimenten des Süßen Sees bei Eisleben. *B.Sc. Thesis*

Co-supervised Student Theses

L.C. Meier (2007): Bestimmung von Gold-Konzentrationen in Peridotiten mit ICP-MS und Standardaddition. *B.Sc. Thesis*

C. Wutzke (2008): Gold-, Rhodium- und Gehalte anderer hochsiderophiler Elemente in Peridotiten. *B.Sc. Thesis*

Acknowledgements

First of all I would like to thank Prof. Dr. Harry Becker for offering me this PhD thesis and the great scientific supervision. His wide scientific background and strong analytical mind were impressive and inspiring to me.

I am very thankful to Prof. Dr. Gerhard Franz for being the second referee of the thesis.

Special thanks go to Dr. Frank Wombacher for his help and assistance concerning ICP-MS analysis, data handling, discussions and support provided throughout this work. Thanks for keeping the merits up during late shifts in the office.

Dr. Konrad Hammerschmidt is acknowledged for help and support in the TIMS laboratory, and for being a competent advisor for all kinds of questions related to mass spectrometry, analytical issues and data interpretation.

Ms. Monika Feth is thanked for invaluable support in all areas of laboratory operations and general organization.

I am very thankful to Dr. David van Acken for help and discussions related to highly siderophile element analysis, and for support in the TIMS lab.

Corinna Wutzke and Marc Weynell are acknowledged for assistance during sample preparation, digestion and chemical separation procedures.

Thanks go to Dr. Uwe Wiechert for discussions and helpful suggestions on analytical issues.

Dr. Kai Rankenburg is acknowledged for providing additional meteorite samples and for discussions on cosmochemical aspects of highly siderophile elements.

Dr. Rudolph Naumann and Andrea Gottsche are thanked for XRF and S analysis conducted at the GFZ in Potsdam.

Generous supply of Apollo samples by CAPTEM and the lunar sample curator (G. Lofgren) is gratefully acknowledged. Dr. Jutta Zipfel is acknowledged for supplying a sample of the lunar meteorite DaG400. Thanks to T. McCoy, M. Wadhwa, F. Brandstetter, A. Greshake, D. Ebel, J.-P. Lorand and S. Gao for supplying samples.

The members of the geochemistry department of the Freie Universität Berlin are gratefully acknowledged for providing a stimulating and delightful atmosphere. Thank you Ms. Feth, Ms. Schreiber, Bi, Corinna, Wiebke, Susanne, Olga, Harry, Frank, Uwe, Kai, Mr. Hammerschmidt, Christian, Marc, Timo and Clemens. It was a pleasure to work and discuss with you.

Eleonore Rauch is acknowledged for proof reading.

My wife Johanna, my two children Janosch and Ida, my family and friends are acknowledged for their help, support and understanding.